UNIVERSITY OF LIVERPOOL

Development of stem cell-derived hepatocyte models

Thesis submitted in accordance with the requirements of the University of Liverpool for the degree of Doctor in Philosophy

By

Christopher Steven Pridgeon

August 2019

Declaration

This thesis is the result of my own work. The material contained within this thesis has not been presented, nor is currently being presented, wholly, or in part, for any other degree or qualification.

Christopher Steven Pridgeon

This research was undertaken at the Department of Molecular and Clinical Pharmacology and the MRC centre for Drug Safety Science of the University of Liverpool

Table of contents

Abstract

Stem cell derived models of hepatocytes have potential in toxicity testing and regenerative medicine. Despite global efforts drug-induced liver-injury (DILI) remains a major concern for the pharmaceutical and healthcare industries and is a considerable cause of morbidity and mortality. Therefore, efforts are being made to reduce its incidence through toxicity screening to prevent the release of unsafe compounds to market. Current models of DILI are flawed, either lacking in terms of physiological relevance in the case of hepatic cell lines or in terms of reproducibility and availability in the case of human primary hepatocytes (hPH). Stem cell-derived hepatocyte models offer a theoretically unlimited source of potentially high-quality hepatocytes for toxicity testing. However, currently they are hindered by lack of maturity compared with hPH as in the case of pluripotent stem cell-derived hepatocyte-like cells (PSC-HLCs), or are incompletely phenotyped, in the case of human liver organoids.

Hypoxic conditions improve the stemness of PSCs, in addition, during embryogenesis cells are exposed to hypoxic conditions. Furthermore, there is a range of oxygen concentration across the liver lobule which is implicated in their phenotype. We hypothesised that iPSC-HLCs differentiated under hypoxic conditions (5% O_2) would adopt a perivenous phenotype with higher CYP expression. Two differentiations protocols, one growth factor-based, the other small molecule-based were also compared. These results showed little difference between oxygen conditions but suggested that cells differentiated under traditional normoxic conditions experience some degree of hypoxia. Additionally, we found little difference between differentiation protocols, suggesting the cheaper, and more reproducible small molecule-based protocol should be used in future studies.

Human liver organoids derived from EpCAM-positive cells were established and their phenotype was examined using iTRAQ. These results showed that organoids offer good recapitulation of the phenotype of hPH particularly regarding transporter phenotype.

The current demand for donor organs outstrips supply. Consequently, there have been efforts in recent years to find alternate sources of cells and tissue for transplant. PSCs offer a potentially unlimited source of cells for this purpose. However, the risks associated with the use of stem cells for transplant are incompletely understood. There are concerns regarding the tumorigenic potential of stem cells used for transplant, based not only on the inherent ability of pluripotent cells to form teratomas *in vivo* but also regarding the more insidious genetic changes introduced during isolation and culture.

The effects of the 20q11.21 amplicon, a common aberration occurring in approximately 20% of PSC-lines after extended culture and providing a selective advantage *in vitro* were examined when differentiated into HLCs and injected intrasplenically into SCID mice. We generated luminescent PSCs with known 20q11.21 status, tracked their engraftment over approximately 4 months. Our results demonstrated worsened liver histology and increased luminescence in animals injected with cells containing the amplicon.

These studies revealed little no advantage to the use of hypoxic conditions for the production of HLCs but suggest potential for the future use of hyperoxia. The investigation into the proteomic phenotype of organoids revealed a good approximation of many liver specific genes including CYPs, phase II enzymes and transporters but were hindered by the inability to successfully cryopreserve the organoids. Despite issues with engraftment, the presence of 20q11.21 appears to worsen liver histology, future studies should screen against its use. Repeat studies should consider the use of alternate animal models to better facilitate cell engraftment

Acknowledgements

I would like to thank my supervisors at the University of Liverpool, Prof. Chris Goldring, Dr. Mike Cross and Prof. Kevin Park for their help and guidance during by PhD studies. I would also like the thank the Integrative Toxicology Training Partnership, for their financial support, and in particular, Andy Smith, for organising the training week each year.

Whilst working at the University of Liverpool I have been lucky enough to work with many gifted scientists who have enabled me to pursue my studies. I would like to express my gratitude to all my colleagues in the department and beyond. Specifically, I would like to thank Fang Zhang for her guidance and attention to detail which has made me a better scientist. I would like to thank James 'Maverick Renegade' Heslop, the stem cell guru. Your patient tutelage has been invaluable, and much of the work in this thesis would not have been possible without it. Thank you also to Pete Metcalfe for being an endless source of interesting conversation and for teaching my first hands-on experience in cell culture. Also, thank you to Shiva Seyed-Forootan, I am immensely grateful for your tutelage and support.

I would also like to extend my gratitude to Team Liver, the tireless efforts of so many individuals, with mad dashes to the hospital to collect specimens and late-night isolations have ultimately made large parts of this thesis possible.

Outside the lab, I would like to thank my friends and family for supporting me throughout my PhD. Thank you to the University of Liverpool Jiu Jitsu club for all the training sessions and social events. Finally, thank you to Fiona for your unfailing patience and support during this PhD.

List of publications

Chris S. Pridgeon, Shiva Seyed Forootan, Fang Zhang, Nicholas Harper, Daniel Palmer, Emanuele Ricci, Peter W. Andrews, Harish Poptani, David C. Hay, B. Kevin Park, Chris E. P. Goldring, *In vivo* tumorigenicity of the 20q11.21 amplicon in a differentiated liver cell engraftment model. *Manuscript in preparation.*

Lynch, S., **Pridgeon, C.S.**, Duckworth, C.A., Sharma, P., Park, B.K., Goldring, C.E.P., 2019. Stem cell models as an *in vitro* model for predictive toxicology. Biochem. J. 476, 1149–1158. doi:10.1042/BCJ20170780

Wong, M.W., **Pridgeon, C.S.**, Schlott, C., Park, B.K., Goldring, C.E.P., 2018. Status and use of induced pluripotent stem cells (iPSCs) in toxicity testing, Methods in Pharmacology and Toxicology. doi:10.1007/978-1-4939-7677-5_10

Pridgeon, C.S., Schlott, C., Wong, M.W., Heringa, M.B., Heckel, T., Leedale, J., Launay, L., Gryshkova, V., Przyborski, S., Bearon, R.N., Wilkinson, E.L., Ansari, T., Greenman, J., Hendriks, D.F.G., Gibbs, S., Sidaway, J., Sison-Young, R.L., Walker, P., Cross, M.J., Park, B.K., Goldring, C.E.P., 2018. Innovative organotypic *in vitro* models for safety assessment: aligning with regulatory requirements and understanding models of the heart, skin, and liver as paradigms. Arch. Toxicol. doi:10.1007/s00204-018-2152-9

Goldring, C., Weaver, R., Kramer, B., Klingmueller, U., Oppelt, A., Van der Water, B., Commandeur, J., Guillouzo, A., Naisbitt, D., French, N., Kitteringham, N., **Pridgeon, C.**, Knolle, P., Sidaway, J., Sison-Young, R., Kamalian, L., Mercer, A., Faulkner, L., Pieters, R., Ingelman-Sundberg, M., Kevin Park, B., Park, B.K., 2017. 4.13 Drug-Induced Liver Injury: Mechanism-Informed Prediction in Drug Development, in: Comprehensive Medicinal Chemistry III. Elsevier, pp. 217–238. doi:10.1016/B978-0-12-409547-2.12384-4

Heslop, J.A., Kia, R., **Pridgeon, C.S.**, Sison-Young, R.L., Liloglou, T., Elmasry, M., Fenwick, S.W., Mills, J.S., Kitteringham, N.R., Goldring, C.E., Park, B.K., 2017. Donor-dependent and other nondefined factors have greater influence on the hepatic phenotype than the starting cell type in induced pluripotent stem cell derived hepatocyte-like cells. Stem Cells Transl. Med. 6, 1321–1331. doi:10.1002/sctm.16-0029

Pridgeon, C.S., Zhang, F., Heslop, J.A., Nugues, C.M.L., Kitteringham, N.R., Park, B.K., Goldring, C.E.P., 2016. Application of Pluripotent Stem Cells in Drug-Induced Liver Injury Safety Assessment, in: Will, Y., McDuffie, J.E., Olaharski, A.J., Jeffy, B.J. (Eds.), Drug Discovery Toxicology. Wiley, Hoboken, New Jersey, pp. 331–345. doi:10.1002/9781119053248.ch21

Kia, R., Kelly, L., Sison-Young, R.L.C., Zhang, F., **Pridgeon, C.S.**, Heslop, J.A., Metcalfe, P., Kitteringham, N.R., Baxter, M., Harrison, S., Hanley, N.A., Burke, Z.D., Storm, M.P., Welham, M.J., Tosh, D., Küppers-Munther, B., Edsbagge, J., Starkey Lewis, P.J., Bonner, F., Harpur, E., Sidaway, J., Bowes, J., Fenwick, S.W., Malik, H., Goldring, C.E.P., Kevin Park, B., 2015. MicroRNA-122: A novel hepatocyte-enriched *in vitro* marker of drug-induced cellular toxicity. Toxicol. Sci. 144, 173–185. doi:10.1093/toxsci/kfu269

1 General Introduction

1.1 Adverse drug reactions and drug-induced liver-injury

Despite concerted global effort, adverse drug reactions (ADRs) are still a major concern for the pharmaceutical and healthcare industries. Drug-induced liver-injury (DILI) is the class of adverse drug reactions discussed herein. DILI is a leading cause of acute liver failure in the UK and the US (O'Grady, 2005; Reuben et al., 2010) and is responsible for 6.5-6.7% of all hospital admissions where 0.15-0.32% of which culminate in death (Lazarou et al., 1998; Pirmohamed, 2004). A recent study investigated the incidence of DILI in the Icelandic population and found an incidence of 19.1 cases per 100,000 individuals per year (Björnsson et al., 2013) this is similar to a previous study carried out in France which reported an incidence of 13.9 cases of DILI per 100,000 individuals per year (Sgro et al., 2002). An important caveat to the Icelandic study is that patients with paracetamol (acetaminophen, APAP) toxicity were excluded from the total estimate which have been shown by other studies to account for nearly half the cases of DILI (Larson et al., 2005). The incidence of DILI has been shown to increase in hospital inpatients to 1.4%, approximately 100-fold higher than in the general population (Meier et al., 2005).

Concomitantly, unexpected hepatotoxicity discovered post-marketing is the largest single cause of drug retractions; between 1953 and 2013, 81 drugs were withdrawn worldwide due to hepatotoxicity, 18% of the total number of retractions (Onakpoya et al., 2016), the largest proportion followed by immunotoxicity and cardiotoxicity. Drug withdrawals are expensive to the pharmaceutical industry, a recent study showed that developing a new compound to the point of market approval costs, on average, $2.558 billion, increasing to $2.87 billion when post-marketing research and development costs are included (DiMasi et al., 2016). These huge sums of money are wasted in the case of toxicity being detected post-marketing leading to withdrawal. These figures include the costs of compounds which were unsuccessful in the development pipeline, highlighting the unsatisfactory nature of current toxicity detection techniques at the early stages of drug development which ideally should prevent progression of unsuitable compounds to the expensive later stages of toxicity testing.

In addition to the large sums of money wasted on unsuccessful compounds, a great deal of time and effort are invested into unsuccessful compounds which could have been more effectively used developing other projects had toxicity been detected sooner. Therefore, for reasons of cost, resource management and most crucially, health, it is imperative to

develop techniques for rigorously detecting hepatotoxicity during the early stages of drug development.

DILI can typically be divided into two classes, idiosyncratic and predictable. Predictable DILI is epitomised by the type of toxicity cause by paracetamol overdose. The toxicity is dose-dependent and occurs in all individuals with sufficient dose. In the case of paracetamol, toxicity occurs when the normal detoxification mechanisms are overcome, therefore although the toxic dose may differ from person to person due to inter-individual heterogeneity, toxicity will always occur with sufficient dose. Under normal conditions, paracetamol is metabolised by sulfation and glucuronidation and to a minor extent by CYP2E1 and CYP1A2 to the reactive metabolite N-acetyl-p-benzoquinone imine (NAPQI) which is then conjugated and detoxified by the intracellular reducing agent, glutathione (GSH). Under conditions of overdose, the intracellular pools of GSH are depleted and NAPQI instead binds to cellular macromolecules, leading to dysfunction and eventually necrotic cell death. Thusly the characteristic focal necrosis in the pericentral regions of the liver, where CYP2E1 is expressed most highly is indicative of paracetamol toxicity.

On the contrary, idiosyncratic DILI is poorly understood, it does not occur in all individuals and does not always follow dose-response patterns, typically occurring at therapeutic levels above a certain threshold. Idiosyncratic DILI is rare; thus, it is often difficult to predict in clinical trials or preclinical trials. However idiosyncratic DILI is thought to be responsible for 13% of cases of ALF in the US (Ostapowicz, 2002) and therefore is a major concern. There is some evidence that factors such as age, sex and liver disease status can influence the occurrence of idiosyncratic DILI (Hussaini and Farrington, 2007), in addition some genetic and immune factors appear to predispose an individual (Fontana, 2014; Hussaini and Farrington, 2007).

Specific human leukocyte antigen (HLA)-types can predispose an individual towards idiosyncratic DILI. HLA-type refers to the highly polymorphic variants of the gene complex which encodes the major histocompatibility complex, a key component of the immune system which presents antigen fragments to the innate immune system and is also involved in leveraging the adaptive immune system. For example, HLA-B*-5701 predisposes individuals to DILI when taking flucloxacillin and also predisposes towards abacavir hypersensitivity (Kim and Naisbitt, 2016). Interestingly however, HLA-B*-5701 is only a weak positive marker for flucloxacillin toxicity affecting only approximately 1 in 100 patients with the polymorphism but is strongly predictive of abacavir hypersensitivity.

Similarly, HLA-DRB1*16: 01-DQB1*05: 02 increases the incidence of liver injury from flupirtine (Daly et al., 2009; Nicoletti et al., 2016). However, despite knowledge of these predisposing factors, these toxicities are still classed as idiosyncratic DILI because the toxic effects do not manifest in all individuals with the 'at-risk' HLA-type. Involvement of HLA-types in DILI suggest an immune component to idiosyncratic DILI. Typically, although many patients may develop symptoms like idiosyncratic DILI, they are very mild (alanine aminotransferase (ALT) <3x ULN) and are tolerated out with continued use of the drug, this phenomenon is termed clinical adaptation. Current opinion holds that idiosyncratic DILI represents a failure of the liver to adapt to the presence of a drug or its metabolite which acts as a hapten, stimulating an immune response against the hepatocytes where the hapten is produced.

The role of immune tolerance in idiosyncratic DILI has recently been demonstrated in two mouse models firstly by Metushi *et al.* where transgenic mice with an impaired immune tolerance phenotype were treated with amodiaquine producing a slightly greater extent of liver injury than immune tolerance-competent mice. Following this experiment, the authors tested amodiaquine on wild-type mice producing transient liver injury which resolved with clinical adaptation. When PD-1(-/-) mice were treated with both amodiaquine and anti-CTLA4 (preventing immune tolerance), the liver injury produced was severe and sustained, indicating the relevance of immune tolerance to idiosyncratic DILI.

1.2 Structure of the liver

The liver is the major hub of xenobiotic metabolism, it responds to a wide variety of xenobiotic compounds and attempts to convert them into non-toxic by-products. Hepatocytes make up most of the cells in the liver, approximately 80% by mass and 60% of the total cell number. They contain many liver-enriched enzymes involved in xenobiotic metabolism, most notably transporters and the cytochromes P450 (CYPs). The liver is strategically positioned as the first pass organ after absorption from the gastrointestinal tract, and therefore receives the highest dose of absorbed xenobiotics. In addition to xenobiotic metabolism, the liver is also responsible for secreting serum proteins such as albumin and α1-antitrypsin and producing urea. The liver is also implicated in the regulation of blood glucose; glycogen is stored and released from the liver under the control of insulin and glucagon secreted from the pancreas.

The liver is divided into lobes; each of these lobes is made up of smaller lobules which are roughly hexagonal in cross-section and fit together in a lattice. Blood enters the lobule through the portal triad (periportal region), the blood then flows along the lobule via the sinusoid and drains through the central vein (the pericentral region, figure 1). Along the sinusoid, hepatocytes are tightly packed together where they perform xenobiotic metabolism and other functions during the passage of blood. These hepatocytes exhibit a spectrum of phenotypes along the sinusoid specialising in different areas of xenobiotic metabolism. For example, expression of CYP2E1, responsible for the metabolism of paracetamol and ethanol is restricted to pericentral regions of the liver (Dicker and Cederbaum, 1991). This explains the localised pericentral damage seen during paracetamol overdose and presents a challenge to *in vitro* models of drug-induced liver injury where the zonation of the lobule is not intact which must nonetheless be able to detect toxicity to all zones of the liver.

Oxygen tension varies across the liver lobule, upon entry blood is highly oxygenated and is depleted of oxygen across the lobule. This gradient in oxygen is functional in determining

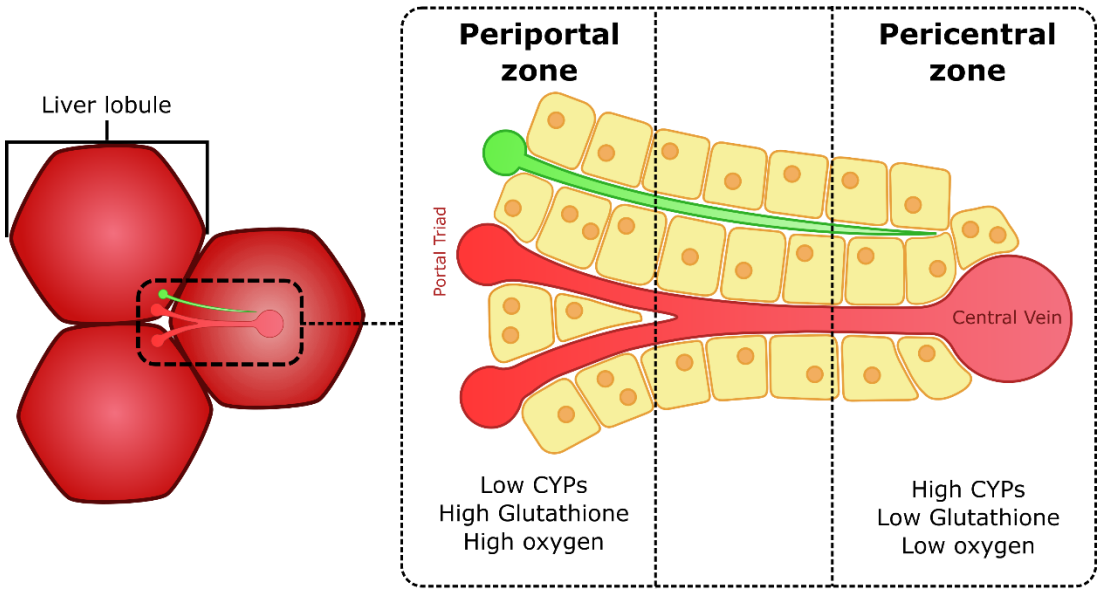

Figure 1

Diagram of zonation across the liver lobule - Hepatocytes vary substantially depending on their location in the liver. For example, the expression of CYP2E1 and glutathione is higher in pericentral regions of the liver lobule and lower in the periportal zones which can functionally affect cells during paracetamol overdose. The levels of oxygen are higher in the periportal zone and decrease as blood flows towards the pericentral zone. This helps drive the change in phenotype of the hepatocytes across the lobule.

the phenotype of hepatocytes and plays a role in determining the expression of the various hypoxia inducible factors that govern this phenotypic change (Kietzmann, 2017). The effects of oxygen on the maintenance and differentiation of hepatocytes and hepatocyte-like cells (HLCs) are poorly understood and will be revisited in chapter 3.

1.3 Models of Hepatotoxicity

Currently, a battery of tests and predictions are used to inform the decisions made during the drug discovery and development process. These include *in silico*, *in vivo* and *in vitro* techniques before compounds are tested in humans. However, these techniques are imperfect, *in silico* models are informed by *in vitro* and *in vivo* data and are not entirely discriminatory in their identification of toxic compounds. Furthermore, it is difficult to ascertain whether false positives are being reported which may lead to unnecessary attrition of potentially useful drugs and the results may be difficult to interpret.

1.3.1 In vivo models

In vivo models involve the use of animals as surrogate models for humans, typically using mice, rats, dogs, mini-pigs or the cynomolgus monkey. The use of animals for research is an ethically challenging topic which has been contentious for well over a century (Saffron, 1975). Because of their similarity to humans, research on great apes has been deemed unethical across the EU and they are no longer used for research in the UK or the EU except in cases where there is direct benefit to the tested species or in the case of a life-threatening condition to humans where no other species can be used (Institute of Medicine and National Research Council, 2011). Whilst ethical concerns regarding the great apes are important, they also represent the closest non-human *in vivo* model for testing of new compounds and the ban of their use forces animal testing to be carried out in lower mammals where there are issues with translatability of findings to humans (Hackam, 2007). Despite some issues with translatability, testing in animal models is still required before first-in-man studies for a new compound (Committee for Medicinal Products for Human Use, 2007) which may be interpreted as confidence in their efficacy. Through initiatives such as the NC3Rs based on 'The Principles of Humane Experimental Technique' (Russell and Burch, 1992) there are drives to replace, refine and reduce animal research, including the use of improved and complex *in vitro* models.

The drive to reduce the use of animals in pharmaceutical testing is not solely ethical. The issues with translatability of findings in animals to humans are challenging. This is well-

demonstrated in the clinical trials of fialuridine, a nucleoside analogue developed for the treatment of hepatitis B which ultimately led to the deaths of 33% of the treated cohort in clinical trials with a further 2 patients receiving emergency liver transplants. The toxicity of fialuridine was unexpected and animal trials in mice, rats, dogs, and primates were not successfully predictive. It has since been demonstrated that the absence of toxicity in animal models was likely due to the lack of mitochondrial expression of the nucleoside transporter ENT1 which is found in humans but not in the tested animals. This was confirmed in studies with TK-NOG mice, which showed hepatotoxicity in response to fialuridine but only when the animals had humanised livers (Xu et al., 2014).

In addition to the fialuridine trial, several other high-profile failures of drugs in first-in-man studies demonstrate the inadequacy of animal models to sufficiently predict human toxicity. These studies include the TGN1412 trial, where despite the use of animal studies for the novel CD28 'superagonist' and use of a dose 500 times lower than found to be safe in animals all six of the patients suffered from cytokine storm and were hospitalised (Suntharalingam et al., 2006). Additionally, recent trials for the fatty acid amide hydrolase inhibitor BIA 10-2474 were conducted in France, animals studies were not predictive of the toxicity observed in first-in-man trials where five patients suffered neurological injuries and a sixth died (Moore, 2016).

1.3.2 In vitro models

With regards to drug hepatotoxicity, *in vitro* models use both single cell types and combinations to identify toxic compounds. These models include the use of cancer cell lines such as the ubiquitous HepG2 or Huh-7, human primary hepatocytes (hPH) and primary hepatocytes from other model species and stem cell-derived models.

1.3.2.1 Human primary hepatocytes

Freshly isolated hPH are considered the gold standard *in vitro* model for predicting hepatotoxicity in humans, because of their high metabolic relevance to humans, hPH express xenobiotic metabolism enzymes, and transporters at similar levels to those found in human liver which is necessary to faithfully recapitulate the DILI environment. However, hPH have several disadvantages, including scarcity due to the need for donor tissue or cadaveric liver, inter-donor variability including expression of cytochrome P450s and transporters. For example, CYP2D6 is involved in the metabolism of approximately 25% of drugs on the market but is highly variable in the human population (Kroemer and Eichelbaum, 1995; Teh and Bertilsson, 2012). Approximately 10% of the Caucasian

population are CYP2D6 null and a further 7% are CYP2D6 ultra-rapid metabolisers (Steijns and Van Der Weide, 1998; Stüven et al., 1996); this variation can confound repeat studies using hPH as it is highly unlikely that several hPH isolations from the same individual will occur and thus experimental repeats will use cells with different genetic origin. It is possible to cryopreserve hPH so that they may be used on several occasions although the loss of mature phenotype and viability which occurs renders the process sub-optimal (Terry et al., 2010, 2006). Furthermore, even though hPH may be cryopreserved, there is a hard limit on the number of cells which can be used from any single donor determined by the number of cells isolated at the time of tissue donation and since hPH are non-proliferative in vivo, they may only be cryopreserved on a single occasion.

The final issue confounding the use of hPH is dedifferentiation. Dedifferentiation is characterised by the progressive loss of mature hepatic characteristics including expression of xenobiotic metabolism enzymes and transporters, loss of the characteristic morphology and eventually loss of cell viability. Dedifferentiation begins immediately after the liver tissue is isolated from the host blood supply. Large scale changes in expression of MicroRNAs have been observed in as little as 30 minutes after isolation (Lauschke et al., 2016). Because of the rapid dedifferentiation of hepatocytes their useful lifespan in vitro is typically considered to be only a few days (Rowe et al., 2013). Practically, this means that hPH are useful mainly for acute toxicity testing, which is problematic considering that many drugs exhibit toxicity only after chronic use. Indeed, idiosyncratic DILI often only presents after prolonged use of a drug.

1.3.2.2 Immortalised cell lines

Immortalised cell lines are heavily used in toxicity testing. Despite some disadvantages, their ease of use and low cost have often made them the *in vitro* model of choice for hepatotoxicity testing. Immortalised cell lines are derived from cancers and have the capacity to replicate indefinitely. The capacity for infinite replication in combination with other hallmarks of cancer cells (Hanahan and Weinberg, 2011) such as loss of contact inhibition and increased proliferation rate make them useful *in vitro* models for rapid, high-throughput toxicity screening.

There are several immortalised cell lines commonly used for hepatotoxicity testing, (HepG2, Huh-7 and HepaRG) which are favoured for their ease of use and low cost. They also represent a static line that is suitable for experimental repeats and can be expected to yield similar results. By contrast, hPH from different donors may produce differing results

depending on their gene and protein expression profiles (Gerets et al., 2012). In addition, immortalised cell lines may be used for toxicity testing where minimal or no bioactivation is required. For example, a recent study showed the utility of HepG2 cells in mitochondrial toxicity testing where the metabolic plasticity of Warburgian cells is advantageous (Kamalian et al., 2015).

The lack of physiological relevance to human liver, is the main limitation of all immortalised cell lines used for hepatotoxicity testing. It has been shown that the gene expression of 251 drug metabolising enzymes and transporters of several commonly used hepatoma cell lines (including HepG2 and Huh-7) correlated poorly to hPH from 4 donors (Guo et al., 2011) although some improvements have been observed in 3D culture, as will be discussed in section 1.7. Additionally, the static nature of immortalised cell lines means that they are unlikely to show any substantial improvement over time whereas stem cell differentiation protocols and protocols for the isolation and maintenance of hPH are dynamic and constantly improving. Furthermore, immortalised cell lines represent the phenotype of only a single donor which is limiting when considering the low frequency of some genotypes susceptible to idiosyncratic DILI in the population.

1.3.2.3 Stem cell-derived models

Stem cells are undifferentiated cells capable of differentiating to other cell types; they are described based on their capacity to differentiate. Totipotent cells can differentiate into all cell types including all germ layers and extraembryonic tissue; only cells in the first few divisions after embryogenesis are totipotent. Despite recent controversial reports, totipotent stem cells have not been derived from adult cells (Obokata et al., 2014b, 2014a). Pluripotent cells can differentiate into cells of all germ layers. Induced pluripotent stem cells (iPSCs) and embryonic stem cells (ESCs) fall under this category. Multipotent cells can differentiate towards several cell types but fewer than pluripotent stem cells, for example, haematopoietic cells that can differentiate into several blood cell types are considered multipotent.

Embryonic stem cells and pluripotent stem cells are often compared as both are commonly used in the field. Embryonic stem cells are derived from the inner cell mass of discarded fresh or frozen blastocysts. However, the use of embryonic material is politically and ethically controversial (Lo and Parham, 2009) and also encumbered by scarcity of donor embryonic tissues.

Induced pluripotent stem cells (iPSCs) were recently discovered and derived in human cells by the Yamanaka group (Takahashi et al., 2007; Takahashi and Yamanaka, 2006). By overexpressing four factors, commonly known as the Yamanaka factors, Oct4, Sox2, Klf2 and c-Myc, a differentiated cell can be reverted to a pluripotent state. This sidesteps many of the confounding ethical issues surrounding the use of embryonic stem cells (ESCs) whilst also offering some advantages unique to iPSCs. One such advantage is the ability to use most cell types as the starting cell, practically this means the iPSCs can be relatively simply derived from easily accessible cells such as fibroblasts or nucleated blood cells. In addition, iPSCs can be isolated from individuals with known phenotype. The advantages of this are mainly twofold, since cells retain the phenotype of the donor individual through isolation, reprogramming and differentiation, cells can be isolated from individuals with a known rare phenotype in order to model it *in vitro* (Raya et al., 2009). Moreover, iPSCs are candidates for personalised medicine in the individual from which they were derived, since they will not be recognised as foreign upon transplantation during cell therapy. Once derived, iPSCs can be differentiated into any somatic cell type. This is typically achieved by use of a differentiation protocol which relies on mimicking the conditions found during embryogenesis to produce the desired cell type. These protocols typically take the form of sequential addition of growth factors to the culture medium though other techniques can also be used such as small molecule mimics of growth factors and environmental triggers.

Furthermore, the use of iPSCs is advantageous as the donor phenotype is known and can be replicated in the resultant cells. This phenomenon has been exploited several times in recent years, and several disease modelling iPSC cell lines have been developed (Dimos et al., 2008; Ebert et al., 2009; Soldner et al., 2009; Ye et al., 2009). Using gene correction, iPSC lines may be effectively 'cured' of genetically based diseases. Examples of this approach include: Parkinson's disease, where LRRK2 mutant iPSCs were generated and corrected (Nguyen et al., 2011; Reinhardt et al., 2013); α1-antitrypsin deficiency (Yusa et al., 2011); congenital erythropoietic porphyria (Bedel et al., 2012) and Fanconi anaemia (Raya et al., 2009). iPSCs are also advantageous insofar as the risk for immune rejection with transplanted cells to the original donor are circumvented.

Acute liver failure is responsible for many deaths each year and liver- or liver cell transplant is often the only curative solution. iPSCs can be differentiated into HLCs and may be useful to treat such cases of liver failure. Indeed, humanisation of animal livers has been achieved in recent years with human iPSC-derived HLCs (iPSC-HLCs) (Takebe et al., 2014). These cells were able to rescue animals from otherwise fatal liver damage (Takebe et al., 2014). The

use of iPSC-HLCs could also allow for cell transplant without the use of long-term immunosuppression and its associated effects and offer an appealing model for toxicity testing given their renewable nature and ability to reproducibly model rare phenotypes.

There is concern that stem cell therapies may pose an oncogenic risk to the recipient. This is due not only to the teratoma-forming ability of the undifferentiated cells but also due to possible accumulation of mutations in the culture of iPSCs. The rate of mutations in iPSCs is incompletely understood, one study indicated that around half of the 6-12 mutations found in protein coding genes over extended iPSC culture were synonymous and that of the remaining mutations, no enrichment in cancer-causing genes was observed (Cheng et al., 2012). Whilst other groups have found that iPSC rapidly accumulate significant mutations in culture such as the gain of 20q11.21, a large duplication that appears to confer a survival advantage to the cells *in vitro* by increased expression of the anti-apoptotic gene, BCL-XL (Nguyen et al., 2014).

The mRNA and miRNA profiles of hESCs differs from the profiles of iPSCs and the differentiation propensity of early-passage iPSCs is reported to be skewed in favour of the cell type of origin. However, this bias towards the original cell type appears to be lost with

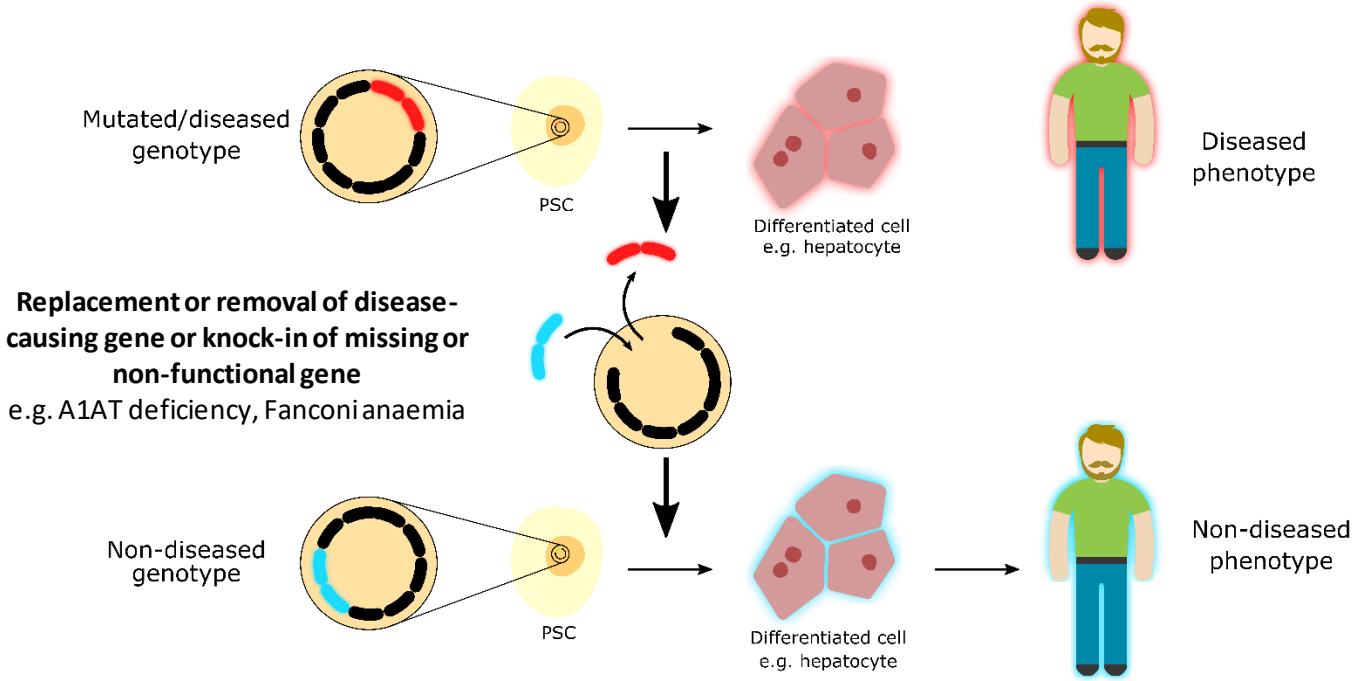

Figure 2

Schematic of gene correction in iPSCs derived from a diseased patient – Replacement of disease-causing genes is possible using genetic techniques. Since iPSCs maintain the phenotype of the donor from which they were derived it is possible to correct the defect and produce non-disease cells in vitro. Eventually, it may be possible to transplant non-diseased cells of matching genotype into diseased patients once key safety concerns have been addressed.

increased passage number. A recent study in our laboratory comparing the differentiation propensity of iPSCs towards iPSC-derived HLCs derived from donor-matched fibroblasts and hepatocytes found no inherent advantage conferred by deriving iPSCs from the same cell type as the target differentiated cell (Heslop et al., 2017).

iPSCs may be derived from any mature nucleated cell through overexpression of four transcription factors known as the Yamanaka factors: Oct4, Sox2, Klf-2 and c-myc. This technique was pioneered by the Yamanaka group in 2006, first in mice (Takahashi and Yamanaka, 2006) and subsequently in humans (Takahashi et al., 2007). Many methods of delivery have been assessed to produce iPSCs ranging from integration of additional copies of the genes to direct transfection of the proteins. These methods can largely be divided into two groups, integrative and non-integrative methods where the integrative methods rely in the integration of the chosen pluripotency factors into the genome of the cell. Integrative methods are generally more efficient than their non-integrative counterparts but come with the caveat that the cells are being genetically modified, this can cause disruption to the cell's normal functions and is an oncogenic risk. This concern is heightened by the integration of potent oncogenes such as c-Myc and in sum, means that iPSCs produced by integrative methods are not considered suitable for use in cell therapies in humans due to concerns of tumorigenicity.

By contrast, non-integrative methods are generally more inefficient than their integrative counterparts, sometimes by a large margin but they are advantageous insofar as that no genes are integrated into potentially oncogenic or otherwise potentially dangerous positions in the genome. Non-integrative methods include non-integrating or replication deficient viruses such as Sendai virus and direct transfection with RNA molecules or proteins to effect pluripotency (Gonzalez et al., 2011). PSCs produced by these methods are considered suitable for cell therapies.

Stem cells are undifferentiated, that is, they are not committed towards any mature cell fate. This is similar to the cells found in the embryo during the very early periods of development prior to gastrulation where the three germ layers are formed. Directed differentiation of stem cells is a process which aims to mimic embryogenesis *in vitro* to produce a mature cell fate. Crucially, unlike embryogenesis, a directed differentiation protocol typically aims to produce only a single cell type rather than a whole organism.

During differentiation, cells are directed through a series of developmental checkpoints which correlate to stages of embryogenesis. For example, when producing hepatocyte like

cells, definitive endoderm is the first checkpoint the cells reach followed broadly by hepatic endoderm and subsequently HLCs. The cells are guided through these checkpoints by timed sequential addition of growth factors. The focus of chapter 3 and will be in the generation of HLCs from iPSCs or ESCs. There are a range of protocols that have been developed over the past decade to produce HLCs, some of which are summarised below and in Table 1.

Early differentiation protocols used embryoid body formation to produce HLCs, wherein undifferentiated cells are allowed to form clusters and differentiate spontaneously (Itskovitz-Eldor et al., 2000). However, this approach is now uncommon with most differentiations being initially performed in monolayer culture. The stochastic nature of non-directed differentiation of HLCs leads to unsatisfactory reproducibility and purity of the resultant cells. Early experiments with embryoid body formation showed the capability of ESCs to produce HLCs *in vitro* (Hamazaki et al., 2001) and *in vivo* (Choi et al., 2002).

Early directed differentiation protocols used a single stage to induce hepatic differentiation; for example, the addition of sodium butyrate to hESCs, resulted in 10-15% purity of HLCs (Rambhatla et al., 2003). Shirahashi *et al.* showed 20% FBS, human insulin and dexamethasone plated on collagen-I, improved albumin synthesis in human and murine ESCs (Shirahashi et al., 2004). Schwartz *et al*. showed that addition of FGF4 and BMP2 in embryoid bodies plated on collagen-I improved expression of several mature hepatic markers including albumin, HNF1 and several CYP enzymes amongst others (Schwartz et al., 2005).

Multi-stage differentiation protocols are currently the commonly used type of protocol, which as previously described involves directing cells towards several developmental checkpoints during differentiation, mimicking embryogenesis. Teratani *et al*. demonstrated an early multi-stage directed hepatic differentiation in similar format to those currently in murine embryonic stem cells and used leukaemia inhibitory factor and retinoic acid in cells cultured on gelatine followed by HGF, FGF1 and FGF4 in ESM on gelatine followed by oncostatin M (OSM) on collagen (Teratani et al., 2005). This protocol demonstrates the general format of HLC differentiation protocols commonly used today, though the exact details and growth factors vary greatly and have been refined over the past decade. A summary of hepatocyte-like cell differentiation protocols is presented in Table 1.

Reference	Differentiation method			Differentiation efficiency (%)	Notable findings
	Cell type	Culture format	Differentiation factors		
Chien et al., 2015	hPSC	Co-culture with MEF, EB formation	AA, FGF4, BMP2, HGF, KGF, OSM, DEX, miR122	–	Improvement in hepatic phenotype when miR-122 used in differentiation in 3D. Increased expression of AFP, CYP2E1, CYP3A4. Improved Urea secretion and LDL uptake.
Zhang et al., 2014	hPSC	Nanopillar	AA, FGF2, BMP4, OSM, HGF, Dex	>80	Protocol paper. Spheroid size examined.
Subramanian et al., 2014	hESC	Ultra-low Attachment	AA, Wnt3a, FGF2, FGF4, HGF, Follistatin	80	*AFP*, *ALB*, *CX32*, *ARG1*, *HNF4A*, *FVII*, ASGPR-1 and PEPCK significantly increased in 3D. Increased and sustained albumin secretion in 3D vs. 2D.
Baharvand et al., 2006	hESC	Embryoid bodies followed by collagen scaffold	aFGF, HGF, OSM, Dex	44-60	Earlier expression of Albumin and G6P in 3D. Increased AFP and urea production in 3D vs. 2D
Pettinato et al., 2016	hPSC	Embryoid bodies in agarose microwells	FGF2, AA, TGF-ß. FGF4, BMP4. WIF-1, DKK-1. HGF, OSM.	80	Novel use of wnt inhibitors. Increased albumin, AFP and fibrinogen secretion and in intracellular urea concentration with inhibitor. ALB CK18 CYP1B1, 2C9, 2B6 3A4, 3A7 and 1A2 expression increased with inhibitor use.
Gieseck et al., 2014	hPSC	RAFT	AA, FGF2, BMP4, LY-294002, CHIR99021. HGF, OSM.	>95	Improved phenotype in 3D culture. Increased expression of CYP3A4, ABCC2, UGT1A1 and decreased expression of AFP and CYP3A7.

Chitrangi et al., 2017	hMSC	Multiple synthetic scaffolds	HGF, FGF4. OSM, Dex	47.23-68.19	Comparison of synthetic scaffolds: dextran–gelatin, chitosan–hyaluronic acid and gelatin–vinyl acetate. Reduced AFP expression and increased HNF4a, ALB, G6P α1AT in 3D
Takayama et al., 2013	hESC, hPSC	Nanopillar	AA, FGF2. FOXA2, AA, FGF2. FOXA2, HNF1α, HGF, FGF1, -4 & -10. HGF, OSM, FGF4, Dex.	-	Increased ALB, CYP1A1, CYP1A2, CYP3A7, CYP2B6, CYP2C8, CYP2C19 CYP2E1, UGT1A1, UGT1A3, GSTA1, MDR1, BCRP, MRP2, SLCO1B3, SLCO2B1, NTCP, OCT1, OAT2, ABCB4, ABCC3 ABCC6, AhR, CAR, PXR and PPARα in 3D vs. 2D
Leclerc et al., 2017	hPSC	Biochip with flow	AA. FGF2, BMP4. HGF, OSM.	-	Increased HIF, HNF4α, CD144, CD31, ALB, CYP3A4 and CYP1A2 in 3D vs. 2D
Cipriano et al., 2017	hMSC	Ultra-low attachment, hollow fibre bioreactor	EGF, FGF2. HGF, FGF2, FGF4, DMSO. OSM, Dex, DMSO.	-	Increased AFP, CYP3A4, urea production and glucose consumption in 3D.
Takayama et al., 2017	hPSC	Monolayer	FGF2. AA. BMP4, FGF4. HGF, EGF, HGF. OSM.	99.997	Used sequential laminin basement layer to generate highly purified HLCs
Siller et al., 2015	hPSC	Monolayer	CHIR99021. DMSO. Dihexa, Dex	83.2-91.0	Use of small molecule-based protocol to generate HLCs
Heslop et al., 2017	hPSC	Monolayer	AA, WNT3a. DMSO. HGF, OSM, Dex.	-	In-house protocol used for routine generation of HLCs in Liverpool

Table 1

Hepatocyte-like cell differentiation protocols – differentiation protocols using both 2D and 3D culture techniques. This summary highlights the similarities between protocols in recent years. Generally, the use of growth factors has remained constant, e.g. AA, HGF, OSM, HGF etc. Other alterations to differentiations protocols have produced the largest changes seen in recent years such as the movement towards 3D cultures and the use of advanced basement matrices such as laminins allowing for greater purity in differentiated cells. Starting cell type and culture conformation and major growth factors used are shown. Differentiation efficiency is shown if reported. Abbreviations: AA - Activin A, aFGF - Acidic fibroblast growth factor, AFP - Alpha foetoprotein, ALB - Albumin, ARG1 - Arginase 1, ASGPR-1 - Asialoglycoprotein receptor 1, BMP2 - Bone morphogenic protein 2, CX32 - Connexin 32, CYP - Cytochrome P450, DEX - Dexamethasone, DKK-1 - Dickkopf-related protein 1, DMSO - Dimethyl sulfoxide, EB - Embryoid body, EGF - Epidermal growth factor, FGF2 - Fibroblast growth factor 2, FGF4 - Fibroblast growth factor 4, FVII - Factor 7, G6P - Glucose 6-phosphate, hESC - Human embryonic stem cell, HGF - Hepatocyte growth factor, HLC - Hepatocyte-like cell, hMSC - Human mesenchymal stem cell, HNF4a - Hepatocyte nuclear factor 4α, hPSC - human pluripotent stem cell, KGF - Keratinocyte growth factor, LDL - Low density lipoprotein, MEF - Mouse embryonic fibroblast, OSM - Oncostatin M, PEPCK - Phosphoenolpyruvate carboxykinase, RAFT - Real Architecture for 3D tissues, TGF-B - Transforming growth factor β, UGT - Uridine 5'-diphospho-glucuronosyltransferase, WIF-1 - Wnt inhibitory factor 1

Although HLCs can now be differentiated in large numbers with acceptable purity there are still caveats to their use as models of hepatic toxicity. The primary disadvantage encumbering their use is their lack of functional maturity when compared with hPH in terms of expression of xenobiotic metabolism enzymes and transporters necessary for recapitulation of hepatic toxicity. Though improvements have been reported, there is still no catch-all protocol for producing HLCs with functional maturity to match hPH. Various attempts have been made to improve maturity of HLCs in addition to various combinations of cytokines, some of which will be discussed in the following paragraphs.

One such attempt to improve maturity of iPSCs utilises miR-122, a highly-conserved and hepatocyte-enriched microRNA that has been shown by several studies to improve the differentiated status of HLCs when overexpressed in stem/progenitor cells (Chien et al., 2015; Davoodian et al., 2014; Deng et al., 2014; Doddapaneni et al., 2013). Conversely, removal of miR-122 prevents hepatocytes forming from hepatoblasts in zebrafish (Xu et al., 2013) and the loss of miR-122 in liver cancer is correlated with the loss of the mature hepatic phenotype (Coulouarn et al., 2009).

A recent study delivered miR-122 complexed with PU-PEI (polyurethane-graft-short-branch polyethyleneimine copolymer in nanostructured amphipathic carboxymethyl-hexanoyl chitosan), to iPSCs and enhanced the maturation of iPSC HLCs. The miR122-iPSC HLCs expressed higher levels of gene and protein markers for hepatic function compared to miR-scrambled-iPSC HLCs including increased expression of CYP2E1, CYP3A4 and AFP and enhanced LDL uptake and urea secretion (Chien et al., 2015).

Shan et al. identified small molecules classed as functional and proliferative hits via high-throughput screening using hPH co-cultured with fibroblasts (Shan et al., 2013). Two of these compounds, FH1 and FPH1, were able to improve longevity and induce proliferation of typically non-replicative hPH in *ex vivo* culture. These compounds also showed promise in iPSC differentiation leading to an increased tendency to differentiate towards the hepatic lineage and exhibiting improved phenotypic maturity with improved albumin expression and phase I-III enzyme expression comparable to hPH, notably, BSEP was reported to reach equal levels to those found in hPH. These results are promising improvements to the phenotype of iPSC-HLCs (Shan et al., 2013).

Avior *et al*. hypothesised that the acquisition of some mature hepatic characteristics in foetal hepatocytes is driven by the change in nutrition source and exposure to gut flora in neonates. Lithocholic acid and vitamin K_2 have been shown to induce PXR and CAR expression and were investigated in this study for their potential to drive the maturation of ESC-HLCs. When added to differentiating ESC-HLCs, lithocholic acid and vitamin K_2 were shown to improve the expression of

CYP2C9 and CYP3A4 and increase the ability of the ESC-HLCs to correctly predict toxicity in known hepatotoxins (Avior et al., 2015). These results demonstrate the importance of a broad understanding of the physiological changes that drive liver maturation *in vivo* and suggest that environmental cues should also be considered for differentiation protocols.

Similarly to environmental cues, it is also important to consider the culture environment of stem cells. ESCs and iPSCs are commonly cultured on mouse embryonic fibroblasts (MEFs) or Matrigel, however both culture techniques rely on animal-derived components and are not ideal for the culture of human cells. Therefore, alternative culture matrices have been investigated including laminins and several attachment glycoproteins such as vitronectin and fibronectin. If stem cells are to be used in large-scale applications such as drug toxicity testing or in cell therapies, it is important to consider the challenges in production of a large number of cells whilst resisting spontaneous differentiation. Techniques such as those described here may help increase the stability of iPSCs and ESCs in culture.

Laminins are highly specific cell-adhesion proteins expressed at certain developmental stages of embryonic development. Their use as a basement matrix has been shown to improve cell proliferation in iPSCs but not ESCs (Lam and Longaker, 2012). Several laminin isoforms including laminin (LN)-511, -521 and -332 have been investigated as basement matrices for ESCs or iPSCs. The specificity of laminins arises from the expression pattern of integrins on the cell surface, laminins have an α and a ß subunit. Miyazaki *et al.* showed the dominant integrin subunits in hESCs were α6 and ß1 which bound most strongly to LN-332 which could be used as a basement matrix whilst retaining pluripotency (Miyazaki et al., 2008). Similarly, Rodin *et al.* used LN-511 alone and LN-521 in combination with E-cadherin both of which are also dependent on integrin α6ß1, to culture hESCs and hiPSCs. In the case of LN-511 hESCs and hiPSCs were cultured for 4 months without loss of pluripotency or abnormal karyotype (Rodin et al., 2010). The combination of LN-521 in combination with E-cadherin was sufficient for the long-term culture of hESCs without the use of ROCK inhibitors (Rodin et al., 2014). Additionally, Takayama *et al.* recently demonstrated a differentiation protocol for the highly efficient production of HLCs by changing the laminins used over the differentiation protocol, initially, a mixture of LN111 and -511 was used which was then replaced with LN-111 alone, followed by LN-111 and collagen IV (Takayama et al., 2017). These results demonstrate the utility of laminins in stem cell culture to control the type of cells present in culture, due to the specificity of laminins to certain tissue types they will be useful either in the maintenance of undifferentiated cells or the purification of cells during differentiation.

Vitronectin and fibronectin are cell-attachment proteins which, similarly to laminins, interact with integrins. Both have been investigated as potential basement matrices to support the undifferentiated growth of ESCs and iPSCs. Fibronectin, whilst able to support the growth of iPSCs and ESCs by attachment to the α6ß1 integrin, when compared with Matrigel and laminins was shown to be inferior in term of cell attachment and proliferation (Lam and Longaker, 2012). Vitronectin has shown promise in several studies as a defined substrate to support the growth of ESCs and iPSCs, attaching to cells by the αVß5 integrin and supporting growth and proliferation (Braam et al., 2008; Rowland et al., 2010).

1.4 Modulation of oxygen concentration in stem cell cultures

In addition to basement matrix, the amount of oxygen in the culture environment has been shown to be important for the undifferentiated maintenance of stem cells. Indeed, hypoxic conditions are necessary for the early stages of mammalian embryo development (Dunwoodie, 2009).

Directed ESC or iPSC differentiation protocols aim to closely mimic the conditions found during embryonic development in order to produce cells as close as possible to their *in vivo* counterparts. During development the concentrations of oxygen available to the developing embryo are considerably lower than to cells cultured in atmospheric oxygen levels, typically between 1.5-5.3% (Badger et al., 2012). Moreover, the concentration of oxygen is known to vary across the liver lobule from 30-65 mmHg O_2 and influences the phenotypic difference between periportal and perivenous hepatocytes (Kietzmann, 2017).

Hepatotoxicity is often exacerbated by the metabolic enzymes enriched in the liver, a prime example of which is the metabolism of paracetamol to NAPQI, its reactive metabolite, predominantly by CYP2E1. Since the expression of CYP2E1 and other metabolic enzymes is enriched in the pericentral zone, this hepatocyte phenotype may be of more interest in hepatotoxicity testing than that of a periportal hepatocyte which deal more with other hepatic functions.

In addition to differentiation of stem cells, expansion and long-term maintenance can be challenging. Stem cells often differentiate spontaneously during culture and hypoxic conditions have been shown to reduce the occurrence of this (Ezashi et al., 2005; Prasad et al., 2009). Hypoxic conditions appear to increase 'stemness' in many types of stem cell cultures including dental pulp, mesenchymal, embryonic, pluripotent, and tendon-derived stem cells (Ahmed et al., 2016; Badger et al., 2012; Ejtehadifar et al., 2015; Forsyth et al., 2006; Zhang and Wang, 2013). In this case, an increase in stemness refers to an increased tendency for stem cells to divide without differentiating and show increased expression of pluripotency markers such as Sox2, Nanog and Oct4. The increase

in 'stemness' has been shown to be related to an increase in notch signalling under hypoxic conditions. Moreover, hypoxic culture has been shown to reduce the spontaneous differentiation associated with long-term culture of ESCs (Ezashi et al., 2005) and to reduce the burden of oxidative stress and the incidence of chromosomal aberrations which are associated with protracted stem cell culture (Forsyth et al., 2006).

Oxygen concentration has also been shown to modulate the way in which ESCs attach to their basement matrix. Kumar et al. showed that αVβ5 (the integrin mainly responsible for attachment to vitronectin) and CD44 (responsible for hyaluronic acid attachment) were shown to be modulated by oxygen and that ESCs switched under hypoxic conditions.

1.5 Complex Hepatic Models Including iPSC-HLC models

Advances in complex culture systems seem likely to improve the application of iPSCs in drug safety assessment. Previous studies have compared conventional 2D monolayer culture with complex 3D and co-culture systems for phenotype and functionality. Compared to 2D, 3D or co-culture systems generally produce more physiologically relevant characteristics including: better inflammatory pathways with cytokine profiles in response to toxins more similar to those found *in vivo* (Cantòn et al., 2010); better xenobiotic metabolism capacity including increased expression of xenobiotic metabolism enzymes and albumin (Bokhari et al., 2007; Elkayam et al., 2006), and formation of more *in vivo*-like cell morphology, polarisation and organisation (Bissell et al., 2002; Liu et al., 2004). These characteristics were achieved by recreating a physiological microenvironment (heterogeneous cell types, spatial architecture, mechanical and chemical composition of extracellular matrices) which improves cell-cell and cell-extracellular matrix interactions, and restores molecular and stromal signaling (e.g. cytokines, integrin, adhesion molecules) (Astashkina and Grainger, 2014).

The interaction of hepatocytes with other non-parenchymal cells such as Kupffer cells, endothelial cells and stellate cells is crucial to maintaining the pharmacological responses of the liver. Non-parenchymal cells activate inflammatory pathways and the release of growth factors and reactive oxygen species in response to toxins; therefore, they are important for inducing and regulating DILI. Efforts have been made to develop complex culture systems, with the aim of maintaining hepatic cells for longer *in vitro* without significant depletion of the normal hepatocyte functions (Roth and Singer, 2014). Examples of these culture approaches include micropatterning (Zeng et al., 2007), spheroid culture (Fey and Wrzesinski, 2012; Ohkura et al., 2014; Takayama et al., 2013; Wang et al., 2015), bioreactors (Caralt et al., 2014; Shafa et al., 2012) and culture incorporating flow (Clark et al., 2014; Vivares et al., 2015).

1.6 Co-culture

Co-culture models combine multiple cell types in the same system, initially these experiments were performed in 2D transwells where the cells are separated by a permeable membrane but have since been combined with 3D-culture (Lan and Starly, 2011; Nagamoto et al., 2012). hPH co-cultured with non-parenchymal cells such as Kupffer cells showed improved function (Rose et al., 2016). Micropatterned co-culture (MPCC) has been developed with the intent of producing a stable and functional hepatic model for drug screening. hPHs were seeded into a micropatterned extracellular matrix and surrounded by fibroblasts. This culture system maintained the hepatic phenotype and functions including enzyme activity, gene expression, and albumin secretion for up to 6 weeks and was supportive of hepatitis C viral infection, Plasmodium *falciparum* and P. *vivax* life cycles (Khetani and Bhatia, 2008; March et al., 2015).

Recently, iPSC-HLCs were shown to have better predictivity of hepatotoxicity in MPCC than in conventional culture, with sensitivity and specificity comparable to hPH (Ware et al., 2015). iPSC-HLCs in MPCC were treated with 47 drugs (37 known hepatotoxicants and 10 non-liver toxicants). IC_{50} values (concentration that decreased the measured endpoints by 50%) for assays of albumin, urea and ATP were used for binary decisions of toxicity. iPSC-HLCs in MPCC had 65% sensitivity for hepatotoxicants (24 out of 37) compared with hPH-MPCCs at 70% sensitivity and 35% in conventional culture. Nagamoto *et al.* showed improved maturation of iPSC-HLCs with upregulation of CYP gene expression and albumin secretion when co-cultured with murine fibroblasts and collagen-I where an intact sheet of fibroblasts was overlaid onto the HLCs (Nagamoto et al., 2012).

Recently, Takebe *et al.* produced liver buds consisting of human iPSCs differentiated towards hepatic endoderm in combination with human umbilical vein endothelial cells and mesenchymal stem cells (Takebe et al., 2014). The liver buds were transplanted into NOD SCID mice where they integrated into the vasculature of the animal and showed characteristics of mature hepatocytes. These results show the importance of the complex signaling cues present *in vivo* to the maturation of iPSC-HLCs. These cues are largely unknown and are therefore difficult to replicate *in vitro* though their replication may lead to an improved phenotype for iPSC-HLCs.

1.7 3-Dimensional culture

Traditional cell culture is performed in 2-dimensional (2D) plates where the cultured cells are allowed to spread flat. Three-dimensional (3D) culture attempts to better mimic *in vivo* conditions by allowing formation of microtissues. 3D culture techniques vary widely but can be broadly divided into the scaffold-based techniques and scaffold-free techniques. Scaffold-based techniques use a

matrix for the cells to adhere to, these scaffolds may be either biological or synthetic in nature and each provides certain advantages and disadvantages. With scaffold-based techniques, cells are mechanically held together and develop cell adhesion over time. Scaffold-free techniques do not include a scaffold for the cells to attach to, instead relying on the deposition of extracellular matrix from the cells and the formation of cell-cell junctions.

The use of biological-scaffold based 3D-culture for hepatic models has been attempted in several studies. For example, recently hESC-HLC spheroids were produced using an algimatrix scaffold. hESCs were differentiated in monolayer culture to definitive endoderm and transferred to 3D algimatrix scaffolds (Ramasamy et al., 2013). Spheroids of varying size were formed, with size dependent on seeding density. These spheroids showed improved expression of differentiation markers and maturation such as apolipoprotein F, tryptophan dioxygenase, and CYP3A4 compared with 2D differentiation. In addition, spheroids have been produced using the HepG2 cell line embedded in Matrigel. These spheroids appeared to improve the maturation status of the HepG2 cells, producing rudimentary bile canaliculi inducing cell polarity and modestly increasing expression of some xenobiotic metabolism enzymes and transporters including CYP2E1, -1A2 and -2D6 and UGT1A1 -2A3 and -2B4 amongst others. The spheroids also showed increased expression of albumin, AhR and PxR (Ramaiahgari et al., 2014).

Another biological scaffold-based approach has been used in the generation of regenerative liver organoids from EpCAM positive hepatic progenitor cells. These cells were embedded in BME2 matrix to form organoids which could be differentiated to both the hepatic and biliary lineages (Broutier et al., 2016; Huch et al., 2015). This is an interesting model of liver regeneration *in vitro* which may help to alleviate the scarcity of highly functional liver cells that previously, only hPH could provide.

Gieseck *et al.* reported an improvement in cell maturation by transferring fully differentiated iPSC HLCs in 2D culture to the proprietary *Real Architecture for 3D Tissues* (RAFT) system as single cells or small epithelial clumps (Gieseck et al., 2014). RAFT creates cell-seeded hydrogels by mixing cells with neutralised collagen in a 96-well format. Compared to 2D culture, cells in 3D clumps showed a more hepatocyte-like gene profile of hepatic markers and CYP3A4 activity was maintained for 75 days. Polarisation and bile canaliculi formation were also induced in 3D clump culture, highlighting the importance of maintaining cell-cell interactions for the hepatic phenotype.

Decellularised tissues are perhaps the most ambitious type of biological scaffolds. They aim to remove the cells from donor tissue to leave an extracellular matrix scaffold. This scaffold is then repopulated with cells from another source, such as HLCs (Bao et al., 2016). In combination with spheroid culture prior to seeding the scaffold, decellularised scaffolds were shown to improve

secretion of albumin and urea when compared to 2D or scaffold-free culture and also increased expression of several hepatic genes including CYP1A1, CYP1A2, Albumin and AFP in HLCs (Bao et al., 2016).

The alternative to scaffold-based culture techniques is scaffold-free culture. Many studies have utilised scaffold-free techniques to produce hepatic spheroids. These techniques typically rely on the use of specialised cell culture equipment including ultra-low attachment plates, micropatterned plates and hanging drop plates. The cells are then left to self-aggregate forming cell-cell links and depositing their own ECM.

Ultra-low attachment plates have an inert, hydrophilic and neutrally-charged coating which prevents cell attachment, forcing cells to form 3D structures. This technique is advantageous due to its relatively low cost and ease of use but has disadvantages in that the size of spheroids may only be controlled by the number of cells added to the well limiting the total number of spheroids that can be produced simultaneously. Spheroids have been produced using ultra-low attachment plates from a plethora of cell types including hPH (Bell et al., 2016; Hendriks et al., 2016), iPSC-HLCs (Subramanian et al., 2014) and cancer cell lines (Hutchinson and Kirk, 2011).

Nanopillar or micropatterned plates are other methods that have been used to generate hepatic spheroids. Nanopillar plates were first developed in 2004 and use a microscale architecture to direct cell attachment and enable the simultaneous production of many spheroids of equal size (Otsuka et al., 2004). Initially, rat primary hepatocytes (rPH) were used to demonstrate the formation of spheroids in these plates showing albumin secretion at consistent levels for one month (Otsuka et al., 2004). Nanopillar plates have subsequently been used in the formation of hepatic spheroids and have been shown to improve hepatic functions and more closely recapitulate hepatocyte polarity when compared with 2D culture (Fukuda et al., 2006; Takahashi et al., 2010).

Recently, Takayama *et al.* used nanopillar plates in differentiation of ESC- and iPSC-HLCs to improve the maturity of the hepatic phenotype in the resultant spheroids (Takayama et al., 2013). These spheroids exhibited improved albumin secretion and expression of metabolic enzymes and transporters including CYP1A1, CYP1A2, CYP2E1, MDR1 and others. Furthermore, iPSC-HLCs in spheroid culture were shown to have increased sensitivity when compared with HepG2 spheroids to several known hepatotoxicants including nefazodone, clozapine, amiodarone and dantrolene amongst others. Similarly, Zhang *et al.* used micropatterned plates which utilised small cavities in place of nanopillars to produce iPSC-HLC spheroids which exhibited an improved hepatic phenotype when compared with 2D culture (Zhang et al., 2014). The 96-well (or higher) format of

micropatterned plates makes them amenable to high-throughput screening a sought-after property in novel hepatic models.

Tong *et al.* recently developed a novel approach to incorporating flow into hPH spheroid models. Using a glass coverslip and a membrane treated with polyethylene glycol they were able to immobilise spheroids. The authors report that constraining the spheroids reduced the loss of the cells during medium changes and improved their phenotype relative to collagen-sandwich culture. Perfused constrained culture produced an increase in CYP2B1/2 and CYP3A2 activity and CYP1A2 was increased in constrained culture regardless of the incorporation of flow (Tong et al., 2016).

In summary, these studies demonstrate the importance of 3D architecture in the maturity and stability of hepatic cell models. This is unsurprising given the increased similarity to physiological conditions which 3D models can reproduce which 2D models cannot.

1.8 Organoids

The liver is highly regenerative, capable of reforming liver mass even after extensive hepatectomy. The mechanisms surrounding this regeneration are incompletely understood, though it is thought that two major mechanisms exist to repopulate the hepatocytes after damage. In the case of acute damage such as hepatectomy, the hepatocytes are induced to re-enter the cell cycle and rapidly produce more hepatocytes, this mechanism of hepatocyte regeneration has been demonstrated in a recent lineage tracing experiment and is thought to be the homeostatic mechanism by which hepatocytes are produced (Yanger et al., 2014). The secondary method relies on the liver resident stem cells known as the oval cells, which are thought to be found at the tips of the biliary tree. The existence of these cells has been the subject of some debate though recent studies have demonstrated their function. The oval cells are bipotent progenitors capable of producing both cholangiocytes and hepatocytes in the 'oval cell response' (Huch et al., 2015). The oval cell response is activated after chronic damage to all hepatocytes in the liver. Until recently, these proliferative responses were not reproducible *in vitro*, however, the recent development of organoid cultures has enabled their recapitulation.

Organoids are 3D cell models that form several organ-specific cell types and self-organise into *in vivo*-like structures. Though organoids are sometimes likened to spheroids, they differ in terms of their derivation and structure. Organoids may be produced from organ-resident or pluripotent stem cells, for example, LGR5+ cells have been used recently in the generation of intestinal and hepatic organoids (Huch et al., 2015; Sato et al., 2009). Organoids are thought to be more genetically stable than PSCs and are also able to recapitulate donor phenotype in a similar manner. For example, α1-

antitrypsin deficiency and Alagille syndrome have both been modelled using hepatic organoids (Huch et al., 2015).

Liver organoids were first produced in 2013 by Huch et al. by expansion of LGR5+ cells in the murine liver, hollow cyst-like structures of epithelial cells were formed (Huch et al., 2013). These cells were found to be part of the liver's regenerative response and were cultured for more than 12 months, by administration of a differentiation medium containing EGF, FGF10, A38-01 and DAPT cells were directed towards a more hepatocyte-like fate showing expression of several mature hepatic markers including albumin and cytochromes P450. These were not expressed at levels equal to those found in hPH, moreover, not all the cells differentiated towards a hepatocyte fate with approximately 10% of the cells adopting a biliary fate instead. Nonetheless, these cells were able to engraft in Fah deficient mice and form functional hepatocytes and reverse otherwise fatal liver damage (Huch et al., 2013).

The same group later published a detailed protocol of a similar procedure in mice and humans, showing the process to isolate organoids from bile duct cells (Chol-Orgs) (Broutier et al., 2016; Huch et al., 2015). This protocol aimed to exploit the oval cell response to produce a mixed population of cholangiocytes and hepatocytes and utilised a similar differentiation technique as before to produce hepatocytes which could be used in transplant or toxicity testing. Moreover, these organoids were demonstrated to recapitulate the phenotype of the donor *in vitro*, in this case, the authors used α1-antitrypsin deficiency and Alagille syndrome as model conditions to demonstrate this effect (Huch et al., 2015). This is significant as this attribute has previously been associated mainly with traditional stem cell model such as iPSCs. Further still, these organoids were shown to be genetically stable, particularly compared with iPSCs which are regarded as unstable in comparison. Liver organoids showed fewer *de novo* base substitutions *in vitro* (63-139) than had previously been reported for iPSCs (1,058-1,808) over a similar period in culture (Huch et al., 2015).

In 2018, the Clever's group published a new protocol for the generation of organoids from human hepatocytes instead of cells from the biliary tree (Hu et al., 2018). This protocol was intended to capture the hepatocyte proliferation response that is thought to be the homeostatic method of hepatocyte regeneration. The new technique uses isolated hepatocytes embedded in a Matrigel matrix which are induced to proliferate using an optimised hepatocyte organoid (Hep-Org) medium (Advanced DMEM/F12 supplemented with: RSPO1, B27 (without vitamin A), EGF, N-acetylcysteine, gastrin, CHIR99021, HGF, FGF7, FGF10, A83-01 and Nicotinamide). These organoids were morphologically distinct from cholangiocyte organoids, displaying a compacted bunch-of-grapes morphology instead of a cystic one. Hep-Orgs demonstrated a superior hepatocyte phenotype to

Chol-Orgs with greater expression of AFP, Albumin, HNF4a, CYP1A2 and CYP3A11 though not to the same level as hPH. Conversely, Chol-Orgs showed greater expression of cholangiocyte markers such as CK19 than either Hep-Orgs or hPH. Hep-Orgs clustered more closely with proliferating hPH than nonproliferating hPH, suggesting recapitulation of the hepatocyte expansion response, indeed experiments with mice with tagged hepatocytes demonstrated that the organoids arose solely from mature hepatocytes. Similarly to Chol-Orgs, Hep-Orgs were also capable of repopulating the murine liver following injury and proliferating therein (Hu et al., 2018).

Organoids are typically cultured in domes of a gel matrix such as Matrigel or BME-2 where they form hollow spherical structures or what is referred to as a 'bunch-of-grapes' morphology (Figure 3). This distinguishes them, in addition to their self-organisation properties from spheroids. Organoids are dependent on the support of the surrounding matrix, whilst a spheroid can maintain its structure independently.

The main advantages associated with organoids compared with PSC-derived cells appears to be the ability to maintain genetic stability over long culture periods whilst retaining the ability to proliferate extensively and form mature cell types with organ-like structures. This contrasts with PSC models which have been reported to accrue genetic aberrations in culture and are currently unable to fully recapitulate the mature hepatic phenotype.

Similarly to iPSC-derived cells, organoids are able to recapitulate the phenotype of the cell from which they were derived. For example, the Clevers lab were able to derive hepatic organoids from a patient with A1AT deficiency which also showed the diseased phenotype (Huch et al., 2015). Furthermore the Tuveson lab were able to derive organoids from pancreatic cancers that recapitulated the progression of the disease *in vitro* (Boj et al., 2015).

However, organoids do not show the same degree of plasticity in their differentiated fate as PSC models which is limited typically to only a few organ-relevant cell types. Conversely, the starting cell type for PSC-models does not appear to influence the ability to form other cell types through differentiation (Heslop et al., 2017). This raises implications for the potential use of organoids in cell therapies, if tissue from the target organ is required to produce organoids, this will necessitate invasive biopsies.

1.9 Perfusion Bioreactors

Perfusion bioreactors aim to restore *in vivo* cellular mechanosensitivity by incorporating flow into cell culture conditions. In these bioreactors, cells are very often seeded into scaffolds combining 3D culture with flow. Cells in this type of culture are continuously perfused with culture medium which is pumped around the cells. Several pumping mechanisms have been employed e.g. pneumatic, peristaltic, gear or propeller and aim to achieve a flow rate that mimics *in vivo* circulation. Culture

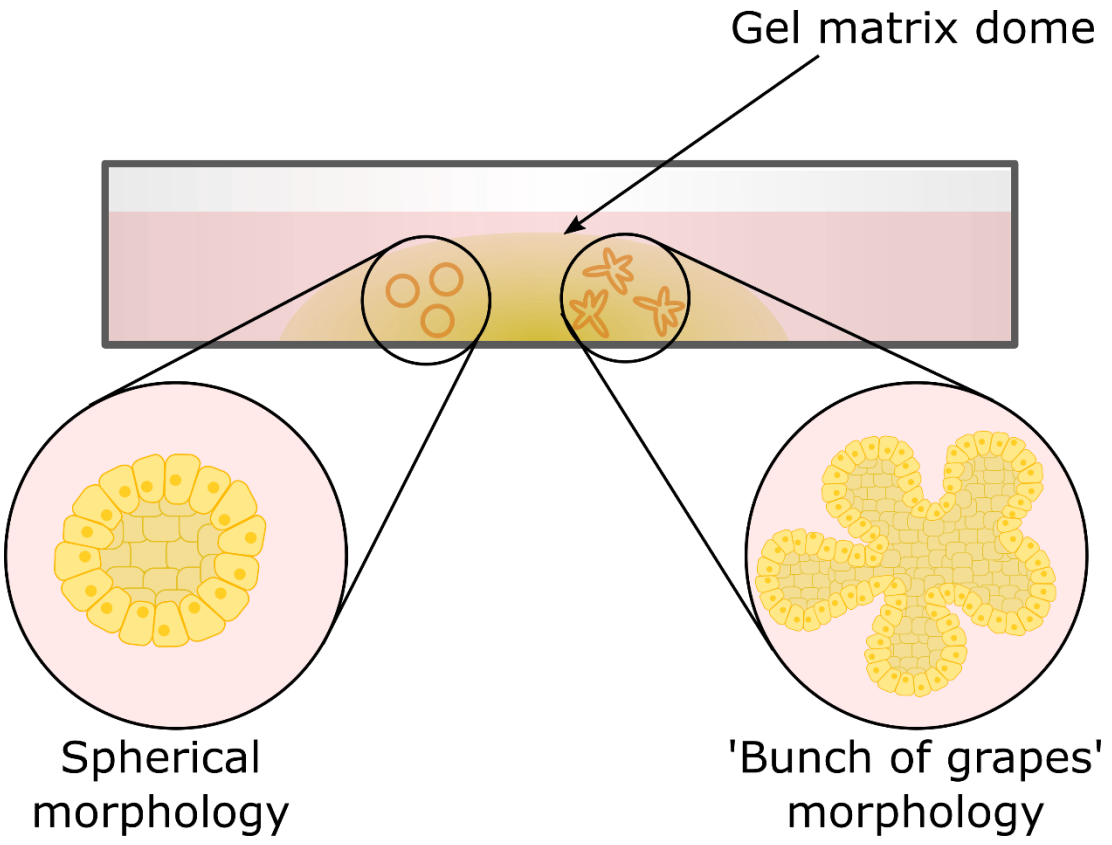

Figure 3

Culture setup and morphology of organoids – Figure shows a cartoon depiction of the culture conformation and morphology of organoids. Organoids are cultured in a gel dome, typically comprised of Matrigel or BME-2 submerged in culture medium. Organoids form either a cystic, spherical morphology (left) or a 'bunch of grapes' morphology (right).

with flow allows continuous exposure of the cell to nutrients and oxygen, as well as *in vivo*-like shear stress, which are important conditions for cell expansion and maturation (Caralt et al., 2014).

Currently, the literature on use of dynamic perfusion culture with iPSCs is limited. One study applied perfusion culture to undifferentiated iPSCs and found an increased proliferation rate (Yoshimitsu et al., 2014). Another study has shown improved phenotype and longevity of iPSC-cardiomyocytes when cultured with flow (Mathur et al., 2015). iPSC derived liver models incorporating flow are emergent but generally in their infancy, several attempts have been made to produce improved hepatic models by using flow. Schepers *et al.* designed a novel microfluidics system to culture iPSC-HLCs in 3D culture and with co-culture with fibroblasts. The results of this study showed increased albumin production in 3D cultured cells and inducible expression of several CYP enzymes including CYP1A1 and CYP2C9 (Schepers et al., 2016).

In addition, several *in vitro* liver models without the use of iPSC-HLC have been produced. Lee *et al.* utilised an osmotic pump to co-culture hPH spheroids with hepatic stellate cells showing an improvement in albumin and urea excretion and enhanced cytochrome P450 enzyme expression (Lee et al., 2013). Darnell *et al*. cultured HepaRG cells in a 3D multicompartment capillary membrane bioreactor under dynamic conditions (Darnell et al., 2011). These cells showed stable P450 metabolic capacity over several weeks, as well as polarity of transporter expression and bile canaliculi formation.

The LiverChip is a dynamic culture perfusion system developed by CN Bio (formerly Zyoxel), that incorporates flow and uses a scaffold to culture cells in 3D. 3D culture with flow has been shown to enhance maturation of iPSC-HLCs and maintain functional hepatocytes with improved viability and longevity and increased ability to predict and distinguish hepatotoxicity of known hepatotoxic compounds from less-toxic analogues (Rowe et al., 2014a, 2014b; Vivares et al., 2015). In the LiverChip system, cells are seeded into coated scaffolds in 12 or 36 wells and perfused via pneumatic micropump-controlled flow, mimicking the architecture of hepatic sinusoids. Clark *et al.* used a modified LiverChip system to identify new therapeutic strategies for metastasis by incorporating the hPHs and non-parenchymal cells (The authors note that a “full complement” of non-parenchymal cells were used but do not further specify) and breast cancer cells in a microfluidic cell culture system incorporating flow (Clark et al., 2014).

In summary, the use of complex culture systems in iPSC HLC differentiation has demonstrated notable advantages in cell maturity and longevity (e.g. albumin and urea secretion maintained for months, gene profile shifting from foetal to mature hepatocyte, sustained and inducible CYP activity over long term). However, more efforts are required to develop methodology to produce more

stable and homogenous iPSC HLCs, as well as to decipher the mechanisms and key signaling pathways involved in hepatocyte differentiation and maturation. Furthermore, the development of reliable, practical and standardised culture systems that are amenable to high-throughput screening should also be considered. Nonetheless, the application of iPSC HLCs in complex culture systems shows great potential for DILI safety assessment, particularly in high-throughput screening and chronic toxicity assessment.

1.10 Alternate uses of hepatocyte-like cells in toxicity assessment

iPSC HLCs currently lack many of the key qualities required to be a one-for-all model of hepatotoxicity; however, that does not preclude the use of iPSC HLCs in modelling other less metabolically dependent endpoints. In the short term, a pragmatic approach should be adopted to find a purpose in which the relatively immature phenotype of iPSC-HLCs is suitable.

One such use is as a model of mitochondrial perturbation. Recent work has shown that HepG2s may provide a model of mitochondrial perturbation that is more amenable to mechanistic studies than human hepatocytes (Kamalian et al., 2015). However, HepG2s are genotypically abnormal and lack physiological translatability; therefore, iPSC HLCs may provide a more physiologically relevant model of this perturbation. Research has shown that iPSC HLCs, like hepatocytes, but unlike pluripotent stem cells, can survive in galactose/ornithine-based culture which forces cells to use oxidative phosphorylation in the absence of glucose (Tomizawa et al., 2013), suggestive of a bio-energetic switch during differentiation to a situation which is more similar to hepatocytes. The use of human iPSC HLCs derived from patients with Alper's syndrome, a disease which increases susceptibility to valproic acid-derived hepatotoxicity, were successfully used to model this increased toxicity compared to control iPSC HLCs (Li et al., 2015). Furthermore, the mechanism of toxicity, more frequent bursts of superoxide generation, was delineated using these cells; therefore, in cases where toxicity is not dependent on metabolism, iPSC HLCs are valuable models of toxicity.

Further, DILI-induced cholestasis may also be modelled. Many drugs associated with cholestasis, such as cyclosporin A, rifampicin and glibenclamide, have been found to be a competitive inhibitor of the bile salt export pump (BSEP) (Böhme et al., 1994; Byrne et al., 2002; Leuthold et al., 2008), preventing the export of bile salts and resulting in their cytotoxic accumulation and consequently, DILI (Krahenbuhl et al., 1994). iPSC HLCs have been shown to have some degree of BSEP activity (Ulvestad et al., 2013) and may therefore be able to triage compounds with cholestatic liability through inhibition of this mechanism.

The advent of gene modulation technology, in the form of Zinc fingers, TALENs and CRISPR/Cas9, also provides the capacity to achieve mechanistic studies of hepatotoxicity. Yusa *et al.* reported such work was feasible in the context of gene therapy, demonstrating that the defective gene in the alpha-1-antitrypsin deficiency could be corrected using zinc finger nucleases in iPSCs and be functional in the resulting HLCs (Yusa et al., 2011). CRISPR/Cas9 knock out technology has also been successfully applied to pluripotent stem cells (Ding et al., 2013) and the differentiation of these cells to HLCs may provide human *in vitro* disease models or equivalents of *ex vivo* cells from knockout mice which are commonly used to understand the mechanisms which underlie hepatotoxicity of a given compound (Musunuru, 2013).

The recapitulation of the patient genotype is a fundamental advantage of iPSC HLCs over more traditional and hESC-derived models of hepatotoxicity. DILI is often idiosyncratic in nature and may occur in only very small numbers of patients, in the case of abacavir, flucloxacillin and flupirtine, which are immune-mediated and associated with specific HLA-types (Daly et al., 2009; Martin et al., 2004; Nicoletti et al., 2016); iPSCs allow for the selection of patients with risk-associated HLA-types. The testing of these HLA-typed HLCs with immune cells with the same HLA-type may provide a unique model of DILI. Such investigation would currently be dependent on the toxicological profile of the drug, i.e. is metabolism required before HLA presentation. Nevertheless, HLA-associated toxicity is currently only feasible in iPSC-based models and the development of a human *in vitro* system able to screen for immune-mediated idiosyncratic DILI would represent a paradigm shift in hepatotoxicity modelling.

Furthermore, once metabolically-competent HLCs are established, simpler iPSC HLC panel-based screening representing the major genotypic variations present in the population (e.g. CYP2D6 null genotype (Takayama et al., 2014)) would enhance current compound screening models utilising the restricted genotypic range of animal strains and cell lines.

1.11 Risks of the use of HLCs for cell therapies

The current demand for donor organs outstrips supply. In addition, there is substantial risk associated with the transplant surgery itself, risk of organ rejection and complications associated with lifelong immunosuppression such as risk of infection and cancer (Adam et al., 2000; Hsu and Katelaris, 2009). Consequently, there have been efforts in recent years to find alternate sources of cells and tissue for transplant. Embryonic stem cells (ESCs) and induced pluripotent stem cells (iPSCs) offer a potentially unlimited source of cells for this purpose. However, the risks associated with the use of stem cells for transplant are incompletely understood. There are concerns regarding the

tumorigenic potential of stem cells used for transplant, based not only on the inherent ability of pluripotent cells to form teratomas *in vivo* but also regarding the more insidious genetic changes introduced during isolation and culture.

The use of liver cells for cell therapy hold promise as an alternative treatment for late-stage liver disease. Whilst the technique has been attempted in both human and animal models there are multiple potential issues to be investigated and overcome before it can be used routinely (Nicolas et al., 2016). Human and porcine primary hepatocytes have been successfully transplanted into humans though concerns of immune rejection and xenozoonosis in the case of animal hepatocytes have been raised (Zhou et al., 2015). Stem cells have the capacity to self-renew whilst maintaining a pluripotent state. Consequently, stem cell derived HLCs are a theoretically unlimited source of hepatocytes for cell therapies. The use of iPSC derived HLCs may also circumvent the need for immunosuppression in recipients since pluripotent stem cells can be derived from any individual.

There is concern that stem cell derived HLCs may pose an oncogenic risk in their recipients. Undifferentiated stem cells are known to readily form teratomas *in vivo*. This is the basis of an *in vivo* teratoma-forming assay where undifferentiated cells are injected into an immunocompromised animal model in order to demonstrate formation of the three major germ layers (Wesselschmidt, 2011). Whilst teratomas are typically benign, there is the possibility for them to become malignant, particularly with solid tumours.

Differentiation protocols are typically less than 100% efficient and an undifferentiated population of cells remain. Currently, it is unclear whether the undifferentiated portion of cells are fully pluripotent or capable of teratoma formation. Previous studies where HLCs were injected into immunocompromised mice have shown tumour formation in the injected animals (Payne et al., 2011). However, a recent study demonstrated that by purification of differentiated cells using Laminin-111, undifferentiated cell populations as low as 0.003% could be achieved, furthermore, these cells were not capable of colony formation despite expression of Tra-1-60, a marker of pluripotency (Takayama et al., 2017). Other studies have also shown no tumour formation in mice injected with HLCs without purification (Basma et al., 2009). In summary, these results show that great care should be taken to remove undifferentiated cells before administration of stem cell-derived cells to patients, the possibility for teratoma formation from undifferentiated cells is clearly extant.

In addition to concerns regarding teratoma formation from undifferentiated cells, there is also the concern that cells accrue mutations over time in culture. These mutations typically confer a survival advantage to the cell *in vitro* such as increased rate of proliferation and decreased differentiation

and are known as culture adaptations (Nguyen et al., 2013). These mutations are of concern for cells intended for transplant or cell therapy since the mechanisms by which cells adapt to culture are similar to some of the characteristics of cancer cells. For example, resistance to cell death and increased proliferation are characteristics associated with cancerous cells and are advantageous to a cell's survival *in vitro* but may pose an oncogenic risk *in vivo* (Hanahan and Weinberg, 2011).

A selective pressure is applied during *in vitro* culture to for stem cells to self-renew. This in part accounts for the recurring patterns of mutations observed in stem cells in culture, in particular, recurrent mutations of chromosomes 12, 17, 20 and X are observed (Amps et al., 2011). The 20q11.21 amplicon is one such common mutation, occurring in as many as 20% of ESC and iPSC lines after prolonged culture and confers a survival advantage (Amps et al., 2011). The 20q11.21 minimal amplicon is approximately 0.55Mb in length and encodes HM13, ID1, BCL2L1, KIF3B and an immature form of miR-1825. The amplicon size is variable and can also encode other nearby genes, including the potential oncogene, TPX2. Recent studies have demonstrated that BCL2L1 is likely to be the key driver of the survival advantage observed in carrier cells (Avery et al., 2013; Nguyen et al., 2014). Although not the source of the survival advantage conferred *in vitro*, ID1 is another gene expressed in the 20q11.21 minimal amplicon that is a potential oncogene.

A recent study demonstrated that BLC2L1 is responsible for the improved survival of cells expressing gain of 20q11.21. BCL2L1 encodes BCL-XL which was shown to have 3-fold increased protein expression and 2.3-fold increased mRNA expression in cells with the gain of 20q11.21 compared to wild-type (Nguyen et al., 2014). This is of particular concern for cells intended for transplant as BCL-XL is a classical proto-oncogene that exerts an anti-apoptotic effect. BCL2L1 also encodes BCL-XS, a pro-apoptotic protein. However, this has been shown to be the minor splice variant and was not detectable at the protein level (Nguyen et al., 2014). Overexpression of BCL-XL improves cell survival by reducing apoptosis during passaging when cell-to-cell contact is lost. This increase in protein expression confers a significant survival advantage over wild-type and cells with the amplification have double the colony-forming efficiency of wild-type cells (Nguyen et al., 2014).

1.12 Objectives

In this thesis we investigated a range of emerging stem cell-derived models of hepatotoxicity, including iPSC, ESC-derived HLCs and human hepatic organoids. In addition, we examined the effects of a commonly-occurring genetic aberration in the HLCs on the tumorigenic potential of hepatocyte like cells in immunocompromised mice.

Specifically, we examined the effects of the amplicon 20q11.21 which occurs frequently in pluripotent cells which have been extensively cultured. We produced luminescent hESC lines with known 20q11.21 status and differentiated them to HLCs before injecting them intrasplenically into the acutely damaged livers of immunocompromised mice. We hypothesised that presence of the 20q11.21 amplicon would predispose carrier cells to tumour formation *in vivo*.

The second major project of this thesis compared the effects of hypoxic culture conditions on the differentiation of normoxic culture conditions and also examined two differentiation protocols, one traditional and one based on small molecules (Table 1) (Heslop et al., 2017; Siller et al., 2015). We hypothesised that hypoxic culture would produce a culture environment closer to that of a pericentral hepatocyte with the associated increase in CYP expression and other markers of a pericentral phenotype. We also sought to determine whether the cheaper small molecule-based protocol performed as effectively as a more traditional growth factor-based approach.

The third project of this thesis examined the use of human liver organoids derived from EpCAM+ cholangiocytes as a model of hepatotoxicity. We established protocols in our lab for the isolation, culture, cryopreservation and differentiation of human liver organoids and then assessed their proteomic phenotype. Using this data, we sought to determine if human liver organoids derived from this cell population were a good approximation of the phenotype of hPH and human liver.

2 Methods

2.1 Stem Cells

2.1.1 Derivation

The iPSCs in chapter 3 were derived in-house from human primary hepatocytes and fibroblasts using the CytoTune II Sendai virus reprogramming kit (Thermo Fisher Scientific, Paisly, UK) as detailed in Heslop et al. (2017).

2.1.2 Maintenance

2.1.2.1 General maintenance

For routine maintenance, medium was changed daily. For iPSCs cultured on growth factor-reduced (GFR)-Matrigel (Corning, Flintshire, UK), Essential 8 medium was used (Table 2, all Thermo Fisher Scientific). ESCs were cultured in NutriStem hPSC XF Medium (Corning). Cells were passaged 1:4 approximately every 5-6 days or when approaching confluency.

2.1.2.2 Preparation of culture plates

During these works, PSCs were almost exclusively cultured in multiwell tissue culture plates prepared by one of two methods. These methods were: coating with GFR-Matrigel, and coating with laminin-521 (ln-521, Biolamina, Stockholm, Sweden).

2.1.2.2.1 GFR-Matrigel

Growth factor reduced Matrigel (GFR-Matrigel) was used as a basement matrix for iPSC culture. 125µL aliquots of GFR-Matrigel were thawed on ice and diluted to 12mL with DMEM (Sigma-Aldrich, Dorset, UK) under aseptic conditions. DMEM was kept ice cold during this procedure to prevent the GFR-Matrigel from solidifying prematurely. The diluted GFR-Matrigel was then plated out using half culture volume for the plate in question (Table 3). Matrigel was left to solidify for 1 hour at room temperature before being transferred to a CO_2 incubator at 37 °C for later use. Before use in iPSC culture, the DMEM used to dilute the GFR-Matrigel was removed.

2.1.2.2.2 Lamninin-521

Ln-521 was used as a basement matrix for the culture of ESCs. Ln-521 aliquots were thawed at room temperature and were diluted 1:20 with DPBS (Life Technologies). Ln-521 solution was plated at 1.5 mL per well of a 6-well plate and then incubated either overnight at 4 °C or for 2 hours at 37 °C.

2.1.2.3 Passaging

2.1.2.3.1 iPSCs

Non-enzymic passaging was employed for the routine maintenance of PSCs. For passage of iPSCs, gentle cell dissociation reagent (GCDR, Stemcell Technologies, Cambridge, UK) was used. Medium

was removed and the cells were washed once with 1 mL of GCDR. A further 1 mL of GCDR was added and incubated at room temperature for approximately 6 minutes or until the appearance of a white 'halo' effect was noted microscopically around the cells indicating detachment. GCDR was then removed taking care not to dislodge the cells. The loosened cells were then scraped into culture medium and plated out into GFR-Matrigel prepared tissue culture plates.

2.1.2.3.2 ESCs

Non-enzymic passaging was also employed for the routine maintenance of ESCs. Culture medium was removed, and cells were washed twice with phosphate buffered saline Without calcium or magnesium (Thermo Fisher Scientific). Cells were then incubated in prewarmed 0.5 mM EDTA (Sigma Aldrich, Dorset, UK) at 37 °C for 5 minutes. After 5 minutes the cells were checked for signs of detachment, indicated by the cells 'balling up'. If detachment was not observed cells were incubated at 37 °C for an additional 1-2 minutes and rechecked up to a maximum of 10 minutes. Once detachment was observed, the EDTA was gently removed and replaced with culture medium and the cells were scraped. The cells were gently agitated by pipetting up and down to break up larger clusters and plated into ln-521 prepared tissue culture plates.

2.1.2.4 Cleaning

iPSCs often differentiate spontaneously in culture, it was necessary to manually remove the unwanted differentiated cells. Differentiated cells were removed under aseptic conditions using an Evos XL Core microscope (Thermo Fisher Scientific). Cells were assessed for differentiation morphologically and were scraped away using a small pipette tip.

2.1.2.5 Cryopreservation

iPSCs were cryopreserved in liquid nitrogen for long-term storage. Cells were washed once with GCDR to remove culture medium and detached from the culture plate by incubating with fresh GCDR for 6-8 minutes at room temperature. The cells were frequently checked until the appearance of a white halo was noted indicating detachment. GCDR was then removed and replaced with 1 mL of freezing medium. Cells were scraped into this medium, transferred to cryovials and frozen at -80 °C using a Mr. Frosty™ Freezing Container (Thermo Fisher Scientific) following the manufacturer's usage instructions. After 24-hours at -80 °C, the cryovials were transferred to liquid nitrogen storage.

2.1.2.6 Thawing

Cells were thawed from liquid nitrogen by quickly transferring the cells to a 37 °C water bath and gently swirling until a small pellet of ice remained in the cell suspension. This suspension was then transferred to aseptic conditions and the volume was increased to 10mL using the intended culture medium in order to dilute the dimethyl sulfoxide (DMSO) in the freezing medium. The cell

suspension was then centrifuged (200*g*, 10 minutes) and the supernatant discarded. The pellet was resuspended in culture medium and immediately transferred to prepared culture plates increasing the volume to culture volume (Table 3) where necessary and swirled to ensure even distribution of the cells. The plates were then transferred to a CO_2 incubator overnight to allow the cells to attach. Medium was changed 24 hours later.

2.1.2.7 Hypoxia

Some work in chapter 3 was carried out under hypoxic conditions; 'normoxic' conditions were a humidified 5% CO_2 atmosphere at 37 °C, other gases uncontrolled. Cells in hypoxic conditions were treated identically to those cultured under normal conditions with the exception that they were cultured in a Whitley H35 HEPA Hypoxystation (Don Whitley Scientific, West Yorkshire, UK). The controlled atmosphere was 90% N_2, 5% O_2, 5% CO_2 and 70-80% humidity at 37 °C. Small adjustments to the humidity of the atmosphere (within the range of 70-80%) were made as necessary to prevent excessive condensation inside the instrument.

Culture under hypoxic conditions precluded any cleaning of spontaneously differentiating cells and any microscopy that was performed on cells under hypoxic conditions was done quickly in plates wrapped in film to reduce loss of the atmosphere inside.

2.1.3 Differentiation

Several protocols for the differentiation of iPSCs to HLCs were used and compared during these works.

2.1.3.1 Protocol 1

Figure 4 shows schematic overviews of the two differentiation protocols used in chapter 3. Figure 4A shows the protocol taken from Heslop et al. (2017), which uses a serum-free, growth-factor based approach. The protocol is 22 days in length and is divided into three major stages, specification of definitive endoderm, from day 1-5, which is also divided into two subsections: day 1-3 where cells are treated with Wnt3a and activin A, and days 4-5 where cells are treated with Activin A alone; specification of hepatic endoderm from day 6-12 where cells are treated with DMSO and hepatic maturation where cells are treated with HGF, OSM and dexamethasone This protocol will be referred to as protocol 1.

iPSCs were grown to >80% confluency on GFR-Matrigel-coated plates. Twenty-four hours prior to initiation of differentiation, 10μM Y-27632 ROCK inhibitor was added to E8 medium. To initiate differentiation, cells were first washed with PBS before incubation with Accutase (Stemcell Technologies) at 37 °C until cell detachment was observed. Once cells started to detach, the

remainder of the cells were washed from the plate by gently pipetting the Accutase over the cells. The Accutase and cells were transferred to a centrifuge tube and any remaining cells were washed off the plate and added to the centrifuge tube with a volume of PBS equal to the volume of Accutase used. The cell suspension was centrifuged (200 *g*, 10 minutes) and the supernatant discarded.

Once pelleted, the cells were transferred into differentiation medium 1 (Table 2) supplemented with 10µM Y-27632 ROCK inhibitor (Sigma Aldrich). These cells were transferred to freshly prepared GFR-Matrigel-coated plates and incubated under the chosen oxygen conditions for 24 hours. Medium was changed daily until day 5 of differentiation omitting Y-27632 ROCK inhibitor after day 1 and Wnt3a after day 3. On day 6 the medium was changed to differentiation medium 2 (Table 2) and changed every other day for 7 days. On day 12, the medium was changed to differentiation medium 3 (Table 2) and changed daily for 10 days.

2.1.3.2 Protocol 2

Figure 4B shows the protocol taken from Siller et al. (2015) This protocol is 17 days in length and uses small molecules in place of traditional growth factors and contains serum during the final stage. Similarly to the protocol shown in Figure 4A, this protocol is divided into three major sections. The first section (day 1-2) uses a 24-hour pulse of CHIR99021 to direct definitive endoderm specification followed by 24 hours without treatment. The second stage (day 3-7) drives hepatic specification via treatment with DMSO. The third stage directs hepatic maturation using Dihexa and dexamethasone. The exact composition of each media in both protocols is shown in chapter 2. All subsequent analyses using iPSCs were undertaken on either fully differentiated cells, collected at the end of the differentiation protocol. This protocol will be referred to as protocol 2.

iPSCs were grown to >80% confluency on GFR-Matrigel-coated plates. Twenty-four hours prior to initiation of differentiation, 10µM Y-27632 ROCK inhibitor was added to culture medium. To initiate differentiation, cells were first washed with PBS before incubation with Accutase at 37 °C until cell detachment was observed. Once cells started to detach, the remainder of the cells were washed from the plate by gently pipetting the Accutase over the cells. The Accutase and cells were transferred to a centrifuge tube and any remaining cells were washed off the plate and added to the centrifuge tube with a volume of PBS equal to the volume of Accutase used. The cell suspension was centrifuged (200 *g*, 10 minutes) and the supernatant discarded.

Once pelleted, the cells were transferred into differentiation medium 4 (Table 2) for 24 hours. On day 2 the medium was changed to differentiation medium 4 without CHIR99021 for a further 24 hours. On day 3 the medium was changed to differentiation medium 2 (Table 2) and changed every

other day for 5 days. On day 8 the medium was changed do differentiation medium 5 (Table 2) and changed daily for 10 days.

2.1.3.3 Tumorigenicity Chapter Protocol

ESCs were grown to 30-60% confluency on ln-521-coated plates in NutriStem medium. On day 1 medium was changed to differentiation medium 1 (Table 2) and changed daily for 3 days. On day 4, medium was changed to differentiation medium 2 (Table 2) and changed every other day for 5 days. On day 9 the medium was initially changed to differentiation medium 6 (Table 2), though for reasons discussed in chapter 5 this was later changed to differentiation medium 7 (Table 2). In both cases, the medium was changed daily for 4 days.

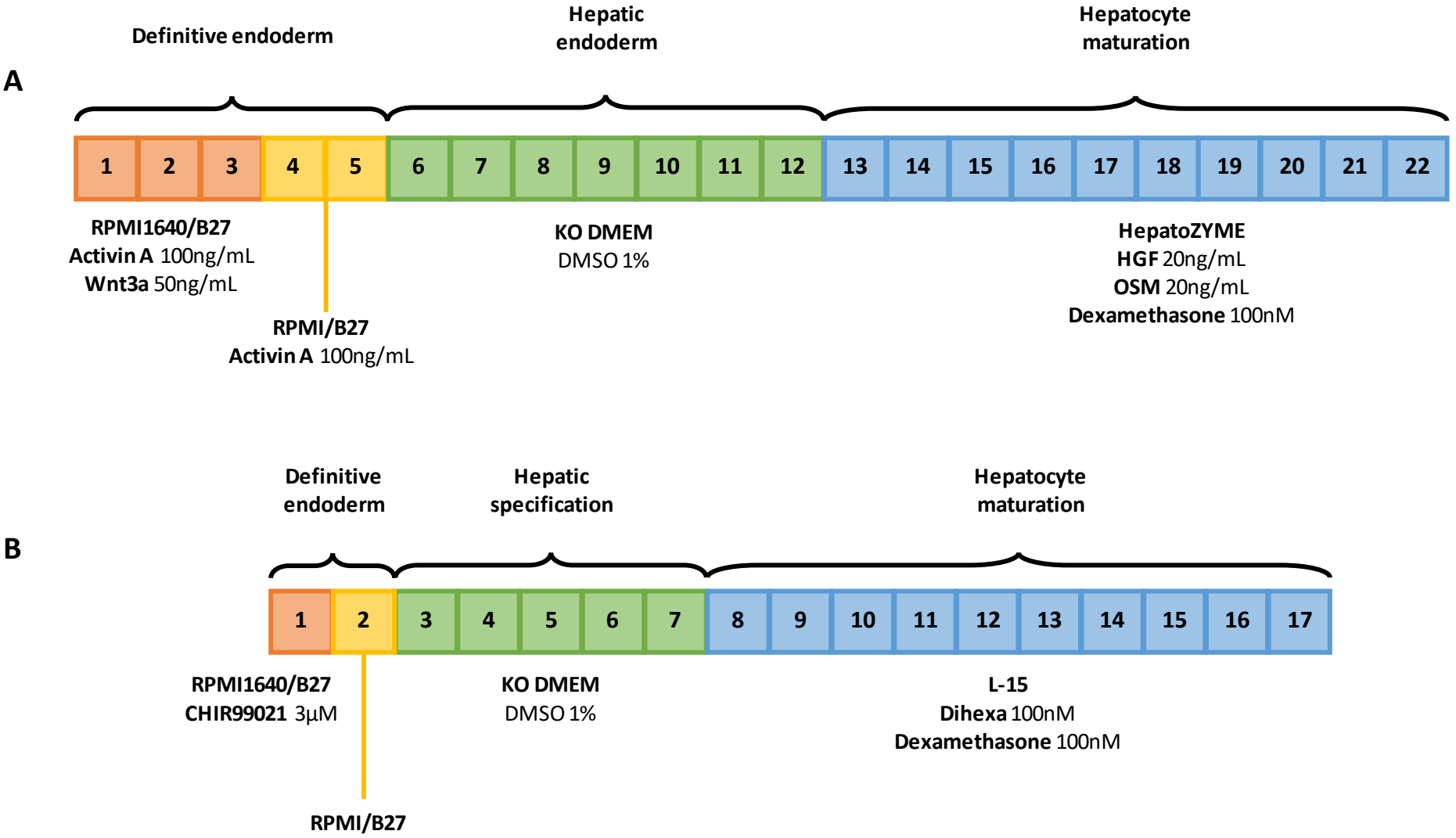
A
Definitive endoderm
Hepatic endoderm
Hepatocyte maturation
1 2 3 4 5 6 7 8 9 10 11 12 13 14 15 16 17 18 19 20 21 22
RPMI1640/B27
Activin A 100ng/mL
Wnt3a 50ng/mL
RPMI/B27
Activin A 100ng/mL
KO DMEM
DMSO 1%
HepatoZYME
HGF 20ng/mL
OSM 20ng/mL
Dexamethasone 100nM
B
Definitive endoderm
Hepatic specification
Hepatocyte maturation
1 2 3 4 5 6 7 8 9 10 11 12 13 14 15 16 17
RPMI1640/B27
CHIR99021 3µM
RPMI/B27
KO DMEM
DMSO 1%
L-15
Dihexa 100nM
Dexamethasone 100nM

Figure 4

Schematic of differentiation protocols used in chapter 3 – **(A)** Overview of protocol 1 as described by Heslop et al. (2017) **(B)** Overview of protocol 2 as described by Siller et al. (2015).

Each section of the differentiation protocols is colour-coded, orange and yellow indicated formation of definitive endoderm, green indicates hepatic specification and blue indicates hepatocyte maturation. The culture medium used, and major additives and their concentrations are indicated below each section and are covered in full detail in chapter 2. Abbreviations: B27 - B27-supplement, DMSO – Dimethyl sulfoxide - HGF - Hepatocyte growth factor, KO DMEM - Knockout Dulbecco's modified Eagle's medium, L-15 - Leibovitz's L-15, OSM - Oncostatin M, RPMI 1640 - Roswell Park Memorial Institute 1640

2.1.4 Embryoid body formation

Undifferentiated hESCs in 6-well plate format were disassociated using gentle cell disassociation reagent and scraped into KSR medium (Table 2) supplemented with 10µM Y-27632 ROCK inhibitor. If the cells were previously cultured on MEFs, they were removed by gravitational separation and cells plated in 24-well non-tissue culture treated plates in triplicate (1:1 ratio). After 24 hours, cells were resuspended by gently pipetting medium up and down and transferred to a new plate to reduce attachment. Medium was changed every 48 hours without ROCK inhibitor. For gene expression comparisons, cells were cultured for 16 days before lysing in QIAzol (Qiagen, Manchester, UK). For characterisation experiments, cells were cultured for 7 days, before transfer to attachment factor coated 24-well tissue culture treated plates for re-attachment. Cells were cultured for a further 7 days before fixing with 4% (v/v) paraformaldehyde (PFA, Sigma Aldrich) for immunofluorescence assessment.

2.1.5 Staining

Cells were prepared for immunofluorescence at day 8 of the ESC differentiation protocol, embryoid bodies were also prepared identically.. All solutions containing normal donkey serum were centrifuged (15,000 *g*, 6 minutes) prior to use avoiding pellets when pipetting. Cells were fixed for 15 minutes in 4% PFA and washed 3 times in Dulbecco's PBS (Thermo Fisher Scientific). Fixed wells were blocked with 10% normal donkey serum (Abcam, Cambridge UK).

Primary antibodies were diluted in 1% normal donkey serum and 0.1% triton in DPBS. Rabbit anti-human HNF4α antibody (Santa Cruz Biotechnology, Heidelberg DE) was diluted 1:50 and rabbit anti-human αSMA and Tuj-1 antibodies (Abcam) were diluted 1:100 and 1:500 respectively. Wells were incubated with primary antibody at room temperature for 2 hours and washed 3 times with DPBS. The secondary antibody was Alexa Fluor 488 donkey anti-rabbit (Thermo Fisher Scientific); both antibodies were diluted 1:750 in the same solution as the primary antibodies and incubated in darkness for 2 hours at room temperature then washed 3 times in DPBS.

Hoechst staining was performed, using Hoechst stain (Sigma Aldrich) diluted 1:75,000 in DPBS. Wells were incubated in darkness for 15 minutes before washing 3 times in DPBS leaving a fourth wash in the wells to prevent the samples from becoming dry. Wells were visualised using a Zeiss Observer Z.1 fluorescence microscope (Carl Zeiss, Cambridge, UK).

2.1.6 Flow Cytometry

Flow cytometry was used to assess the proportion of cells expressing differentiation markers throughout differentiation. Unless otherwise noted, all centrifugation steps are 1,000 g, 10 minutes. Culture medium was removed, and the cells were washed with PBS (without Ca^{2+} or Mg^{2+}). The cells were detached with Accutase by incubating at 37 °C for approximately 6 minutes until detachment was observed. Once the cells had detached, the Accutase was diluted with an equal volume of PBS and centrifuged. The supernatant was discarded, and the pellet resuspended in 10 mL PBS before centrifuging again. The supernatant was discarded and the pellet resuspend in cold fixation buffer (Table 2) at room temperature for 30 minutes. After fixation, the buffer was diluted with PBS and centrifuged, the supernatant was discarded and the pellet was resuspended in permeabilisation buffer (Table 2) and incubated at room temperature for 20 minutes. After permeabilisation, the permeabilisation buffer was diluted with PBS and centrifuged again. The supernatant was discarded, and the pellet was resuspended in blocking buffer for 30 minutes at room temperature. After blocking, the buffer was again diluted and removed by centrifugation. The pellet was then resuspended in fluorescence-activated cell sorting (FACS) buffer with the primary antibody (HNF4a, Santa Cruz, Heidelburg, Germany) diluted 1:50 an incubated overnight at 4 °C.

After incubation with the primary antibody, the buffer was diluted with PBS and removed by centrifugation. This step was repeated twice before resuspending the pellet in FACS buffer (table 2) with the secondary antibody diluted 1:750. Care was taken to work in darkness where possible with the photosensitive secondary antibody. The cells were incubated with the secondary antibody at room temperature for 2 hours in darkness. The secondary antibody solution was diluted with PBS as before and centrifuged and the supernatant was discarded to remove unbound secondary antibody. The pellet was resuspended in 1 mL PBS. 1µM DAPI was added immediately before flow cytometry analysis using the FACS Canto II (BD Biosciences).

2.2 Organoids

2.2.1 Production of conditioned medium

Medium conditioned by RSPO1 or Wnt3a producing cells was required in the composition of several organoid media (Table 2). As directed by Broutier et al. (2016), Cultrex® HA-R-Spondin1-Fc 293T Cells and L Wnt-3A (ATCC® CRL-2647™) cells were obtained from AMS Biotechnology and LGC Standards (Middlesex, UK) respectively.

Cells were expanded in Wnt3a- or RSPO1-conditioned growth medium into 500 cm^2 plates, once at 70% confluency; the medium was changed to Wnt3a- or RSPO1-conditioned harvest medium and

incubated for 1 week for conditioning. The conditioned harvest medium was centrifuged (500 *g*, 5 minutes, 8 °C) to remove any cells before storage. Wnt3a-conditioned medium was stored at 4 °C for up to 6 months; RSPO1-conditioned medium was stored at -20 °C for up to 6 months.

2.2.2 Isolation and culture of hepatic organoids

Organoids were derived from human liver tissue as described in Broutier et al. (2016) and in detail below.

2.2.3 Tissue Collection

Tissue specimens were collected from Aintree Hospital, Liverpool, UK from waste tissue from hepatobiliary surgeries. Full patient consent and ethical approval from the relevant institutional review boards (National Research Ethics Service REC ref: 11/NW/0327) was received.

Resected tissue was transported in ice-cold HEPES buffered saline (Table 2) and transferred to organoid basal medium (Table 2) and stored at 4 °C until isolation a maximum of 48 hours later.

2.2.4 Single-cell isolation

For human organoids, approximately 1g of tissue was used per isolation. The tissue was dissociated under aseptic conditions using scissors into pieces no larger than 1 mm^3. These pieces were washed twice in organoid wash medium (Table 2) by pipetting the pieces up and down to remove excess blood, floating tissues and fat. The pieces of tissue were allowed to sediment gravitationally and the wash medium was discarded. The washed pieces were then resuspended in 10 mL human organoid digestion buffer (Table 2) and agitated gently at 37 °C for 30 minutes. The suspension was then vigorously pipetted up and down to break up tissue pieces. Depending on the extent of tissue digestion, the digestion buffer was either returned to gentle agitation at 37 °C for a further 10 minutes (repeating this step until sufficient digestion was observed to a maximum of 90 minutes) or proceeded to filtration.

Digestion was considered complete once the suspension contained 80-100% single cells. The volume of the digested suspension was increased to 15 mL with organoid wash medium and passed through a 70 µm filter. The volume was then increased to 50 mL using ice-cold organoid wash medium and centrifuged (300 *g*, 5 minutes, 4 °C). The supernatant was discarded and the pellet was resuspended in 15 mL of ice-cold organoid wash medium and centrifuged twice (300 *g*, 5 minutes, 4 °C), discarding the supernatant each time. The cells were resuspended in organoid basal medium and were centrifuged (300 *g*, 5 minutes, 4 °C). The pellet at this point was often very small or not visible to the naked eye.

The supernatant was discarded, and the pellet was resuspended in ice cold BME-2 (AMSBio). Fifty µL per well of a pre-warmed 24-well suspension culture plate was carefully pipetted into a dome shape and transferred to a CO_2 incubator at 37 °C for 10 minutes to fully solidify before adding organoid isolation medium (Table 2) at standard culture volume (Table 3). After 3-4 days, the organoid isolation medium was changed to organoid expansion medium (Table 2) and changed every 3-4 days thereafter.

2.2.5 Fluorescence-activated cell sorting (FACS)

In some cases, the isolation of ductal cells was enriched by sorting for EpCAM-positive cells using FACS. All centrifugation steps were carried out a 400g, 5 minutes at 8 °C unless otherwise noted. The isolation proceeded as described in the single-cell isolation section before resuspending the pelleted material in 5 mL of TrypLE (Thermo Fisher Scientific) supplemented with 10 mg/mL DNAseI (Sigma Aldrich). The suspension was triturated using a fine pipette tip e.g. 200 µL, and incubated at 37 °C for 5 minutes. The suspension was repeatedly checked until >90% of the suspension was single cells. 10 mL of cold wash medium was added to stop the digestion and the cells were pelleted by centrifugation; this step was repeated once at 500 *g*. The pelleted material was resuspended in 5 mL of wash medium and passed through a 40 µm filter to leave only single cells. The cells were counted using a haemocytometer and divided into an experimental and negative control with 90% of the material being used for the experimental group. The cells were pelleted by centrifugation (400 *g*, 5 minutes, 8 °C) and resuspended in FACS blocking solution (Table 2) for 20 minutes on ice. The cells were pelleted by centrifugation and resuspended in 500 µL wash medium supplemented with 5 µg DNAseI and 10 µM ROCK inhibitor (Y-27632) before proceeding to antibody incubation. The antibody used was APC-conjugated anti-human EpCAM (Biolegend, London, UK) diluted 1:1000 and incubated for 1 hour on ice in darkness. The cells were washed twice with 3 mL wash medium and pelleted by centrifugation. The cells were resuspended in 500 µL wash medium with 10 µM ROCK inhibitor (Y-27632). Both the negative control and the experimental sample were divided into DAPI-positive and DAPI-negative samples and were sorted using a BD FACS ARIA III. The sorted sample was then plated in BME-2 domes as described in the previous section.

2.2.6 Passaging

Organoids were passaged approximately two weeks after initial isolation and passaged based on density thereafter, once organoids became too dense for their BME-2 domes. Suspension plates were prewarmed to 37 °C. The BME-2 dome was disrupted by triturating with a 1 mL pipette tip in 500 µL organoid basal medium. Up to three domes were then combined into a single 15 mL tube and the volume was increased to 15 mL basal medium. This suspension was pipetted up and down to

break up the BME-2 and centrifuged (200 *g*, 5 minutes, 8 °C). 13 mL of the supernatant was aspirated, and the organoids were resuspended in the remaining medium with a 200 µL tip in order to break the organoids apart. The tube was filled with cold basal medium and centrifuged (250 *g*, 5 minutes, 8 °C) to wash out any remaining BME-2 and the supernatant was discarded. The remaining cells were resuspended in BME-2 and 50 µL domes were pipetted into the prewarmed plates and allowed to solidify at 37 °C for 10 minutes before adding organoid expansion medium.

2.2.7 Cryopreservation

Cryopreservation of organoids was performed identically to passaging but instead of resuspending in BME-2 for plating after dissociation of the domes, cryopreservation medium was added. Either CS10 (STEMCELL Technologies) or Cell recovery medium (Thermo Fisher Scientific) was used and the suspension was cooled at a rate of 1 °C per minute to -80 °C using a Mr Frosty before transferring to liquid nitrogen for long term storage.

To recover organoids from cryopreservation, the suspension was rapidly warmed using a water bath at 37 °C until a small piece of ice remained floating in the tube. The volume was then increased to 10 mL using organoid basal medium and centrifuged (300 *g*, 5 minutes, 4 °C). The supernatant was discarded, and the pellet resuspended in BME2 and plated in domes as described previously.

2.2.8 Differentiation

Once grown to high density, organoids were considered ready for differentiation towards a hepatocyte phenotype. Organoids were passaged as described previously and cultured in organoid differentiation medium 1 (Table 2) for 5 days, changing the medium every 2-3 days. On day 6 the medium was changed to human organoid differentiation medium 2 (Table 2) and changed every 3 days until day 15.

2.2.9 Organoid harvesting

The procedure for harvesting organoids for analysis was identical to the procedure for passaging until the point that the organoids would normally be resuspended in BME-2. At this point the organoid fragments were washed with PBS to remove any remaining culture medium before lysing in Isobaric Tagging for Relative and Absolute Quantification (iTRAQ) buffer.

2.2.10Western Blotting

Protein samples were lysed in radioimmunoprecipitation assay (RIPA) buffer (Sigma Aldrich) and separated via SDS-PAGE on 10% acrylamide tris-HCl gel (ProtoGel 30% acrylamide solution, ProtoGel resolving buffer and ProtoGel stacking buffer were obtained from AGTC Bioproducts, Hessle, UK).

Separated protein bands were transferred to nitrocellulose membrane (GE Healthcare, Amersham, UK), transfer was checked using Ponceau Red stain, blocked with 10% blotting-grade blocker (Bio-Rad, Hemel Hempstead, UK) at room temperature for 1 hour and probed with rabbit anti-cytochrome P450 3A4 (1:3000) or rabbit anti-albumin (1:3000) antibody (Overnight, 2% (w/v) blocking-grade blocker in tris buffered saline with tween 20 (TBST)) and mouse anti-ß-actin antibody (15 min, 1:10000, 2% (w/v) blotting grade blocker in TBST) (all Abcam). Secondary incubation was with anti-rabbit IgG-peroxidase (1 hour, 1:5000, 2% (w/v) blotting grade blocker in TBST) or anti-mouse IgG-peroxidase (1 hour, 1:10000, 2% (w/v) blotting grade blocker in TBST) as appropriate. Samples were visualised via chemiluminescence using Western Lighting Plus-ECL (Perkin Elmer), and visualised in a darkroom with Amersham Hyperfilm ECL (GE Healthcare). Once visualised, densitometry analysis was performed using ImageJ software (Schneider et al., 2012).

2.3 Tumorigenicity Study

2.3.1 Ethics

These techniques were performed by personal licence holders according to the regulations defined within the project licence granted under the Animals (Scientific Procedures) Act 1986 and approved by the University of Liverpool ethics committee. Animals were housed at a constant temperature and humidity with free access to food and water and a 12-hour like/dark cycle and were acclimatised for at least 7 days before any procedures. Animals were humanely sacrificed using a rising concentration of carbon dioxide according to the Humane Killing of Animals Under Schedule 1 to the Animals (Scientific Procedures) 1 Act 1986.

2.3.2 Animals used

Fox Chase SCID beige mice (SCID beige) were used for these studies. SCID beige mice carry the mutations *Prkdcscid* and *Lystbg*, which combined, produce severe B and T lymphocytopenia and defective natural killer cells. Animals were obtained from Charles River (Massachusetts, US).

2.3.3 CCl_4 dosing

Carbon tetrachloride was administered via intraperitoneal injection to produce acute liver injury. To the best of our knowledge, acute dosing with CCl_4 had not previously been attempted with SCID beige mice. Doses of 1.0, 0.4 and 0.2 mL/kg in olive oil were used. Response to CCl_4 was determined by ALT activity and histological examination of liver after sacrifice. 0.2 mL/kg was determined to be the optimal dose tested to cause liver injury without excessive mortality in the animals.

2.3.4 Intrasplenic injection of hepatocyte-like cells

Animals were treated with 0.2 mL/kg CCl_4 by intraperitoneal injection to induce liver injury. After 72 hours, animals were anaesthetised with isoflurane and prepared for surgery. The spleen was exposed and injected with 1x 10^6 HLCs. Gentle pressure was maintained on the injection site for at least 1 minute to prevent bleeding and backflow of the injected cells. The surgical wound was sutured closed and the animals were recovered in warmed boxes before returning to their cages. The animals were observed for 2 hours after surgery to check for signs of excessive distress or discomfort and checked daily for 7 days thereafter. The same procedure was followed for the injection of undifferentiated cells, substituting the cell type where appropriate.

2.3.5 Imaging protocols

In vivo bioluminescence was detected using an IVIS spectrum (Perkin Elmer, Buckinghamshire, UK). Animals were imaged 1 week after surgery and every 1-2 weeks thereafter. Prior to imaging, animals were weighed and anaesthetised with isoflurane. Luciferin (15 mg/mL) was administered by intraperitoneal injection at a volume of 10 µL/g for a final dose of 150 µg/g. Animals were imaged from the front and from the side using the automatic setting to determine exposure time. After imaging, the animals were recovered in a warmed box before returning them to their cages.

2.3.6 Sacrifice and ex vivo imaging

Animals were sacrificed once signs of discomfort or ill health began to occur, typically around 6 months of age. Prior to sacrifice animals were anaesthetised and imaged as previously described. Immediately after imaging and without allowing animals to wake from anaesthesia, animals were administered luciferin by intraperitoneal injection for a second time and sacrificed using a rising concentration of CO_2. After death was confirmed, blood was recovered by cardiac puncture and organs were retrieved. The spleen, liver, kidneys and lungs were retrieved, and luminescence was detected using an IVIS spectrum with exposure determined by automatic settings. Tissues were then stored either in 4% paraformaldehyde (PFA) or snap-frozen in liquid nitrogen.

2.3.7 Immunohistochemistry

Immunohistochemistry was performed at Leahurst Campus, Liverpool by specialists and were scored by a veterinary histopathologist (Thoolen et al., 2010, Table 9). Liver and spleen tissues were fixed in PFA for 24–48h, were trimmed and routinely embedded in paraffin wax. Consecutive 4 µm thick sections were prepared and routinely stained with haematoxylin and eosin (HE). Individual selected cases were further examined with both histochemistry (PAS and Alcian-PAS) or subjected to immunohistochemical labelling. For the latter technique, a Dako Autostainer Link 48 was used.

Following removal and re-hydration, EnVisionTM FLEX Peroxidase Blocking Reagent was used to quench endogenous peroxides. Before addition of the primary antibodies (against Vimentin (clone V9, Dako, 1:500), Pan-Cytokeratin (clones AE1/AE3, Dako, 1:200) and GFAP (Dako, Z 0334, 1:1000)), goat serum and Fab Fragment (unconjugated Affinipurified Fab fragments goat anti-mouse IgG, Stratech Scientific, Ely, UK) blocking steps were serially applied. Following this, slides were incubated with the EnVisionTM anti-mouse FLEX/HRP labelled polymer for 20 minutes, rinsed and then incubated with the EnVisionTM FLEX DAB + Substrate Chromogen System. Slides were finally counterstained with EnVisionTM FLEX Haematoxylin, then rehydrated and mounted as per routine histology.

2.3.8 qPCR

2.3.8.1 RNA Extraction

All samples for RNA analysis were lysed in 700 µL QIAzol and stored at -80 °C until used. The miRNeasy kit (Qiagen) was used following the manufacturer's protocol. Briefly, samples were thawed and allowed to equilibrate to room temperature for approximately five minutes. 140 µL chloroform (Thermo Fisher Scientific) was added to each sample and mixed thoroughly by vortexing for 15 seconds. Samples were then incubated at room temperature for 2-3 minutes before centrifugation (12,000 *g*, 4 °C, 15 minutes). The upper aqueous phase was pipetted into a clean tube without disturbing the interphase and the remainder was discarded. At this point the remainder of the process was either fully automated using the QIAcube protocol 'Purification of total RNA, including small RNAs, from animal tissues and cells (aqueous phase)' (Qiagen), or proceeded manually, as follows.

Ethanol (100%, 1.5 volumes) was added to the aqueous phase and mixed thoroughly. The sample was then passed through the RNeasy mini column by centrifugation (17,000 *g*, 15 seconds, room temperature). 700 µL of buffer RWT was next passed through the column by centrifuging in the same manner, the flow through was discarded. 500 µL of buffer RPE was then passed through the column in the same manner discarding the flow through, this step was repeated once. The RNA was then eluted into 50 µL RNAse-free water by centrifugation as in previous steps. In order to retrieve as much RNA as possible this step was repeated once using the flow through of the previous run. The RNA concentration of the eluate was determined using a NanoDrop ND-1000 spectrophotometer (Thermo Fisher Scientific).

2.3.8.2 Reverse Transcription

Reverse transcription was performed using the Improm II Reverse Transcription Kit (Promega, Southampton, UK) using the following protocol. RNA samples were diluted with RNAse-free water to

1000 ng in 24 µL and 1 µL oligodT was added to each sample. These samples were then heated to 70 °C before cooling on ice. The reaction mixture was prepared as directed by the manufacturer and 25 µL was added to each reaction. Each sample was mixed thoroughly by pipetting and heated to 25 °C for 5 minutes, 42 °C for 1 hour and 70 °C for 15 minutes before cooling on ice. cDNA was stored at -20 °C until further use.

2.3.8.3 qPCR

SYBR Green and TaqMan chemistry were used in this thesis, the chemistry used is noted on each occasion. qPCR experiments were carried out using 384-well plates and loading was automated using a Qiagility (Qiagen) robot where possible.

For TaqMan chemistry the volume of each reaction mixture was 20 µL and contained 10 µL TaqMan Gene Expression Master Mix (Thermo Fisher Scientific), 1 µL primers (Thermo Fisher Scientific), 9 µL RNAse-free water and cDNA. Once combined, the plate was sealed and vortexed briefly to mix before centrifugation (4,000 *g*, 1 minute) to collect liquid at the bottom of the wells. Experiments were run using a ViiA7 instrument (Thermo Fisher Scientific) following a protocol of: 95 °C for 10 minutes followed by 40 cycles of 95 °C for 15 seconds and 60 °C for 60 seconds.

For SYBR green chemistry the volume of each reaction mixture was 25 µL and contained 12.5 µL SYBR Green JumpStart Taq ReadyMix (Sigma Aldrich), 1 µL each of forward and reverse primers (Eurofins Genomics, Ebersberg, Germany) each at 10 µM, 0.25 µL Rox passive reference dye, 8.25 µL of RNAse-free water and 2 µL cDNA. The amount of cDNA was occasionally increased, reducing the volume of RNAse-free water for low-abundance targets. Experiments were run using a ViiA7 instrument following a protocol of: 95 °C for 10 minutes followed by 40 cycles of 95 °C for 15 seconds and 60 °C for 1 minute.

Data was processed using the $2^{-\Delta\Delta CT}$ method (Livak and Schmittgen, 2001) in Microsoft Excel.

2.3.9 iTRAQ Analysis

2.3.9.1 Preparation

In preparation for iTRAQ analysis samples were lysed in iTRAQ buffer, cell samples were initially lysed by vortexing, tissue samples were lysed using a steel ball and an oscillating mill. Lysed samples were sonicated three times using a sonicating probe ensure complete disruption of any cells in the sample before being centrifuged at 18,000 *g* at 4 °C to remove any insoluble debris from the sample. The supernatant was transferred to a new tube and stored at -80 °C for further processing.

2.3.9.2 Bradford assay

It is imperative that the loading of each sample is even for iTRAQ analysis. A Bradford assay was performed to determine the concentration of protein in each sample prepared as described above. A standard curve of bovine serum albumin was constructed at the following concentrations: 0.25, 0.2, 0.15, 0.1, 0.05, and 0.025 mg/mL and a blank sample. Samples were diluted in distilled water and 20 µL of each diluted sample and standard were loaded into a 96-well flat-bottomed microtitre plate. Bradford assay dye reagent (Bio-Rad) was diluted 1:4 with ultrapure water and 200 µL was added to each well. Absorbance was measured at 570 nm and protein concentration was determined by linear regression to the standard curve.

2.3.9.3 Coomassie stain

A Coomassie stain was performed in order to confirm accurate determination of protein concentration via Bradford assay. Samples were diluted to 1 mg/mL in x4 Laemmli buffer (Bio-rad), prepared according to the manufacturer's instructions and denatured at 85 °C for 10 minutes before cooling on ice. Samples were loaded into a 10% polyacrylamide gel, run at 90V for 10 minutes then at 170V until the dye front approached the bottom of the gel. After electrophoresis, the proteins were fixed for 1 hour in 7% glacial acetic acid and 40% (v/v) methanol. After fixation, the gel was stained using freshly prepared Coomassie stain (4 parts colloidal Coomassie stain (0.1% (w/v) Coomassie brilliant blue G-250 in 2% (w/v) phosphoric acid, 10% (w/v) ammonium sulphate) to 1 part methanol) for 2 hours. After staining, the gel was destained for 60 seconds with agitation using 10% acetic acid in 25% (v/v) methanol. Following destaining, the gel was rinsed once in 25% (v/v) methanol before destaining at least overnight in 25% (v/v) methanol with agitation on an orbital shaker.

After destaining, the gel was imaged using a GS-800 calibrated imaging densitometer (Bio-Rad) and relative density of each gel lane was assessed using Quantity One software (Bio-Rad).

2.3.8.4 iTRAQ

iTRAQ analysis was performed by specialist technicians as follows. 100 µg protein in 20 µL was denatured using SDS, reduced using tris(2-carboxyethyl) phosphine (TCEP) and capped with methyl methanethiosulfonate (MMTS) according to the manufacturer's protocol (8-plex, Sciex, Cheshire, UK). Samples were digested overnight with trypsin and labelled with iTRAQ isobaric tags 113-121. Samples were subjected to cation exchange chromatography, to remove unbound trypsin and reagent and then diluted to 4 mL with 10 mM potassium dihydrogen phosphate/25% ACN (w/v). The pH was adjusted to <3 using phosphoric acid prior to fractionation on a Polysulfoethyl A strong cation-exchange column (200 × 4.6 mm, 5 µm, 300 Å; Poly LC, Columbia, MD). Fractions of 2 mL

were collected and were dried by centrifugation under vacuum (SpeedVac, Eppendorf). Fractions were reconstituted in 1 mL of 0.1% TFA and were subsequently desalted using a mRP Hi Recovery protein column 4.6 x 50 mm (Agilent, Stockport, UK) on an Infinity 1260 HPLC system (Agilent) prior to mass spectrometric analysis.

Desalted fractions were reconstituted in 40 μL 0.1% formic acid and 3 μL aliquots were delivered into a Triple TOF 6600 (Sciex) via an Eksigent NanoLC 400 System (Sciex) mounted with a NanoAcquity 5 μm, 180 μm x 20 mm C_{18} trap and 1.7 μm, 75 μm X 250 mm analytical column (Waters, Herts, UK). A NanoSpray III source was fitted with a 10 μm inner diameter PicoTip emitter (New Objective, MA, USA). A gradient of 2−50% ACN/0.1% formic acid (v/v) over 90 min was applied to the columns at a flow rate of 300 nL/min. The mass spectrometer was operated in positive ion mode (Analyst TF1.7) with survey scans of 250 ms, MS/MS accumulation time of 100 ms and with monitoring of the 25 most intense ions (total cycle time 2.75 s). Data were searched using ProteinPilot 5 software (Sciex) against the latest UniProt database with iTRAQ as a variable modification and MMTS as the cysteine alkylating reagent. The reversed database was used as a decoy to determine the false discovery rate (FDR) for protein identification, and only those proteins identified within a 1% FDR were evaluated further. Data from iTRAQ analyses were processed using Partek (Partek Incorporated, Missouri, USA).

2.4 Medium and buffer compositions

Medium name	Base medium	Additives	Serum free?	Notes
Media				
Freezing medium	DMEM-F12 (Thermo Fisher Scientific, Dorset, UK)	20% (v/v) KnockOut Serum Replacement, 1 mM L-glutamine (Sigma-Aldrich, Dorset UK), 100 µM MEM Non-Essential Amino Acids, 200 µM 2-mercaptoethanol, 10% (v/v) DMSO (Thermo Fisher Scientific)	Yes	
MEF medium	DMEM (Sigma-Aldrich)	15% Embryonic stem-cell FBS (Thermo Fisher Scientific) 1% (v/v) penicillin/streptomycin (Thermo Fisher Scientific)	No	
KSR	DMEM-F12	20% (v/v) KnockOut Serum Replacement, 1% (v/v) GlutaMAX (Thermo Fisher Scientific), 100 µM MEM Non-Essential Amino Acids, 200 µM 2-mercaptoethanol, 4 ng/mL FGF2 (Thermo Fisher Scientific)	Yes	
Essential 8 medium	Essential 8 basal medium	Essential 8 supplement (Thermo Fisher Scientific), 1% (v/v) penicillin/streptomycin	Yes	Essential 8 supplement was added immediately prior to use and used within 7 days of storage at

	(Thermo Fisher Scientific)			4 °C
Differentiation medium 1	RPMI-1640 (Sigma-Aldrich)	B27 supplement, 100ng/mL Activin A (Peprotech), 50ng/mL Wnt3a (RnD Systems, Oxfordshire UK)	Yes	
Differentiation medium 2	Knockout DMEM (Thermo Fisher Scientific)	20% (v/v) KnockOut Serum Replacement, 1% (v/v) GlutaMAX, 100 µM MEM Non-Essential Amino Acids, 200 µM 2-mercaptoethanol, 1% (v/v) DMSO	Yes	
Differentiation medium 3	HepatoZYME-SFM (Thermo Fisher Scientific)	10nM dexamethasone (Sigma-Aldrich), 20 ng/mL oncostatin M (PeproTech, London UK), 20 ng/mL hepatocyte growth factor (PeproTech)	Yes	Recombinant growth factors were added immediately prior to use to prevent degradation at 4 °C
Differentiation medium 4	RPMI-1640	B27 supplement	Yes	
Differentiation medium 5	Leibovitz's L-15 (Thermo Fisher Scientific)	8.3% tryptose phosphate broth, 8.3% embryonic stem-cell FBS, 10 µM hydrocortisone 21-hemisuccinate, 0.5% (v/v) insulin, transferrin, selenium, 1% (v/v) GlutaMAX, 50ng/mL sodium-L-ascorbate, 100 nM dexamethasone, 100 nM dihexa (Active Peptide, Cambridge, MA, USA)	No	
Differentiation medium 6	Leibovitz's L-15	8.3% tryptose phosphate broth, 8.3% embryonic stem-cell FBS, 10 µM hydrocortisone 21-hemisuccinate, 1	No	Use of this medium composition was eventually halted, due to the high acidity of 0.2% ascorbic

		µM Insulin (bovine pancreas), 1% GlutaMAX, 0.2% ascorbic acid, 100 nM dexamethasone, 20 ng/mL oncostatin M, 10 ng/mL hepatocyte growth factor		acid causing poor viability in resultant cells and substituted for differentiation medium 7
Differentiation medium 7	Leibovitz's L-15	8.3% tryptose phosphate broth, 8.3% embryonic stem-cell FBS, 10 µM hydrocortisone 21-hemisuccinate, 1 µM insulin (bovine pancreas), 1% GlutaMAX, 50ng/mL sodium-L-ascorbate, 100 nM dexamethasone, 20 ng/mL oncostatin M, 10 ng/mL hepatocyte growth factor	No	
Organoid basal medium	Advanced DMEM/F12	1% penicillin/streptomycin, 1% GlutaMAX, 10mM 4-(2-hydroxyethyl)-1-piperazineethanesulfonic acid (HEPES)	Yes	Store at 4 °C for up to 1 month
Organoid wash medium	DMEM (high glucose, GlutaMAX and pyruvate)	1% FBS, 1% penicillin/streptomycin	No	Store at 4 °C for up to 1 month
Organoid expansion medium	Organoid basal medium	2% B27 supplement (without vitamin A), 1% N2 supplement, 1 mM N-acetylcysteine, 10% (v/v) RSPO1-conditioned medium, 10 mM nicotinamide, 10 nM recombinant human [Leu15]-gastrin I, 50 ng/mL recombinant human EGF, 100 ng/mL recombinant	No	Store at 4 °C for up to 2 weeks

		human FGF10, 25 ng/mL recombinant human HGF, 10 µM Forskolin, 5 µM A83-01.		
Organoid isolation medium	Organoid expansion medium	25 ng/mL recombinant human Noggin, 30% (v/v) Wnt3a-conditioned medium and 10 µM Rho kinase (ROCK) inhibitor (Y-27632)	No	Store at 4 °C for up to 2 weeks
Organoid differentiation Medium 1	Organoid expansion medium	25 ng/mL BMP7	No	
Organoid differentiation medium 2	Organoid basal medium	2% B27 supplement, 1:100 N2 supplement, 1 mM N-acetylcysteine, 10 nM recombinant human [Leu15]-gastrin I, 50 ng/mL recombinant human EGF, 25 ng/mL recombinant human HGF, 0.5 µM A83-01, 10 µM DAPT, 3 µM dexamethasone, 25 ng/mL BMP7, 100 ng/mL recombinant human FGF19	No	Store at 4 °C for up to 2 weeks
RPSO1 growth medium	DMEM	10% FBS, 150 µg/ml Zeocin	No	Store at 4 °C for up to 1 week.
RPSO1 conditioned medium	Advanced DMEM/F12 (Thermo Fisher Scientific)	1% penicillin/streptomycin, 1% GlutaMAX and HEPES 10 mM	No	Store at 4 °C for up to 1 month. Once conditioned, store at -20 – -80 °C for up to 6 months

Wnt3a growth medium	DMEM	10% FBS, 1% penicillin/streptomycin, 300 µg/mL Zeocin	No	Store at 4 °C for up to 1 week.
Wnt3a conditioned medium	DMEM	10% FBS, 1% penicillin/streptomycin	No	Store at 4 °C for up to 1 month. Once conditioned, store at -20 – -80 °C for up to 6 months
Buffers				
Phosphate buffered saline (PBS)	Distilled water	137 mM NaCl, 2.6 mM KCl, 8.1mM Na_2HPO_4 and 1.4 mM KH_2PO_4 Adjust pH to 7.4 with HCl	N/A	
Fixation buffer	PBS	2 % paraformaldehyde	N/A	
Permeabilisation buffer	PBS	0.1 % Triton X-100	N/A	
FACS buffer	PBS	0.5 % normal donkey serum and 0.05% Sodium Azide (NaN_3)	N/A	
Blocking reagent	PBS	2.5 % normal donkey serum	N/A	
HEPES buffered saline	Distilled water	10mM x 4-(2-hydroxyethyl)-1-piperazineethanesulfonic acid (HEPES), 5mM KCl, 136mM NaCl, 0.5% (w/v) glucose, pH adjusted to 7.6 with HCl	N/A	

Table 2

Table of media and buffer compositions – detailed composition of each buffer and medium used throughout this thesis. Basal medium and all additive are shown. Abbreviations: BMP7 - Bone morphogenic protein 7, DMEM - Dulbecco's modified Eagle's medium, DMSO - Dimethyl sulfoxide, EGF - Epidermal growth factor, FBS - Foetal bovine serum, FGF10 - Fibroblast growth factor 10, FGF19 - Fibroblast growth factor 19, FGF2 - Fibroblast growth factor 2, HGF - Hepatocyte growth factor, MEM - Modified Eagle's medium, PBS - Phosphate buffered saline, RPMI-1640 - Roswell Park Memorial Institute 1640, RSPO1 - R-spondin 1

Culture Vessel Type	Area (cm^2)	Routine culture volume (mL)
6-well plate	9.5	2
12-well plate	3.8	1
24-well plate	1.9	0.5
48-well plate	0.95	0.25
96-well plate	0.32	0.1
25cm^2 square dish	625	100
T25 flask	25	5
T75 flask	75	9
T175 flask	175	21

Table 3

Table of standard culture volumes – list of culture vessels and the standard volumes used during tissue culture

3 Effects of hypoxia on the production of hepatocyte-like cells from induced pluripotent stem cells using two protocols

3.1 Introduction

iPSC-HLCs made using the best current protocols are not sufficiently mature for transplantation in humans and their phenotype is a hindrance to their use in toxicity testing. They display a phenotype closer to that of an immature foetal hepatocyte and lack features such as cytochromes P450, phase II enzymes and transporters at physiological levels and also express markers of immaturity such as AFP at high levels As such there have been many attempts over recent years to improve upon differentiation protocols for HLCs and other cell types.

Differentiation protocols to produce HLCs have advanced from initially undirected differentiation, where cells were allowed to spontaneously differentiate or very simple directed protocols with only a single stage to enrich for a hepatic fate, to the more complex and familiar protocols that are currently common. These protocols are most often comprised of three main stages: definitive endoderm specification, hepatic endoderm specification and hepatic maturation which may be subdivided into smaller sections. For example, in our previous work we utilised a common type of three-stage growth factor-based differentiation protocol (Heslop et al., 2017).

Specifically, this protocol uses activin A and Wnt3A followed by activin A alone for definitive endoderm specification (Figure 4). Activin A is a TGF-β family member commonly used to manipulate the nodal pathway. The nodal pathway is a key element of left-right asymmetry and the patterning process and initial generation of mesoderm and endoderm during embryogenesis. Endoderm specification requires high levels of activation of the nodal pathway compared with mesoderm which leads to the production of anterior primitive streak cells and in turn activates mixer homeoproteins beginning a cascade which ultimately upregulates endoderm-related genes such as Sox17 whilst downregulating mesoderm inducing genes (Shen, 2007; Sui et al., 2013). Wnt signalling is another commonly manipulated pathway in the differentiation of pluripotent cells to definitive endoderm. The Wnt pathway is activated repeatedly throughout embryo development and is involved in definition of the anterior/posterior axis as well as in patterning (Sokol, 2011). Though the Wnt pathway itself induces a mesodermal fate if continuously activated it is required for efficient generation of the primitive streak from which definitive endoderm is derived (Sui et al., 2013).

DMSO was used for hepatic endoderm specification in this protocol. DMSO has been shown to drive differentiation by downregulating genes associated with 'stemness' including Oct-4, Sox-2, Nanog and Rex-1 (Czysz et al., 2015; Pal et al., 2012). After specification with DMSO, cells are considered hepatoblasts, the bipotent progenitor cell type that can give rise to only two types of cell, hepatocytes or cholangiocytes. FGF10 and BMP4 are also commonly used for the definition of hepatic endoderm and likely more closely mimic embryogenesis but were not used in the protocols in this work (Hannan et al., 2013).

Hepatocyte growth factor (HGF) is commonly used in the differentiation of HLCs to activate c-Met and drive hepatocyte maturation. After formation of the foregut from the definitive endoderm, HGF is secreted from the mesenchyme of the liver and septum transversum and is implicated in the migration, proliferation and survival of hepatoblasts. Moreover, once the hepatoblasts have formed, it is responsible, in conjunction with glucocorticoid hormones, Wnt signalling and oncostatin M (OSM) for the differentiation of the foetal hepatocytes. OSM is secreted from the hematopoietic cells of the embryonic liver and induces metabolic maturation of the hepatocytes by activating the GP130 receptor and the JAK/STAT3 signalling pathways (Zorn, 2008).

The growth factors used during the differentiation of HLCs are often altered to better mimic the conditions found during embryogenesis. However, no current protocol has been able to produce cells which fully recapitulate the phenotype of human primary hepatocytes (hPH) suggesting that there are other factors at play in the generation of fully functional hPH from iPSCs. In addition to the modulation of the growth factors, environmental and physical characteristics of the differentiation protocol can be altered. Three-dimensional culture (e.g. spheroids, bioreactors) and co-culture with non-parenchymal cell types have shown promise to improve the maturity of iPSC-HLCs. However, similarly to modulation of growth factors, no combination of these factors has been able to fully recapitulate the phenotype of adult hPH.

Another practical aspect to consider in the differentiation of iPSC-HLCs is cost. In order to produce enough iPSC-HLCs for large-scale experimentation or transplantation the cost of differentiation materials such as growth factors may become prohibitively high. In a recent study, a differentiation protocol using small molecules in place of traditional growth factors was demonstrated (Siller et al., 2015). Specifically, this protocol uses small molecules to replace key growth factors during differentiation. During the first stages of differentiation CHIR99021 is substituted where activin A/Wnt3a would typically be used. CHIR99021 is a

potent inhibitor of glycogen synthase kinase 3 and a Wnt pathway activator. The Wnt pathway is associated with patterning in embryonic development and is commonly activated in protocols producing endoderm cells, the authors demonstrate that addition and removal of CHIR99021 over 48 hours is sufficient to induce definitive endoderm differentiation (Siller et al., 2015). The second stage of differentiation uses DMSO to drive differentiation which is also commonly used in growth factor-based protocols and was discussed previously. The third stage of the differentiation protocol replaces HGF with N-hexanoic-Tyr-Ile-(6) aminohexanoic amide (Dihexa), an HGF mimetic, in combination with dexamethasone and hydrocortisone-21-hemisuccinate. The advantages to this approach are several; firstly, the cost of such a protocol is greatly reduced when compared with traditional growth factor-based approaches. In addition, the variability in reagents can be reduced since there is no biological component in their production.

However, it has not yet been fully determined whether the resultant cells are as well differentiated as their growth factor-derived counterparts. Since the effects of many growth factors are pleiotropic and often incompletely understood, it cannot be determined with certainty that a small molecule will perfectly mimic all the pathways that the growth factor would interact with. For example, Dihexa, the HGF mimic used in the protocol described has been shown to activate c-Met, the main pathway through which HGF operates, but has not been shown to interact with heparan sulphate or dermatan sulphate which HGF also interacts with, these discrepancies may impact upon differentiation (Benoist et al., 2014).

The use of hypoxic conditions for the routine culture of iPSCs is well established. Hypoxic conditions have been shown to reduce the levels of spontaneous differentiation and therefore aid in long term culture of iPSCs (Ezashi et al., 2005; Prasad et al., 2009; Zhang and Wang, 2013). The rationale behind this technique are readily apparent when the oxygen levels during embryogenesis are considered, particularly compared with typical cell culture conditions where the oxygen level is not controlled from the atmosphere (Dunwoodie, 2009). Hypoxic conditions have been shown to increase the expression of NANOG in iPSCs compared with atmospheric oxygen whilst leaving cellular reactive oxygen species unaffected and also to maintain notch expression (Guo et al., 2013; Prasad et al., 2009).

Similarly, oxygen tension in the liver is variable across the lobule and thought to be tied to its function (Kietzmann, 2017). The partial pressure of oxygen ranges from 60-65 mmHg in

the periportal region to 30-35 mmHg in the perivenous region (Jungermann and Kietzmann, 2000). Compared with the partial pressure of atmospheric oxygen (approximately 160 mmHg) this equates to 8-4% atmospheric oxygen across the lobule. The phenotype of hepatocytes changes across the lobule, cells periportal region experience a higher oxygen tension and are more specialised for gluconeogenesis and glutathione synthesis. Conversely hepatocytes in the perivenous region experience a comparatively low oxygen tension and are specialised for glucose uptake and express higher levels of CYPs, essential proteins for xenobiotic metabolism (Kietzmann, 2017). Moreover, there is evidence that cultured primary hepatocytes are better able to resist dedifferentiation under hypoxic conditions (Guo et al., 2017), though the situation is complex as improvements in function and longevity under very high oxygen conditions and worsened survival in hypoxia have also been demonstrated (Kidambi et al., 2009).

We hypothesised that the use of hypoxia in the culture and differentiation of HLCs may produce a more physiological environment and improve the phenotype of the resultant cells. Previous studies have used hypoxic conditions to generate HLCs from Wharton's Jelly-derived mesenchymal stem cells and showed expression of hepatocyte-specific genes including Albumin, CYP3A4 and A1AT in addition to glycogen storage and LDL uptake (Prasajak and Leeanansaksiri, 2013). Si Tayeb et al. also demonstrated the use of transient hypoxic conditions during the hepatic endoderm stages of differentiation to HLCs using iPSCs (Si-Tayeb et al., 2010). Using this protocol, it was shown that highly efficient differentiation could be achieved, however, a comparison to normoxic conditions was not made.

We also sought to compare the small molecule-based protocol described by Siller et al. to the growth factor based protocol we have used in previous studies (Heslop et al., 2017; Siller et al., 2015) and characterise the phenotype of these cells in greater depth than has previously been attempted using iTRAQ and qPCR. The effects of hypoxic culture were examined during differentiation towards HLCs using both differentiation protocols using iTRAQ in the same manner. We hypothesised that by more closely mimicking the levels of oxygen found during embryogenesis the phenotype of the HLCs would be closer to that of hPH. It was also considered that by differentiating cells under hypoxic conditions the resultant phenotype may be closer to that of a perivenous hepatocyte, with greater expression of cytochromes P450 enzymes and other concomitant changes associated with hepatocytes from this region of the liver lobule. Specifically, we differentiated several human iPSC lines under both standard cell culture conditions using atmospheric oxygen and

under a controlled hypoxia atmosphere (5% oxygen) using both differentiation protocols. To the best of our knowledge, this is the first attempt to differentiate iPSCs under controlled hypoxic conditions and directly compare them to HLCs differentiated under normoxic conditions

Name	Sex	BMI	Age at isolation	Original cell type	Diagnosis	Co-morbidities
Liv4FA	Male	27.9	66	Fibroblast	Colorectal carcinoma with liver metastases	Type II diabetes mellitus
Liv6HB	Female	31.2	63	Hepatocyte	Colorectal carcinoma with liver metastases	Hypertension, Chronic liver disease, Type II diabetes mellitus
Liv6HE						
Liv7HE	Male	32.1	27	Hepatocyte	Focal nodular hyperplasia	None

Table 4

Donor details of iPSC lines used in chapter 3 - Liv4FA was used for assessment of the phenotype of undifferentiated cells cultured under hypoxic conditions, the remaining cell lines were used for differentiation and iTRAQ and qPCR analysis. Information from each tissue donor for iPSC lines. Sex, BMI at time of surgery, age at time of surgery, cell type of origin, patient diagnosis and known comorbidities are shown.

3.2 Results

In this study 4 iPSC lines were used, Liv4FA was used for assessment of undifferentiated phenotype (Figure 6) and Liv6HB, Liv6HE and Liv7HE were used for assessment of phenotype once differentiated (Figure 7-15). These lines were isolated from skin or surgical excess liver tissue obtained with informed consent from patients undergoing hepatobiliary surgery at Aintree Hospital, Liverpool, UK during a previous study from our lab (Heslop et al., 2017). The details associated with each line including age at isolation, sex etc. are shown in Table 4. Each line follows the same naming convention in which the last three characters inform the details of the cell type. For example, one line used was Liv6HE, in this case the number indicates the donor, 'H' indicates the cell type of origin, and 'E' indicates the number of the clone.

3.2.1 iPSCs cultured in hypoxic conditions show gene expression changes

Figure 6 shows qPCR analysis of Liv4FA iPSCs cultured under hypoxic conditions compared to the same cells cultured under non-oxygen-controlled conditions analysed using qPCR with SYBR green chemistry. Cells were cultured under hypoxic conditions for at least 3 passages prior to experimentation to enable adaptation to the culture conditions. Data are presented as fold difference ($2^{-\Delta\Delta CT}$) relative to iPSCs cultured under normoxic conditions with either GAPDH or β-actin as a control gene. Figure 6A shows the expression of four hypoxia-inducible genes, EPO, HIF1A, HSP70 and VEGFA. Although there were no significant changes, there was a trend towards increased expression of all genes under hypoxic conditions. Figure 6B shows expression of the pluripotency markers OCT4, SOX2 and NANOG, expression is increased in hypoxia in all cases and is significantly higher for SOX2 and NANOG, as determined by a student's t-test. Figure 6C shows expression of the NRF-2 pathway markers, GCLC, HO-1 and NRF-2, both HO-1 and NRF-2 are significantly increased in hypoxic conditions.

3.2.2 iPSC-HLCs show hPH-like morphology

Micrographs of Liv6HE iPSC-HLCs differentiated under each of the tested conditions i.e. both differentiation protocols under normoxic and hypoxic conditions (Figure 5). Undifferentiated cells are also shown for comparison (Figure 5E). Scale bars are 100 µm. Figure 5A and Figure 5B show the morphology of iPSC-HLCs differentiated using protocol 1 under normoxic and hypoxic conditions respectively, characteristic polygonal morphology associated with hepatocytes is visible in several locations. Figure 5C and Figure 5D show the

morphology of iPSC-HLCs differentiated using protocol 2 under normoxic and hypoxic conditions respectively, polygonal morphology can be observed in both images. Though not apparent at the presented magnification, multinucleate cells, a characteristic trait of hPH, were not observed in differentiated cells under any condition. Figure 5E shows the morphology of undifferentiated iPSCs, the tight, smooth colony formation and small cell size and small cytoplasm are of note. Figure 5F shows the morphology of hPH 24-hours after isolation for the purposes of comparison.

3.2.4 iTRAQ analysis shows incomplete differentiation of iPSC-HLCs

iTRAQ analysis was performed on iPSCs differentiated to HLCs under each condition. Additionally, undifferentiated iPSCs pooled from each line were included as a comparator alongside pooled hPH from several donors. Each condition was tested in triplicate and results were pooled for the subsequent analyses in figures Figure 7-14.

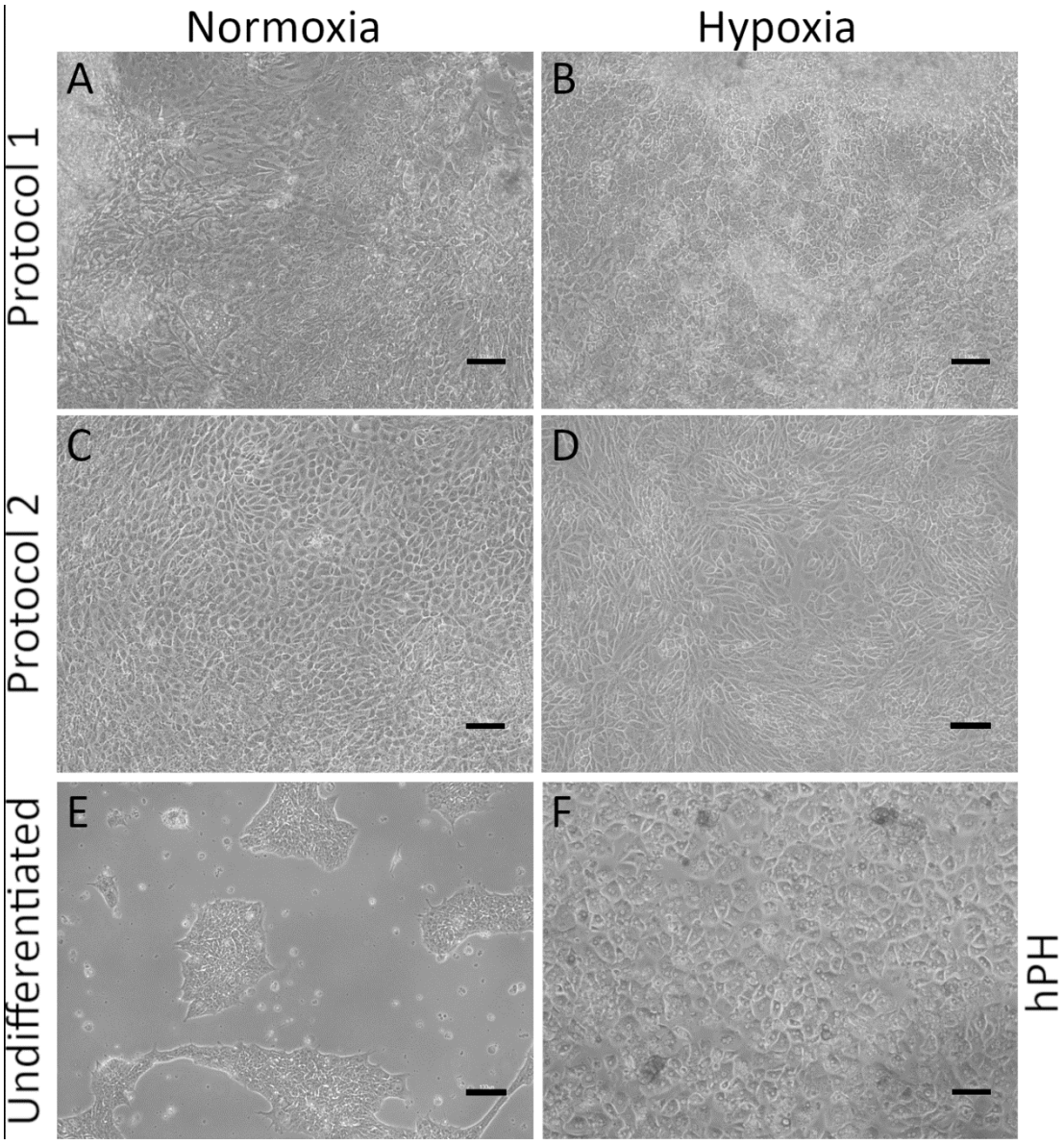

Figure 5

Micrographs of iPSC-HLCs differentiated using protocol 1 & 2 under normoxic and hypoxic conditions show differences in morphology – (A) iPSC-HLCs differentiated using protocol 1, normoxia. **(B)** iPSC-HLCs differentiated using protocol 1, hypoxia. **(C)** iPSC-HLCs differentiated using protocol 2, normoxia. **(D)** iPSC-HLCs differentiated using protocol 2, hypoxia. **(E)** undifferentiated iPSCs in normoxic conditions, though the morphology does not change when cultured under hypoxic conditions. **(F)** hPH 24-hours after isolation in 2D culture show characteristic polygonal morphology and multinucleate cells.

Scale bars are 100 µm. Polygonal morphology is apparent in panels B-D but not in panel A. iPSC-HLCs in panels A-D are smaller than hPH in Panel F. Abbreviations: hPH – human primary hepatocytes

3.2.5 Hierarchical clustering analysis (HCA)

HCA was performed using Partek, the results of this analysis are shown in Figure 7 in which each bar represents a single protein and each column represents a single sample. Figure 7 is colour coded, green bars indicate downregulation and red bars indicate upregulation relative to a pooled control of all samples in the iTRAQ run. In the labelling of this figure, protocol 1 and 2 are abbreviated to 'Hes' and 'Sill', normoxia and hypoxia are abbreviated to 'Norm' and 'Hypo', respectively. The dendrogram shows how closely each sample is related with shorter branches representing more similar samples.

hPH cluster strongly together and are also highly separated from all other samples. 'Sil_norm_1' and 'Sil_norm_2' cluster most closely to iPSCs out of all samples though all other iPSC-HLCs cluster shortly thereafter except for 'Hes_hypo_2' and 'Hes_hypo_3' which cluster together and away from all other iPSC-HLC lines. From these data it is apparent that iPSC-HLCs have diverged from iPSCs but still cluster more closely to them than to HLCs.

3.2.6 Principal component analysis

PCA was performed on the dataset using Partek, the results of which are shown in Figure 8. The three principal components shown in Figure 8 account for 60.6% of the variability of the data with 33.1% assigned to PC1, 16.8% assigned to PC2 and 10.7% assigned to PC3. Similarly to HCA (Figure 7), iPSCs are separated from hPH and iPSC-HLCs along PC1, hPH separate from iPSC-HLCs mainly along PC2 and PC3 and iPSC-HLCs tend to cluster more closely with one another. As shown in the HCA, 2 data points from 'Hes hypo' separate from the majority of other iPSC-HLCs.

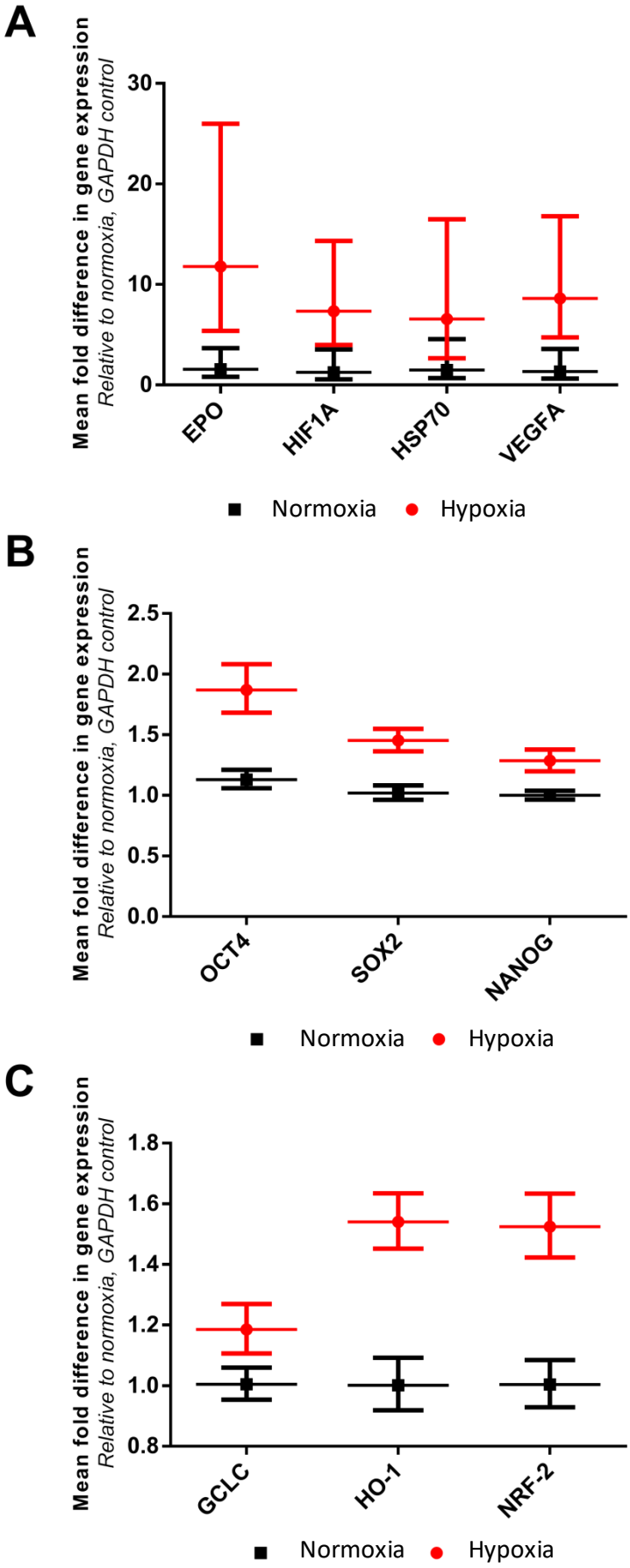

Figure 6

qPCR analysis of Liv4FA iPSCs cultured under normoxic and hypoxic conditions – **(A)** Change in expression of hypoxia inducible genes EPO, HIF1A, HSP70, VEGFA. **(B)** Change in pluripotency associated genes OCT4 SOX2 NANOG. **(C)** Change in expression of NRF-2 pathway related genes GCLC HO-1, NRF-2.

Cells were cultured under hypoxic or normoxic conditions for at least three passages prior to experimentation to allow acclimatisation. qPCR completed using SYBR green chemistry. All panels use Liv4FA iPSCs (Table 4). Graphs show mean fold difference in gene expression. Fold difference was calculated using the $2^{-\Delta\Delta CT}$ method according to Livak and Schmittgen (2001) fold differences are relative to iPSCs cultured under normoxic conditions and normalised to GAPDH. Data points show mean fold difference, error bars denote error calculated as per the $2^{-\Delta\Delta CT}$ method. Asterisks (*) indicate significant differences, tested using an unpaired, two-tailed Student's t-test. Increased number of asterisks denotes smaller p-values, * = ≤ 0.05, ** = ≤ 0.01, *** = ≤ 0.001. n=3

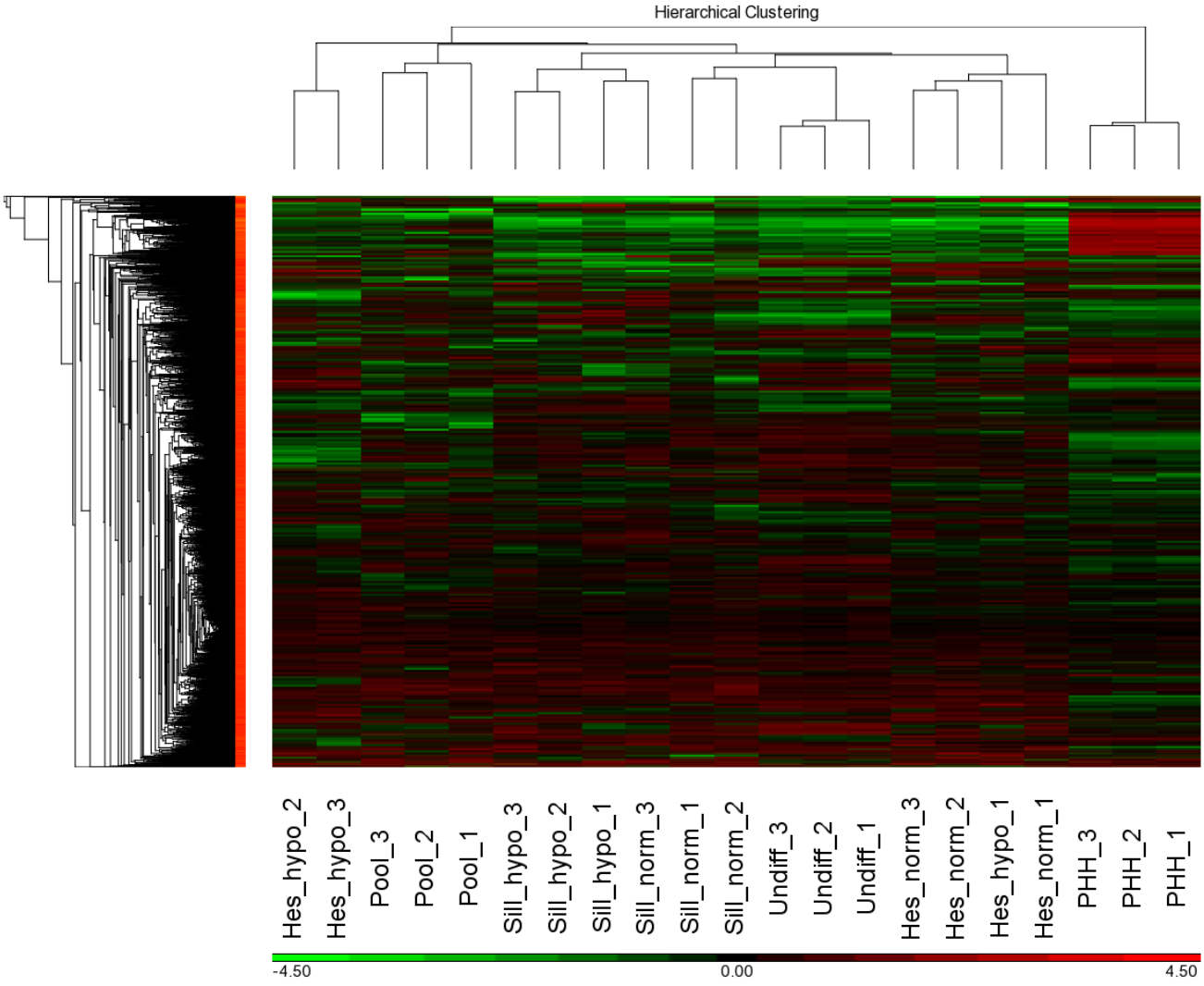

Figure 7

Hierarchical clustering analysis of iPSC-HLCs differentiated using protocol 1 & 2 under normoxic and hypoxic conditions – Hierarchical clustering analysis performed using Partek. Data pooled from three separate experimental runs. Green bars indicate downregulation compared to a pooled control, red bars represent upregulation. The dendrogram indicates how closely each sample clusters with shorter branches indicating greater similarity. Samples names refer to the following conditions: Hes_norm – Protocol 1, normoxic conditions; Hes_hypo – protocol 1, hypoxic conditions; Sil_norm – protocol 2, normoxic conditions; Sil_hypo – protocol 2, hypoxic condition; Undif – Undifferentiated iPSCs; PHH – Pooled primary human hepatocytes; Pool – technical iTRAQ pool, duplicate sample of pooled control used to normalise data.

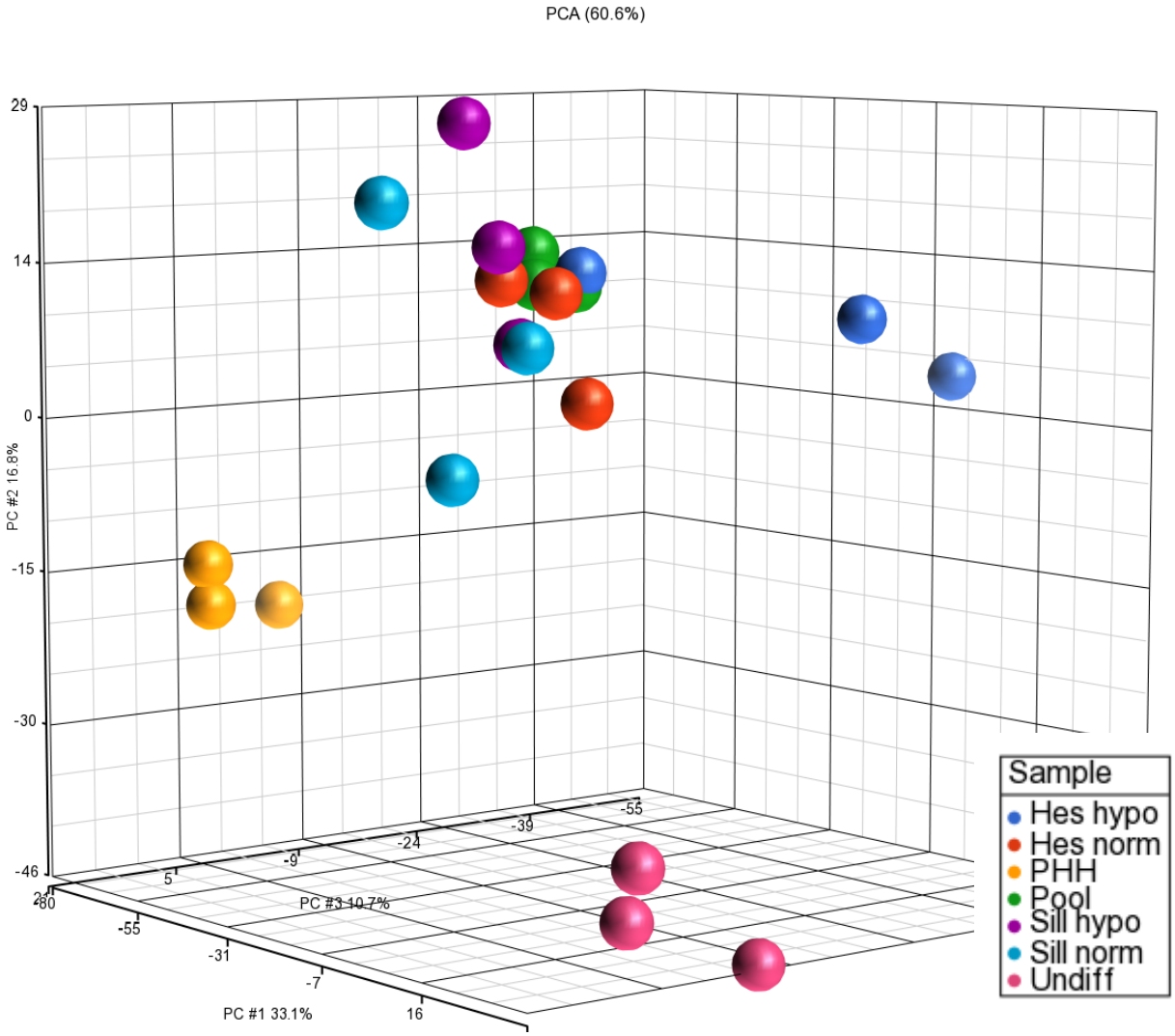

Figure 8

Principal component analysis of iPSC-HLCs differentiated using protocol 1 & 2 under normoxic and hypoxic conditions – Principle component analysis performed using Partek. Data pooled from three separate experimental runs. PC1 accounts for 33.1% of the variability, PC2 accounts for 16.8% of the variability, PC3 accounts for 10.7% of the variability. Samples are colour-coded ad show in the figure legend. Samples names in the figure legend refer to the following conditions: Hes norm – Protocol 1, normoxic conditions; Hes hypo – protocol 1, hypoxic condtions; Sil norm – protocol 2, normoxic conditions; Sil hypo – protocol 2, hypoxic condition; Undiff – Undifferentiated iPSCs; PHH – Pooled primary human hepatocytes; Pool – technical iTRAQ pool, duplicate sample of pooled control used to normalise data.

3.2.7 Liver-specific genes

Three lists of liver-specific genes were compiled based on the detected proteins in the iTRAQ analyses, categorised as either 'CYPs', 'Phase II' or 'Transporters'. The dataset was interrogated for expression of these genes which were plotted on bar charts (Figure 9-14). In each case, blue bars represent non-significant changes ($p>0.05$), whilst red bars indicate significant changes ($p \leq 0.05$) as determined by ANOVA, using Partek. Positive fold differences indicate higher expression in the first comparator. A complete list of the proteins in each group, abbreviations used, exact values and associated significance (shown in Figure 9-14) are tabulated in Appendix 1 (page 235).

3.2.7.1 Cytochromes P450

Figure 9 shows protein expression of CYPs in iPSC-HLCs differentiated according to protocol 1. Figure 9A and Figure 9B show CYP expression in iPSC-HLCs differentiated in normoxia and hypoxia respectively, compared to iPSCs. In both cases, all CYPs except CYP2S1 are upregulated. In Figure 9A all changes were significant except for CYP4A11 and CYP2D6. In Figure 9B all the changes shown were significant except for CYP2A6. Figure 9C and Figure 9D show CYP expression in iPSC-HLCs differentiated in normoxia and hypoxia respectively, compared to hPH, expression of all CYPs was significantly higher in hPH except for CYP 2S1 which was not significantly different. Figure 9E shows a comparison of iPSC-HLCs differentiated under normoxia and hypoxia. CYP2D6 was significantly higher in hypoxia whilst CYP2A6 was significantly higher in normoxia. All other proteins were non-significantly increased in iPSC-HLCs differentiated in hypoxia, except CYP3A4 which was non-significantly increased in normoxia.

Figure 10 shows the CYP expression profile of iPSC-HLCs differentiated using protocol 2 normoxia and hypoxia. Figure 10A and Figure 10B show iPSC-HLCs differentiated in normoxia and hypoxia respectively, versus iPSCs. In both graphs all proteins are significantly upregulated in iPSC-HLCs, except CYP2S1 which is significantly downregulated. Figure 10C and Figure 10D shows the same iPSC-HLCs compared to hPH. In this case, all the proteins are significantly lower than in hPH except for CYP2S1 which, in Figure 10C is non-significantly higher in iPSC-HLCs and in Figure 10D, is significantly increased. Figure 10E shows a comparison of CYP expression between iPSC-HLCs differentiated using protocol 2 under normal and hypoxic conditions. All proteins are non-significantly increased in normoxic conditions except CYP2S1 which is significantly decreased.

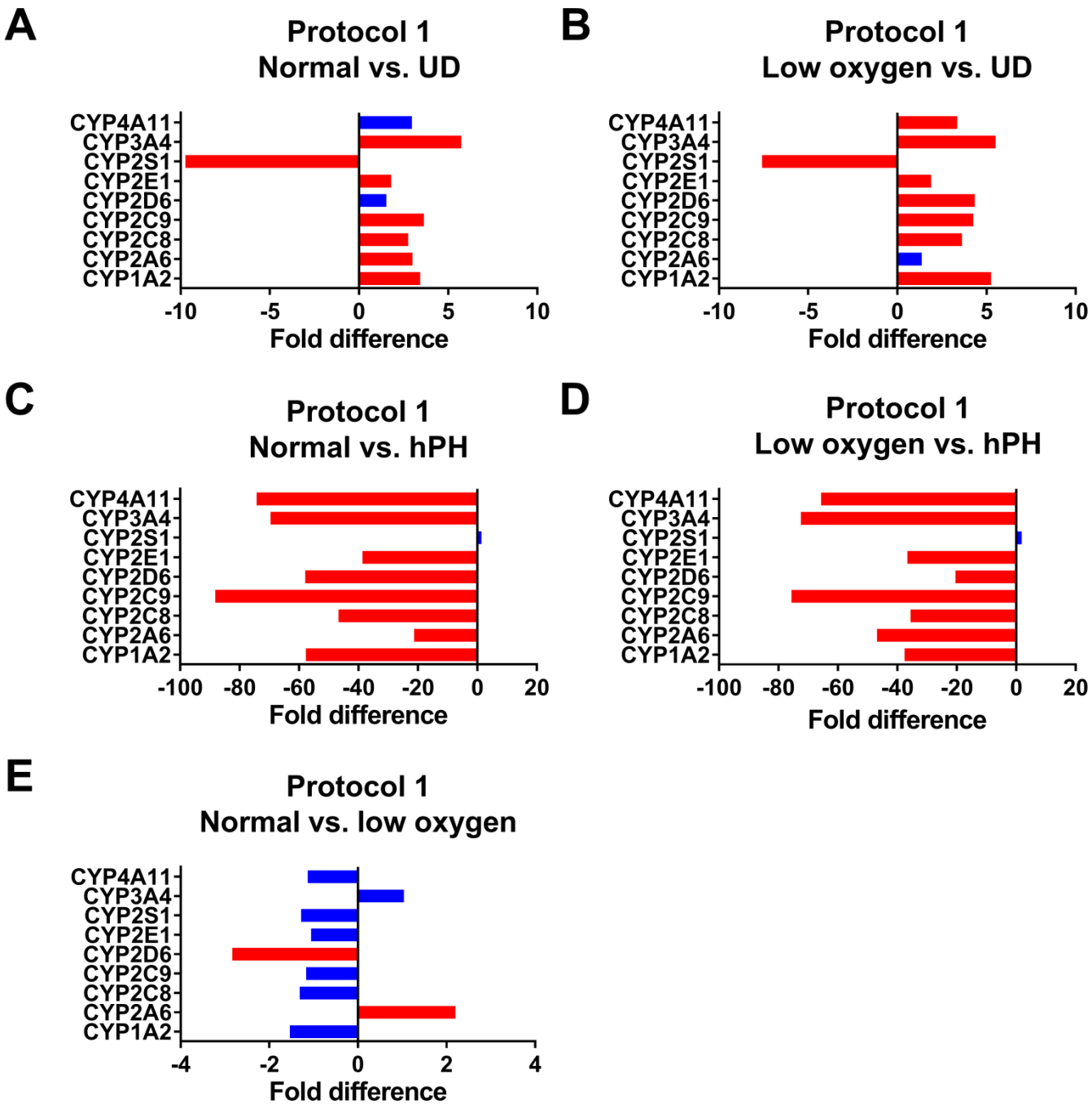

Figure 9

Cytochromes P450 expression in iPSC-HLCs differentiated using protocol 1 - (A) Normoxic iPSC-HLCs versus UD. **(B)** Hypoxic iPSC-HLCs versus UD. **(C)** Normoxic iPSC-HLCs versus hPH. **(D)** Hypoxic iPSC-HLCs versus hPH. **(E)** Normoxic iPSC-HLCs versus hypoxic iPSC-HLCs.

Graphs showing the fold difference in CYP expression in iPSC-HLCs differentiated using protocol 1, analysed by iTRAQ. Positive values indicate higher expression in the first comparator, bars in red show significant changes $p \leq 0.05$ determined by ANOVA blue bars are non-significant. Exact values for these changes, and associated significance are shown in Appendix 1. Abbreviations: UD – undifferentiated iPSCs, hPH – human primary hepatocytes, CYP – Cytochrome P450, iPSC-HLCs – induced pluripotent stem cell-derived hepatocyte-like cells.

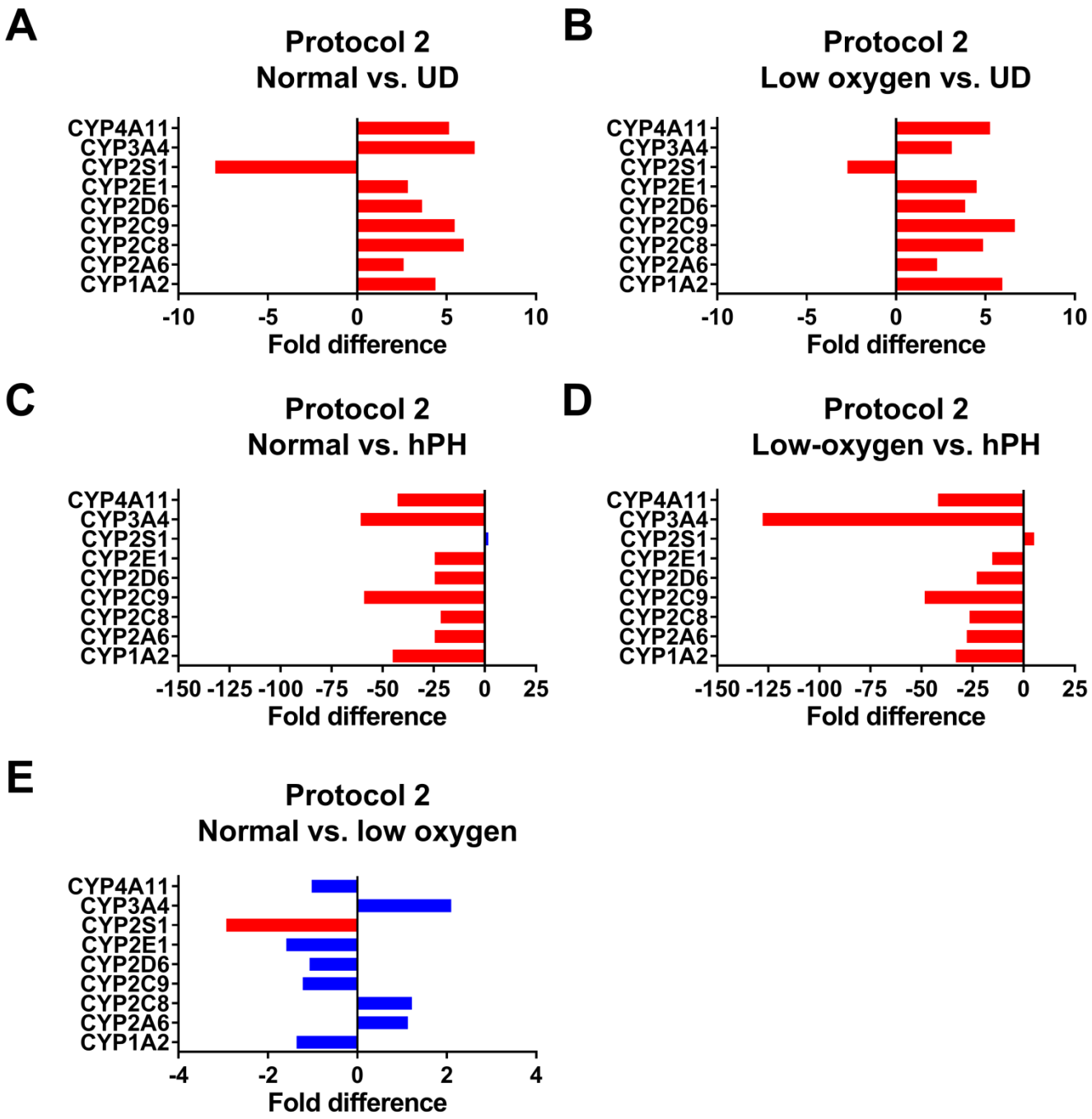

Figure 10

Cytochromes P450 expression in iPSC-HLCs differentiated using protocol 2 - (A) Normoxic iPSC-HLCs versus UD. **(B)** Hypoxic iPSC-HLCs versus UD. **(C)** Normoxic iPSC-HLCs versus hPH. **(D)** Hypoxic iPSC-HLCs versus hPH. **(E)** Normoxic iPSC-HLCs versus hypoxic iPSC-HLCs.

Graphs showing the fold difference in CYP expression in iPSC-HLCs differentiated using protocol 2, analysed by iTRAQ. Positive values indicate higher expression in the first comparator, bars in red show significant changes $p \leq 0.05$ determined by ANOVA blue bars are non-significant. Exact values for these changes, and associated significance are shown in Appendix 1. Abbreviations: UD – undifferentiated iPSCs, hPH – human primary hepatocytes, CYP – Cytochrome P450, iPSC-HLCs – induced pluripotent stem cell-derived hepatocyte-like cells.

3.2.7.2 Phase II metabolism

Figure 11 shows the phase II metabolism phenotype of iPSC-HLCs differentiated using protocol 1. Figure 11A and Figure 11B show normoxic and hypoxic iPSC-HLCs versus undifferentiated iPSCs. In Figure 11A UGT2B7, UGT2B10, UGT1A6, SULT1A1, MGST3, GSTO1, GSTK1, GSTA2 and COMT are all significantly higher in iPSC-HLCs, other changes are non-significant. In Figure 11B, UGT2B7, UGT2B10, SULT1A1, GSTO1, GSTK1, COMT and CAT are all significantly higher in iPSC-HLCs whilst GSTP1 is higher in iPSCs, other changes are non-significant. Figure 11C and Figure 11D show normoxic and hypoxic iPSC-HLCs respectively, versus hPH. In Figure 11C, all proteins were significantly higher in hPH except for GSTP1, which was significantly higher in iPSC-HLCs and NQO1, MGST3, GSTM3 and GSTM2 which were not significantly different. In Figure 11D, all genes were significantly higher in hPH except for GSTP1 and NQO1, which were significantly higher in iPSC-HLCs. MGST3, GSTM2 and GSTM3 were not significantly different. Figure 11E shows the comparison of phase II metabolism phenotype between normoxia and hypoxia. UGT1A4 is significantly higher in hypoxia whilst GSTK1 is significantly higher in normoxia, other changes were non-significant.

Figure 12 shows the phase II metabolism phenotype of iPSC-HLCs differentiated using protocol 2. Figure 12A and Figure 12B show normoxic and hypoxic iPSC-HLCs respectively, versus iPSCs. In Figure 12A, UGT2B7, UGT2B10, SULT1A1, GSTO1, GSTM2, GSTM3, GSTK1 and COMT are all significantly higher in iPSC-HLCs, other changes are non-significant. In Figure 12B, UGT2B7, UGT2B10, SULT1A1, MGST3, GSTO1, GSTM3, GSTK1 and COMT are all significantly higher in iPSC-HLCs, NQO1 and GSTP1 are significantly higher in iPSCs, other changes are non-significant. Figure 12C and Figure 12D show normoxic and hypoxic iPSC-HLCs respectively, versus hPH. In Figure 12C, all proteins were significantly higher in hPH, except for GSTP1, GSTM2 and GSTM3 which were significantly higher in iPSC-HLCs and NQO1 and MGST3 which were not significantly different. In Figure 12D, all proteins were significantly higher in hPH except for GSTP1 and GSTM3 which were significantly higher in iPSC-HLCs and NQO1, MGST3 and GSTM2 which were not significantly changed. Figure 12E shows the comparison in phase II metabolism enzymes between normoxia and hypoxia. SULT1A1 and GSTM2 are significantly higher in normoxia, other changes were not significant.

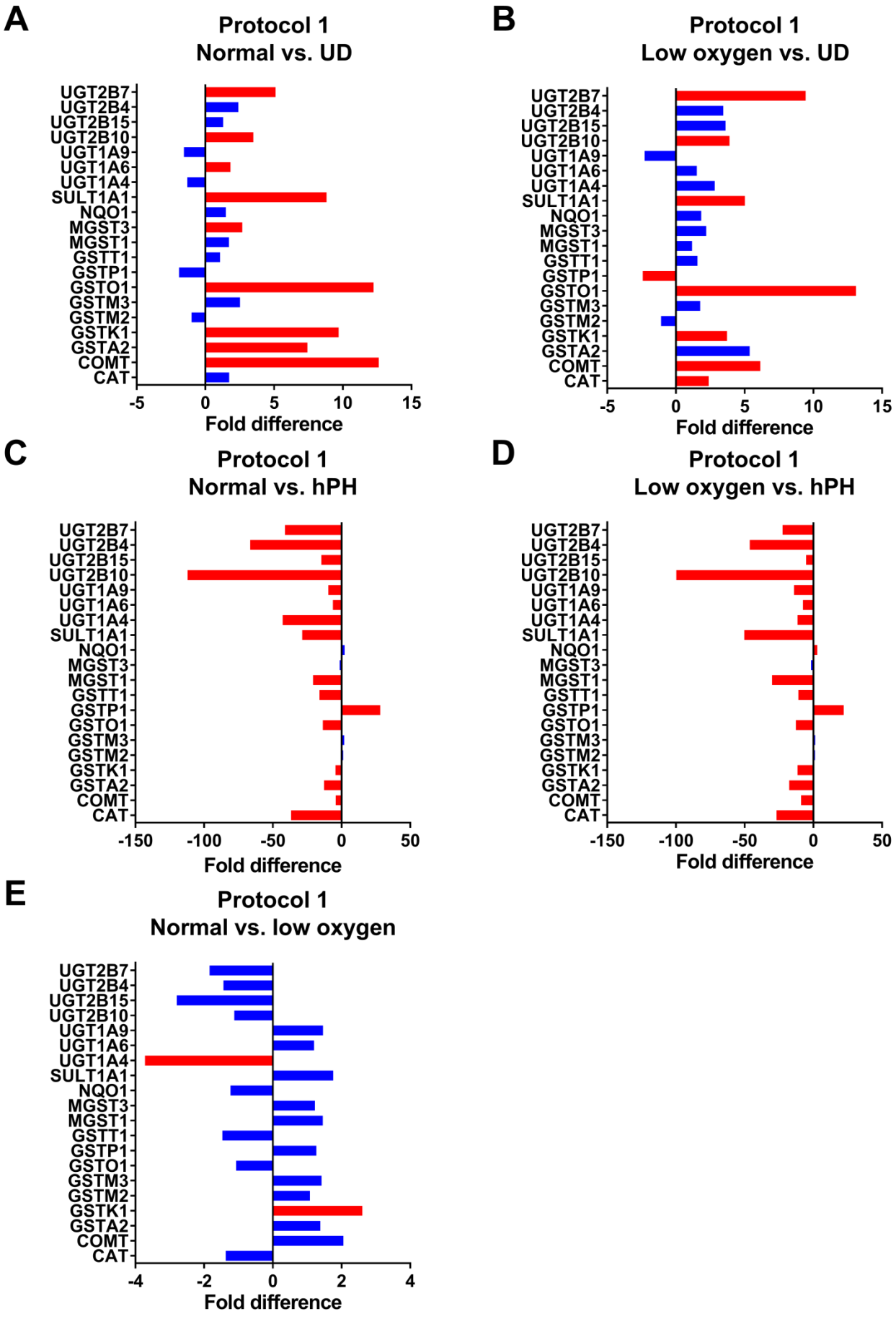
A
Protocol 1
Normal vs. UD
UGT2B7
UGT2B4
UGT2B15
UGT2B10
UGT1A9
UGT1A6
UGT1A4
SULT1A1
NQO1
MGST3
MGST1
GSTT1
GSTP1
GSTO1
GSTM3
GSTM2
GSTK1
GSTA2
COMT
CAT
-5
0
5
10
15
Fold difference
B
Protocol 1
Low oxygen vs. UD
UGT2B7
UGT2B4
UGT2B15
UGT2B10
UGT1A9
UGT1A6
UGT1A4
SULT1A1
NQO1
MGST3
MGST1
GSTT1
GSTP1
GSTO1
GSTM3
GSTM2
GSTK1
GSTA2
COMT
CAT
-5
0
5
10
15
Fold difference
C
Protocol 1
Normal vs. hPH
UGT2B7
UGT2B4
UGT2B15
UGT2B10
UGT1A9
UGT1A6
UGT1A4
SULT1A1
NQO1
MGST3
MGST1
GSTT1
GSTP1
GSTO1
GSTM3
GSTM2
GSTK1
GSTA2
COMT
CAT
-150
-100
-50
0
50
Fold difference
D
Protocol 1
Low oxygen vs. hPH
UGT2B7
UGT2B4
UGT2B15
UGT2B10
UGT1A9
UGT1A6
UGT1A4
SULT1A1
NQO1
MGST3
MGST1
GSTT1
GSTP1
GSTO1
GSTM3
GSTM2
GSTK1
GSTA2
COMT
CAT
-150
-100
-50
0
50
Fold difference
E
Protocol 1
Normal vs. low oxygen
UGT2B7
UGT2B4
UGT2B15
UGT2B10
UGT1A9
UGT1A6
UGT1A4
SULT1A1
NQO1
MGST3
MGST1
GSTT1
GSTP1
GSTO1
GSTM3
GSTM2
GSTK1
GSTA2
COMT
CAT
-4
-2
0
2
4
Fold difference

Figure 11

Phase II enzyme expression in iPSC-HLCs differentiated using protocol 1 -- (A) Normoxic iPSC-HLCs versus UD. **(B)** Hypoxic iPSC-HLCs versus UD. **(C)** Normoxic iPSC-HLCs versus hPH. **(D)** Hypoxic iPSC-HLCs versus hPH. **(E)** Normoxic iPSC-HLCs versus hypoxic iPSC-HLCs.

Graphs showing the fold difference in Phase II enzyme expression in iPSC-HLCs differentiated using protocol 1, analysed by iTRAQ. Positive values indicate higher expression in the first comparator, bars in red show significant changes $p \leq 0.05$ determined by ANOVA blue bars are non-significant. Exact values for these changes, and associated significance are shown in Appendix 1. Abbreviations: UD – undifferentiated iPSCs, hPH – human primary hepatocytes, iPSC-HLCs – induced pluripotent stem cell-derived hepatocyte-like cells, UGT - Uridine 5'-diphospho-glucuronosyltransferase, SULT - Sulfotransferase, NQO - NAD(P)H dehydrogenase [quinone] 1, MGST - Microsomal glutathione S-transferase, GST - Glutathione S transferase, COMT - Catechol O methyl transferase, CAT - Catalase

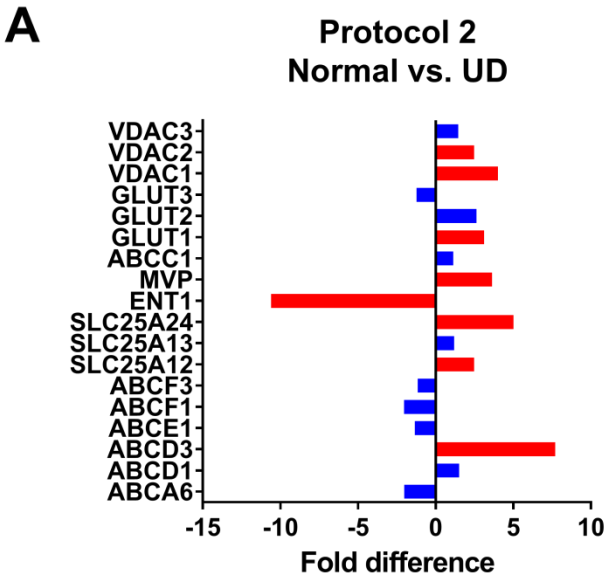
A
Protocol 2
Normal vs. UD
VDAC3
VDAC2
VDAC1
GLUT3
GLUT2
GLUT1
ABCC1
MVP
ENT1
SLC25A24
SLC25A13
SLC25A12
ABCF3
ABCF1
ABCE1
ABCD3
ABCD1
ABCA6
-15 -10 -5 0 5 10
Fold difference

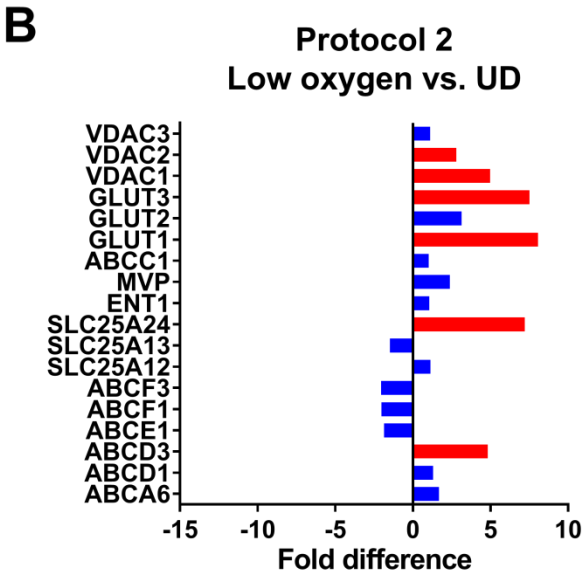
B
Protocol 2
Low oxygen vs. UD
VDAC3
VDAC2
VDAC1
GLUT3
GLUT2
GLUT1
ABCC1
MVP
ENT1
SLC25A24
SLC25A13
SLC25A12
ABCF3
ABCF1
ABCE1
ABCD3
ABCD1
ABCA6
-15 -10 -5 0 5 10
Fold difference

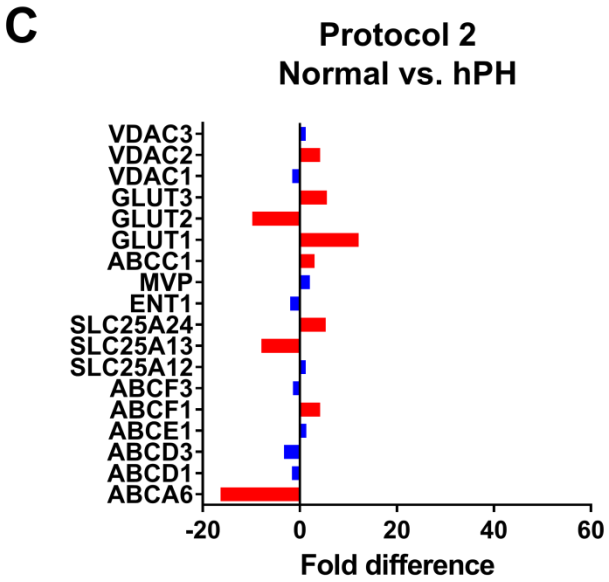
C
Protocol 2
Normal vs. hPH
VDAC3
VDAC2
VDAC1
GLUT3
GLUT2
GLUT1
ABCC1
MVP
ENT1
SLC25A24
SLC25A13
SLC25A12
ABCF3
ABCF1
ABCE1
ABCD3
ABCD1
ABCA6
-20 0 20 40 60
Fold difference

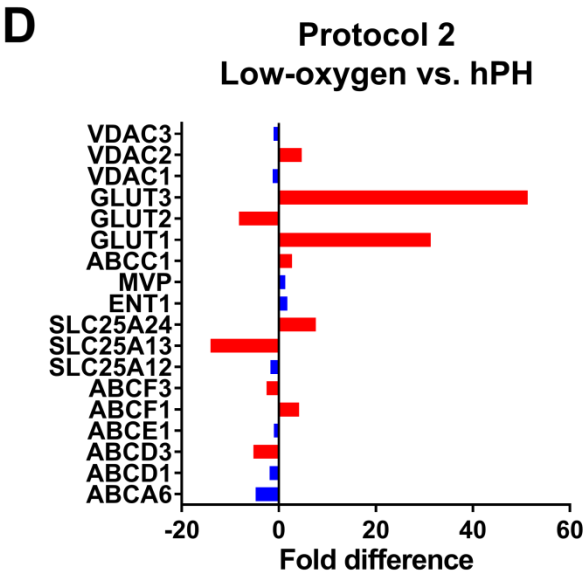
D
Protocol 2
Low-oxygen vs. hPH
VDAC3
VDAC2
VDAC1
GLUT3
GLUT2
GLUT1
ABCC1
MVP
ENT1
SLC25A24
SLC25A13
SLC25A12
ABCF3
ABCF1
ABCE1
ABCD3
ABCD1
ABCA6
-20 0 20 40 60
Fold difference

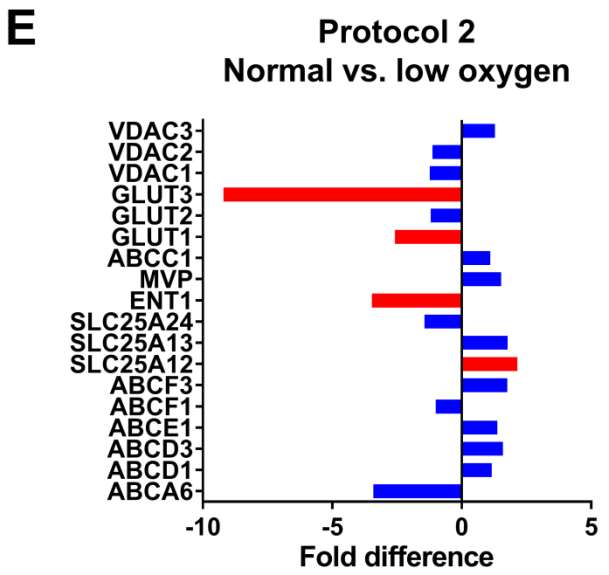
E
Protocol 2
Normal vs. low oxygen
VDAC3
VDAC2
VDAC1
GLUT3
GLUT2
GLUT1
ABCC1
MVP
ENT1
SLC25A24
SLC25A13
SLC25A12
ABCF3
ABCF1
ABCE1
ABCD3
ABCD1
ABCA6
-10 -5 0 5
Fold difference

Figure 12

Phase II enzyme expression in iPSC-HLCs differentiated using protocol 2 - **(A)** Normoxic iPSC-HLCs versus UD. **(B)** Hypoxic iPSC-HLCs versus UD. **(C)** Normoxic iPSC-HLCs versus hPH. **(D)** Hypoxic iPSC-HLCs versus hPH. **(E)** Normoxic iPSC-HLCs versus hypoxic iPSC-HLCs.

Graphs showing the fold difference in Phase II enzyme expression in iPSC-HLCs differentiated using protocol 2, analysed by iTRAQ. Positive values indicate higher expression in the first comparator, bars in red show significant changes $p \leq 0.05$ determined by ANOVA blue bars are non-significant. Exact values for these changes, and associated significance are shown in Appendix 1. Abbreviations: UD – undifferentiated iPSCs, hPH – human primary hepatocytes, iPSC-HLCs – induced pluripotent stem cell-derived hepatocyte-like cells, UGT - Uridine 5'-diphospho-glucuronosyltransferase, SULT - Sulfotransferase, NQO - NAD(P)H dehydrogenase [quinone] 1, MGST - Microsomal glutathione S-transferase, GST - Glutathione S transferase, COMT - Catechol O methyl transferase, CAT - Catalase

3.2.7.3 Transporters

Figure 13 shows transporter expression in iPSC-HLCs differentiated using protocol 1. Figure 13A and Figure 13B show the comparison of iPSC-HLCs differentiated in normoxia and hypoxia respectively versus iPSCs. In Figure 13A, VDAC1, VDAC2, GLUT1, MVP, SLC25A24, ABCD3 and ABCD1 are all significantly upregulated, whilst ENT1 is significantly downregulated, all remaining changes were non-significant. In Figure 13B, VDAC1, VDAC2, VDAC3, GLUT3, MVP and SLC25A24 are significantly upregulated and ENT1 and ABCF1 are significantly downregulated, all remaining changes were non-significant. Figure 13C and Figure 13D show the comparison iPSC-HLCs differentiated in normoxia and hypoxia respectively, versus hPH. In Figure 13C VDAC2, GLUT3, GLUT1, ABCC1, MVP, SLC25A24 and ABCF1 are significantly increased and GLUT2, SLC25A13 and ABCA6 are significantly decreased, all other changes are non-significant. In Figure 13D, VDAC2, VDAC3, GLUT1, GLUT3, MVP, SLC25A24 and ABCF1 are significantly upregulated and GLUT2, SLC25A13 and ABCD3 are significantly downregulated, all other changes were non-significant. Figure 13E shows the comparison of transporter phenotype between cells differentiated in normoxia and hypoxia. VDAC2 and VDAC3 are significantly higher in hypoxia and ABCD3 is significantly higher in normoxia, all other proteins were not significantly changed.

Figure 14 shows transporter expression in iPSC-HLCs differentiated using protocol 2. Figure 14A and Figure 14B show the comparison of iPSC-HLCs differentiated in normoxia and hypoxia respectively, versus iPSCs. In Figure 14A VDAC1, VDAC2, GLUT1, MVP, SLC25A24, SLC25A12 and ABCD3 are significantly higher in iPSC-HLCs. ENT1 is significantly higher in iPSCs, remaining changes are non-significant. In Figure 14B VDAC1, VDAC2, GLUT1, GLUT3, SLC25A24 and ABCD3 were all significantly higher in iPSC-HLCs, no other changes were significant. Figure 14C and Figure 14D show the comparison of iPSC-HLCs in normoxia and hypoxia respectively versus hPH. In Figure 14C, VDAC2, GLUT1, GLUT3, ABCC1 and ABCF1 were all significantly higher in iPSC-HLCs. GLUT2, SLC25A24 and ABCA6 were all significantly higher in hPH, other changes were non-significant. In Figure 14D, VDAC2, GLUT1, GLUT3, ABCC1, SLC25A24 and ABCF1 are significantly higher in iPSC-HLCs. GLUT2, SLC25A13, ABCF3 and ABCD3 were all significantly higher in hPH, remaining changes were non-significant. Figure 14E shows a comparison of the transporter phenotype between normoxic and hypoxic iPSC-HLCs. SLC25A12 is significantly higher in normoxic conditions whilst GLUT1, GLUT3 and ENT1 are significantly higher under hypoxic conditions, remaining changes are non-significant.

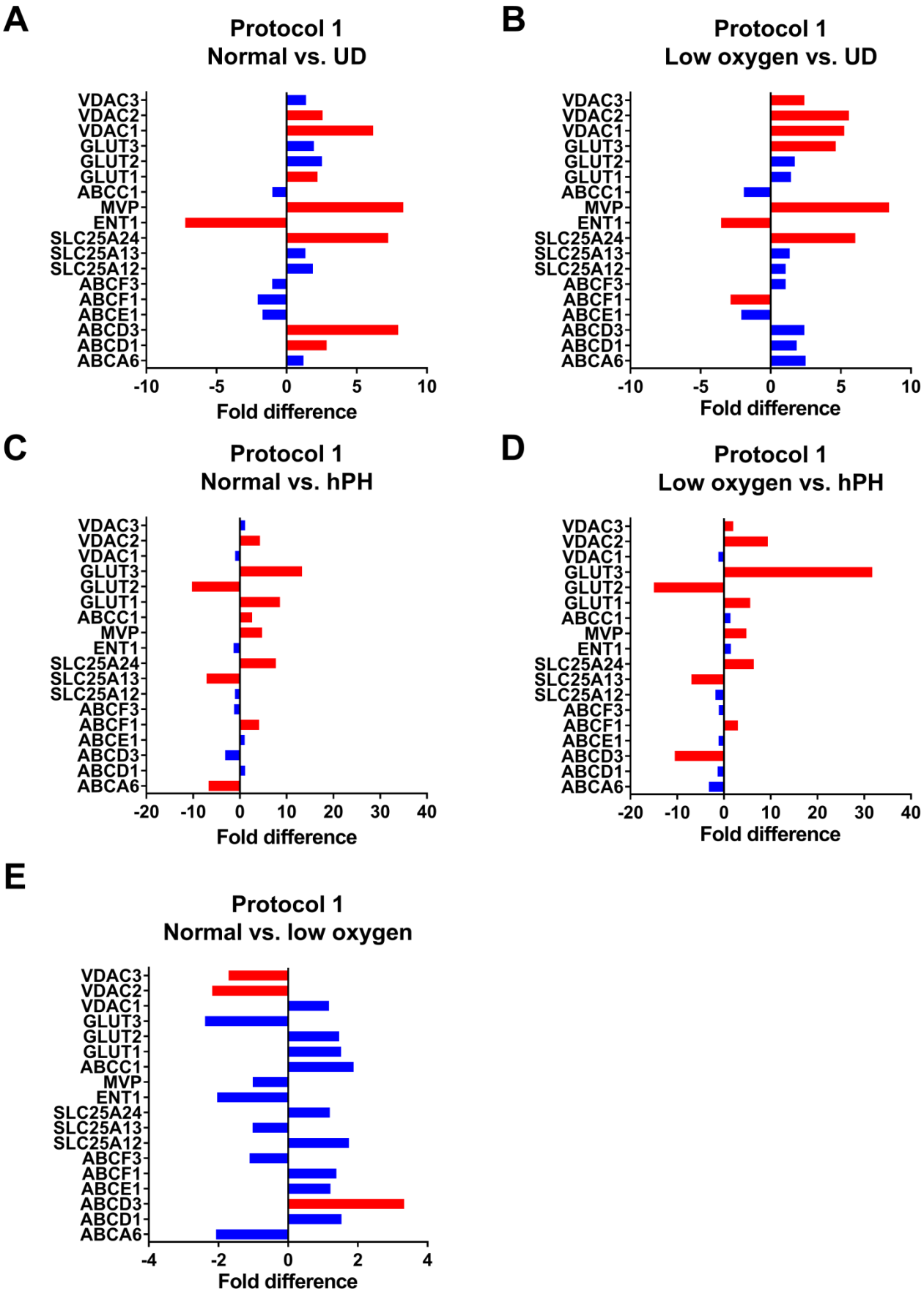
A
Protocol 1
Normal vs. UD
VDAC3
VDAC2
VDAC1
GLUT3
GLUT2
GLUT1
ABCC1
MVP
ENT1
SLC25A24
SLC25A13
SLC25A12
ABCF3
ABCF1
ABCE1
ABCD3
ABCD1
ABCA6
-10 -5 0 5 10
Fold difference
B
Protocol 1
Low oxygen vs. UD
VDAC3
VDAC2
VDAC1
GLUT3
GLUT2
GLUT1
ABCC1
MVP
ENT1
SLC25A24
SLC25A13
SLC25A12
ABCF3
ABCF1
ABCE1
ABCD3
ABCD1
ABCA6
-10 -5 0 5 10
Fold difference
C
Protocol 1
Normal vs. hPH
VDAC3
VDAC2
VDAC1
GLUT3
GLUT2
GLUT1
ABCC1
MVP
ENT1
SLC25A24
SLC25A13
SLC25A12
ABCF3
ABCF1
ABCE1
ABCD3
ABCD1
ABCA6
-20 -10 0 10 20 30 40
Fold difference
D
Protocol 1
Low oxygen vs. hPH
VDAC3
VDAC2
VDAC1
GLUT3
GLUT2
GLUT1
ABCC1
MVP
ENT1
SLC25A24
SLC25A13
SLC25A12
ABCF3
ABCF1
ABCE1
ABCD3
ABCD1
ABCA6
-20 -10 0 10 20 30 40
Fold difference
E
Protocol 1
Normal vs. low oxygen
VDAC3
VDAC2
VDAC1
GLUT3
GLUT2
GLUT1
ABCC1
MVP
ENT1
SLC25A24
SLC25A13
SLC25A12
ABCF3
ABCF1
ABCE1
ABCD3
ABCD1
ABCA6
-4 -2 0 2 4
Fold difference

Figure 13

Transporter expression in iPSC-HLCs differentiated using protocol 1 - (A) Normoxic iPSC-HLCs versus UD. **(B)** Hypoxic iPSC-HLCs versus UD. **(C)** Normoxic iPSC-HLCs versus hPH. **(D)** Hypoxic iPSC-HLCs versus hPH. **(E)** Normoxic iPSC-HLCs versus hypoxic iPSC-HLCs.

Graphs showing the fold difference in transporter expression in iPSC-HLCs differentiated using protocol 1, analysed by iTRAQ. Positive values indicate higher expression in the first comparator, bars in red show significant changes $p \leq 0.05$ determined by ANOVA blue bars are non-significant. Exact values for these changes, and associated significance are shown in Appendix 1. Abbreviations: UD – undifferentiated iPSCs, hPH – human primary hepatocytes, iPSC-HLCs – induced pluripotent stem cell-derived hepatocyte-like cells, VDAC - Voltage dependent anion channel, GLUT - Glucose transporter, ABC - ABC transporter, MVP - Major vault protein, ENT - Equilibrative nucleoside transporter, SLC - Solute carrier

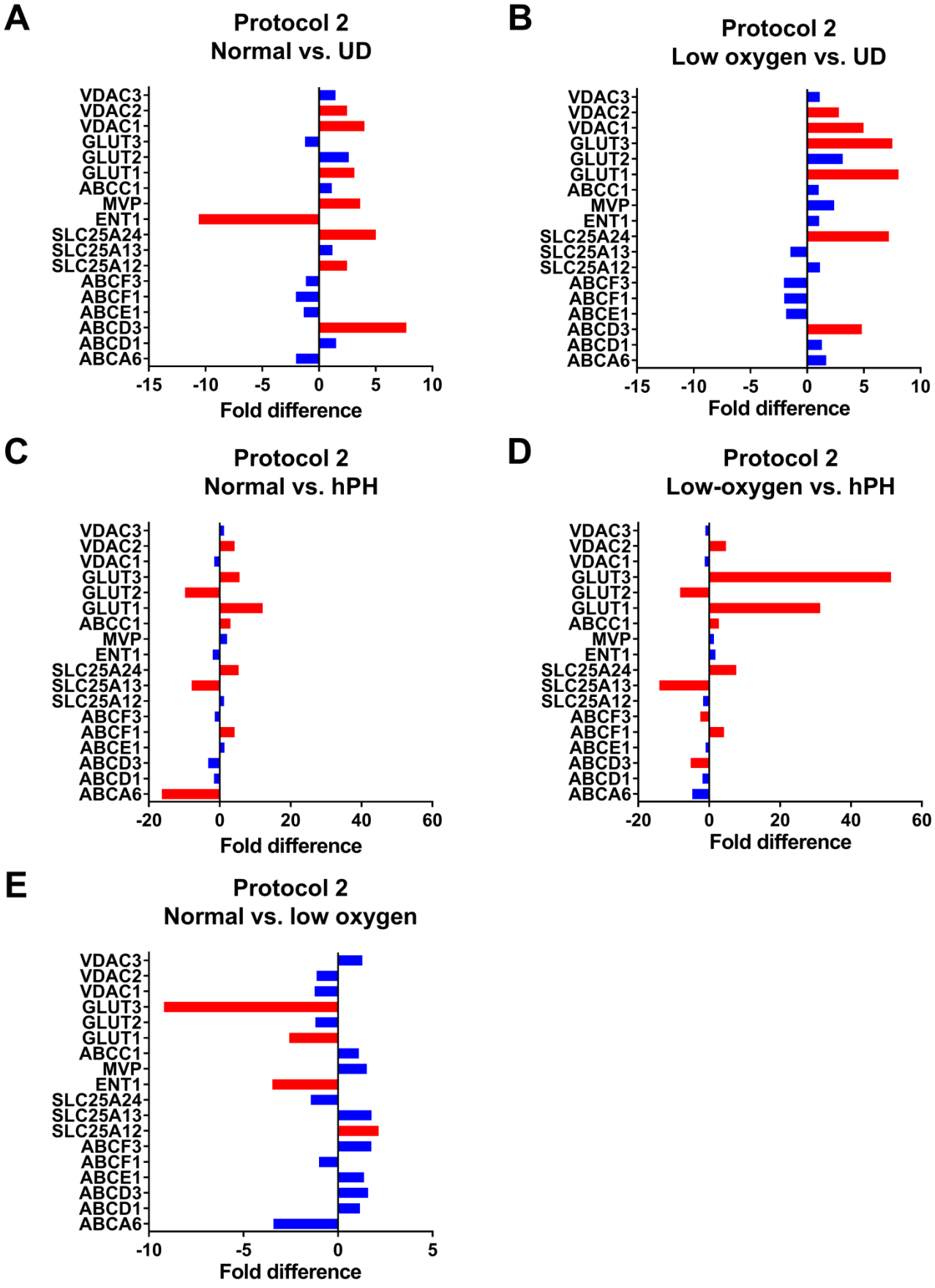
A
Protocol 2
Normal vs. UD
VDAC3
VDAC2
VDAC1
GLUT3
GLUT2
GLUT1
ABCC1
MVP
ENT1
SLC25A24
SLC25A13
SLC25A12
ABCF3
ABCF1
ABCE1
ABCD3
ABCD1
ABCA6
-15 -10 -5 0 5 10
Fold difference
B
Protocol 2
Low oxygen vs. UD
VDAC3
VDAC2
VDAC1
GLUT3
GLUT2
GLUT1
ABCC1
MVP
ENT1
SLC25A24
SLC25A13
SLC25A12
ABCF3
ABCF1
ABCE1
ABCD3
ABCD1
ABCA6
-15 -10 -5 0 5 10
Fold difference
C
Protocol 2
Normal vs. hPH
VDAC3
VDAC2
VDAC1
GLUT3
GLUT2
GLUT1
ABCC1
MVP
ENT1
SLC25A24
SLC25A13
SLC25A12
ABCF3
ABCF1
ABCE1
ABCD3
ABCD1
ABCA6
-20 0 20 40 60
Fold difference
D
Protocol 2
Low-oxygen vs. hPH
VDAC3
VDAC2
VDAC1
GLUT3
GLUT2
GLUT1
ABCC1
MVP
ENT1
SLC25A24
SLC25A13
SLC25A12
ABCF3
ABCF1
ABCE1
ABCD3
ABCD1
ABCA6
-20 0 20 40 60
Fold difference
E
Protocol 2
Normal vs. low oxygen
VDAC3
VDAC2
VDAC1
GLUT3
GLUT2
GLUT1
ABCC1
MVP
ENT1
SLC25A24
SLC25A13
SLC25A12
ABCF3
ABCF1
ABCE1
ABCD3
ABCD1
ABCA6
-10 -5 0 5
Fold difference

Figure 14

Transporter expression in iPSC-HLCs differentiated using protocol 2 - **(A)** Normoxic iPSC-HLCs versus UD. **(B)** Hypoxic iPSC-HLCs versus UD. **(C)** Normoxic iPSC-HLCs versus hPH. **(D)** Hypoxic iPSC-HLCs versus hPH. **(E)** Normoxic iPSC-HLCs versus hypoxic iPSC-HLCs.

Graphs showing the fold difference in transporter expression in iPSC-HLCs differentiated using protocol 2, analysed by iTRAQ. Positive values indicate higher expression in the first comparator, bars in red show significant changes $p \leq 0.05$ determined by ANOVA blue bars are non-significant. Exact values for these changes, and associated significance are shown in Appendix 1. Abbreviations: UD – undifferentiated iPSCs, hPH – human primary hepatocytes, iPSC-HLCs – induced pluripotent stem cell-derived hepatocyte-like cells, VDAC - Voltage dependent anion channel, GLUT - Glucose transporter, ABC - ABC transporter, MVP - Major vault protein, ENT - Equilibrative nucleoside transporter, SLC - Solute carrier

3.2.8 Expression of liver and hypoxia related genes

qPCR analysis was undertaken on a panel of genes which were unlikely to be readily detected by iTRAQ analysis due to low protein expression of these genes (Figure 15). These genes included mainly transcription factors where the protein levels are low. A complete list of the genes analysed, their fold differences and associated significance is shown in Appendix 2. Values are presented as fold difference ($2^{-\Delta\Delta Ct}$) relative to undifferentiated iPSCs and were tested in triplicate, the control gene is GAPDH. Significant changes are indicated by an asterisk (*) and a connecting bar between the significantly changed samples (* =$p \leq 0.05$, ** = $p \leq 0.01$), determined using a two-tailed, unpaired Student's t-test. Significance testing was not performed relative to hPH.

Figure 15 A-I shows gene expression in Liv6HB, there were no significantly changed values in in panels B, D, E, F, G, H or I. Figure 15A shows fold difference in FOXA2 expression, Protocol 1, hypoxia (P1H) shows significantly higher expression than both protocol 2, normoxia (P2N) and protocol 2, hypoxia (P2H). Figure 15C shows fold difference in HNF4a expression, P1H shows significantly higher expression than P2H and P2N.

Figure 15 J-R shows gene expression in Liv6HE, there were no significant changes in panels J and L. Panel K shows significantly higher VEGF expression in P2H than in P2N. Panel M shows significantly increased expression of NRF2 in protocol 1, normoxia (P1N) cells over P1H and P2N. P2N shows significantly increased NRF2 expression compared to P1H and P2H, which in turn shows significantly greater NRF2 expression than P1H. In panel N the expression of ALDOA is significantly increased in P1N compared to P2N. Panel O shows significantly increased HSF1 expression in P1N over P1H, P2H and P2N. P1H shows significantly less HSF1 expression than P1N and P2H. Panel P shows significantly increased HIF1A expression in P1N versus P1H. Panel Q shows expression of CTNNB1, P1N has significantly increased expression versus P1H, P2N and P2H. P1H shows significantly less CTNNB1 expression than P2N and P2H. Panel R shows NANOG expression, P2N is significantly higher than P2H.

Figure 15 S-AA shows gene expression in Liv7HE, there were no significant changes in panels W and AA. Panel S shows significantly higher expression of FOXA2 in P1N versus P2N and P2H. Panel T shows significantly higher expression of VEGFA in P1N, than in P2N and P2H. Panel U shows significantly higher expression of HNF4a in P1N, than in P1H, P2N and P2H. Panel V shows significantly higher expression of NRF2 in P1N, than in P2N and P2H. Panel X shows significantly higher expression of HSF1 in P1N, than in P2N and P2H. Panel Y

shows significantly lower expression of HIF1 in P1H, than in P2N and P2H. Panel Z shows CTNNB1 expression, P2N is significantly increased over P1N.

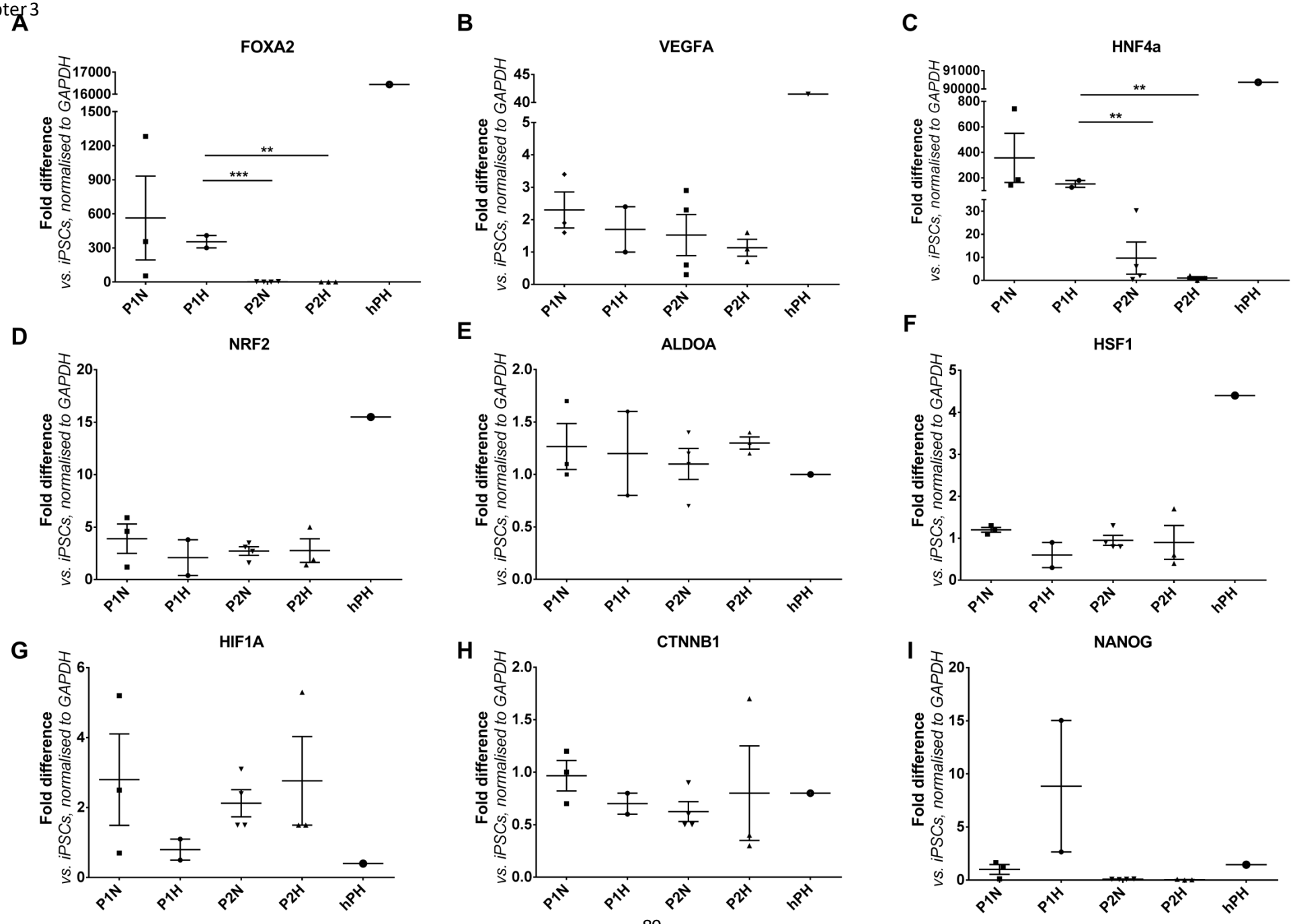
A
FOXA2
Fold difference
vs. iPSCs, normalised to GAPDH
17000
16000
1500
1200
900
600
300
0
**
***
P1N
P1H
P2N
P2H
hPH
B
VEGFA
Fold difference
vs. iPSCs, normalised to GAPDH
45
40
5
4
3
2
1
0
P1N
P1H
P2N
P2H
hPH
C
HNF4a
Fold difference
vs. iPSCs, normalised to GAPDH
91000
90000
800
600
400
200
30
20
10
0
**
**
P1N
P1H
P2N
P2H
hPH
D
NRF2
Fold difference
vs. iPSCs, normalised to GAPDH
20
15
10
5
0
P1N
P1H
P2N
P2H
hPH
E
ALDOA
Fold difference
vs. iPSCs, normalised to GAPDH
2.0
1.5
1.0
0.5
0.0
P1N
P1H
P2N
P2H
hPH
F
HSF1
Fold difference
vs. iPSCs, normalised to GAPDH
5
4
3
2
1
0
P1N
P1H
P2N
P2H
hPH
G
HIF1A
Fold difference
vs. iPSCs, normalised to GAPDH
6
4
2
0
P1N
P1H
P2N
P2H
hPH
H
CTNNB1
Fold difference
vs. iPSCs, normalised to GAPDH
2.0
1.5
1.0
0.5
0.0
P1N
P1H
P2N
P2H
hPH
I
NANOG
Fold difference
vs. iPSCs, normalised to GAPDH
20
15
10
5
0
P1N
P1H
P2N
P2H
hPH

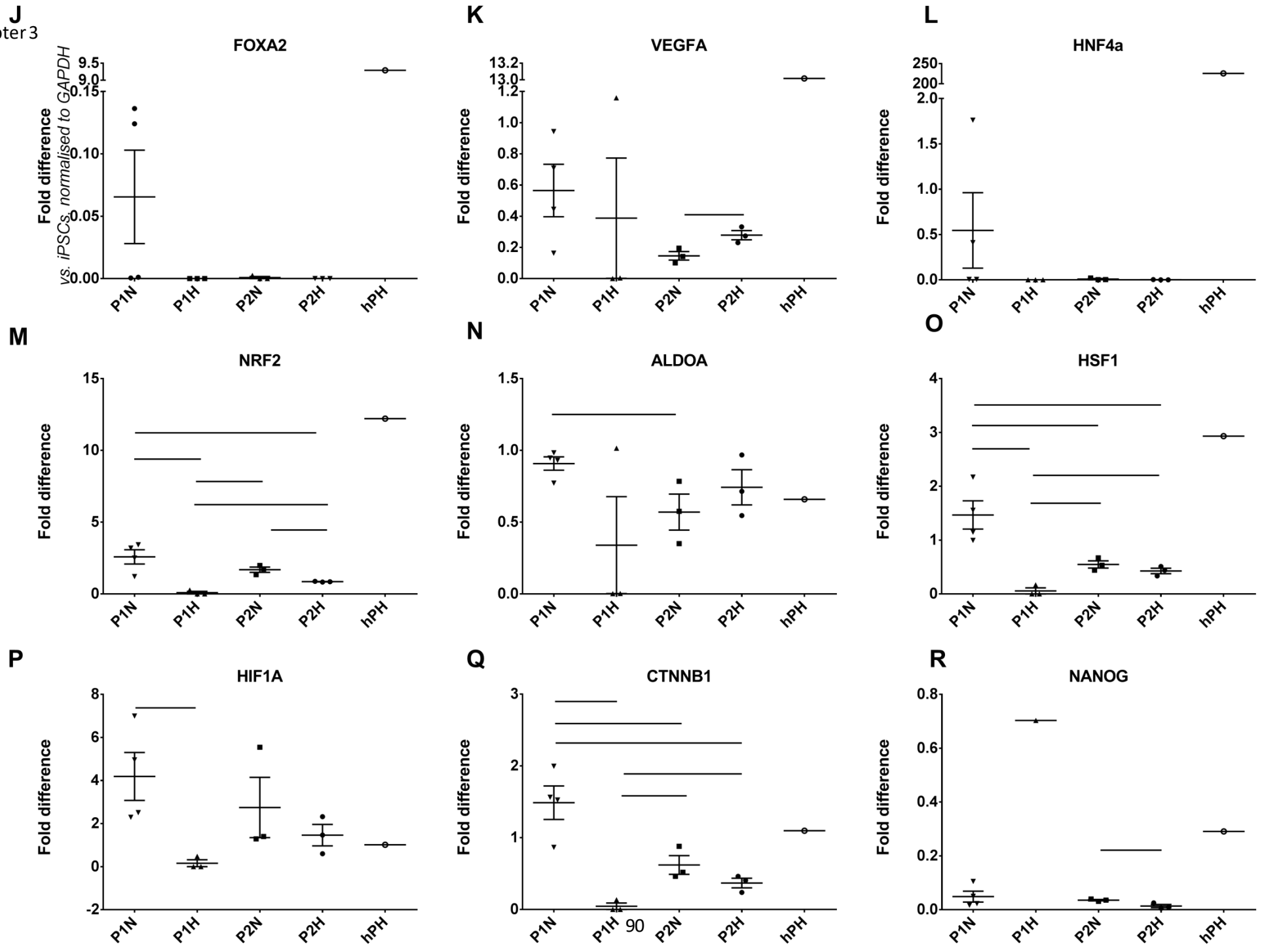
J
FOXA2
K
VEGFA
L
HNF4a
M
NRF2
N
ALDOA
O
HSF1
P
HIF1A
Q
CTNNB1
R
NANOG
Fold difference
vs. iPSCs, normalised to GAPDH
P1N
P1H
P2N
P2H
hPH

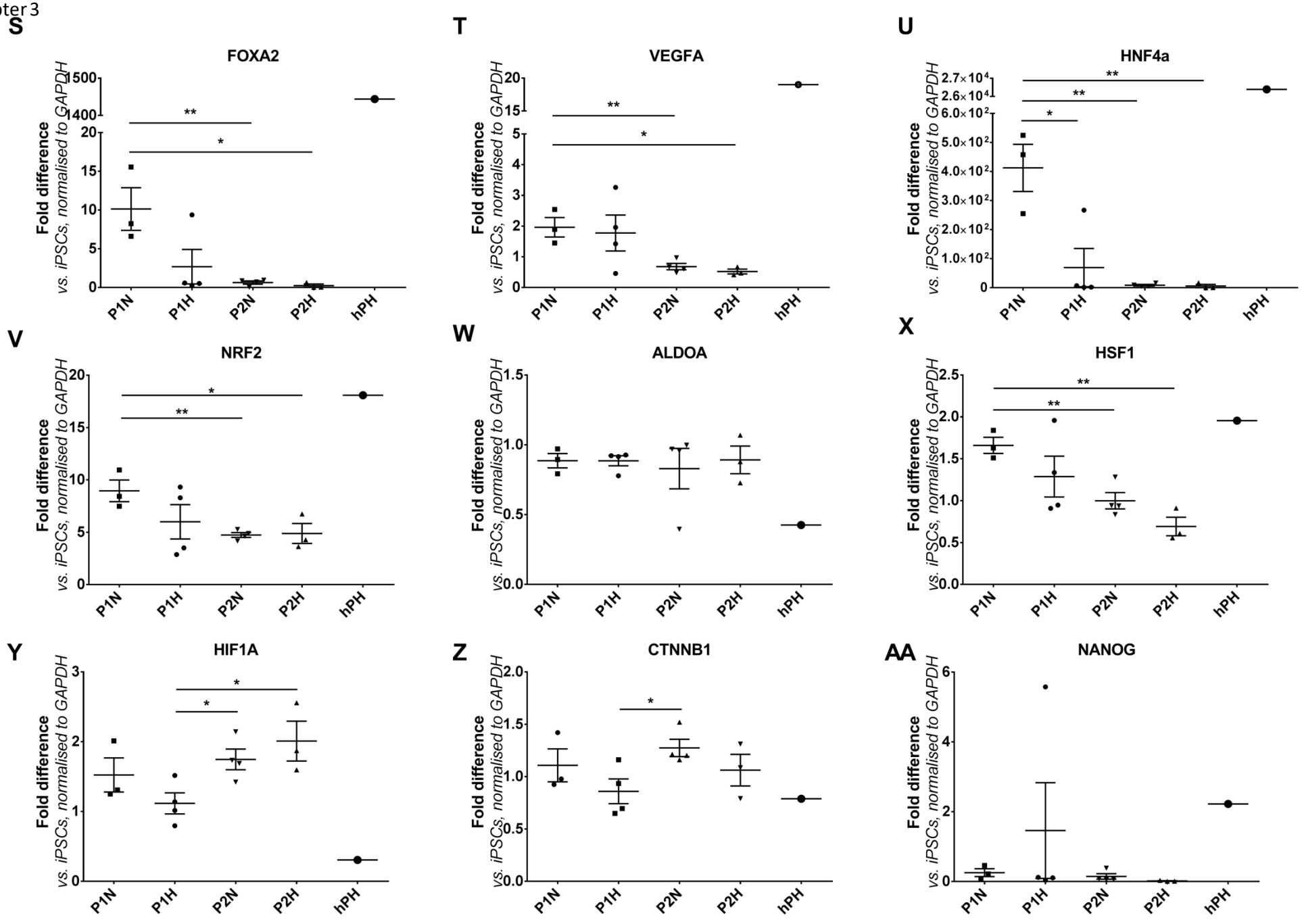
S
FOXA2
T
VEGFA
U
HNF4a
V
NRF2
W
ALDOA
X
HSF1
Y
HIF1A
Z
CTNNB1
AA
NANOG
Fold difference
vs. iPSCs, normalised to GAPDH
P1N
P1H
P2N
P2H
hPH

Figure 15

qPCR analysis of iPSC-HLCs differentiated using protocol 1 and 2 under normoxic and hypoxic conditions shows trend toward increased expression under normoxic conditions and protocol 1 – (A-I) Fold difference in FOXA2, VEGFA HNF4α, NRF2, ALDOA, HSF1, HIF1A, CTNNB1 and NANOG in PSC-HLCs derived from Liv6HB versus undifferentiated iPSCs. **(J-R)** Identical analysis as performed in section A-I using iPSC-HLCs derived from Liv6HE **(S-AA)** Identical analysis as performed in section A-I using iPSC-HLCs derived from Liv7HE

Graphs show mean fold difference in gene expression for the gene in the graph title. Fold difference was calculated using the $2^{-\Delta\Delta CT}$ method (Livak and Schmittgen, 2001) using line-matched normoxic iPSCs as a calibrator and GAPDH as a control gene. Horizontal bars show mean fold difference, data points show exact values of each replicate, error bars denote standard deviation of the mean. Horizontal bars with asterisks (*) indicate significant differences, tested using an unpaired, two-tailed Student's t-test. Increased number of asterisks denotes smaller p-values, * = ≤ 0.05, ** = ≤ 0.01, *** = ≤ 0.001. Exact fold difference values, standard deviation and p-values are shown in Appendix 2. Details of each iPSC line are shown in Table 4. There is a trend towards increased gene expression under normoxic conditions and using protocol 1, though the results are inconsistent between cell lines. Abbreviations: ALDOA - Aldolase A, FOXA2 - Forkhead box protein A2, GAPDH - Glyceraldehyde 3-phosphate dehydrogenase, HIF1A - Hypoxia inducible factor 1A, HLC - Hepatocyte-like cell, HNF4a - Hepatocyte nuclear factor 3a, HSF1 - Heat shock factor 1, iPSC - Induced pluripotent stem cell, NRF2 - Nuclear factor erythroid 2-related factor 2, P1H - Protocol 1 hypoxia, P1N - Protocol 1 normoxia, P2H - Protocol 2 hypoxia, P2N - Protocol 2 normoxia, VEGFA - Vascular endothelial growth factor A, hPH, - human primary hepatocytes

3.3 Discussion

iPSC-HLCs potentially offer an unlimited source of hepatocytes for a range of uses from transplant to toxicity testing. They are particularly valuable since they can be derived non-invasively from patients and can theoretically mimic the phenotype of their donor. However, despite numerous attempts to improve differentiation, their phenotype is generally considered to be closer to that of an immature foetal hepatocyte (Baxter et al., 2015). These attempts have included alteration of both the chemical and physical properties of differentiation to more closely mimic the process of embryonic development. In this study we have assessed the performance of two differentiation protocols and the effects of oxygen modulation on the differentiation of iPSCs to iPSC-HLCs. Protocol 1 uses a more traditional growth factor-based approach whilst protocol 2 uses small molecules to mimic the effects of growth factors. We used a hypoxic environment (5% O_2, 5% CO_2, 90% N_2) in comparison to standard tissue culture conditions where only CO_2 was mechanically controlled, atmospheric gases provided the remaining gas composition.

3.3.1 Effects of hypoxia on undifferentiated iPSCs

The positive effects of hypoxia on the pluripotency of iPSCs have been known for some time, we sought to confirm these results in our lab. Liv4FA iPSCs were cultured under hypoxic conditions for several passages and their expression of pluripotency markers, hypoxia-inducible genes, and NRF2-related genes was assessed by qPCR (Figure 6). When cells were cultured in 5% O_2, small but significant increases in the pluripotency markers, SOX2 and NANOG were observed (Figure 6B). The increase in OCT4 was of similar magnitude but did not achieve significance. These findings agree with literature reports of improved pluripotency in hypoxia. We also examined the gene expression of several hypoxia inducible genes, all the tested genes showed increased expression which confirmed that 5% O_2 was sufficient to induce a hypoxia response in iPSCs (Figure 6A). Finally, we also examined the gene expression of three NRF-2 pathway-related genes. The NRF-2 pathway is the master regulator of the cellular response to oxidative stress which may be expected to be active under hypoxic conditions (Mutter et al., 2015). Indeed, NRF-2 and HO-1, an NRF-2-regulated gene, were both significantly upregulated in hypoxic iPSCs versus normoxic (Figure 6C). Taken together, these results show that 5% O_2 induces far-reaching effects in gene expression in iPSCs and is sufficient to drive a hypoxia response and improve pluripotency.

3.3.2 Morphological differences between conditions

Figure 5 shows the morphology of Liv6HE HLCs differentiated under each condition in comparison to hPH and iPSCs. Polygonal morphology, like that of hPH (Figure 5F) can be observed in panels B-D. However, this morphology is not apparent in Figure 5A and in Figure 5B-D the size of these cells is generally smaller than hPH. Moreover, there are no multinucleate cells observable in iPSC-HLCs, which are apparent in hPH. Conversely, the morphology is different to that exhibited by iPSCs in Figure 5E where the cells are smaller and compacted.

Whilst morphology is not necessarily required for the biochemical phenotype of the iPSC-HLCs, it follows that a perfect recapitulation of hPH would also recapitulate their morphology. Whilst difficult to quantify, the morphology of iPSC-HLCs differentiated using protocol 1 appears to be slightly improved under hypoxic conditions and the morphology of cells differentiated using protocol 2 appears to be largely unchanged in either oxygen condition. Moreover, the morphology of the cells in Figure 5A is the least like hPH, suggesting some shortcomings of this protocol.

3.3.3 iTRAQ Analyses

HCA and PCA were both performed on the iTRAQ dataset to examine if any large-scale changes occurred due to the differentiation protocols or oxygen conditions (Figure 7 & 8). Both of these analyses showed that iPSC-HLCs were not strongly separated based on any of the tested conditions with the exception of two iterations of P1H, the reasons for this are unclear but are also observed in Figure 15 during qPCR analysis where VEGFA and ALDOA expression in 2/3 points for P1H are very low compared to the third point. It is unclear whether these two data points are spurious since, the third point separates from these two but clusters closely with the points from other protocols.

Furthermore, iPSC-HLCs do not cluster closely with hPH. This has been shown repeatedly by other studies (Table 1) and it was not expected that alteration of the oxygen level would cause iPSC-HLCs to fully recapitulate the phenotype of hPH, rather that hypoxia may provide one of many necessary incremental improvements in the phenotype might be observed and used in combination with other approaches e.g. 3D culture, co-culture etc. Similarly, it is promising that iPSC-HLCs do not cluster closely with iPSCs, this shows that the differentiation protocols have altered the phenotype towards that of an hPH, albeit incompletely.

3.3.3.1 Cytochromes P450 expression

CYPs are an essential part of the phase I metabolism performed by hepatocytes, therefore reproduction of their expression is essential for an accurate hepatic phenotype. We selected a panel of CYPs and examined their expression using the iTRAQ dataset (Figures 9 & 10, Appendix 1). Figure 9 shows the expression of CYPs in iPSC-HLCs differentiated using protocol 1. Panel A shows the changes in CYP expression between normoxia and undifferentiated cells. The magnitude of these changes was small and only CYP3A4 and CYP2S1 exceed a fold-change magnitude of 5. CYP2S1 is repeatedly downregulated during the process of differentiation (Figure 9 & 10) and is the only CYP whose expression is close to that of hPH (Figure 9C-D & 10C-D), this is a positive indicator for the phenotype of iPSC-HLCs as CYP2S1 is implicated mainly in extrahepatic xenobiotic metabolism and the decrease in expression moves the phenotype closer to that of hPH (Saarikoski et al., 2005). Figure 9B shows the CYP expression of iPSC-HLCs differentiated under hypoxic conditions, the pattern of expression is largely similar to normoxia. Moreover, there is a trend towards increased expression of most CYPs, this is visualised in Figure 9E when compared with cells differentiated under normoxic conditions. It should be stressed that the magnitude of all these changes are small compared to hPH, as shown in Figure 9C and 6D, regardless of oxygen conditions, the expression remains lower.

Using protocol 2, all CYPs except CYP2S1 were significantly increased over undifferentiated cells (Figure 10). However, there was no clear trend between normoxia and hypoxia (Figure 10E), CYP2S1 was the only significantly altered protein which was significantly higher under hypoxic conditions and the magnitude of all other changes was less than 2.5. Similarly to protocol 1, when compared to hPH, iPSC-HLCs express lower levels of CYPs (Figure 10C & D).

3.3.3.2 Phase II metabolism enzymes expression

We next examined the expression of phase II metabolic enzymes in iPSC-HLCs differentiated under each condition. The majority of proteins were unchanged or only changed by a small magnitude. In Figure 11A, the upregulation of GSTK1 and COMT are of interest because the large change in expression during differentiation reduces the difference between hPH and these proteins to less than 5-fold indicating more complete differentiation. GSTK1 is a member of the GSTK family or the mitochondrial GSTs. It is primarily expressed in the mitochondria of the liver, kidney and adrenal glands in humans. Similar expression of GSTK1 is a positive phenotypic indicator for iPSC-HLCs, particularly since it may indicate the adaptation of the mitochondria to a hepatic phenotype.

In the comparison of phase II phenotype between oxygen conditions (Figure 11C & D) the majority of proteins are expressed more highly in hPH. When oxygen conditions are compared, the magnitude of the changes is small overall (Figure 11E). UGT1-4 is significantly increased in iPSC-HLCs differentiated under hypoxic conditions, whilst GSTK1 is significantly higher under normoxic conditions. Overall, there is no consistent improvement in phase II phenotype for either oxygen condition using protocol 1.

Under normoxic conditions, COMT, GSTK1, UGT1-4 and UGT2B10 were significantly upregulated versus undifferentiated cells and also had a fold difference greater than 5 (Figure 11D). Under hypoxic conditions, COMT, GSTK1, GSTO1, UGT2B10 and UGT2B7 were significantly upregulated and had fold differences greater than 5 (Figure 11E). Interestingly, the significantly downregulated proteins, GSTP1 and NQO1 are both modulated by the NRF2 pathway, suggesting a decrease in NRF2 activity in the cells differentiated in hypoxia (Mutter et al., 2015; Satoh et al., 2002).

Compared to hPH, the majority of proteins has significantly lower expression, though GSTP1 and GSTM3 are significantly higher in iPSC-HLCs in both oxygen conditions (Figure 12B & C). Under normoxic conditions GSTM3 is also significantly increased in iPSC-HLCs. For protocol 2, SULT1A1 and GSTM2 are significantly upregulated in normoxia over hypoxia, (Figure 12E). However, the magnitude of this change, and all other changes, are small.

3.3.3.3 Transporter Expression

We next examined transporter expression Figure 13 & 14, Appendix 1). With protocol 1, normoxia, VDAC1, MVP, SLC25A24 and ABCD3 are significantly increased by greater than 5-fold and ENT1 is significantly downregulated by greater than 5-fold (Figure 13A). Under hypoxic conditions VDAC1, VDAC2, SLC25A24 and MVP were significantly increased by greater than 5-fold (Figure 13B). Both protocols show good expression of MVP, the major structural component of the vault organelle (Berger et al., 2009). Vaults may be involved in chemoresistance, as MVP is overexpressed in some multidrug resistant cancer cell lines and is therefore a positive indicator for the phenotype of iPSC-HLCs (Scheffer et al., 1995).

The transporter phenotype appears to be relatively well reproduced in iPSC-HLCs (Figure 13C & D). The majority of changes were either small or non-significant compared to hPH. Of the significantly changed proteins, 3 show small changes (<5-fold) and all except GLUT3 show only modest changes (<15-fold). Increased GLUT3 expression under hypoxic conditions (Figure 13B & 14B) may be an effect of oxygen modulation. GLUT3 is a widely expressed hypoxia-responsive high affinity glucose transporter which is upregulated in

response to hypoxia via the HIF1a pathway, typically in combination with GLUT1 (Mobasheri et al., 2005). However, it is also possible that high expression of GLUT3 is indicative of poor maturation as it is also highly expressed in embryonic tissues before birth and also aids in the maintenance of pluripotency under hypoxic conditions (Christensen et al., 2015; Mobasheri et al., 2005).

Both VDAC2 and VDAC3 are significantly higher in hypoxic conditions and ABCD3 is significantly higher in normoxic conditions (Figure 13E). ABCD3 shows the largest significant change in expression, this change may be due to oxygen modulation. ABCD3 is expressed on the membrane of liver peroxisomes whose activity is dependent on the availability of molecular oxygen as an electron acceptor (Schönenberger, 2015). However, the magnitude of changes in Figure 13E are low overall, suggesting that oxygen modulation had little effect.

When differentiated in normoxia using protocol 2, iPSC-HLCs the majority of changes are small or non-significant (Figure 14A-B). In comparison to hPH, the phenotype is favourable with 9 and 8 proteins non-significantly different to hPH in normoxia and hypoxia respectively (Figure 14C & D). Moreover, in panel C, 4 of the significantly altered proteins show small fold differences (<5-fold) and all except ABCA6 show only modest fold differences (<15-fold).

It is interesting that ENT1 is downregulated during differentiation (Figure 13A & B, 14A). ENT1 is repressed by HIF1 in response to hypoxia providing cardioprotective effects in mice (Eltzschig et al., 2005; Rose et al., 2010). This explains the downregulation observed in Figure 13B (hypoxia) but not the downregulation observed in Figure 13A and 14A (normoxia), or the lack of an effect in Figure 14B (hypoxia). Taken together, these results suggest that the changes in ENT1 are not related to the oxygen tension and may instead represent a more general shift towards a hepatic phenotype (Figure 13C-D, 14C-D). ENT1 is implicated in the toxicity of fialuridine (McKenzie et al., 1995; Xu et al., 2014). The expression of ENT1 was not significantly different to hPH and therefore, iPSC-HLCs from each condition could reasonably be expected to model fialuridine toxicity.

3.3.4 Effects of hypoxia on gene expression in iPSC-HLCs

Though global proteomic analysis was performed on iPSCs, there are shortcomings of the technique that require supplementation with gene expression analysis. Very low abundance proteins, such as some transcription factors can be challenging to detect using iTRAQ. A panel of relevant genes were examined using qPCR (Figure 15, Appendix 2, page

243). In each iPSC-HLC line there was a trend towards increased FOXA2 expression in P1N, though the trend is only significant in 6HE. FOXA2 was also significantly increased in P1H relative to protocol 2 in Liv6HB. FOXA2, also known as hepatocyte nuclear factor 3a is considered a 'pioneer factor', whose expression drives hepatocyte specification and activates expression of genes such as AFP and albumin (Friedman and Kaestner, 2006). High expression of FOXA2 is a positive indicator of phenotype in iPSC-HLCs for these reasons, however it should be noted that the expression in hPH is dramatically higher than in iPSC-HLCs indicating their relative immaturity.

VEGFA expression was generally higher using protocol 1 (Figure 15 B, K, T), and was significantly higher in Liv7HE P1N versus protocol 2 but was variable. In Liv6HE, VEGFA expression was significantly higher in low oxygen, though only in protocol 2. VEGFA is an angiogenesis factor and hypoxia responsive gene (Ahmed et al., 2016), so increased expression in low oxygen conditions is expected (Figure 15K) but it is not clear why there should be increased expression in P1H (Figure 15T). The reasons for the high degree of variability, particularly in Liv6HE are unclear, though it is apparent that none of the lines or protocols show full maturity, as the expression in iPSC-HLCs is similar to that of undifferentiated iPSCs and in hPH, expression is approximately 10-40-fold higher.

HNF4a is the most abundant DNA-binding protein in the liver where it regulates the expression of HNF1a and also genes related to gluconeogenesis and lipid metabolism (Chandra et al., 2013). Like FOXA2, HNF4a was expressed most highly in P1N and generally showed increased expression in protocol 1 overall. In Figure 15U, HNF4a expression is significantly higher in P1N than P1H, P2N and P2H and in Figure 15C expression in P1H was significantly increased over both P2N and P2H. Increased expression of HNF4a is a good indicator of hepatic maturity, though expression is still lower than in hPH.

NRF2 was also examined, some NRF2-related proteins were also investigated by iTRAQ (Figure 11 & 12), though direct assessment of the NRF2 transcript may also be informative. As previously discussed, NRF2 is the master regulator of the cellular response to oxidative stress. Some caution should be placed in the interpretation of NRF2 by qPCR due to the mechanism of NRF2 regulation. NRF2 is continuously expressed, translated and subsequently degraded when bound by KEAP1, under conditions of oxidative stress, the degradation of the protein is impaired, which then enters the nucleus (Mutter et al., 2015). Nonetheless, NRF2 pathway activation is implied by increased transcription and it is interesting NRF2 shows increased expression in P1N iPSC-HLCs where it is significantly

higher than P1H and P2H Figure 15M & V. Additionally, P2N also shows increased NRF2 expression and is significantly increased over P1H and P2H (Figure 15M). This suggests an increased degree of oxidative stress in cells in a normoxic environment.

HSF1 is a transcription factor which governs the response to proteotoxic stressors such as heat or hypoxia amongst other functions (Dayalan Naidu and Dinkova-Kostova, 2017; Vihervaara and Sistonen, 2014). Interestingly, HSF1 was most highly expressed in P1N, where it was significantly higher than P1H, P2N and P2H (Figure 15O & X). In addition, both P2N and P2H show significantly increased HSF1 expression over P1H (Figure 15O). This is contrary to the expectation that hypoxic conditions would induce HSF1 expression and though the changes are small this suggests activation of a hypoxia response under normoxic conditions. Similarly, the pattern of HIF1A expression is somewhat unclear, HIF1A is the master regulator of the cellular hypoxia response and is induced in response to hypoxic conditions (Majmundar et al., 2010). In Figure 15P, HIF1A is significantly increased in P1N over P1H and in Figure 15Y HIF1A expression is significantly increased in P2N and P2H over P1H. It is expected that HIF1A would show greater expression in cells differentiated under hypoxic conditions, but this is not always the case. The lack of upregulation of HIF1A in iPSC-HLCs is unexpected because HIF1A induction was shown in undifferentiated cells (Figure 6), suggesting either that this upregulation was lost during differentiation or the hypoxia response is being induced under normoxic conditions.

CTNNB1 is both a structural protein in adherens junctions and a major ligand in the Wnt signalling pathway which is involved in many developmental processes, the maintenance of pluripotency and definition of the perivenous phenotype in the liver (Sokol, 2011). The changes in CTNNB1 expression in Figure 15H, Q & Z were small. Nonetheless, some conditions significantly changed CTNNB1 expression. In Figure 15Q, CTNNB1 expression was significantly increased in P1N over P1H, P2N and P2H and was also significantly increased in P2H and P2N over P1H. Similarly, in Figure 15Z P2N is significantly increased over P1H. Increased expression of CTNNB1 implies increased activation of the Wnt signalling pathway, and may be indicative of several factors, e.g. immaturity, perivenous phenotype. However the fold differences are small and similar to the level of expression found in hPH which were not enriched for perivenous cells. These results also allude to the difficulty inherent with iPSC lines in that even clones from the same donor and cell type (Figure 15Q & Z) show differing results possibly due to an altered tendency to differentiate, these findings are in agreement with our previous work which shows that clonal and donor differences

contribute more than cell type of origin to the overall phenotype of iPSC-HLCs (Heslop et al., 2017).

Finally, the expression of NANOG was also examined in iPSC-HLCs (Figure 15 I, R & AA). NANOG is a transcription factor which aids in maintenance of pluripotency and supresses differentiation, therefore it is expected that expression would be lower in differentiated cells compared with iPSCs. Indeed, NANOG generally showed lower expression in iPSC-HLCs than in iPSCs, though only a single significant change was observed in Figure 15 R where P2N showed slightly increased expression over P2H. In Figure 15 I, R & AA for P1H, some data points are dramatically higher than the majority of other differentiations. These data may represent poorly differentiated cells and indicate the possibility of variation between experimental runs present with growth factor-based protocols. The relatively high expression of NANOG observed in hPH is also of interest, at approximately 2-fold higher than in iPSCs, this is an unexpected result and the reasons for increased expression of a pluripotency factor in mature cells is unclear.

3.3.5 A perivenous phenotype?

We hypothesised that the use of lower oxygen during differentiation may produce iPSC-HLCs with a perivenous phenotype. The phenotype of hepatocytes changes across the liver lobule with those in the periportal region specialising in gluconeogenesis and glutathione synthesis whilst those in the perivenous region specialise in glycolysis and show high expression of CYPs (Colnot and Perret, 2011). In addition, the perivenous phenotype *in vivo* is characterised by low oxygen and high expression of hypoxia inducible factors and Wnt signalling (Kietzmann, 2017). To determine if a perivenous phenotype was produced in hypoxic iPSC-HLCs we examined markers of both the periportal and perivenous zones. As previously stated, Wnt signalling is increased in perivenous hepatocytes and CTNNB1, a major Wnt pathway ligand was examined in Figure 15H, Q & Z, CTNNB1 was not consistently increased in hypoxic iPSC-HLCs, indeed in several cases there was increased signalling under normoxic conditions (Figure 15Q & Z). CYP expression is also higher in perivenous hepatocytes, notably CYP1A2 and CYP2E1 (Colnot and Perret, 2011), these proteins were detected in iTRAQ analysis (Figure 9 & 10) but were not significantly changed between oxygen conditions. CDH1, ARG1, PCK1/2 and CPS1 show increased expression in periportal hepatocytes (Sekine et al., 2009). These proteins were detected in iPSC-HLCs by iTRAQ analysis and shown in Appendix 1. Of these proteins, only CDH1 and PCK2 were significantly changed in protocol 2 and 1 respectively. CDH1 was increased 2.2-fold in

hypoxic iPSC-HLCs. However, contrary to expectation PCK2 was increased by approximately 1.4-fold in normoxic iPSC-HLCs.

These results suggest that culture under hypoxic conditions did not produce a perivenous phenotype in iPSC-HLCs. The reasons for this are initially unclear, and made more so by the loss of HIF1A activation despite maintenance of the hypoxic environment (Figure 15P & Y). It may be the case that cells under normoxic conditions are experiencing some degree of hypoxia due to the diffusion of oxygen throughout the medium. In static cultures like those used herein, the penetration of oxygen into the culture medium is low, reaching saturation slowly, particularly considering the deoxygenation of liquids that occurs during autoclaving, though we did not autoclave the culture medium it is probable that it was autoclaved by the manufacturer (Somerville and Proctor, 2013). Furthermore, Somerville and Proctor (2013) suggest that cells grown below a depth of 1 mm experience anaerobic conditions. Given the use of 6-well plates and 2 mL culture volume, the depth of medium in each condition was approximately 2.1 mm, therefore it is probable that the oxygen concentration perceived by the cells under both normoxic and hypoxic conditions is lower than may initially be expected.

Because the diffusion of oxygen into the culture is governed by Fick's law where the concentration gradient of oxygen between gas and liquid and the thickness of the liquid is considered, the time to reach equilibrium will be slowed by hypoxia, moreover the consumption of oxygen by cells at the bottom of the liquid should be considered for the time taken to reach equilibrium and can potentially prevent the formation of equilibrium in highly metabolically active cells (Place et al., 2017). Considering these factors, Place et al. calculated the depth of culture medium where cellular oxygen demand meets rate of diffusion for a range of cell types and oxygen concentrations under typical (normoxic) incubator conditions. The depth for ESCs was calculated and was assumed to be similar to iPSCs at 7.1 mm and 8.7 mm to produce conditions similar to a periportal hepatocytes (60 mmHg O_2), or perivenous hepatocytes (40 mmHg O_2) respectively, this is greater depth than was used in the experiments herein so the cells likely were not oxygen-starved, however, hepatocytes have a higher metabolic rate than iPSCs (Place et al., 2017). The maximum depth for rat hepatocytes was also calculated and was assumed to be similar to that of iPSC-HLCs, to achieve similar oxygen concentrations in these cells a maximum medium depth of 1.1 and 0.9 mm for periportal and perivenous respectively would be required. Therefore, the depth of medium used in these experiments likely starved even the normoxic iPSC-HLCs of oxygen, effectively producing hypoxic conditions over the course of

differentiation as the metabolic demand of the cells increased and explaining the lack of separation between oxygen conditions (Place et al., 2017). Effectively, the cells under hypoxic conditions became increasingly hypoxic over the course of differentiation and may have even reached conditions of near anoxia. This realisation helps to explain the increased failure rate of differentiations that was casually observed under hypoxic conditions (data not shown), cells were likely already fragile from oxygen starvation and more prone to detachment and death.

3.3.6 Conclusions

In summary, these results show that there is no strong advantage to the use of hypoxia during differentiation of iPSCs to iPSC-HLCs. The differences in expression of genes between oxygen conditions was typically small and inconsistent between iPSC lines suggesting that clonal variation and other non-defined factors contribute more strongly to the variations in expression observed. There were also similar results for the comparison of differentiation protocols, the majority of differences observed between either protocol were small and inconsistent. HCA did not reveal strong separation based on either oxygen conditions or differentiation protocol and PCA showed that all four conditions clustered relatively closely together compared to iPSCs and hPH.

These results also revealed higher variability in iPSC-HLCs produced using protocol 1. There are two data points for P1N in Figure 7 & 8 which separate strongly from the other iPSC-HLCs and high variability in gene expression was frequently observed in HLCs differentiated using protocol 1 in Figure 15. This may represent increased variability from the growth factor-based protocol. Given the minimal advantages observed in using the growth factor-based protocol 1 it seems prudent that future studies should use the cheaper and faster small molecule-based protocol 2. Though the possibility that improved differentiation may be observed with the protocol 1 with more thoroughly optimised differentiation conditions cannot be ruled out. Furthermore, since no major advantage appears to have been conferred to the hepatocyte phenotype during differentiation under hypoxia, we suggest that either normal oxygen levels or even high oxygen levels based on the increased oxygen demand of more metabolically active differentiated hepatocytes should be used for future studies. These results also agree with published literature regarding the beneficial effects of hypoxia on the pluripotency of iPSCs (Figure 6). Therefore, future studies should maintain and grow iPSCs under hypoxic conditions and increase the levels of available oxygen to cells over the course of differentiation in order to meet the increasing oxygen demand. Considering the level of oxygen available to cells in culture as described by Place et al.

(2017), the exact oxygen composition of the differentiation atmosphere could be adjusted to closely match that of perivenous or periportal hepatocytes.

4 Assessing the proteome of human liver organoids and their potential as models for hepatotoxicity

4.1 Introduction

Organoids are a recently developed type of 3D culture which produce miniaturised organ-like structures in a supportive matrix such as Matrigel or BME-2 (Sato et al., 2009). It is anticipated that they will be useful in the production of large quantities of mature cells in a physiologically-relevant architecture which may be then useful for toxicity testing or transplant. Organoids have been derived from several tissues including brain, pancreas, kidney, intestine and liver. Organoids are derived from either pluripotent or adult stem cells and even cancer cell lines and self-assemble in 3D culture in a range of conformations including hollow cysts and dense 'bunch-of-grapes' structures. Although organoids have only recently been developed, they have already seen widespread use, for example they have been used to model: organ development and microcephaly in the brain (Lancaster et al., 2013), infectious diseases including Cryptosporidium *parvum* (Castellanos-Gonzalez et al., 2013) and rotaviruses (Finkbeiner et al., 2012), genetic diseases including familial multiple intestinal atresia (Bigorgne et al., 2014), cystic fibrosis (Dekkers et al., 2013), α1-antitrypsin deficiency and Alagille syndrome (Huch et al., 2015). Moreover, drug efficacy screening has been performed on pancreatic organoid cultures showing function of several compounds including cetuximab and nutlin-3a whilst simultaneously demonstrating the possibility of high-throughput screening for organoid cultures (Van De Wetering et al., 2015).

Previous studies using human hepatic organoids have made extensive use of RNA quantification techniques such as RNAseq and microarrays. However, it is well understood that although RNA expression is a worthwhile method to examine cell phenotype there are often discrepancies between the levels of RNA expression and the levels of protein expression observed. It has been shown that the correlation between mRNA and protein expression may be as low as 40-50% (Schwanhüusser et al., 2011; Vogel and Marcotte, 2012). Since, in most cases, proteins are the functional product of gene expression, a more accurate depiction of the true phenotype of human liver organoids can be obtained by examining the proteome rather than mRNA.

In this chapter, we have focussed on the production of human organoids derived from liver resident stem cells and their differentiation towards a hepatocyte fate. We sought to reproduce the work demonstrated in Broutier *et al.* (2016). Initially we established organoids from several human donors using surgical waste liver tissue and optimised the isolation technique for our laboratory. These optimisations included the use of FACS to

select for EpCAM-positive cells and more straightforward crude isolations of the cells. Once established, we sought to examine the proteomic phenotype of human Chol-Orgs when differentiated towards a hepatocyte fate, a key omission in the published data until this point.

4.2 Results

4.2.1 Rapid isolation of tissue after excision improves isolation success in human liver organoids

In the protocol published by Broutier et al. (2016) the authors state that liver tissue may be stored for up to 48 hours at 4 °C in organoid basal medium (Table 2) prior to isolation. We performed several isolations on tissue at various time points after resection of the tissue and noted a negative correlation between the time after resection and the success of the organoid isolation. Isolations performed less than 24 hours after resection. These were successful in up to 80% of cases with a precipitous drop in efficiency after this point. This is not in agreement with Broutier et al., wherein they reported this reduction in efficiency only after 48 hours.

4.2.2 FACS does not improve isolation success from human liver organoids

During this work, we sought to optimise the isolation of Chol-Orgs from human liver tissue. In Broutier et al. (2016), the authors discuss the use of FACS as an optional step to isolate EpCAM-positive cells as the progenitor cells which give rise to Chol-Orgs. Figure 16 shows the gating used on the FACS Aria III to sort the EpCAM-positive cells from the crude cell population. Cells were isolated from human liver tissue on three occasions and stained for EpCAM using an APC conjugated antibody and the nuclei were stained using DAPI. Gating was established during the first run and identical gating was used in each subsequent experiment. Gating aims to remove non-relevant cells or debris from the final cell suspension. In this case, the first two gates remove cell debris and clusters of cells respectively. The third gate uses DAPI-stained nuclei to detect viable cells. The fourth gate removes cells which were negative for APC, and consequently EpCAM-negative.

The gating for each experiment in Figure 16 shows a maximum of 10,000 events, only a small portion of the total cell population was allocated for establishing and confirming gating and therefore, only 5,024 events were recorded for experimental run 3 where the

cell count was very low. The breakdown of events at each gate can be seen in sections F, L and R. Based on these results, it can be observed that the proportion of EpCAM-positive cells in these sample are low, contributing between 0.7 and 4.0% of the total number of cells. This is unsurprising given that EpCAM-positive cells are typically found around the bile ducts and comprise a small proportion of the whole liver cell number.

After concentration of EpCAM-positive cells by FACS had been achieved, the cells were plated in BME-2 as normal and were monitored for signs of organoid growth. However, very few organoids were observed to arise from these sorted cells (Figure 18A-B). The number of organoids arising from this method was not quantified but was visually determinable as lower than the numbers of organoids arising from the crude isolation.

4.2.3 Human liver organoids established in culture have cystic morphology

Figure 18C-D shows the typical morphology of the Chol-orgs that were derived. These results agree with the published literature, which also show the characteristic cystic morphology. The size of the organoids varied greatly in some cases up to several millimetres in diameter and visible to the naked eye. However, in most cases organoids were smaller.

It is noteworthy that some organoids displayed a dense morphology, as though the cystic structure had collapsed. We were not able to investigate these organoids more closely due to the inability to separate them from the whole population, but it is unclear whether these organoids represent cells spontaneously differentiating towards a hepatocyte fate, as this morphology is more common in differentiated organoids, or whether these are organoids that have collapsed and failed to proliferate (Figure 18C-F).

4.2.4 Human liver organoids can be cryopreserved and thawed

A protocol for cryopreservation was presented in Broutier et al. (2016), we sought to replicate this procedure in our lab. We used two commercial freezing media to cryopreserve organoids, Recovery Cell Culture Freezing Medium and CryoStor CS10. Cryopreservation was performed as described previously and organoids were stored in liquid nitrogen for at least one week and up to 4 months. Both media were found to perform similarly and it was possible to recover organoids even at the longest time points tested with characteristic cystic morphology re-emerging within one week of thawing (Figure 20).

However, we noted that the proliferation rate of organoids that had been cryopreserved for long periods was substantially damaged. Though we were not able to easily depict this quantifiably. This greatly extended the time taken to produce reasonable quantities of organoids to approximately 3 months, in lines where similar proliferation occurred in 2-3 weeks prior to cryopreservation.

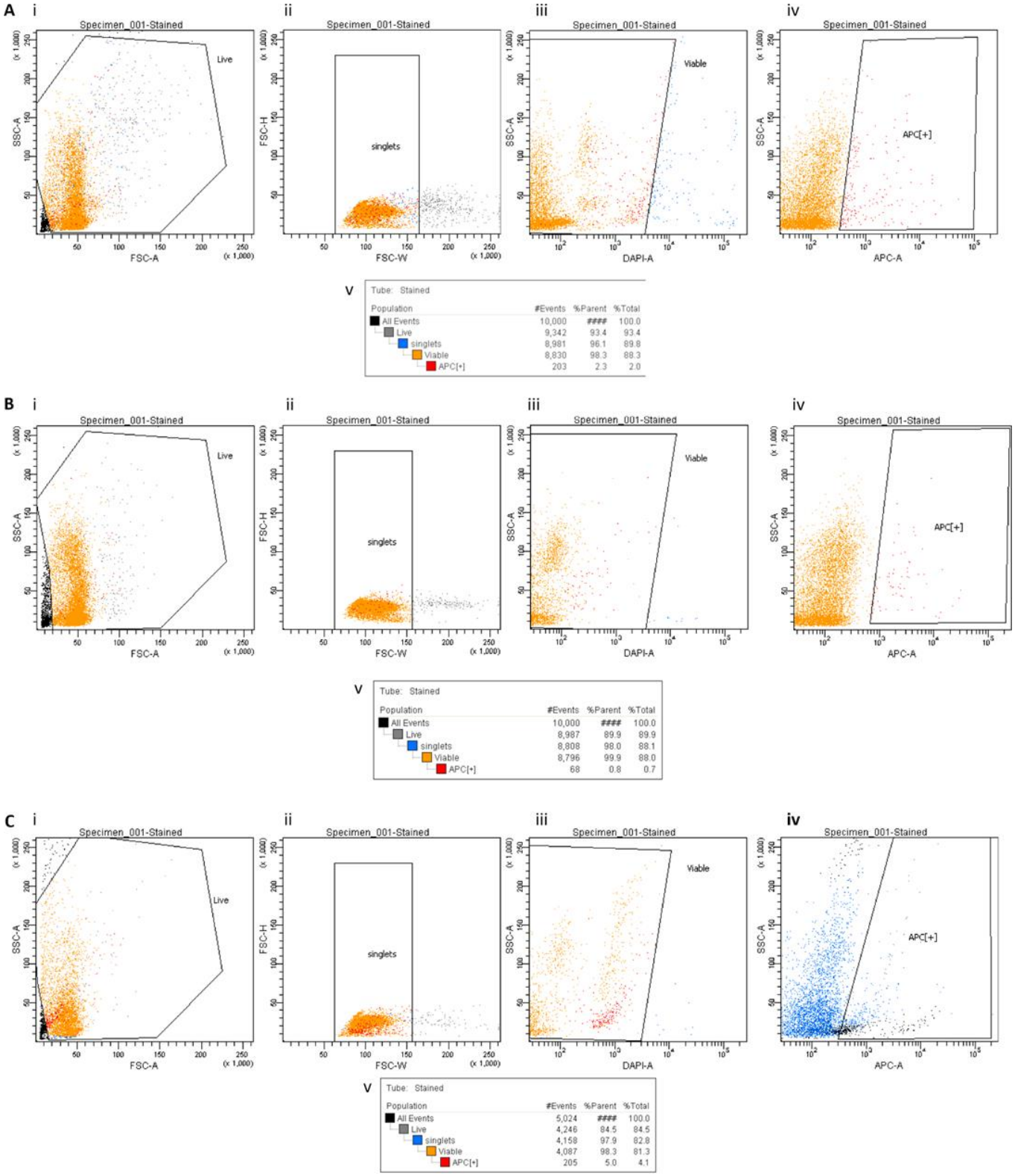

Figure 16

Sort reports for fluorescence activated cell sorting enrichment of EpCAM-positive cells in three liver specimens – (A) Gating for enrichment of EpCAM-positive cells from crude liver cell suspension in a single donor. The crude suspension was stained for EpCAM with an APC conjugated probe and DAPI as a viability stain. (i) Gating used to select for live cells. (ii)

Gating used to select for single cells. (iii) Gating used to select for viable cells, determined by absence of DAPI staining. (iv) Gating used to select for EpCAM-positivity, determined by presence of APC staining. (v) tabulation of number of events passing through each gate **(B)** Identical sort for EpCAM-positive cells as shown in section A in a separate donor. Gates in sections i-iv sort for the same criteria as section A **(C)** Identical sort for EpCAM-positive cells as shown in section A in a separate donor. Gates in sections i-iv sort for the same criteria as section A

Each point represents a single event e.g. a single cell. Points outside the gating are not included in subsequent panels. Points in each section are colour-coded as shown in section v, these colours are based on the gate at which the cell was excluded, points in grey indicate live cells, points in blue indicate singlets, points in amber indicate viable cells and points in red indicate EpCAM-positive cells. Colour coding is incomplete for section C-iv. These data were generated using a FACS Aria III (BD Biosciences) and analysed using FACSDiva (BD Biosciences).

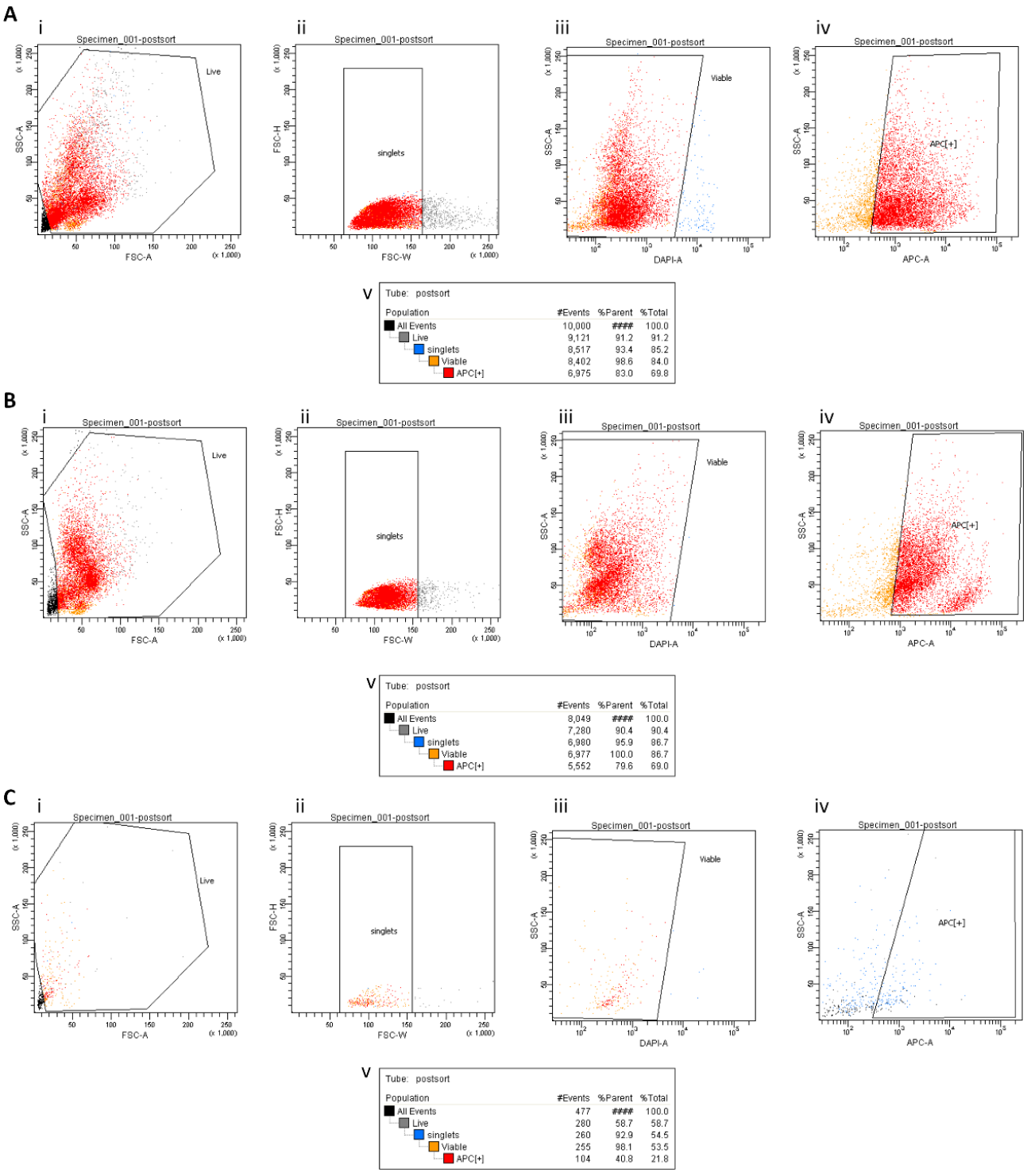

Figure 17

Post-sorting reports for fluorescence activated cell sorting enrichment of EpCAM-positive cells in three liver specimens – (A) Identical gating to that used in Figure 16A to confirm successful gating for enrichment of EpCAM-positive cells in the previous report. The cells sorted in this figure are taken from the sorted cells in Figure 16A. (i) Gating used to select for live cells. (ii) Gating used to select for single cells. (iii) Gating used to select for viable cells, determined by absence of DAPI staining. (iv) Gating used to select for EpCAM-

positivity, determined by presence of APC staining. (v) tabulation of number of events passing through each gate **(B)** Identical sort for EpCAM-positive cells as shown in section A in a separate donor. Gates in sections i-iv sort for the same criteria as section A **(C)** Identical sort for EpCAM-positive cells as shown in section A in a separate donor. Gates in sections i-iv sort for the same criteria as section A.

Each point represents a single event e.g. a single cell. Points outside the gating are not included in subsequent panels. Points in each section are colour-coded as shown in section v, these colours are based on the gate at which the cell was excluded, points in grey indicate live cells, points in blue indicate singlets, points in amber indicate viable cells and points in red indicate EpCAM-positive cells. Colour coding is incomplete for section C-iv. These data were generated using a FACS Aria III (BD Biosciences) and analysed using FACSDiva (BD Biosciences).

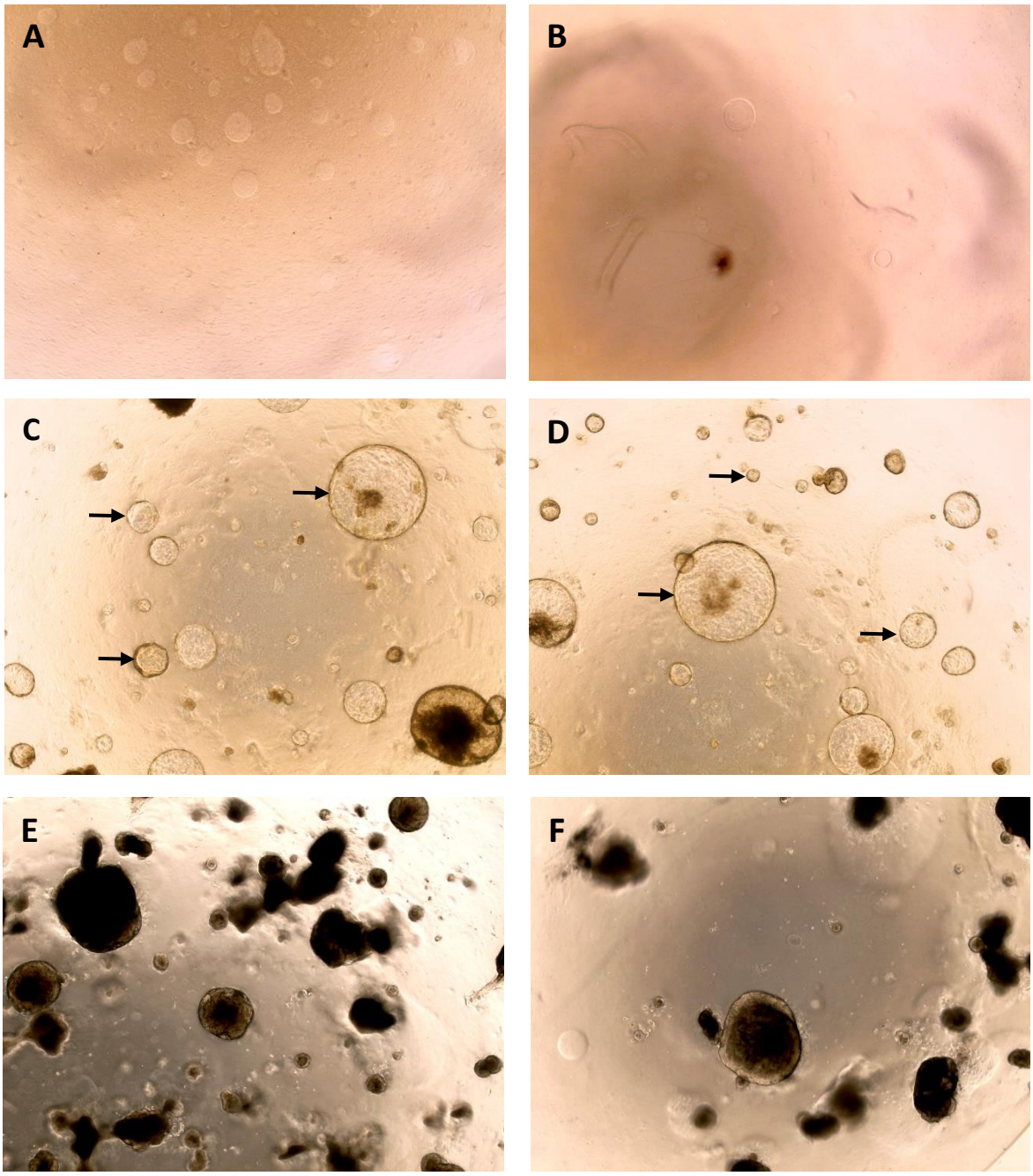

Figure 18

Micrographs showing organoids isolated by fluorescence activated cell sorting enrichment or crude plating, and after differentiation – **(A-B)** Representative brightfield micrographs of cells plated after FACS sorting of EpCAM-positive cells. No organoids are visible, the faint ring-structures are bubbles in the BME-2 matrix. No further outgrowth was noted from cells isolated using fluorescence activated cell sorting enrichment. **(C-D)** Representative brightfield micrographs of donor 1 organoids at passage 1-2 after isolation using the 'crude-plating' method (Table 5). Cystic organoid structures are visible in a range of sizes (black arrows show examples). Some dark structures are also visible at this stage

which may represent collapsed or dead organoids. **(E-F)** Representative brightfield micrographs of donor 1 organoids at day 15 of differentiation. There is a stark change in the appearance of the organoids which have mostly become dark and opaque. The cause of the gross change in appearance is unclear but was interpreted to be a result of the differentiation process.

Images were captured using an EVOS XL Core microscope, 4x magnification.

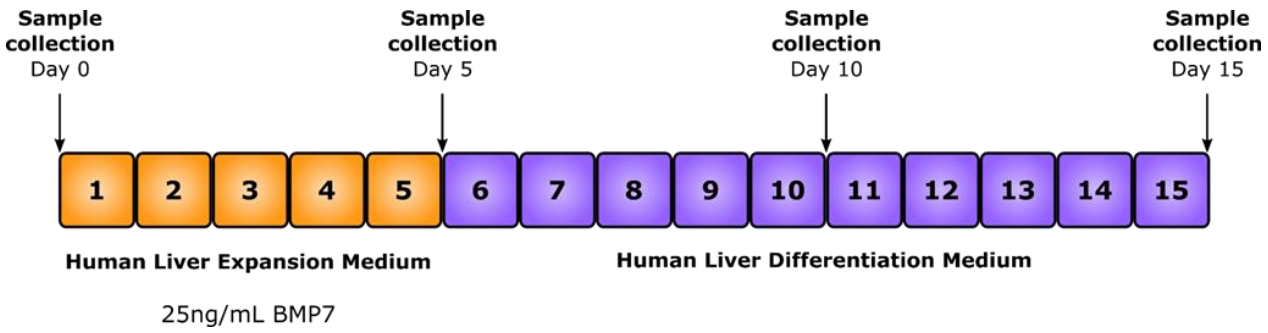

Figure 19

Chol-org liver differentiation protocol and sample collection points – Protocol for the differentiation of Chol-orgs to a hepatocyte-like fate taken from Broutier et al. (2016). Organoids were grown to acceptable density and passaged immediately prior to differentiation and differentiated over a period of 15 days. Medium was changed every 2-3 days as described in chapter 2. Steps in the differentiation protocol are colour-coded, days 1-5 in orange, use human liver expansion medium (Table 2, page 49) supplemented with 25ng/mL BMP7, days 6-15 in purple use human liver differentiation medium (Table 2). Samples were collected for iTRAQ analysis throughout the differentiation process, at day 0, 5, 10 and 15. Abbreviations: BMP7 - Bone morphogenic protein 7, iTRAQ - Isobaric tags for relative and absolute quantitation

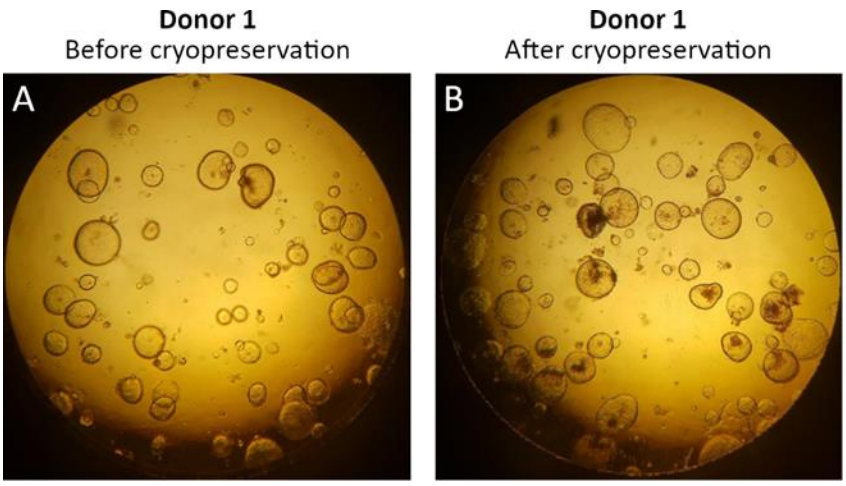

Figure 20

Micrographs showing donor 1 organoids before and after cryopreservation - Representative brightfield images of donor 1 organoids before and after cryopreservation. **(A)** Donor 1 organoids before cryopreservation. Cystic morphology is apparent and few dark structures are present. **(B)** Donor 1 organoids after cryopreservation. Cystic morphology has re-emerged after cryopreservation but an increase in dark structures is visible possibly indicating an increase in the number of dead or damaged organoids.

Pictured organoids were cryopreserved using Recovery™ Cell Culture Freezing Medium, though morphology was not changed when CryoStor CS10 was used.

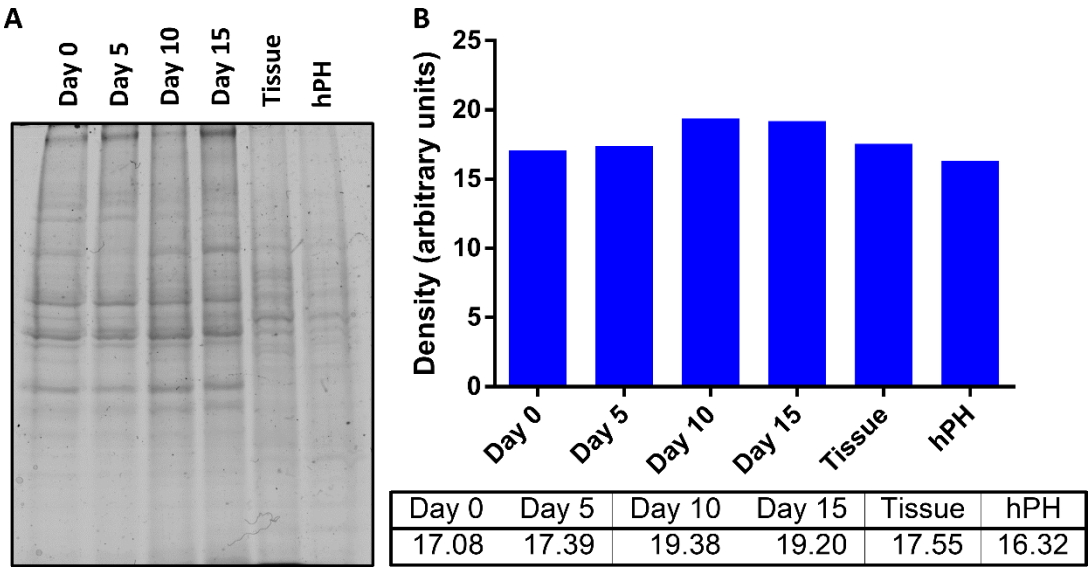

Day 0	Day 5	Day 10	Day 15	Tissue	hPH
17.08	17.39	19.38	19.20	17.55	16.32

Figure 21

Coomassie stain to normalise donor 1 iTRAQ loading – A Coomassie stain was performed to supplement a Bradford assay to ensure even loading of each sample during iTRAQ analysis. **(A)** image of Coomassie stain for each sample used in donor 1 iTRAQ analysis. Captured using a GS-800 calibrated imaging densitometer (Bio-Rad), **(B)** densitometry analysis of the Coomassie stain shown in section A, values are arbitrary units and show even loading in all samples. Exact values are shown for each bar below the graph. Densitometry performed using Quantity One software (Bio-Rad). Abbreviations: hPH – Human primary hepatocytes

4.2.5 Differentiation of Chol-Orgs to hepatocyte fate

Once established in culture, we sought to differentiate the Chol-Orgs to a hepatocyte fate as described in Broutier et al. (2016), an overview of this process can be found in Figure 19. Some morphological changes were observed during this period, particularly the increase in tendency for organoids to become dense clusters that appeared dark under a brightfield microscope (Figure 18 E & F).

Table 5 shows the details of each tissue donor used for analysis in this chapter but is not an exhaustive list of all isolations performed. Two of the donors are female and one is male, all are ethnically white British and have an age range of 20-55. The body mass index of the donors are 25, 27.7 and 18.6 which are defined as overweight, overweight and underweight respectively, by the World Health Organisation (Madden, 2006). The diagnoses of these patients vary for each as does the additional information provided.

Donor #	Sex	Age	BMI	Ethnicity	Diagnosis
1	Male	20	25	White British	Metastatic adrenal carcinoma
2	Female	55	27.7	White British	Colorectal liver metastases
3	Female	41	18.6	White British	Cholangiocarcinoma

Table 5

List of liver tissue donors used for production of human liver organoids – donor numbers and pertinent information of the donors of liver tissue used for organoid isolation. Additional isolations were performed but did not materially contribute to the data displayed in this work and were omitted.

4.2.6 iTRAQ analysis shows proteomic changes during the hepatic differentiation of human liver organoids

Samples of Chol-orgs differentiated towards a hepatocyte fate from donor 1 (Table 5) at day 0, 5, 10 and 15 of the differentiation were produced (Figure 19). An entire 24-well plate was allocated to each sample to ensure sufficient cell material for iTRAQ analysis. Samples were prepared and analysed as described in the methods section. To ensure even loading to each iTRAQ run, Coomassie staining was performed to supplement the Bradford assay. Figure 21A visually demonstrates even loading across these samples, densitometry was performed using Quantity One software (Bio-Rad) and confirms even loading (Figure 21B).

A total of 3343 unique proteins were identified in the sample. Hierarchical clustering analysis was performed, in which each sample was compared against a pooled control. Organoids at day 0 and day 5 clustered together as did organoids at day 10 and day 15. Organoids did not cluster closely with pooled hPH from several donors or donor-matched tissue which clustered more closely to one another than any organoid sample and both clusters of organoids were closer to one another than hPH or liver tissue (Figure 22). Figure 22 is colour-coded to indicate up- or downregulation of each protein detected relative to the pooled control, green indicates downregulation and red indicates upregulation.

A list of liver specific proteins was compiled under the following sections: CYPs, drug metabolism enzymes and transporters (DMETs), NRF2 pathway related genes, transporters, and biomarkers (Table 6). The iTRAQ dataset was interrogated for presence of these proteins and then tested by ANOVA to find any significant differences in expression between the following groups: day 0 and day 5 versus day 10 and day 15, day 0 and day 5 versus hPH, day 0 and day 5 versus liver tissue, day 10 and day 15 versus hPH, and day 10 and day 15 versus liver tissue. Because day 0 and day 5 and day 10 and day 15 clustered closely in hierarchical clustering analysis it was deemed acceptable to treat them as a single group in order to enable statistical analysis. The exact values and associated significance of all the data in Figure 23-28 are also shown in Table 6.

Figures 23-28A show the changes in the protein groups shown in Table 6 for undifferentiated organoids (day 0 and day 5) versus differentiated organoids (day 10 and day 15). None of the proteins in the 'biomarkers' group or the 'NRF2' group were significantly changed (Figure 25A & Figure 27A). In the 'CYPs' group, CYP3A5 expression was significantly higher in differentiated than in undifferentiated organoids, no other tested CYP was significantly altered (Figure 23A). In the 'DMETs' group, NIT1, GGT1, UGT2B15 and UGT2B7 were all significantly higher in differentiated organoids than in undifferentiated (Figure 24A). In the transporters group, ABCF3, ACBB1, SLC12A2, SLC13A5, SLC15A1 and SLC2A2 were all significantly higher in differentiated organoids than in undifferentiated (Figure 26A).

Figures 23-28B show the changes in the protein groups shown in Table 6 for undifferentiated organoids versus hPH. In the 'CYPs' group, CYP4F12 and CYP4V2 are significantly higher in hPH, whilst CYP2S1 is significantly higher in undifferentiated organoids (Figure 23B). In the 'DMETs' group, GGT1, GSTM4 and GSTP1 are all significantly higher in undifferentiated organoids than in hPH. Conversely, GSTA1, GSTT1, CES1, ESD,

UGT2B10 and UGT2B28 are all significantly higher in hPH than in undifferentiated organoids (Figure 24B). In the 'NRF2' section, GSTP1, NQO1 and TRXND1 were all significantly higher in undifferentiated organoids whilst TRXND2 was significantly higher in hPH (Figure 25B). In the 'Transporters' section, SLC2A2, SLC12A2 and ABCF1 were significantly higher in undifferentiated organoids whilst ABCC1 was significantly higher in hPH (Figure 26B). In the 'biomarkers' section, ALT2 was significantly higher in undifferentiated organoids whilst both cytoplasmic and mitochondrial AST were significantly higher in hPH (Figure 27B).

Figures 23-28C show the changes in the protein groups shown in Table 6 for differentiated organoids versus hPH. In the 'CYPs' section CYP2S1 is significantly higher in differentiated organoids, however, CYP1A2, CYP2A6 and CYP2C19 are significantly higher in hPH (Figure 23C). In the 'DMETs' section GSTA1, CES1, UGT2B28 and ESD were all significantly higher in hPH than differentiated organoids. Conversely, GGT1, GSTM4, UGT1A3, GSTP1 and GSTM3 were all higher in differentiated organoids than hPH (Figure 24C). In the 'NRF2' section cytoplasmic TRXND1, NQO1 and GSTP1 were all significantly higher in differentiated organoids than hPH (Figure 25C). In the 'Transporters' section, ABCB1 and ABCF1 were both significantly higher in differentiated organoids than hPH. Conversely bile salt sulfotransferase (SULT2A1) and ABCC1 were both significantly higher in hPH (Figure 26C). In the biomarkers section both cytoplasmic and mitochondrial AST were significantly higher in hPH although ALT2 was significantly higher in differentiated organoids (Figure 27C).

Figure 29 shows volcano plots of the iTRAQ data, produced using Partek. Volcano plots visually represent the change in proteome between organoids versus hepatocytes and liver tissue and between hepatocytes and liver tissue individually. Each point represents a single protein, the x-axis indicates the direction and magnitude of change whilst the y-axis indicates the significance of the change. Therefore, the more the volcano plot 'erupts' the more different the tested samples are. Figure 29A & B show the changes in protein expression between organoids and donor-matched liver tissue and pooled hepatocytes respectively. Both plots show large scale changes in the proteome indicating large difference in protein expression between organoids and these comparators. However, the magnitude and significance of the changes for organoids versus hepatocytes (Figure 29B) tend to be larger than those found between organoids and liver tissue (Figure 29A) Conversely, Figure 29C shows the changes in protein expression between hepatocytes and liver tissue. The differences are not as pronounced as in Figure 29A & B indicating that hepatocytes and liver tissue are more similar to one another than organoids.

4.2.7 Western blot analysis shows expression of mature hepatocyte markers

We performed western blotting on Chol-orgs differentiated towards a hepatocyte fate. We gathered samples at 0-, 5-, 10- and 15-days during differentiation and blotted for hepatic markers, CYP3A4 and albumin (Figure 30). An increase in albumin expression was observed at day 10 and 15 in donor 2 organoids, a small increase in CYP3A4 expression is also observable. These changes are mirrored in the densitometry analysis where the increase in CYP3A4 and Albumin expression can be seen over the process of differentiation. It is noteworthy that in this blot, the levels of β-actin detected in the hPH samples were lower than in the other samples. The protein concentration of each sample was normalised by Bradford and Coomassie assays before blotting, so the reasons for this discrepancy are unclear. Because of this discrepancy, protein levels for densitometry are normalised to donor matched tissue instead of hPH.

Moreover, although western blotting was attempted for donor 3 organoids, we were unable to obtain useful results due to limited cell material. This is likely due to the severely diminished proliferation of cryopreserved organoids. Due to time constraints of this project we were unable to generate additional samples.

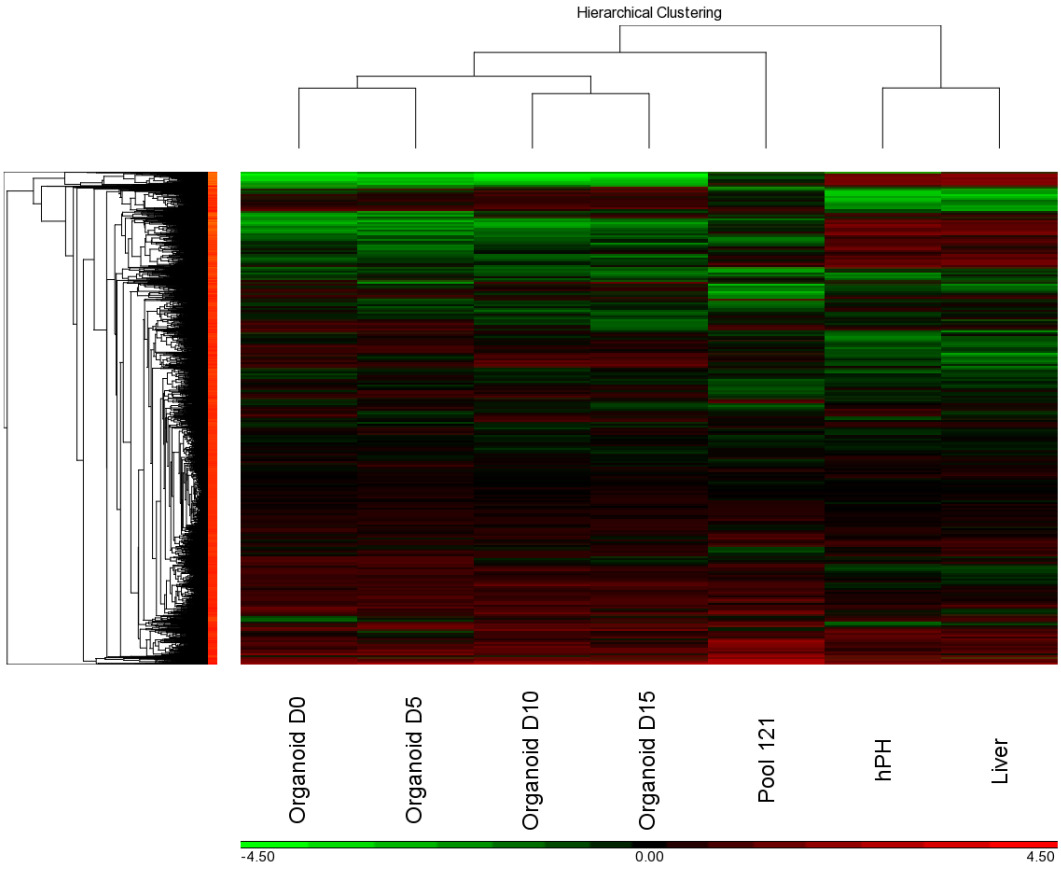

Figure 22

Hierarchical clustering analysis of differentiated organoids, donor-matched liver tissue and hPH – Hierarchical clustering analysis visually represents the similarities between iTRAQ samples. Values shown are relative to Pool 119, pool 121 is identical to pool 119 but was labelled separately and is therefore included in clustering analysis. Green bars represent downregulation, red bars indicate upregulation. The dendrogram indicates how similar each sample is, shorter branches indicate greater similarity. Organoids at day 0 and day 5 cluster together as do organoids at day 10 and day 15. All organoids separate from hPH and liver tissue which cluster together. Produced using Partek.

A

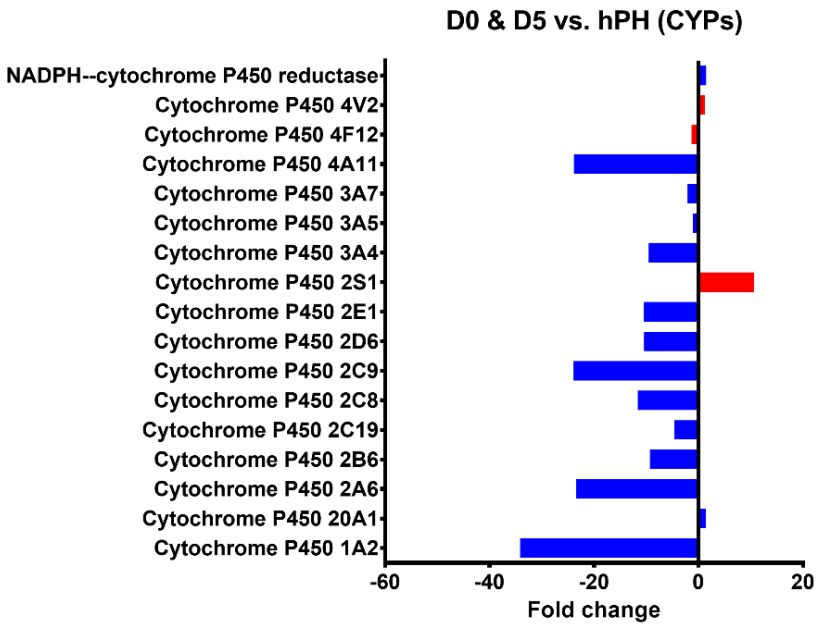
D0 & D5 vs. hPH (CYPs)
NADPH--cytochrome P450 reductase
Cytochrome P450 4V2
Cytochrome P450 4F12
Cytochrome P450 4A11
Cytochrome P450 3A7
Cytochrome P450 3A5
Cytochrome P450 3A4
Cytochrome P450 2S1
Cytochrome P450 2E1
Cytochrome P450 2D6
Cytochrome P450 2C9
Cytochrome P450 2C8
Cytochrome P450 2C19
Cytochrome P450 2B6
Cytochrome P450 2A6
Cytochrome P450 20A1
Cytochrome P450 1A2
-60
-40
-20
0
20
Fold change

B

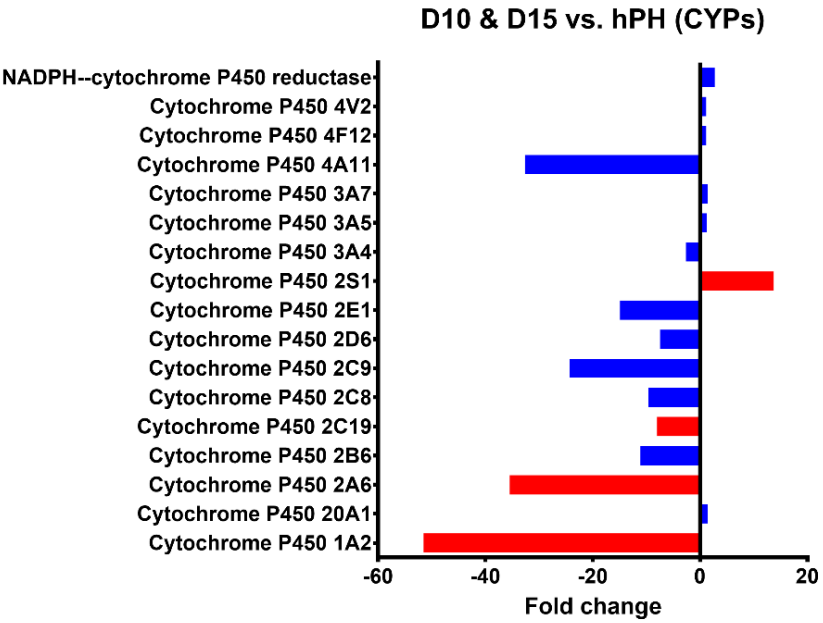
D10 & D15 vs. hPH (CYPs)
NADPH--cytochrome P450 reductase
Cytochrome P450 4V2
Cytochrome P450 4F12
Cytochrome P450 4A11
Cytochrome P450 3A7
Cytochrome P450 3A5
Cytochrome P450 3A4
Cytochrome P450 2S1
Cytochrome P450 2E1
Cytochrome P450 2D6
Cytochrome P450 2C9
Cytochrome P450 2C8
Cytochrome P450 2C19
Cytochrome P450 2B6
Cytochrome P450 2A6
Cytochrome P450 20A1
Cytochrome P450 1A2
-60
-40
-20
0
20
Fold change

C

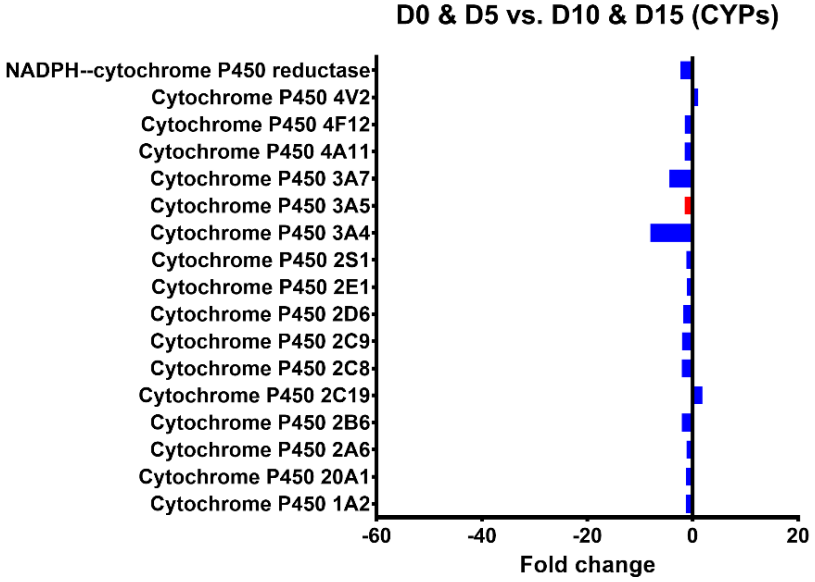
D0 & D5 vs. D10 & D15 (CYPs)
NADPH--cytochrome P450 reductase
Cytochrome P450 4V2
Cytochrome P450 4F12
Cytochrome P450 4A11
Cytochrome P450 3A7
Cytochrome P450 3A5
Cytochrome P450 3A4
Cytochrome P450 2S1
Cytochrome P450 2E1
Cytochrome P450 2D6
Cytochrome P450 2C9
Cytochrome P450 2C8
Cytochrome P450 2C19
Cytochrome P450 2B6
Cytochrome P450 2A6
Cytochrome P450 20A1
Cytochrome P450 1A2
-60
-40
-20
0
20
Fold change

Figure 23

Cytochromes P450 expression in organoids - Graphs showing the fold change in CYP expression in differentiated and undifferentiated organoids analysed by iTRAQ. **(A)** Undifferentiated organoids (day 0 and day 5) versus hPH. **(B)** Differentiated (day 10 and day 15) organoids versus hPH. **(C)** undifferentiated organoids (day 0 and day 5) versus differentiated organoids (day 10 and day 15).

Organoids at day 0 and day 5 and organoids at day 10 and day 15 of differentiation clustered together in Figure 22 and were treated as duplicates for the purposes of analysis. Positive values indicate higher expression in the first comparator, bars in red show significant changes $p \leq 0.05$ determined by ANOVA bars in blue show non-significant changes. Exact values for these changes and abbreviations used in the text are shown in Table 6. Abbreviations: D0 - Differentiation day 0, D5 - Differentiation day 5, D10 - Differentiation day 10, D15 - Differentiation day 15, hPH - Human primary hepatocytes, CYP - Cytochrome P450

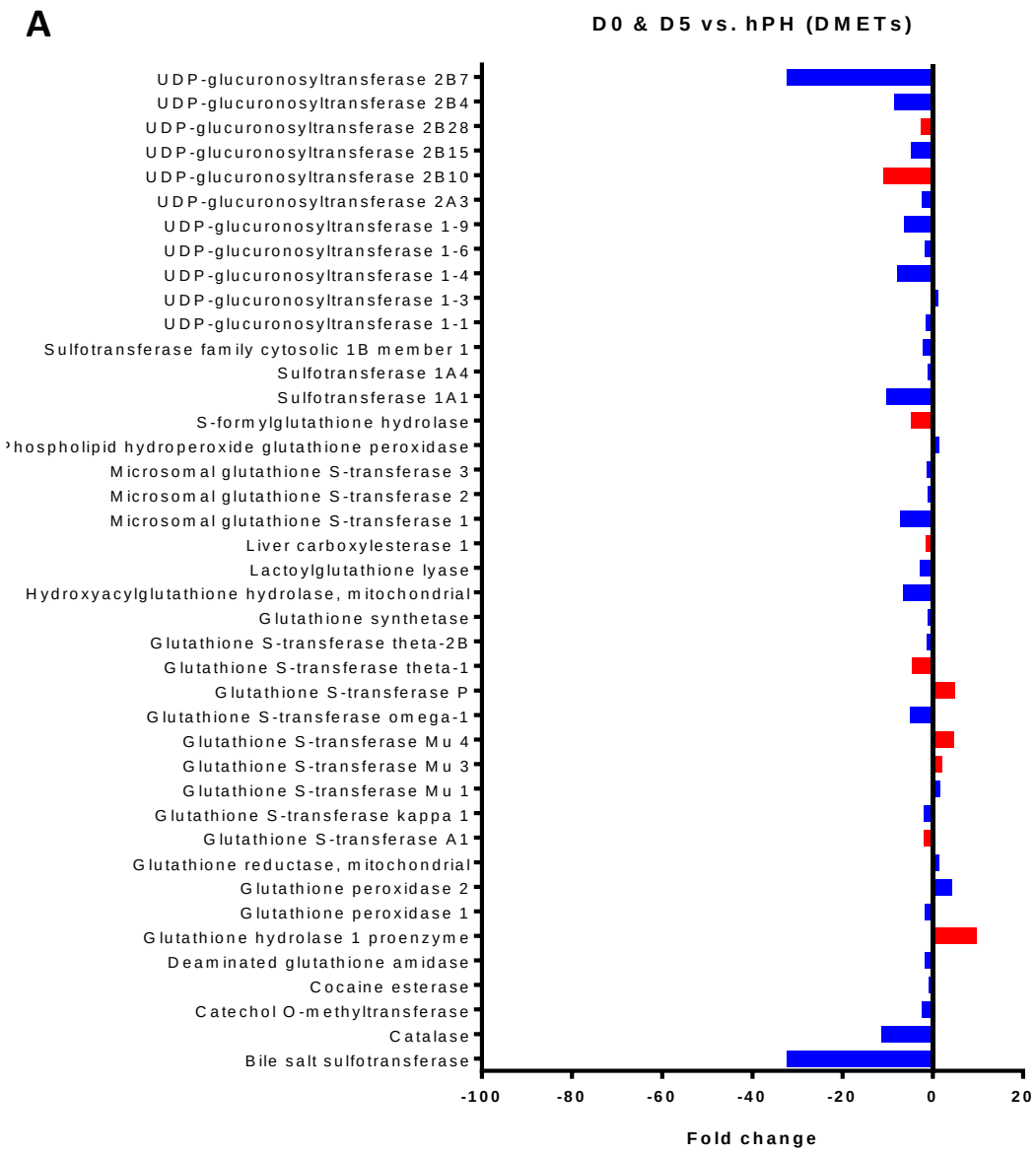
A
D0 & D5 vs. hPH (DMETs)
UDP-glucuronosyltransferase 2B7
UDP-glucuronosyltransferase 2B4
UDP-glucuronosyltransferase 2B28
UDP-glucuronosyltransferase 2B15
UDP-glucuronosyltransferase 2B10
UDP-glucuronosyltransferase 2A3
UDP-glucuronosyltransferase 1-9
UDP-glucuronosyltransferase 1-6
UDP-glucuronosyltransferase 1-4
UDP-glucuronosyltransferase 1-3
UDP-glucuronosyltransferase 1-1
Sulfotransferase family cytosolic 1B member 1
Sulfotransferase 1A4
Sulfotransferase 1A1
S-formylglutathione hydrolase
›hospholipid hydroperoxide glutathione peroxidase
Microsomal glutathione S-transferase 3
Microsomal glutathione S-transferase 2
Microsomal glutathione S-transferase 1
Liver carboxylesterase 1
Lactoylglutathione lyase
Hydroxyacylglutathione hydrolase, mitochondrial
Glutathione synthetase
Glutathione S-transferase theta-2B
Glutathione S-transferase theta-1
Glutathione S-transferase P
Glutathione S-transferase omega-1
Glutathione S-transferase Mu 4
Glutathione S-transferase Mu 3
Glutathione S-transferase Mu 1
Glutathione S-transferase kappa 1
Glutathione S-transferase A1
Glutathione reductase, mitochondrial
Glutathione peroxidase 2
Glutathione peroxidase 1
Glutathione hydrolase 1 proenzyme
Deaminated glutathione amidase
Cocaine esterase
Catechol O-methyltransferase
Catalase
Bile salt sulfotransferase
-100
-80
-60
-40
-20
0
20
Fold change

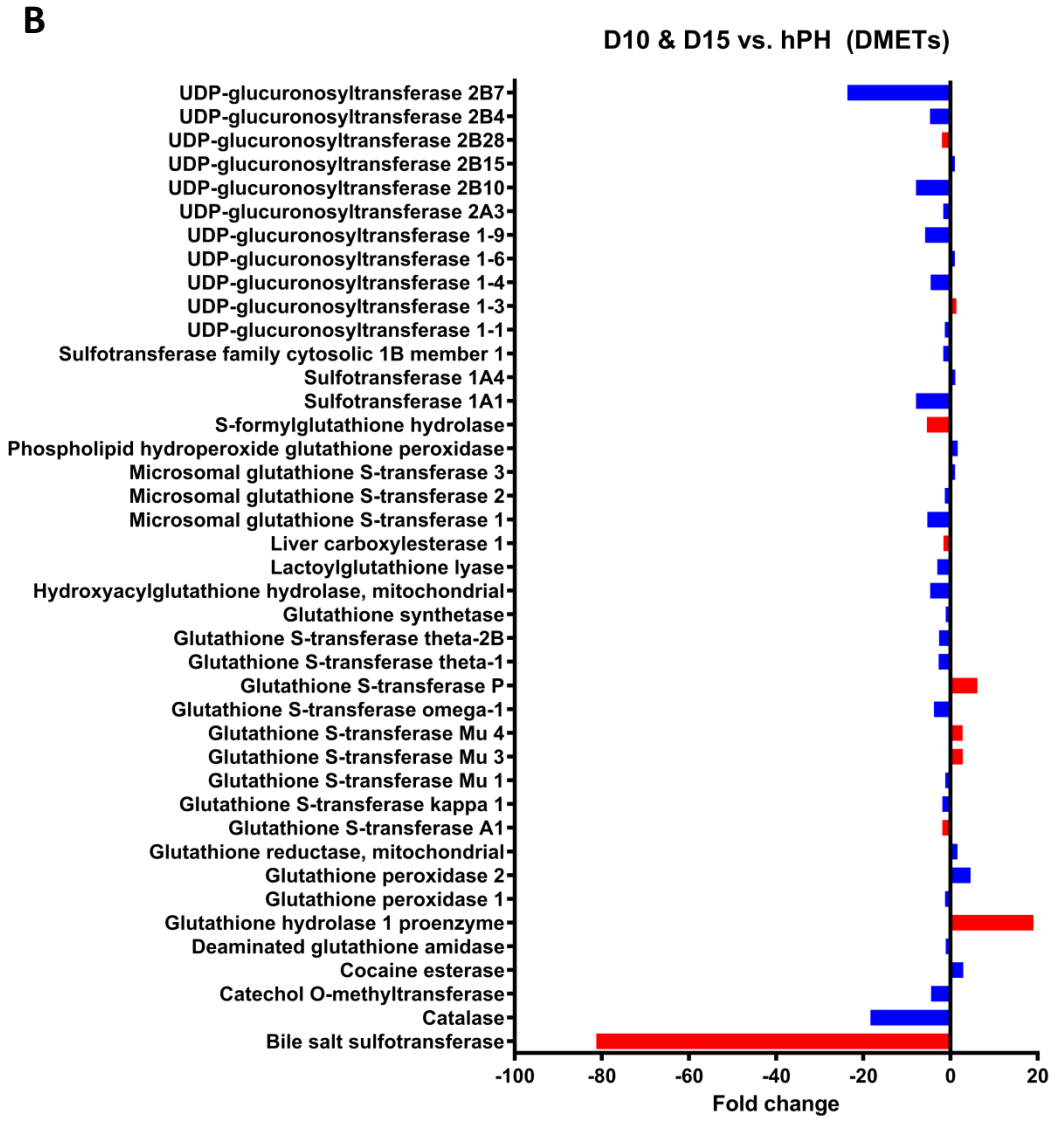
B
D10 & D15 vs. hPH (DMETs)
UDP-glucuronosyltransferase 2B7
UDP-glucuronosyltransferase 2B4
UDP-glucuronosyltransferase 2B28
UDP-glucuronosyltransferase 2B15
UDP-glucuronosyltransferase 2B10
UDP-glucuronosyltransferase 2A3
UDP-glucuronosyltransferase 1-9
UDP-glucuronosyltransferase 1-6
UDP-glucuronosyltransferase 1-4
UDP-glucuronosyltransferase 1-3
UDP-glucuronosyltransferase 1-1
Sulfotransferase family cytosolic 1B member 1
Sulfotransferase 1A4
Sulfotransferase 1A1
S-formylglutathione hydrolase
Phospholipid hydroperoxide glutathione peroxidase
Microsomal glutathione S-transferase 3
Microsomal glutathione S-transferase 2
Microsomal glutathione S-transferase 1
Liver carboxylesterase 1
Lactoylglutathione lyase
Hydroxyacylglutathione hydrolase, mitochondrial
Glutathione synthetase
Glutathione S-transferase theta-2B
Glutathione S-transferase theta-1
Glutathione S-transferase P
Glutathione S-transferase omega-1
Glutathione S-transferase Mu 4
Glutathione S-transferase Mu 3
Glutathione S-transferase Mu 1
Glutathione S-transferase kappa 1
Glutathione S-transferase A1
Glutathione reductase, mitochondrial
Glutathione peroxidase 2
Glutathione peroxidase 1
Glutathione hydrolase 1 proenzyme
Deaminated glutathione amidase
Cocaine esterase
Catechol O-methyltransferase
Catalase
Bile salt sulfotransferase
-100
-80
-60
-40
-20
0
20
Fold change

C

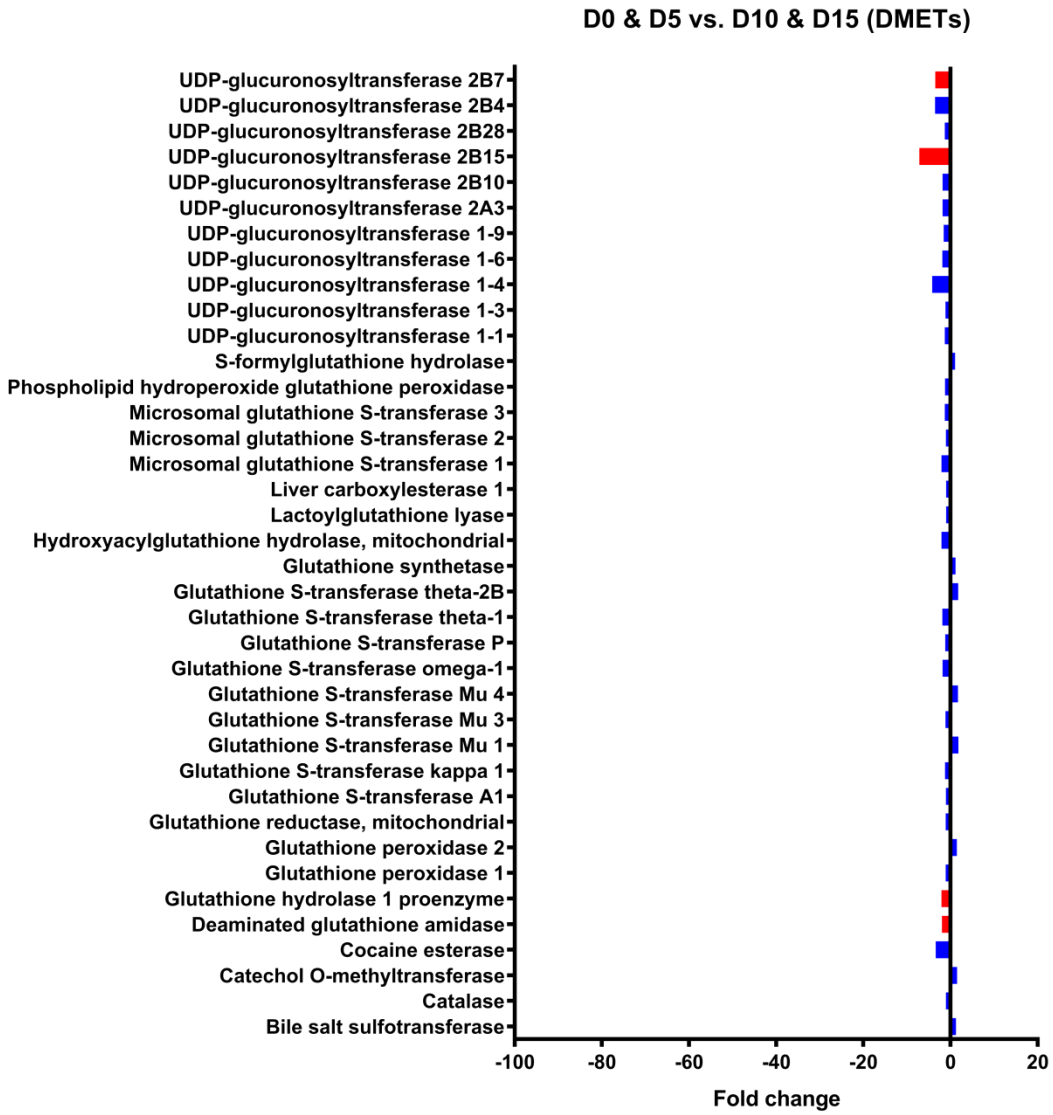
D0 & D5 vs. D10 & D15 (DMETs)
UDP-glucuronosyltransferase 2B7
UDP-glucuronosyltransferase 2B4
UDP-glucuronosyltransferase 2B28
UDP-glucuronosyltransferase 2B15
UDP-glucuronosyltransferase 2B10
UDP-glucuronosyltransferase 2A3
UDP-glucuronosyltransferase 1-9
UDP-glucuronosyltransferase 1-6
UDP-glucuronosyltransferase 1-4
UDP-glucuronosyltransferase 1-3
UDP-glucuronosyltransferase 1-1
S-formylglutathione hydrolase
Phospholipid hydroperoxide glutathione peroxidase
Microsomal glutathione S-transferase 3
Microsomal glutathione S-transferase 2
Microsomal glutathione S-transferase 1
Liver carboxylesterase 1
Lactoylglutathione lyase
Hydroxyacylglutathione hydrolase, mitochondrial
Glutathione synthetase
Glutathione S-transferase theta-2B
Glutathione S-transferase theta-1
Glutathione S-transferase P
Glutathione S-transferase omega-1
Glutathione S-transferase Mu 4
Glutathione S-transferase Mu 3
Glutathione S-transferase Mu 1
Glutathione S-transferase kappa 1
Glutathione S-transferase A1
Glutathione reductase, mitochondrial
Glutathione peroxidase 2
Glutathione peroxidase 1
Glutathione hydrolase 1 proenzyme
Deaminated glutathione amidase
Cocaine esterase
Catechol O-methyltransferase
Catalase
Bile salt sulfotransferase
-100
-80
-60
-40
-20
0
20
Fold change

Figure 24

DMET expression in organoids - Graphs showing the fold change in DMET expression in differentiated and undifferentiated organoids analysed by iTRAQ. **(A)** Undifferentiated organoids (day 0 and day 5) versus hPH. **(B)** Differentiated (day 10 and day 15) organoids versus hPH. **(C)** Undifferentiated organoids (day 0 and day 5) versus differentiated organoids (day 10 and day 15).

Organoids at day 0 and day 5 and organoids at day 10 and day 15 of differentiation clustered together in Figure 22 and were treated as duplicates for the purposes of analysis. Positive values indicate higher expression in the first comparator, bars in red show significant changes $p \leq 0.05$ determined by ANOVA bars in blue show non-significant changes. Exact values for these changes and abbreviations used in the text are shown in Table 6. Abbreviations: D0 - Differentiation day 0, D5 - Differentiation day 5, D10 - Differentiation day 10, D15 - Differentiation day 15, hPH - Human primary hepatocytes, DMET – Drug metabolising enzymes and transporters

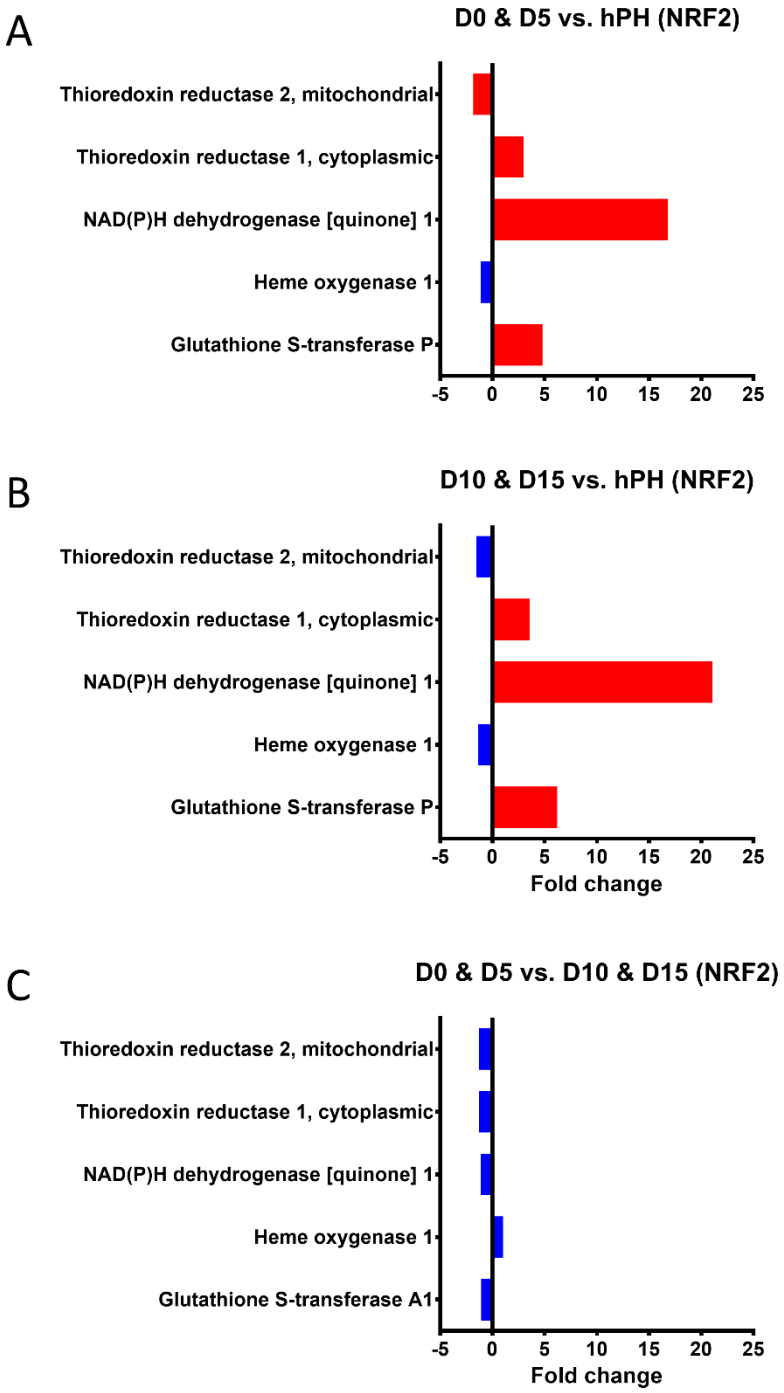
A
D0 & D5 vs. hPH (NRF2)
Thioredoxin reductase 2, mitochondrial
Thioredoxin reductase 1, cytoplasmic
NAD(P)H dehydrogenase [quinone] 1
Heme oxygenase 1
Glutathione S-transferase P
-5 0 5 10 15 20 25
B
D10 & D15 vs. hPH (NRF2)
Thioredoxin reductase 2, mitochondrial
Thioredoxin reductase 1, cytoplasmic
NAD(P)H dehydrogenase [quinone] 1
Heme oxygenase 1
Glutathione S-transferase P
-5 0 5 10 15 20 25
Fold change
C
D0 & D5 vs. D10 & D15 (NRF2)
Thioredoxin reductase 2, mitochondrial
Thioredoxin reductase 1, cytoplasmic
NAD(P)H dehydrogenase [quinone] 1
Heme oxygenase 1
Glutathione S-transferase A1
-5 0 5 10 15 20 25
Fold change

Figure 25

NRF2 pathway expression in organoids - Graphs showing the fold change in NRF2 pathway expression in differentiated and undifferentiated organoids analysed by iTRAQ. **(A)** Undifferentiated organoids (day 0 and day 5) versus hPH. **(B)** Differentiated (day 10 and day 15) organoids versus hPH. **(C)** Undifferentiated organoids (day 0 and day 5) versus differentiated organoids (day 10 and day 15).

Organoids at day 0 and day 5 and organoids at day 10 and day 15 of differentiation clustered together in Figure 22 and were treated as duplicates for the purposes of analysis. Positive values indicate higher expression in the first comparator, bars in red show significant changes $p \leq 0.05$ determined by ANOVA bars in blue show non-significant changes. Exact values for these changes and abbreviations used in the text are shown in Table 6. Abbreviations: D0 - Differentiation day 0, D5 - Differentiation day 5, D10 - Differentiation day 10, D15 - Differentiation day 15, hPH - Human primary hepatocytes, NRF2 – Nuclear factor erythroid 2-related factor 2

A

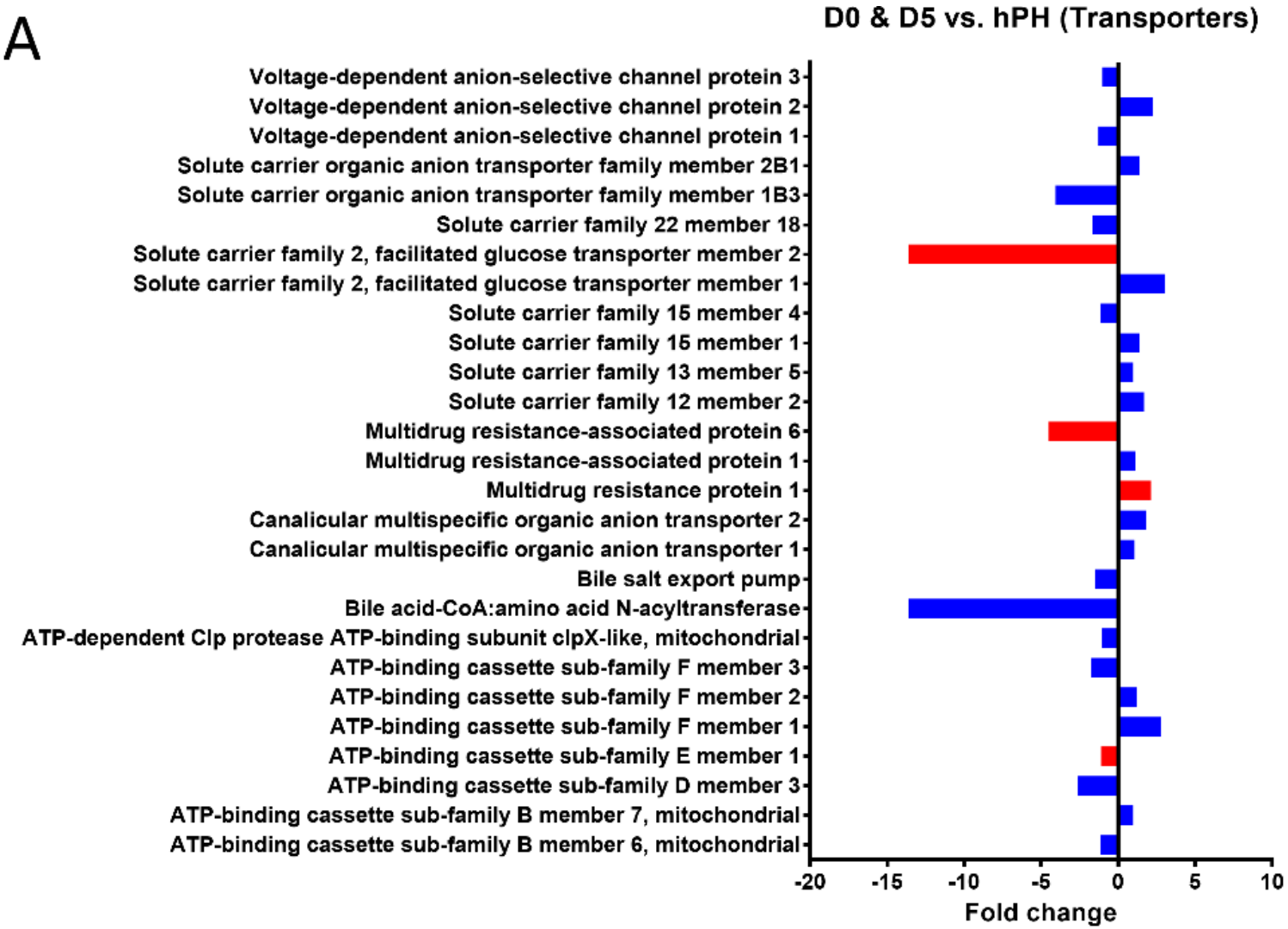
D0 & D5 vs. hPH (Transporters)
Voltage-dependent anion-selective channel protein 3
Voltage-dependent anion-selective channel protein 2
Voltage-dependent anion-selective channel protein 1
Solute carrier organic anion transporter family member 2B1
Solute carrier organic anion transporter family member 1B3
Solute carrier family 22 member 18
Solute carrier family 2, facilitated glucose transporter member 2
Solute carrier family 2, facilitated glucose transporter member 1
Solute carrier family 15 member 4
Solute carrier family 15 member 1
Solute carrier family 13 member 5
Solute carrier family 12 member 2
Multidrug resistance-associated protein 6
Multidrug resistance-associated protein 1
Multidrug resistance protein 1
Canalicular multispecific organic anion transporter 2
Canalicular multispecific organic anion transporter 1
Bile salt export pump
Bile acid-CoA:amino acid N-acyltransferase
ATP-dependent Clp protease ATP-binding subunit clpX-like, mitochondrial
ATP-binding cassette sub-family F member 3
ATP-binding cassette sub-family F member 2
ATP-binding cassette sub-family F member 1
ATP-binding cassette sub-family E member 1
ATP-binding cassette sub-family D member 3
ATP-binding cassette sub-family B member 7, mitochondrial
ATP-binding cassette sub-family B member 6, mitochondrial
-20
-15
-10
-5
0
5
10
Fold change

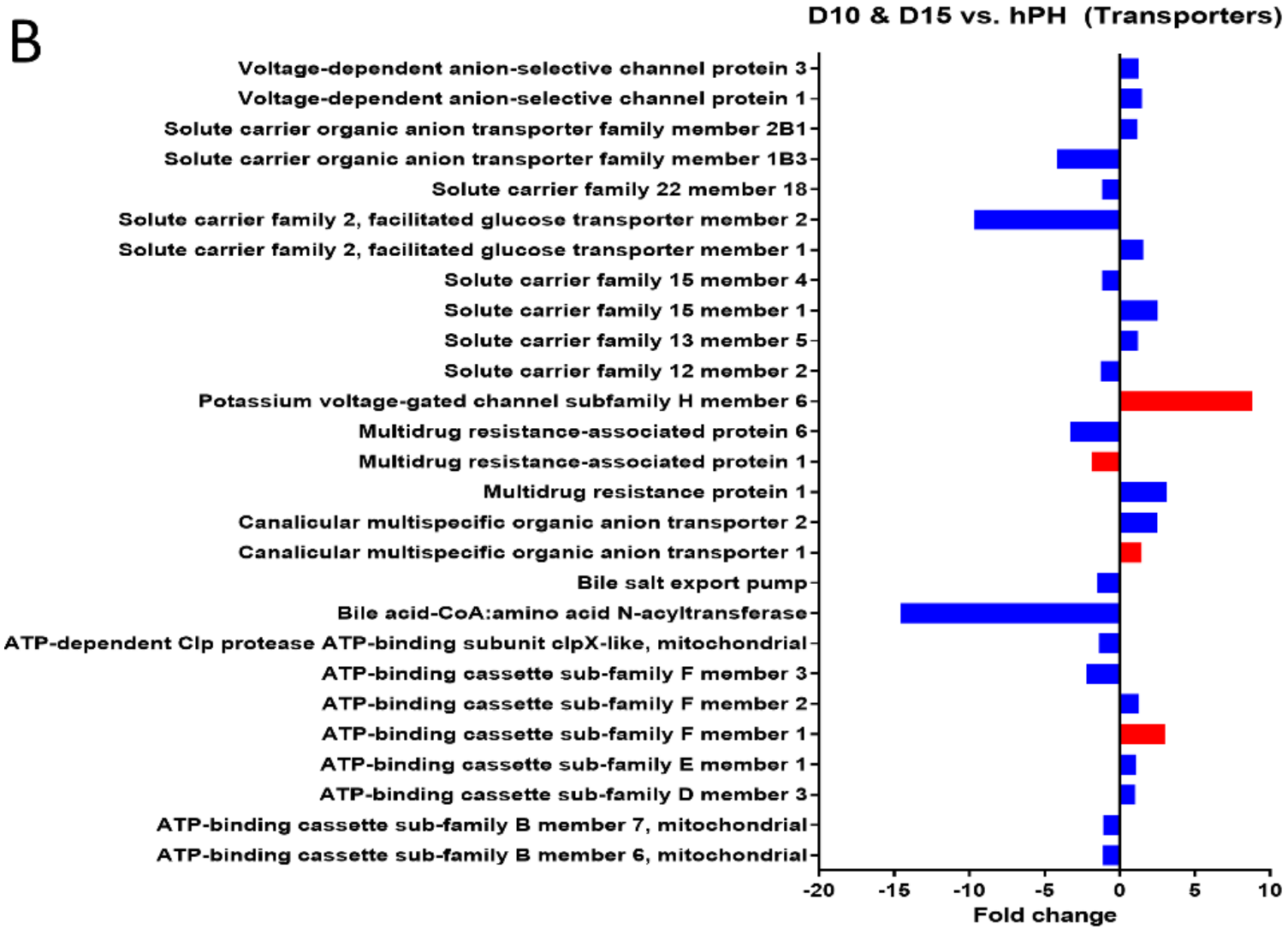
B
D10 & D15 vs. hPH (Transporters)
Voltage-dependent anion-selective channel protein 3
Voltage-dependent anion-selective channel protein 1
Solute carrier organic anion transporter family member 2B1
Solute carrier organic anion transporter family member 1B3
Solute carrier family 22 member 18
Solute carrier family 2, facilitated glucose transporter member 2
Solute carrier family 2, facilitated glucose transporter member 1
Solute carrier family 15 member 4
Solute carrier family 15 member 1
Solute carrier family 13 member 5
Solute carrier family 12 member 2
Potassium voltage-gated channel subfamily H member 6
Multidrug resistance-associated protein 6
Multidrug resistance-associated protein 1
Multidrug resistance protein 1
Canalicular multispecific organic anion transporter 2
Canalicular multispecific organic anion transporter 1
Bile salt export pump
Bile acid-CoA:amino acid N-acyltransferase
ATP-dependent Clp protease ATP-binding subunit clpX-like, mitochondrial
ATP-binding cassette sub-family F member 3
ATP-binding cassette sub-family F member 2
ATP-binding cassette sub-family F member 1
ATP-binding cassette sub-family E member 1
ATP-binding cassette sub-family D member 3
ATP-binding cassette sub-family B member 7, mitochondrial
ATP-binding cassette sub-family B member 6, mitochondrial
-20
-15
-10
-5
0
5
10
Fold change

C

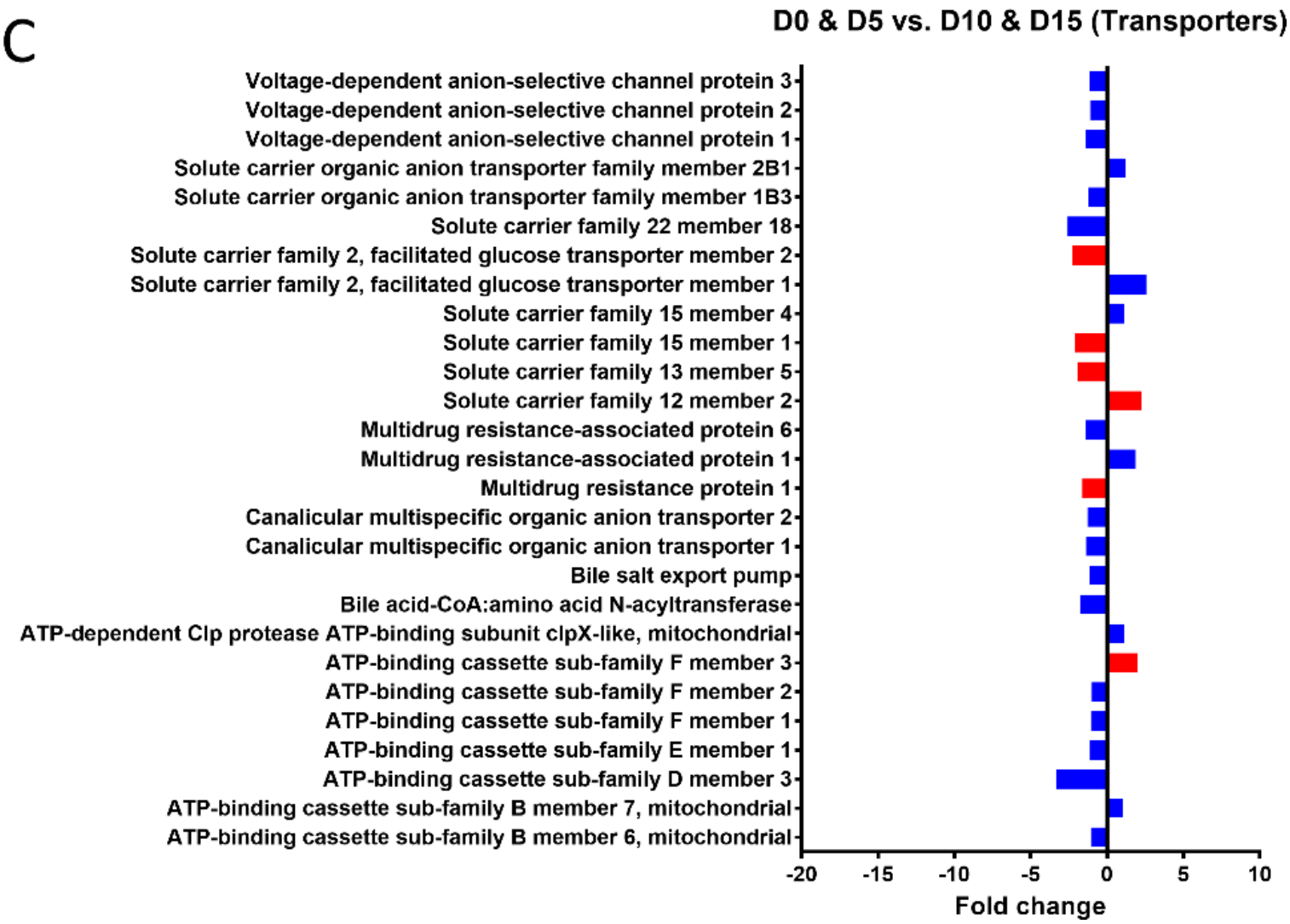
D0 & D5 vs. D10 & D15 (Transporters)
Voltage-dependent anion-selective channel protein 3
Voltage-dependent anion-selective channel protein 2
Voltage-dependent anion-selective channel protein 1
Solute carrier organic anion transporter family member 2B1
Solute carrier organic anion transporter family member 1B3
Solute carrier family 22 member 18
Solute carrier family 2, facilitated glucose transporter member 2
Solute carrier family 2, facilitated glucose transporter member 1
Solute carrier family 15 member 4
Solute carrier family 15 member 1
Solute carrier family 13 member 5
Solute carrier family 12 member 2
Multidrug resistance-associated protein 6
Multidrug resistance-associated protein 1
Multidrug resistance protein 1
Canalicular multispecific organic anion transporter 2
Canalicular multispecific organic anion transporter 1
Bile salt export pump
Bile acid-CoA:amino acid N-acyltransferase
ATP-dependent Clp protease ATP-binding subunit clpX-like, mitochondrial
ATP-binding cassette sub-family F member 3
ATP-binding cassette sub-family F member 2
ATP-binding cassette sub-family F member 1
ATP-binding cassette sub-family E member 1
ATP-binding cassette sub-family D member 3
ATP-binding cassette sub-family B member 7, mitochondrial
ATP-binding cassette sub-family B member 6, mitochondrial
-20
-15
-10
-5
0
5
10
Fold change

Figure 26

Transporter expression in organoids - Graphs showing the fold change in transporter expression in differentiated and undifferentiated organoids analysed by iTRAQ. **(A)** Undifferentiated organoids (day 0 and day 5) versus hPH. **(B)** Differentiated (day 10 and day 15) organoids versus hPH. **(C)** Undifferentiated organoids (day 0 and day 5) versus differentiated organoids (day 10 and day 15).

Organoids at day 0 and day 5 and organoids at day 10 and day 15 of differentiation clustered together in Figure 22 and were treated as duplicates for the purposes of analysis. Positive values indicate higher expression in the first comparator, bars in red show significant changes $p \leq 0.05$ determined by ANOVA bars in blue show non-significant changes. Exact values for these changes and abbreviations used in the text are shown in Table 6. Abbreviations: D0 - Differentiation day 0, D5 - Differentiation day 5, D10 - Differentiation day 10, D15 - Differentiation day 15, hPH - Human primary hepatocytes

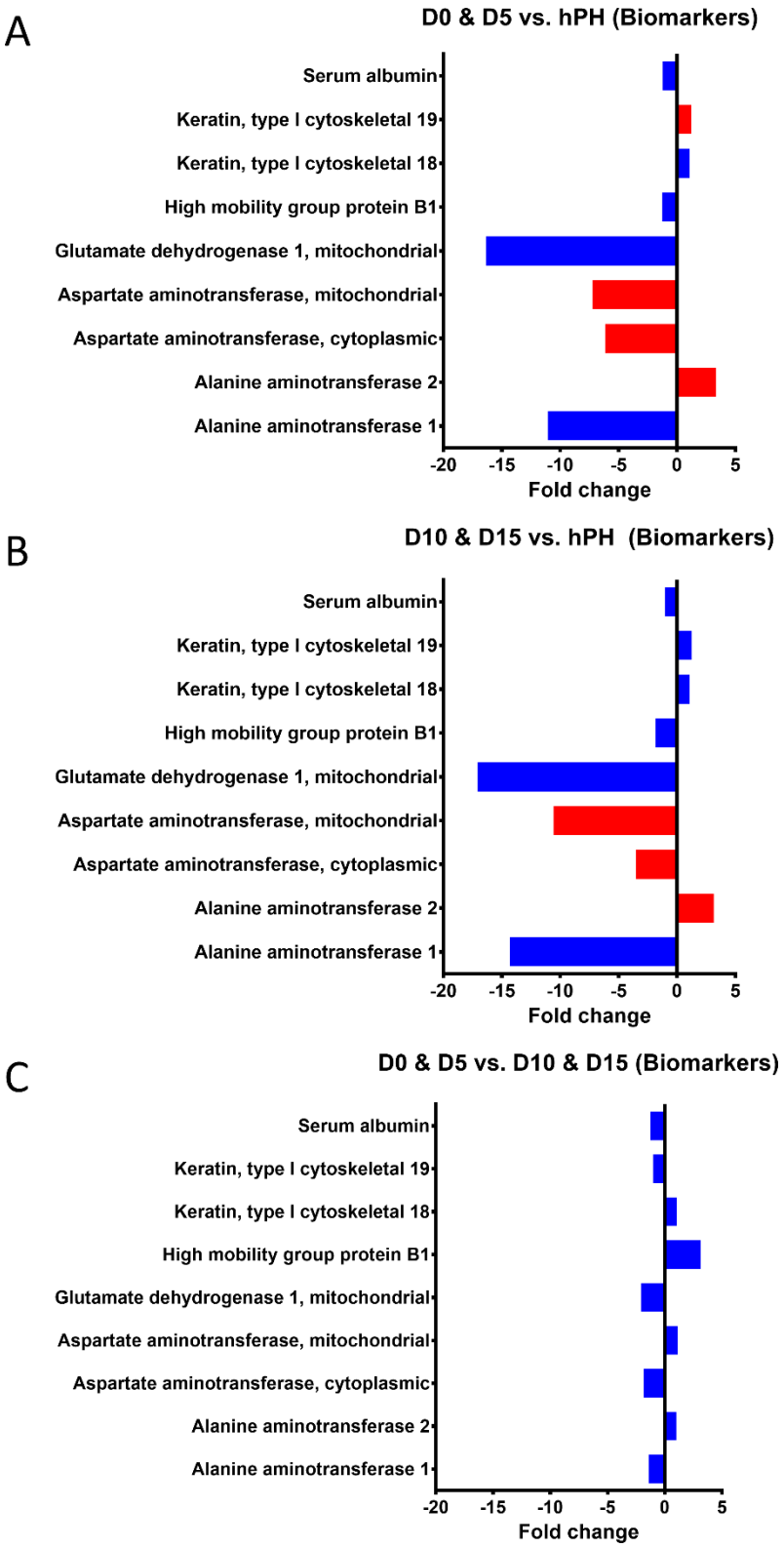

Figure 27

Biomarker expression in organoids - Graphs showing the fold change in expression of biomarkers in differentiated and undifferentiated organoids analysed by iTRAQ. **(A)** Undifferentiated organoids (day 0 and day 5) versus hPH. **(B)** Differentiated (day 10 and day

15) organoids versus hPH. **(C)** Undifferentiated organoids (day 0 and day 5) versus differentiated organoids (day 10 and day 15).

Organoids at day 0 and day 5 and organoids at day 10 and day 15 of differentiation clustered together in Figure 22 and were treated as duplicates for the purposes of analysis. Positive values indicate higher expression in the first comparator, bars in red show significant changes $p \leq 0.05$ determined by ANOVA bars in blue show non-significant changes. Exact values for these changes and abbreviations used in the text are shown in Table 6. Abbreviations: D0 - Differentiation day 0, D5 - Differentiation day 5, D10 - Differentiation day 10, D15 - Differentiation day 15, hPH - Human primary hepatocytes

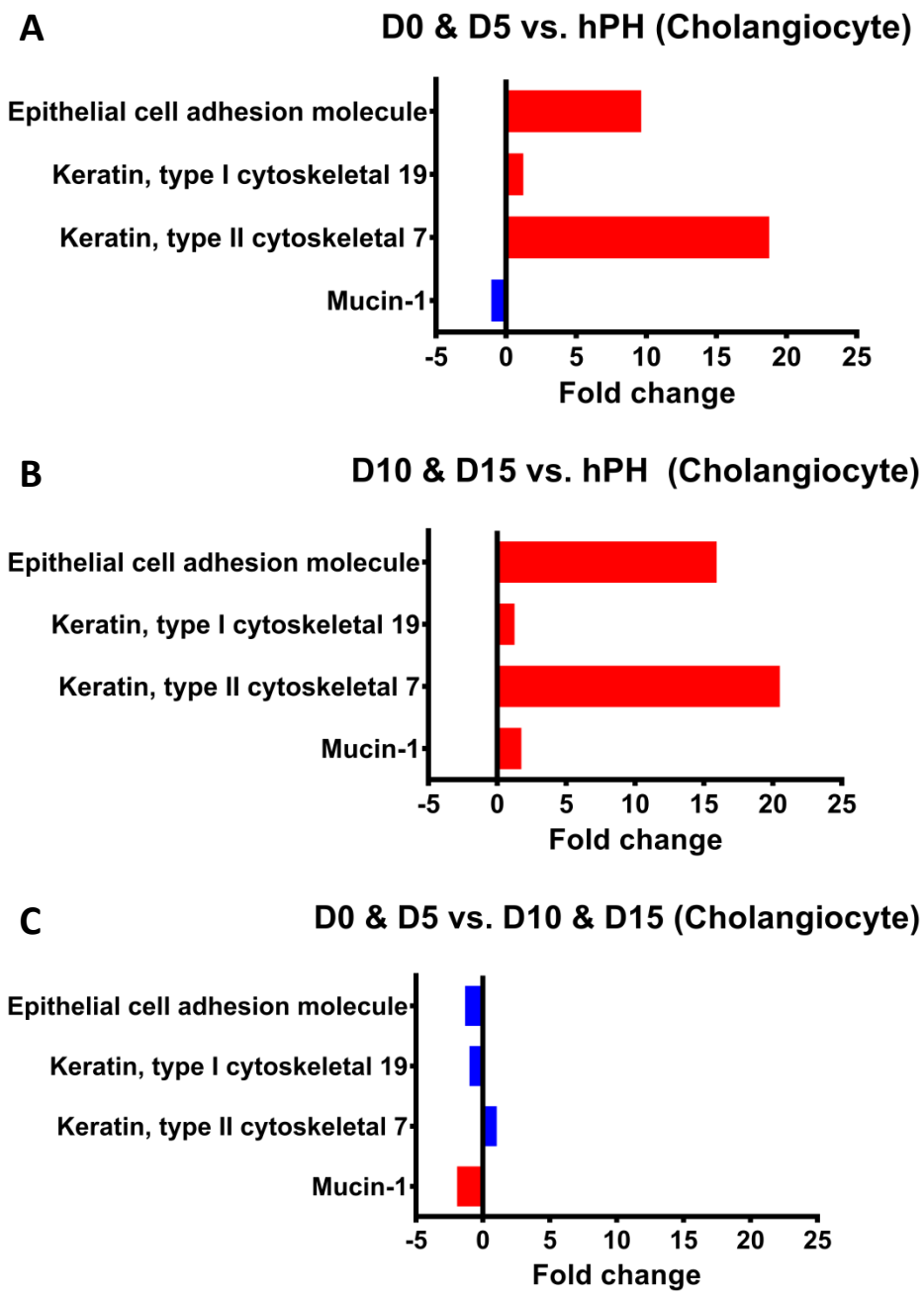

Figure 28

Cholangiocyte marker expression in organoids - Graphs showing the fold change in cholangiocyte marker expression in differentiated and undifferentiated organoids analysed by iTRAQ. **(A)** Undifferentiated organoids (day 0 and day 5) versus hPH. **(B)** Differentiated (day 10 and day 15) organoids versus hPH. **(C)** Undifferentiated organoids (day 0 and day 5) versus differentiated organoids (day 10 and day 15).

Organoids at day 0 and day 5 and organoids at day 10 and day 15 of differentiation clustered together in Figure 22 and were treated as duplicates for the purposes of analysis. Positive values indicate higher expression in the first comparator, bars in red show

significant changes $p \leq 0.05$ determined by ANOVA bars in blue show non-significant changes. Exact values for these changes and abbreviations used in the text are shown in Table 6. Abbreviations: D0 - Differentiation day 0, D5 - Differentiation day 5, D10 - Differentiation day 10, D15 - Differentiation day 15, hPH - Human primary hepatocytes

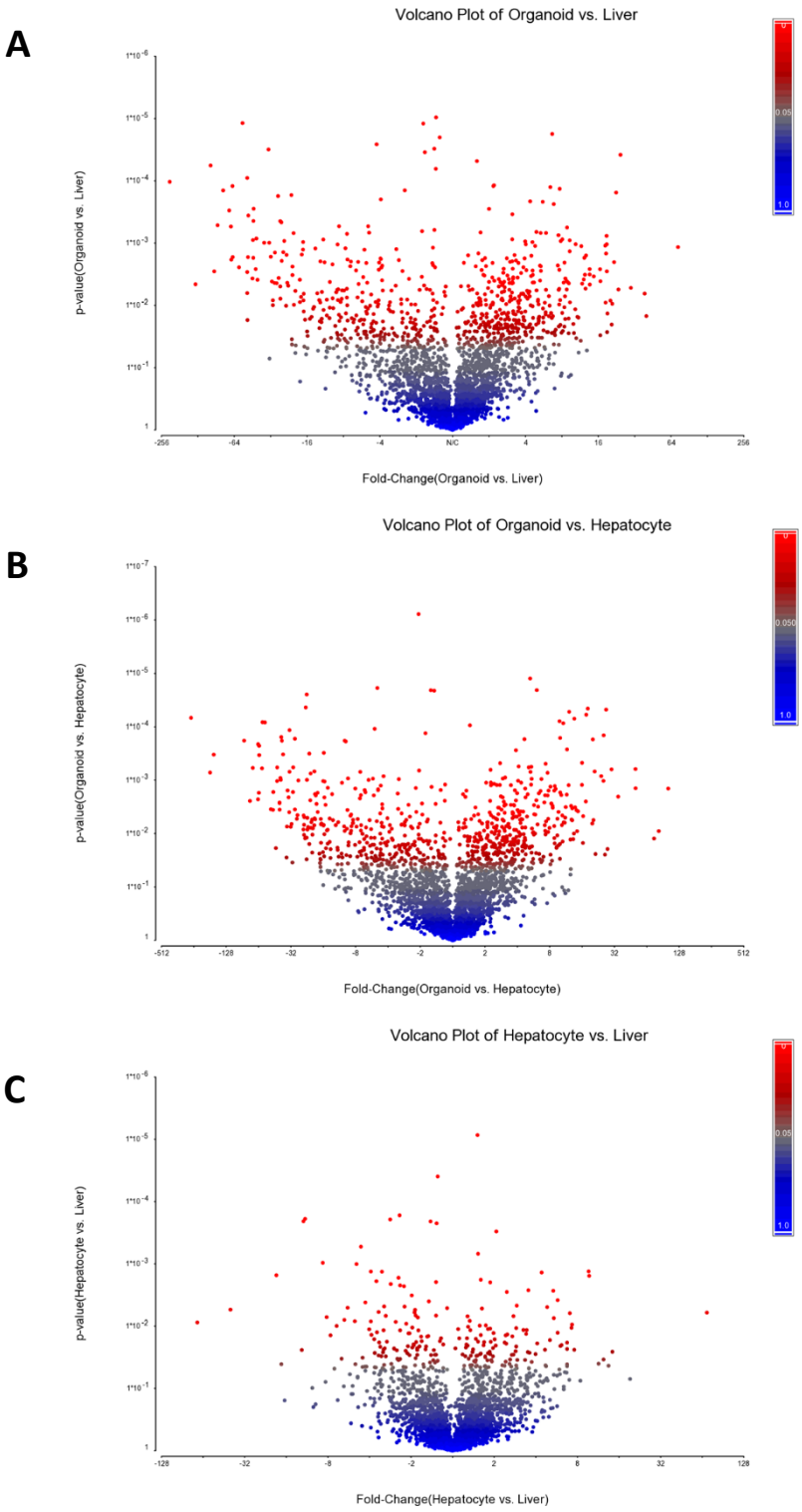

Figure 29

Volcano plots showing changes in protein expression in organoids, hPH and liver tissue – **(A)** Volcano plot showing change in protein expression between differentiated donor 1 organoids (day 10 and day 15) and donor 1 liver tissue. **(B)** Volcano plot showing change in protein expression between differentiated donor 1 organoids (day 10 and day 15) and pooled hPH. **(C)** Volcano plot showing change in protein expression between pooled hPH and donor 1 liver tissue.

C

Chapter 4

Plots showing changes between samples tested during iTRAQ analysis. Values along the x-axis show fold change and values on the y-axis show significance associated with this change. Each point represents a single protein. Significance is colour coded from blue to red, indicating greater or lesser significance respectively. Details of donor 1 are shown in Table 5. Panel A and B show large scale changes between differentiated human liver organoids and tissue and hepatocytes respectively. The differences between tissue and hepatocytes, shown in panel C are smaller and less significant.

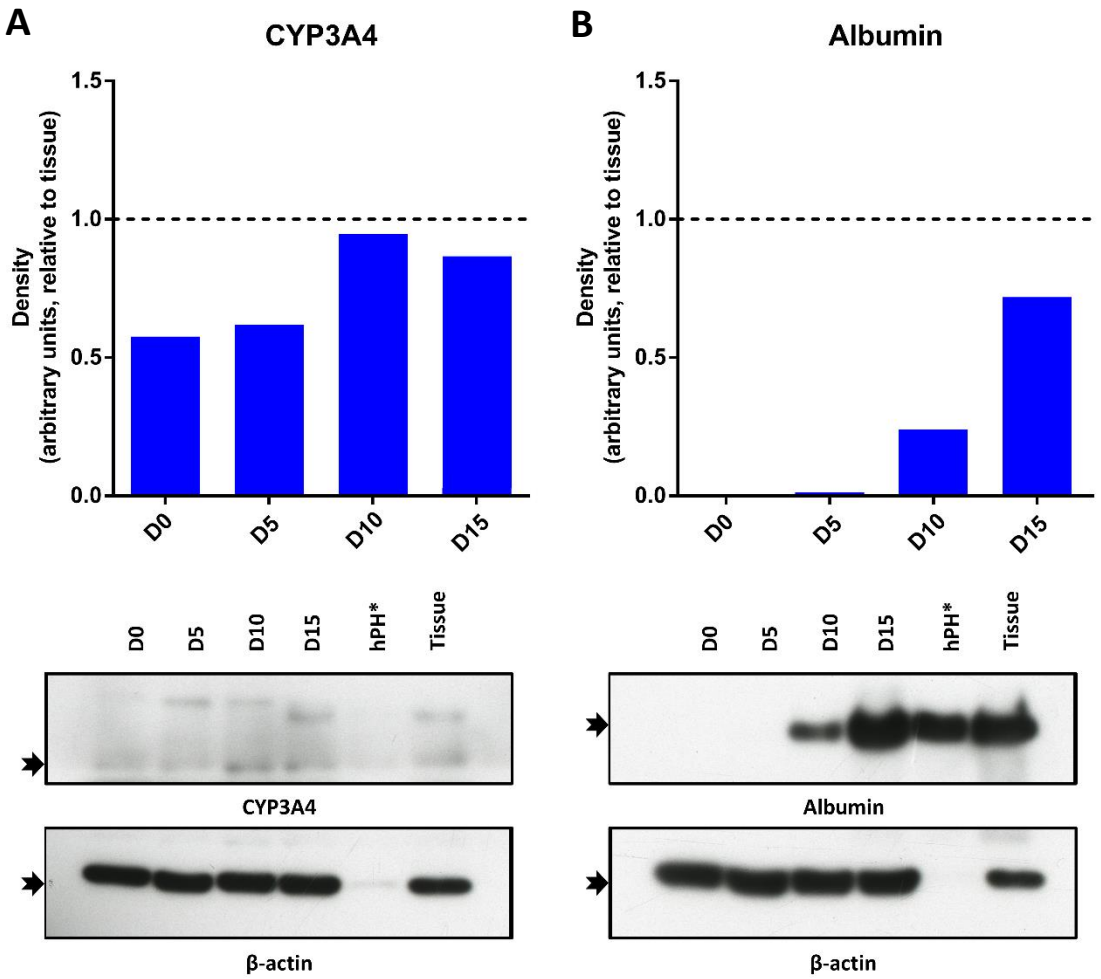

Figure 30

Western blotting of donor 2 organoids for CYP3A4 and Albumin – Western blots were performed on donor 2 organoid samples taken at day 0, 5, 10 and 15 during differentiation. **(A)** western blotting for CYP3A4, density is expressed in arbitrary values relative to donor-matched tissue, which is represented by the dotted line. **(B)** western blotting for albumin, density is expressed in arbitrary values relative to donor-matched tissue, which is represented by the dotted line. Black arrows indicate the bands used for densitometry analysis. Densitometry was performed using ImageJ. hPH*, is included in the images but was not included in further analysis as β-actin density for this sample was spuriously low. Abbreviations: D0 - Differentiation day 0, D5 - Differentiation day 5, D10 - Differentiation day 10, D15 - Differentiation day 15, hPH - Human primary hepatocytes, CYP - Cytochrome P450

Protein name	Abbreviation	Undifferentiated organoids vs. hPH	p-value	Differentiated organoids vs. hPH	Significance	Undifferentiated organoids vs. Differentiated organoids	Significance
CYPs							
Cytochrome P450 1A2	CYP1A2	-34.146	0.055	-51.523	0.049	-1.330	0.307
Cytochrome P450 20A1	CYP20A1	1.410	0.501	1.479	0.473	-1.300	0.473
Cytochrome P450 2A6	CYP2A6	-23.406	0.049	-35.481	0.041	-1.197	0.275
Cytochrome P450 2B6	CYP2B6	-9.290	0.250	-11.117	0.243	-2.099	0.249
Cytochrome P450 2C19	CYP2C19	-4.585	0.049	-8.017	0.026	1.803	0.359
Cytochrome P450 2C8	CYP2C8	-11.623	0.076	-9.683	0.103	-2.080	0.080
Cytochrome P450 2C9	CYP2C9	-23.915	0.083	-24.322	0.093	-2.051	0.151
Cytochrome P450 2D6	CYP2D6	-10.407	0.079	-7.482	0.123	-1.811	0.548
Cytochrome P450 2E1	CYP2E1	-10.439	0.069	-14.928	0.056	-1.153	0.576
Cytochrome P450 2S1	CYP2S1	10.633	0.016	13.740	0.014	-1.213	0.737
Cytochrome P450 3A4	CYP3A4	-9.521	0.251	-2.630	0.606	-8.091	0.157
Cytochrome P450 3A5	CYP3A4	-1.070	0.802	1.259	0.443	-1.556	0.028
Cytochrome P450 3A7	CYP3A7	-2.083	0.417	1.406	0.708	-4.446	0.066
Cytochrome P450 4A11	CYP4A11	-23.842	0.089	-32.659	0.082	-1.563	0.276
Cytochrome P450 4F12	CYP4F12	-1.335	0.107	1.159	0.352	-1.521	0.085
Cytochrome P450 4V2	CYP4V2	1.267	0.228	1.122	0.538	1.028	0.513
NADPH--cytochrome P450 reductase	CPR	1.463	0.600	2.767	0.237	-2.388	0.261
DMETs							
Catalase	CAT	-11.482	0.080	-18.365	0.061	-1.081	0.819

Protein name	Abbreviation	Undifferentiated organoids vs. hPH	p-value	Differentiated organoids vs. hPH	Significance	Undifferentiated organoids vs. Differentiated organoids	Significance
Catechol O-methyltransferase	COMT	-2.543	0.252	-4.487	0.121	1.535	0.581
Cocaine esterase	COCE	-1.009	0.990	2.938	0.230	-3.373	0.217
Deaminated glutathione amidase	NIT1	-1.797	0.181	-1.107	0.796	-1.977	0.025
Glutathione hydrolase 1 proenzyme	GGT1	9.787	0.001	19.055	0.000	-2.080	0.019
Glutathione peroxidase 1	GPX1	-1.820	0.265	-1.282	0.630	-1.112	0.639
Glutathione peroxidase 2	GPX2	4.285	0.182	4.634	0.185	1.466	0.442
Glutathione reductase, mitochondrial	GSR	1.271	0.585	1.652	0.315	-1.096	0.784
Glutathione S-transferase A1	GSTA1	-1.929	0.004	-1.854	0.006	-1.081	0.294
Glutathione S-transferase kappa 1	GSTK1	-1.977	0.152	-1.879	0.194	-1.253	0.423
Glutathione S-transferase Mu 1	GSTM1	1.518	0.196	-1.213	0.521	1.862	0.145
Glutathione S-transferase Mu 3	GSTM3	2.070	0.089	2.858	0.043	-1.159	0.159
Glutathione S-transferase Mu 4	GSTM4	4.613	0.008	2.793	0.029	1.714	0.168
Glutathione S-transferase omega-1	GSTO1	-5.012	0.094	-3.819	0.154	-1.803	0.315
Glutathione S-transferase P	GSTP1	4.801	0.048	6.194	0.038	-1.213	0.738
Glutathione S-transferase theta-1	GSTT1	-4.713	0.022	-2.754	0.073	-1.879	0.201
Glutathione S-transferase theta-2B	GSTT2B	-1.450	0.428	-2.642	0.110	1.778	0.312
Glutathione synthetase	GSS	-1.124	0.700	-1.117	0.730	1.159	0.344
Hydroxyacylglutathione hydrolase, mitochondrial	HAGH	-6.689	0.068	-4.677	0.122	-2.070	0.160
Lactoylglutathione lyase	GLO1	-2.920	0.087	-3.062	0.090	-1.005	0.993
Liver carboxylesterase 1	CES1	-1.537	0.007	-1.592	0.007	-1.005	0.698

Protein name	Abbreviation	Undifferentiated organoids vs. hPH	p-value	Differentiated organoids vs. hPH	Significance	Undifferentiated organoids vs. Differentiated organoids	Significance
Microsomal glutathione S-transferase 1	MGST1	-7.222	0.073	-5.321	0.120	-2.099	0.052
Microsomal glutathione S-transferase 2	MGST2	-1.232	0.420	-1.300	0.349	-1.072	0.579
Microsomal glutathione S-transferase 3	MGST3	-1.282	0.297	1.062	0.794	-1.294	0.308
Phospholipid hydroperoxide glutathione peroxidase	GPX4	1.454	0.206	1.706	0.119	-1.247	0.426
S-formylglutathione hydrolase	ESD	-4.936	0.037	-5.445	0.037	1.081	0.883
UDP-glucuronosyltransferase 1-1	UGT1A1	-1.173	0.851	1.138	0.886	-1.318	0.451
UDP-glucuronosyltransferase 1-3	UGT1A3	-2.242	0.087	-1.660	0.234	-1.170	0.195
UDP-glucuronosyltransferase 1-4	UGT1A4	-1.634	0.190	-1.300	0.458	-4.188	0.275
UDP-glucuronosyltransferase 1-6	UGT1A6	1.162	0.146	1.361	0.032	-1.879	0.496
UDP-glucuronosyltransferase 1-9	UGT1A9	-7.968	0.308	-4.571	0.460	-1.578	0.353
UDP-glucuronosyltransferase 2A3	UGT2A3	-1.727	0.510	1.005	0.996	-1.811	0.169
UDP-glucuronosyltransferase 2B10	UGT2B10	-6.486	0.069	-5.834	0.090	-1.803	0.356
UDP-glucuronosyltransferase 2B15	UGT2B15	-2.406	0.142	-1.652	0.364	-7.145	0.008
UDP-glucuronosyltransferase 2B28	UGT2B28	-10.999	0.032	-7.907	0.054	-1.330	0.101
UDP-glucuronosyltransferase 2B4	UGT2B4	-4.860	0.084	1.019	0.979	-3.565	0.140
UDP-glucuronosyltransferase 2B7	UGT2B7	-2.696	0.002	-1.968	0.009	-3.483	0.011
NRF2 Pathway							
Glutathione S-transferase A1	GSTA1	4.801	0.048	6.194	0.038	-1.081	0.294
Heme oxygenase 1	HO1	-1.127	0.762	-1.368	0.474	1.019	0.945
NAD(P)H dehydrogenase [quinone] 1	NQO1	16.801	0.010	21.086	0.010	-1.122	0.831

Protein name	Abbreviation	Undifferentiated organoids vs. hPH	p-value	Differentiated organoids vs. hPH	Significance	Undifferentiated organoids vs. Differentiated organoids	Significance
Thioredoxin reductase 1, cytoplasmic	TRXND1	2.983	0.004	3.581	0.003	-1.288	0.069
Thioredoxin reductase 2, mitochondrial	TRXND2	-1.825	0.032	-1.521	0.088	-1.294	0.134
Transporters							
ATP-binding cassette sub-family B member 6, mitochondrial	ABCB6	-1.141	0.254	-1.132	0.300	-1.028	0.795
ATP-binding cassette sub-family B member 7, mitochondrial	ABCB7	1.000	1.000	-1.086	0.333	1.052	0.380
ATP-binding cassette sub-family D member 3	ABCD3	-2.598	0.172	1.023	0.970	-3.342	0.097
ATP-binding cassette sub-family E member 1	ABCE1	-1.100	0.628	1.107	0.626	-1.117	0.434
ATP-binding cassette sub-family F member 1	ABCF1	2.823	0.023	3.020	0.023	-1.023	0.934
ATP-binding cassette sub-family F member 2	ABCF2	1.195	0.240	1.276	0.155	-1.014	0.895
ATP-binding cassette sub-family F member 3	ABCF3	-1.754	0.526	-2.218	0.409	2.032	0.036
ATP-dependent Clp protease ATP-binding subunit clpX-like, mitochondrial	CLPX	-1.047	0.922	-1.368	0.545	1.117	0.794
Bile acid-CoA:amino acid N-acyltransferase	BAAT	-13.635	0.086	-14.588	0.093	-1.746	0.106
Bile salt export pump	BSEP	-1.486	0.246	-1.507	0.255	-1.132	0.536
Bile salt sulfotransferase	SULT2A1	-32.310	0.057	-81.283	0.037	1.259	0.464
Canalicular multispecific organic anion transporter 1	ABCC2, MRP2	1.076	0.784	1.452	0.247	-1.355	0.363
Canalicular multispecific organic anion transporter 2	ABCC3	1.825	0.263	2.500	0.143	-1.265	0.649
Multidrug resistance protein 1	ABCB1, MDR1	2.148	0.026	3.119	0.010	-1.622	0.009
Multidrug resistance-associated protein 1	ABCC1, MRP1	1.141	0.832	-1.854	0.382	1.888	0.382
Multidrug resistance-associated protein 6	ABCC6, MRP6	-4.501	0.018	-3.296	0.039	-1.400	0.421

Protein name	Abbreviation	Undifferentiated organoids vs. hPH	p-value	Differentiated organoids vs. hPH	Significance	Undifferentiated organoids vs. Differentiated organoids	Significance
Solute carrier family 12 member 2	SLC12A2	1.696	0.062	8.790	0.257	2.259	0.041
Solute carrier family 13 member 5	SLC13A5	1.003	0.997	-1.265	0.311	-1.950	0.001
Solute carrier family 15 member 1	SLC15A1	1.389	0.339	1.202	0.841	-2.138	0.038
Solute carrier family 15 member 4	SLC15A4	-1.141	0.450	2.547	0.056	1.117	0.299
Solute carrier family 2, facilitated glucose transporter member 1	GLUT1, SLC2A1	3.039	0.143	-1.175	0.393	2.570	0.096
Solute carrier family 2, facilitated glucose transporter member 2	GLUT2, SLC2A2	-13.635	0.044	1.585	0.497	-2.259	0.019
Solute carrier family 22 member 18	SLC22A18	-1.675	0.707	-9.683	0.071	-2.582	0.378
Solute carrier organic anion transporter family member 1B3	SLCO1B3	-4.068	0.083	-1.170	0.913	-1.213	0.705
Solute carrier organic anion transporter family member 2B1	SLCO2B1	1.368	0.096	-4.169	0.091	1.208	0.252
Voltage-dependent anion-selective channel protein 1	VDAC1	-1.290	0.705	1.180	0.317	-1.419	0.479
Voltage-dependent anion-selective channel protein 2	VDAC2	2.249	0.185	1.472	0.593	-1.096	0.528
Voltage-dependent anion-selective channel protein 3	VDAC3	-1.025	0.955	1.253	0.632	-1.127	0.771
Biomarkers							
Alanine aminotransferase 1	ALT1	-11.07	0.098	-14.322	0.089	-1.387	0.456
Alanine aminotransferase 2	ALT2	3.30	0.012	3.148	0.016	1.019	0.942
Aspartate aminotransferase, cytoplasmic	AST, GOT1	-6.16	0.005	-3.532	0.016	-1.837	0.126
Aspartate aminotransferase, mitochondrial	AST, GOT2	-7.22	0.017	-10.568	0.012	1.143	0.147
Glutamate dehydrogenase 1, mitochondrial	GLDH	-16.34	0.115	-17.061	0.126	-2.061	0.093

Protein name	Abbreviation	Undifferentiated organoids vs. hPH	p-value	Differentiated organoids vs. hPH	Significance	Undifferentiated organoids vs. Differentiated organoids	Significance
High mobility group protein B1	HMGB1	-1.29	0.862	-1.820	0.703	3.133	0.079
Keratin, type I cytoskeletal 18	CK18	1.09	0.140	1.067	0.266	1.047	0.255
Keratin, type I cytoskeletal 19	CK19	1.22	0.012	1.253	0.011	-1.005	0.860
Serum albumin	HSA	-1.22	0.291	-1.014	0.940	-1.271	0.237

Table 6

List of liver relevant protein groups from iTRAQ analysis - Names and abbreviations used for the proteins in figures 23-28 divided into five categories: CYPs, DMETs, NRF2 pathway, transporters and biomarkers. Fold change in expression for each protein is shown for three comparisons: undifferentiated (day 0 and day 5) organoids versus hPH, differentiated organoids (day 10 and day 15) versus hPH and undifferentiated organoids versus differentiated organoids. Positive fold changes indicate higher protein expression in the first comparator, negative fold changes indicate greater expression the second comparator. Protein fold changes were produced using iTRAQ and analysis was completed using Partek and Microsoft Excel. Significance associated with the fold change is also shown as a p-value for each comparison. These p-values were produced via ANOVA using Partek, p-values of ≤0.05 were considered significant.

4.3 Discussion

Human liver organoids offer a promising source of differentiated hepatocytes for a range of laboratory and therapeutic uses. However, despite multiple studies examining their gene expression profiles, their proteome has not previously been assessed. Investigation of the hepatic phenotype at the proteomic level gives the best approximation of the true metabolic potential of these cells, since previous studies have demonstrated that gene expression does not necessarily equate to protein expression. In this chapter, we established culture methods for the generation, culture, cryopreservation and differentiation of human liver organoids, based on the work presented by Broutier et al. (2016). We then subjected these organoids to proteomic analysis by iTRAQ and western blotting.

4.3.1 Isolation and culture of human organoids

We attempted to isolate organoids from resected liver tissue on several occasions. It was noted that the probability of success of organoids isolation appeared to negatively correlate with the time since the resection of the tissue. We found that our isolations were successful 80% of the time (n=5) after isolation was performed immediately after the tissue was received. If the tissue was stored at 4 °C, for over 24 hours, as described in Broutier et al. (2016), we noted a precipitous drop in isolation efficiency where isolation was successful in approximately 10% of cases.

The reasons for this discrepancy are not clear, however we suggest that storage at 4 °C for more than 24-hours may lead to the large-scale death of the cells required to establish Chol-orgs *in vitro*. This effect may be compounded by the health of the donors from which the tissue was received. These individuals were undergoing hepatobiliary surgery, typically to remove either primary liver tumours or metastatic tumours from other organs and frequently had poor overall health, e.g. high BMI, polypharmacy etc. These extant health issues may impact upon the health of the cells in the biliary tree and therefore damage the chances of isolation when compared with, for example, an otherwise healthy cadaveric liver. However, we chose not to study this effect further, instead opting to modify our protocol to consistently perform organoid isolations as soon after resection as possible.

We also noted that sorting of EpCAM-positive cells by FACS did not improve isolation efficiency. We attempted FACS sorting of EpCAM-positive cells on three occasions, none of which resulted in the successful establishment of organoids in acceptable quantities and

timeframe. In each isolation we noticed only a very small outgrowth of only very few cells which did not propagate into a successful organoid culture. Conversely, when using an isolation method which did not employ FACS, instead plating cells which had only been enriched by centrifugation, we observed a larger organoid population emerging during a shorter timeframe (Figure 18).

The reasons for this lack of improvement when sorting the cells initially seems paradoxical. EpCAM-positive cells are known to be the progenitor cell type of Chol-orgs and therefore their enrichment in culture should improve isolation success. However, it appears that in our laboratory the enrichment of EpCAM-positive cells in plating was not sufficient to outweigh the loss in viability found caused by the FACS process. This loss in viability can be observed in Figure 17C, where the post-sorting report shows an increase in dead cells, even though these dead cells were gated during the previous sort. The process for staining cells for FACS sorting takes several hours and involves several steps in which the cells must be handled in a suspension, in combination with the mechanical stresses exerted on the cells during FACS, it appears that the viability of these cells is irrecoverably damaged by the process of sorting. Moreover, the process of sorting the cells using FACS was logistically difficult in our laboratory, it is possible that if the time to prepare and sort the cells, and the stresses exerted on them, were minimised then an improvement in plating efficiency could be observed.

The organoids that were isolated showed the characteristic cystic morphology expected from Chol-orgs. This is consistent with previous reports which demonstrated similar morphologies (Hu et al., 2018; Huch et al., 2015). Additionally, we noted that there was a tendency for some organoids to collapse and become dense and dark when observed under a brightfield microscope. The reasons for this behaviour are unclear though there are several possibilities, in some cases we observed this behaviour after the organoids had become larger than 100-200µm, in this case it seems likely that the reasons for the collapse were mechanical due to lack of support from the BME-2 matrix. In other cases, the organoids collapsed when smaller, conditions which would typically be well supported by the BME-2 matrix, in these cases we interpreted this as the death of the organoid though due to the difficulty sorting this type of organoid from other healthy ones, we were not able to confirm this possibility.

4.3.2 Cryopreservation of human organoids

We attempted to reproduce the cryopreservation techniques presented previously by Broutier et al. (2016) with our Chol-orgs. We compared the efficacy of two commercial freezing media, Recovery Cell Culture Freezing Medium and CryoStor CS10. We were able to cryopreserve and revive organoids without issue using both media. However, it quickly became apparent that the organoids were damaged by the cryopreservation process. Despite successful recovery and establishment of the organoids, the rate of proliferation and growth was severely slowed, the interval between passages increased to several months as opposed to approximately 1-3 weeks before cryopreservation.

The reasons for this loss in proliferative potential are likely to be damage and toxicity to the organoids during the freezing process. The freezing medium contains DMSO which is toxic to cells and there is also the possibility of mechanical and temperature damage to the organoids during the disruption steps of the cryopreservation protocol and when freezing. Unfortunately, this damage to the organoid cultures precluded their use in the iTRAQ analyses as was initially planned since it was not possible to generate sufficient cell material in a timely manner.

4.3.3. Differentiation of human organoids

Despite our difficulty in re-establishing proliferative cultures of Chol-orgs we were able to proceed with differentiation towards a hepatic fate in three organoid lines. Of these lines, only donor 1, was differentiated before cryopreservation and consequently, this was the only line used for iTRAQ analysis. Donors 2 and 3 were both differentiated after cryopreservation and therefore the amount of cell material was very low. Ultimately, only Donor 2 yielded enough cell material for successful western blotting (Figure 30).

During the differentiation towards hepatocytes as described in Broutier et al. (2016), we noticed an increase in the number of organoids which changed from a cystic morphology to a dense clustered morphology which was opaque when examined by brightfield microscopy. Some examples of this type of morphology can also be seen in Broutier et al. (2016), however, the authors also present a brightfield image of a differentiated organoids which do not share this morphology. The reasons for this change and discrepancy are unclear.

4.3.4 Proteomic analysis of differentiated organoids

We analysed the proteome of donor 1 organoids throughout differentiation towards hepatocytes using iTRAQ. The results of these analyses are shown in Figures 22-29. Figure 22 shows the hierarchical clustering of the samples, it is noteworthy that organoids at day 0 and day 5 cluster together as do organoids at day 10 and 15, this indicates that the proteome of the organoids is successfully altered by the differentiation procedure, in this case, likely indicating a shift towards a more hepatic phenotype. However, it is also important to note that the organoids do not cluster closely with hepatocytes or tissue, the target tissue type. This shows that although the phenotype has been changed by the differentiation procedure, the differentiated organoids do not fully recapitulate the phenotype of liver tissue or hepatocytes in isolation. The hierarchical clustering also includes a control column, this is due to the experimental setup used, two control samples were included and the one displayed in Figure 22 is not the same control used to normalise the dataset.

4.3.4.1 Cytochromes P450

Next, we examined the dataset for liver specific proteins, to examine the functional relevance of organoids compared with hepatocytes. These proteins are shown in Table 6, and the changes in expression are shown in figures 23-28, significantly changed proteins are also summarised in Table 6. First, we examined expression of CYP proteins, which are key liver-enriched enzymes responsible for the metabolism of 70-80% of all clinically-used drugs (Zanger and Schwab, 2008). There are 57 putative functional CYP enzymes in humans, though not all contribute equally to the number of xenobiotics metabolised. CYP3A4, CYP2C9, CYP2C8, CYP2E1, and CYP1A2 are the most highly expressed *in vivo*, whilst CYP2A6, CYP2D6, CYP2B6, CYP2C19 and CYP3A5 are comparatively less expressed but still important for xenobiotic metabolism (Zanger and Schwab, 2008). Accurate recapitulation of the expression patterns of CYP enzymes are essential for an accurate model of the liver for toxicity testing, not only are they responsible for metabolism of some compounds, there are also cases where CYP enzymes can produce a reactive metabolite which can cause liver injury. A well-known example of this is the metabolism of paracetamol during overdose, the glutathione-based detoxification pathways are exhausted and the CYP-mediated production of the reactive metabolite NAPQI becomes dominant and toxicity is elicited (Holme and Jacobsen, 1986; Ramachandran and Jaeschke, 2018).

Interestingly, in Figure 23C, between differentiated and undifferentiated organoids, the only significantly changed CYP protein was CYP3A5, this is unexpected since 90% of the

Caucasian population are CYP3A5 nonexpressers and donor 1 is of white British ethnicity. CYP3A5 shares 85% sequence homology with CYP3A4 and has been shown to overlap in its target specificity, if a genuine result the increase in CYP3A5 is positive for the hepatic phenotype (Langman et al., 2015). Furthermore, although non-significant, CYP3A4 shows the largest fold difference of any of the CYP proteins in this panel suggesting the acquisition of a more mature hepatic phenotype over the process of differentiation. It is also noteworthy that although non-significant, there is a trend towards increased expression of every CYP protein over differentiation in this panel except CYP4V2 and CYP2C19.

When undifferentiated organoids are compared with hPH (Figure 23A), the majority of proteins were not significantly changed. Though there was a trend to increased expression in hPH. These results are expected, hPH should show a more mature hepatic phenotype than undifferentiated organoids. CYP expression in organoids was also compared to hPH after differentiation (Figure 23B). The majority of changes in CYP expression during differentiation were small, however after differentiation CYP1A2, CYP2A6 and CYP2C8 are all significantly lower in differentiated organoids than in hPH but were not before differentiation suggesting differentiation is having the opposite to the intended effect and causing the phenotype of the organoids to diverge from hPH.

CYP2S1 is consistently upregulated in organoids, before and after differentiation versus hPH. It shares sequence homology with other CYP2 family members and is activated through the aryl hydrocarbon receptor in response to dioxin and hypoxia (Rivera et al., 2007). However, *in vivo* CYP2S1 is most commonly expressed in extrahepatic epithelial tissues and why is it upregulated in hepatic organoids in unclear (Marek et al., 2007; Saarikoski et al., 2005).

4.3.4.2 DMETs

We next examined the expression of DMETs in organoids before and after differentiation and in comparison with hPH. One of the key groups in this panel of proteins are the UDP-glucuronosyltransferases (UGT), a superfamily of 22 enzymes which mainly facilitate glucuronidation, the covalent linkage of glucuronic acid, of lipophilic substrates to increase solubility and facilitate renal excretion (Rowland et al., 2013). Another large group of enzymes in this group are the glutathione-S-transferases, these enzymes facilitate the conjugation of reduced glutathione to various substrates, typically in order to increase their solubility and enable further metabolism (Smith et al., 2013).

When undifferentiated organoids were compared to differentiated (Figure 24C), UGT2B7, UGT2B15, GPX1 and NIT1 were all significantly upregulated. UGT2B7 and UGT2B15 are considered to be among the most important UGTs for xenobiotic detoxification (Rowland et al., 2013). Increased expression of UGT2B7 and UGT2B15 is a positive indicator for the hepatic phenotype of the organoids. NIT1 is implicated in the regeneration of glutathione after deamination and is highly conserved (Peracchi et al., 2017). Glutathione metabolism is important for the detoxification function of the liver and NIT1 expression is likely a positive indicator for the phenotype of human liver organoids.

In comparison to hPH, undifferentiated organoids show several significantly changed proteins. UGT2B10 and GGT1 are significantly changed and have fold changes greater than 5 (Figure 24A). UGT2B10 is implicated in the glucuronidation of tobacco-specific nitrosamines and some antidepressants (Chen et al., 2008; Labriet et al., 2018). It is unsurprising that the expression of this UGT is increased in hPH over undifferentiated organoids, however, after organoid differentiation, the difference in expression is no longer significant (Figure 24B), indicating a trend towards a more mature hepatocyte phenotype.

GGT1 is implicated in the cleavage of extracellular glutathione to facilitate cysteine uptake and the metabolism of compounds which contain a gamma-glutamyl moiety such as metabolites of 3,4-(+/-)-methylenedioxymethamphetamine (MDMA) (Bai et al., 2001; Wickham et al., 2011). This enzyme is typically enriched in renal tissues but is also expressed at low levels in the liver and cholangiocytes (Uhlen et al., 2017). Its significant upregulation in undifferentiated organoids may be indicative of a cholangiocyte phenotype.

When hPH and differentiated organoids are compared, the differences in expression are generally small. Only GGT1, GSTP1, ESD and SULT2A1 are significantly changed by greater than 5-fold (Figure 24B). GSTP1 is a highly polymorphic member of the GST superfamily which has been implicated in chemosensitivity to cisplatin (Sawers et al., 2014). This is a positive indicator for their hepatocyte phenotype, however, that organoid expression should be markedly higher than that of hPH is of concern. GSTP1 has been implicated in the progression of several cancers, this may explain to some extent the increase expression in highly proliferative organoid cultures (Checa-Rojas et al., 2018; Louie et al., 2016; Martignano et al., 2016).

ESD catalyses the regeneration of glutathione from S-formylglutathione, and participates in methane and formaldehyde metabolism (Uotila and Koivusalo, 1974). The lack of expression of this enzyme demonstrates that organoids to not fully recapitulate the hPH

phenotype in all respects. SULT2A1 was significantly higher in hPH by a large magnitude which increased over the differentiation process. SULT2A1 is highly liver enriched catalyses the sulfation of bile acids and a wide array of steroid hormones (Li et al., 2008). SULT2A1 transcription is induced by PXR, FXR and CAR also implicated in the metabolism of some drugs including hydroxytamoxifen (Chatterjee et al., 2005).The reason why this enzyme should diverge from the mature hepatocyte phenotype over the process of differentiation is unclear but is a poor indicator of the hepatic phenotype of organoids, potentially also suggesting that CAR, PXR or FXR are inactive.

4.3.4.3 NRF2 pathway

In addition to its role in oxidative stress, NRF2 has been implicated in the maintenance of the hepatic phenotype during liver regeneration and, when continuously expressed, is also associated with poor prognosis in hepatocellular carcinoma (Beyer et al., 2008; Raghunath et al., 2018; Shin et al., 2013; Zou et al., 2014) The organoids in this study are used with the intention to recapitulate the oval cell response, therefore activation of the NRF2 pathway might be expected.

When differentiated organoids are compared to undifferentiated, none of the NRF2 pathway-associated genes are significantly changed (Figure 25C). Furthermore, the magnitude of the changes observed are very small, all lower than 1.5-fold change. However, this is not the case when compared to hPH (Figure 25A), 3 out of 5 NRF2-related proteins are significantly upregulated in undifferentiated organoids compared to hPH, these proteins include TRXND1, NQO1 and GSTP1. Conversely, TRXND2 is significantly downregulated and HO1 is non-significantly downregulated. Of these changes only NQO1 shows a fold change of greater than 5. NQO1 reduces a wide array of quinones to hydroquinones *in vivo*, this typically prevents oxidative stress but is also a step in the activation of some chemotherapeutics (Oh and Park, 2015; Siegel et al., 2012). Similarly, when differentiated organoids are compared to hPH, the same genes are significantly upregulated, albeit more strongly (Figure 25B). TRXND2 is no longer significantly downregulated and HO-1 remains almost unchanged. Significant upregulation in the majority of NRF2 related genes implies a general activation of the NRF2 pathway which becomes slightly more profound during differentiation. This upregulation of the NRF2 pathway is expected when it is considered that the NRF2 pathway is activated during hepatocyte regeneration (Beyer et al., 2008; Raghunath et al., 2018; Shin et al., 2013; Zou et al., 2014).

4.3.4.4 Transporters

The next panel of proteins that were investigated were transporters. There are several major transporter families included in this panel, including members of the Solute carrier (SLC) family and ATP-binding cassette transporters (ABC transporters). The transporter protein families are among the largest gene families, with 49 known ABC transporters in humans (Vasiliou et al., 2009) and 400 SLC transporters (Perland and Fredriksson, 2017). Transporter proteins are essential for the maintenance of homeostasis for the movement of all manner of soluble molecules across lipid membranes including drugs (Vasiliou et al., 2009). Because of the essential role that transporters play in drug transport it is also necessary that a liver model recapitulates the expression found *in vivo*. For example, ABCC1 actively exports many pharmaceuticals from the cell (e.g. doxycycline, irinotecan, mitomycin C) effectively conferring resistance to the exported compound by lowering the effective exposure (Glavinas et al., 2004; Hodges et al., 2011). If the expression of transporters is not accurately reproduced by a liver model, it is possible that predictions made regarding drug sensitivity will be skewed.

The panel of transporters that were investigated in this study are detailed in Table 6. When differentiated organoids are compared to undifferentiated, there are small changes overall (Figure 26C). When undifferentiated organoids are compared with hPH, GLUT2, ABCC6 and ABCE1 are all significantly higher in hPH, conversely, ABCB1 is higher in undifferentiated organoids (Figure 26A). The large, but non-significant change in expression of BAAT which is higher in hPH is also noteworthy.

That GLUT2 should be more highly expressed in hPH is unsurprising, it is the primary glucose transporter between the liver and the blood and is involved in glucose homeostasis, one of the major functions of the liver though it is also expressed in a range of glucose-sensitive tissues (Thorens, 2015). ABCC6, also referred to as MRP6 is an ABC transporter that is enriched in the liver and kidneys and expressed on the mitochondrial membranes (Martin et al., 2012). Like other ABC transporters it has a wide substrate specificity including some drugs, and is thought to be involved in nilotinib and dasatinib resistance, increased expression in organoids is a positive indicator of hepatocyte phenotype (Eadie et al., 2018).

In the comparison between differentiated organoids and hPH, ABCC6 is significantly higher in hPH and ABCC1 and ABCF1 are significantly higher in organoids (Figure 26B). However, none of the significantly altered genes shows a fold change greater than 5. It is noteworthy

that most transporters in this panel are not significantly changed and the changes that are present are of small magnitude, except for KCNH6, BAAT and GLUT2, which show fold changes above 5. This is a positive general indicator that the transporter phenotype closely matches that of hPH, an essential aspect of the phenotype that some liver models do not fully recapitulate (Gao et al., 2017).

4.3.4.5 Liver Biomarkers

The penultimate panel of proteins that were analysed from the iTRAQ dataset were biomarkers. Biomarkers are used as proxy indicators for larger processes. The biomarkers included in this panel are used as indicators of liver damage with the most commonly used likely being ALT and AST. Indeed, in chapter 5 we examined elevations in ALT in mice as a proxy measurement of liver damage induced by CCl_4. It is important that a liver model accurately reproduces the expression of biomarkers found in whole organisms and other models as this aids their translatability. For example, although it is not included in this panel, miR-122 is a highly translatable biomarker (Kia et al., 2015). It is highly conserved throughout commonly used model species and can be detected in cell cultures and in the circulation of model organisms and patients. The biomarkers in this panel are compared against freshly isolated hPH, it should be considered that there is likely some damage occurring to the cells during isolation which may skew the expression of these biomarkers. Nonetheless, it is expected that organoids should show similar expression in most cases.

When organoids are compared over the process of differentiation, none of the proteins were significantly changed (Figure 27C). However, when compared with hPH, expression of HMGB1, CK18, GLDH and ALT1 in undifferentiated organoids are also not significantly different from hPH although the fold change for GLDH and ALT1 is still large (16.4- and 11.0-fold higher in hPH, respectively) (Figure 27A). These results suggest that undifferentiated organoids have a hepatocyte-like phenotype before the differentiation process, as might be expected from liver progenitor cells. Nonetheless, there are significant differences between hPH and undifferentiated organoids, both forms of AST are significantly decreased by a substantial magnitude and ALT2 is significantly increased by a small margin as is CK19. The pattern of expression is the same in all proteins after differentiation, though the expression in organoids has decreased in every case except cytoplasmic AST (Figure 27B).

AST is a key biomarker that is routinely used in conjunction with ALT to assess liver damage, the use of serum transaminases in this manner is well-established and was first described in the 1950s (Karmen et al., 1955). There are two isozymes of AST, one mitochondrial (AST2)

one cytoplasmic (AST1). Though both isozymes catalyse the transfer of an amino group from aspartate to α-ketoglutarate, their sequences share only approximately 50% identity (McGill, 2016; McPhalen et al., 1992). Both AST and ALT are released by the liver when damaged, though the relative levels of each can inform the type of damage that is occurring, for example, an increased AST/ALT ratio may be indicative of advanced alcoholic liver disease (Nyblom et al., 2004). Similarly, it has been suggested that differential analysis of the isozymes of AST may be informative of the types of liver damage occurring, Kamiike et al. showed that whilst cytoplasmic AST was released quickly after injury, mitochondrial AST was released into circulation after a longer period and more extensive cell damage and suggested that mitochondrial AST is specifically indicative of apoptosis (Kamiike et al., 1989).

That AST should be markedly lower in organoids, even after differentiation is concerning when considering their hepatic phenotype. Ideally, their expression would be similar, to enable simple translation. Whilst it might be possible to account for these differences based on known proteomic screens, this hampers their utility in discovery of new biomarkers if they are not reliably expressed at similar levels. Interestingly, although the differences are still significant after differentiation, the fold difference is decreased for cytoplasmic AST suggesting the possibility of incomplete differentiation to a hepatocyte phenotype, this agrees with the global analyses of the proteome which shows differentiated organoids still cluster with undifferentiated organoids rather than with hPH (Figure 22).

4.3.4.6 Cholangiocyte markers

The final panel of proteins which was analysed were markers of cholangiocytes. Since these organoids are nominally derived from EpCAM-positive cholangiocytes, we investigated whether they retained a cholangiocyte identity before and after differentiation to a hepatic fate. These results should be interpreted with caution since FACS enrichment for EpCAM-positive cells was not used, and therefore the confidence in the exact identity of the starting cell type is lower and the organoids may arise from hepatocytes instead as discussed by Hu et al. (2018).

Four commonly used markers of cholangiocytes were detected by iTRAQ analysis, CK19, CK7, MUC1 and EpCAM. CK7 and CK19 are keratins used for the routine identification of cholangiocytes, neither protein is expressed in healthy hPH but can often be acquired in hepatocellular carcinomas (Matsukuma et al., 2012; Shibuya et al., 2011). Similarly, MUC1

(also epithelial membrane antigen) is expressed in cholangiocytes and other epithelial cell types (Kumagai et al., 2016; Leong et al., 2003). MUC1 is not expressed in healthy hepatocytes but is often acquired in hepatocellular carcinoma (Kim et al., 2014). Increased expression of these proteins implies an adoption of a cholangiocyte-like phenotype. As such, some of the proteins identified in previous panels were assessed for increased expression in cholangiocytes.

All proteins except MUC1 were significantly higher in undifferentiated organoids than in hPH and all were significantly higher after differentiation, and MUC1 was the only significantly changed protein during differentiation (Figure 28). These results suggest that Chol-orgs exhibit some markers of a cholangiocyte phenotype even after differentiation to a hepatocyte fate. The relative expression of several cholangiocyte markers increases during differentiation, contrary to expectation. However, it should be noted that expression in hPH is very low and the relative increase in expression in organoids may appear to be greater for this reason.

GSTP1 expression was higher in organoids than hPH (Figure 25). The degree of GSTP1 expression in hPH is low and it has also been implicated in chemoresistance in cholangiocarcinoma and therefore may represent an acquisition of a more cholangiocyte-like phenotype (Nakajima et al., 2003; Söderdahl et al., 2007). Some transporters which were significantly upregulated may also represent a shift towards a cholangiocyte phenotype, ABCB1 and SLC12A2 are expressed in cholangiocytes (Concepcion et al., 2014; Larbcharoensub et al., 2011). Similarly GGT1, which was significantly upregulated in the 'DMETs' section is also expressed in cholangiocytes (Dianat et al., 2014). These results generally indicate that human liver organoids have at least a partially cholangiocyte-like phenotype but also a hepatocyte like phenotype as discussed in previous sections. A mixed cholangiocyte-hepatocyte phenotype has been reported in previous studies using similar organoids (Huch et al., 2015). It is not clear from these results whether all cells are expressing a mixed phenotype or is there are two distinct populations of cells. A mixed phenotype is unlikely to be appealing as a model of hepatotoxicity since it does not mirror the in vivo situation, though a mixed population of cells may be desirable.

Next we examined how the results of this proteomic analysis matched with the analyses performed by Huch et al. (2015). First the authors measured the phenotype of undifferentiated organoids at different passages, our analysis did not include different passages of the same organoids, but all analyses were completed before passage 10, and

therefore are comparable to the 'early passage' organoids in Huch et al. Moreover, in Huch et al. the comparison is made to tissue, whereas the comparisons in figures 22-27 are made versus hPH, however, (Figure 29C) shows that for the purposes of comparison, these samples are similar. Huch et al showed that serum albumin was undetectable by RT-qPCR, however, we readily detected serum albumin in undifferentiated organoids at only approximately 1.2-fold lower than hPH (Figure 27). Similarly, Huch et al. showed that CK19 was undetectable in hPH and higher in early passage organoids, whilst our data show that CK19 expression is only approximately 1.2-fold higher in undifferentiated organoids than hPH.

Furthermore, Huch et al. also examined the expression of liver-specific genes before and after the differentiation process, notably, serum albumin and CYP3A4. We readily detected both proteins in our analysis and were also able to confirm their expression by western blotting. In this regard, our results match with those of Huch et al. who showed increased expression of both genes during differentiation. When compared against hPH, by proteomic analysis (Figure 23B & 23B), we found reduced, but comparable expression of CYP3A4 and albumin in differentiated organoids (2.63- and 1.01-fold higher in hPH respectively), by western blotting. When compared to donor-matched tissue, our results showed higher expression of CYP3A4 and albumin in differentiated organoids than Huch et al. (approximately 1.13- and 1.28-fold higher in tissue respectively, Figure 30). Additionally, the authors showed an increase in gene expression of CK19 during differentiation, our data shows CK19 remains unchanged throughout differentiation (Figure 28C). These data likely highlight the differences in expression patterns of RNA and protein as previously noted.

4.3.5 Conclusions

Human Chol-orgs can be derived from donor liver tissue in our lab, we have also succeeded in culturing, passaging, cryopreserving and differentiating them to a hepatocyte fate. Global proteomic analysis shows that although there are changes to the proteome of organoids during the process of differentiation, they do not cluster closely with hPH by hierarchical clustering analysis. Closer scrutiny of these data indicates that although the global proteome does not cluster closely with hPH, differentiated organoids show similar expression of key proteins required for drug metabolism and transport. For example, these analyses show that 13 out of 16 detected CYP enzymes were either not significantly different or significantly higher in organoids than in hPH. Furthermore, the panel of DMETs shows that out of 41 proteins, only 4 were significantly higher in hPH, with the remaining genes either non-significantly changed or significantly higher in differentiated organoids.

The NRF2 pathway is highly active in differentiated organoids with significantly higher expression of 3 out of 5 proteins in this panel and none significantly downregulated. The pattern is similar again for transporters where only one protein in this panel is significantly higher in hPH. These findings are further corroborated by western blotting, performed on a separate donor showing expression of CYP3A4 and albumin increasing over the differentiation process to levels comparable to donor-matched liver tissue (Figure 30).

Future studies should aim to increase the statistical power of these experiments. In this study only one donor was differentiated in sufficient quantity to enable proteomic analysis. Additionally, there are many nascent liver models currently under development, 3D cultures of primary and stem cell-derived hepatocytes, systems incorporating flow etc., comparison with these models and other currently used models should be performed. Only once these comparisons have been made at the proteomic level will it be possible to fully determine if liver organoids are a true improvement over extant and upcoming models.

In summary, differentiated Chol-orgs, recapitulate physiologically relevant levels of some, but not all aspects of the hepatic phenotype and some aspects of the cholangiocyte phenotype as may be expected from the cell-type of origin. The incomplete hepatic phenotype may be related to the completeness of differentiation, similar to the difficulty in the stem cell field in driving stem cell-derived HLCs towards a mature phenotype (Baxter et al., 2015). It is also possible that the incomplete recapitulation of the hepatic phenotype is related to the starting cell type. As discussed previously, the organoids described in Broutier et al. (2016) aim to reproduce the oval cell response, which is not the homeostatic mechanism for reproduction of hepatocytes. In a recent paper, the Clevers group demonstrated reproduction of the homeostatic mechanism of hepatocyte repopulation, i.e. division of mature hepatocytes (Hu et al., 2018). Based on the analyses in this paper, is seems likely that they possess a more relevant hepatic phenotype than Chol-orgs when differentiated, though with the caveat that the analyses are RNA based and therefore may not fully represent the true phenotype of the cells (Schwanhüusser et al., 2011; Vogel and Marcotte, 2012).

5 Tumorigenicity of the 20q11.21 amplicon in a differentiated cell engraftment model

5.1 Introduction

Stem cells are capable of several fates, self-renewal, differentiation or death. When cells are cultured in an undifferentiated state a selective pressure is applied to the cells favouring the self-renewal fate. This, in part, accounts for the recurring patterns of mutations observed in stem cells in culture, in particular, recurrent mutations of chromosomes 12, 17, 20 and X are common (Amps et al., 2011). The 20q11.21 amplicon is one such common mutation, occurring in as many as 20% of ESC and iPSC lines after prolonged culture and confers a survival advantage (Amps et al., 2011). The 20q11.21 minimal amplicon is approximately 0.55Mb in length and encodes HM13, ID1, BCL2L1, KIF3B and an immature form of miR-1825. The amplicon size is variable and can also encode other nearby genes, including the potential oncogene, TPX2. Recent studies have demonstrated that BCL2L1 is likely to be the key driver of the survival advantage observed in carrier cells (Avery et al., 2013; Nguyen et al., 2014). Although not the source of the survival advantage conferred *in vitro*, ID1 is another gene expressed in the 20q11.21 minimal amplicon that is a potential oncogene.

Previous studies have demonstrated the application of stem cell derived HLCs in mouse models where the cells have engrafted and become functional in murine liver (Asgari et al., 2013). Additionally, undifferentiated stem cells with known aberrations have been used *in vivo* to demonstrate enhanced tumorigenicity (Ben-David et al., 2014). Here we present the first attempt, to the best of our knowledge, to combine these approaches and use differentiated stem cells with a known genetic aberration *in vivo* to discern the effects of the 20q11.21 amplicon on tumorigenicity after differentiation.

In this study Fox Chase SCID Beige (SCID beige) mice were used. SCID beige mice are albino and carry both the SCID and beige mutations producing a severely immunocompromised mouse demonstrating severe T and B lymphocytopaenia with defective natural killer cells and a rudimentary thymus (Croy and Chapeau, 1990). For the purposes of this study, SCID beige mice were an appropriate model due to their severely immunocompromised status and albino fur which facilitated *in vivo* bioluminescence imaging without shaving. However, when compared with other immunocompromised mouse models such as NOD-SCID etc., SCID beige mice are relatively understudied. For example, at the time of writing, PubMed returns 3668 results for the search term “NOD SCID” but only 311 for the term “SCID beige”. Therefore, it was necessary to determine some aspects of this study for the first

time, such as the required dose of carbon tetrachloride (CCl_4) required to produce acute liver injury.

Acute CCl_4 injury was used in this study to better facilitate cell engraftment into the liver as described by Payne et al. (2011). Though once widely used, the toxicity of CCl_4 has now been recognised for over 70 years (Recknagel, 1967). Despite the restrictions on its use in other fields, CCl_4 is widely used in research as a model hepatotoxin. CCl_4 is activated by a range of cytochromes P450 (CYP2E1, CYP2B1, CYP2B2, CYP3A) into the trichloromethane radical ($CCl_3\cdot$) which in turn may react with oxygen to form the trichloromethylperoxy radical ($CCl_3OO\cdot$) both of which are highly reactive and can damage cellular macromolecules such as DNA and phospholipids. The attack of $CCl_3\cdot$ on DNA is thought to be an initiator of hepatic cancers and $CCl_3OO\cdot$ can initiate a chain reaction which degrades phospholipids of the various cellular membranes. These processes cause sufficient damage, either acutely or chronically to cause cell death (Weber et al., 2003). In this work CCl_4 was administered to induce acute liver damage followed by a period of liver regeneration. Gupta et al. report that if cells are administrated during the period of liver regeneration, the transplanted cells can proliferate along with the host cells, thereby enhancing engraftment (Gupta et al., 1999). However, the authors also report that if cells are administered whilst CCl_4 is still present in the liver the administered cells can also become damaged. Because of this, cells were administered 3 days after acute liver injury, longer than the *in vivo* half-life of CCl_4 of approximately 7 hours (World Health Organisation, 2004).

We hypothesised that the presence of amplicon 20q11.21 confers a survival advantage to carrier cells in vitro. Similarly, differentiated cells which carry the amplification will be more prone to tumour formation when transplanted into the livers of an immunodeficient mouse model. Therefore, human ESCs (hESCs) with known 20q11.21 status were differentiated into HLCs for transplantation into SCID mice. Luminescent hESCs were generated from the MasterShef 7 and MasterShef 8 hESC lines both with and without 20q11.21. These cells were differentiated into HLCs and injected intrasplenically into Fox Chase SCID-beige mice whose livers had been acutely damaged with CCl_4. The engraftment of these cells into the liver was then tracked using *in vivo* luminescence imaging for approximately 4 months and the formation of any malignancies was assessed.

5.2 Results

5.2.1 Characterisation of MasterShef 7 & 8 -fluc clones

Four parental hESC lines were used in this study: MS7N, MS7CNV, MS8N and MS8Ab. Luminescent copies of these cells were produced by nucleofection with the construct shown in Figure 31A and clonally selected using puromycin. Luminescence was confirmed and quantified using the IVIS Spectrum and the two most strongly luminescent cell lines were selected for each parental cell line (Figure 31B). The 20q11.21 status of each cell line is summarised in Table 7.

	-20q11.21	**+20q11.21**
MasterShef 7	MS7N	MS7CNV
MasterShef 8	MS8N	MS8Ab

Table 7

Table of MasterShef hESC lines showing 20q11.21 status – Each MasterShef line was named according to 20q11.21 status, lines denoted as 'N' do not carry the 20q11.21 amplicon, those marked at 'Ab' or 'CNV' contain the 20aq11.21 amplicon. Luminescent cell lines derived from these cells are appended with a 2-character identifier e.g. C7, G7 etc.

5.2.2 SCID-beige mice are highly sensitive to acute carbon tetrachloride toxicity

To better facilitate engraftment of hESC-HLCs into the liver, acute hepatocellular damage was induced using CCl_4. To the best of our knowledge, the dose of CCl_4 for induction of acute liver injury in SCID beige mice has not previously been reported. The range of CCl_4 doses used in other strains of mice varies greatly as high as 10mL/kg (Chen et al., 2018; Wang et al., 2013). We used single doses of 1.0, 0.4 and 0.2 mL/kg of CCl_4. With 1.0 and 0.4 mL/kg, animals became unwell before the end of the study. Using 0.2 mL/kg of CCl_4 demonstrated a substantial degree of liver damage (Figure 31C, D) and ALT elevation (Figure 31E) at 24 and 72 hours after injection. Therefore, for subsequent experiments 0.2 mL/kg was used.

5.2.3 Teratoma formation using undifferentiated hESCs with and without amplicon

Undifferentiated hESCs readily form teratomas in rodents. However, changes in teratoma-forming behaviour in the presence of amplicon 20q11.21 has not previously been investigated. We induced liver injury in 16 male SCID beige mice and after 72 hours, 1×10^6 undifferentiated luminescent MS7N, MS7CNV, MS8N or MS8Ab were injected intrasplenically (n=4). Animals were kept for 4 weeks and imaged weekly. Weights of the animals were monitored three times a week.

In the first week, 14/15 animals showed a bioluminescent signal which increased over time (Figure 32A, Supplementary Figure 1). The intensity of the signals was significantly higher in MS7CNV compared to MS7N in both liver and spleen when imaged *ex vivo* (P=0.0152 and p=0.0002 respectively) though this trend did not continue in MS8Ab and MS8N (Figure 32B). *Ex vivo* imaging demonstrated signal in 14/15 livers and 4/15 spleens in addition to macroscopically observable cystic lesions.

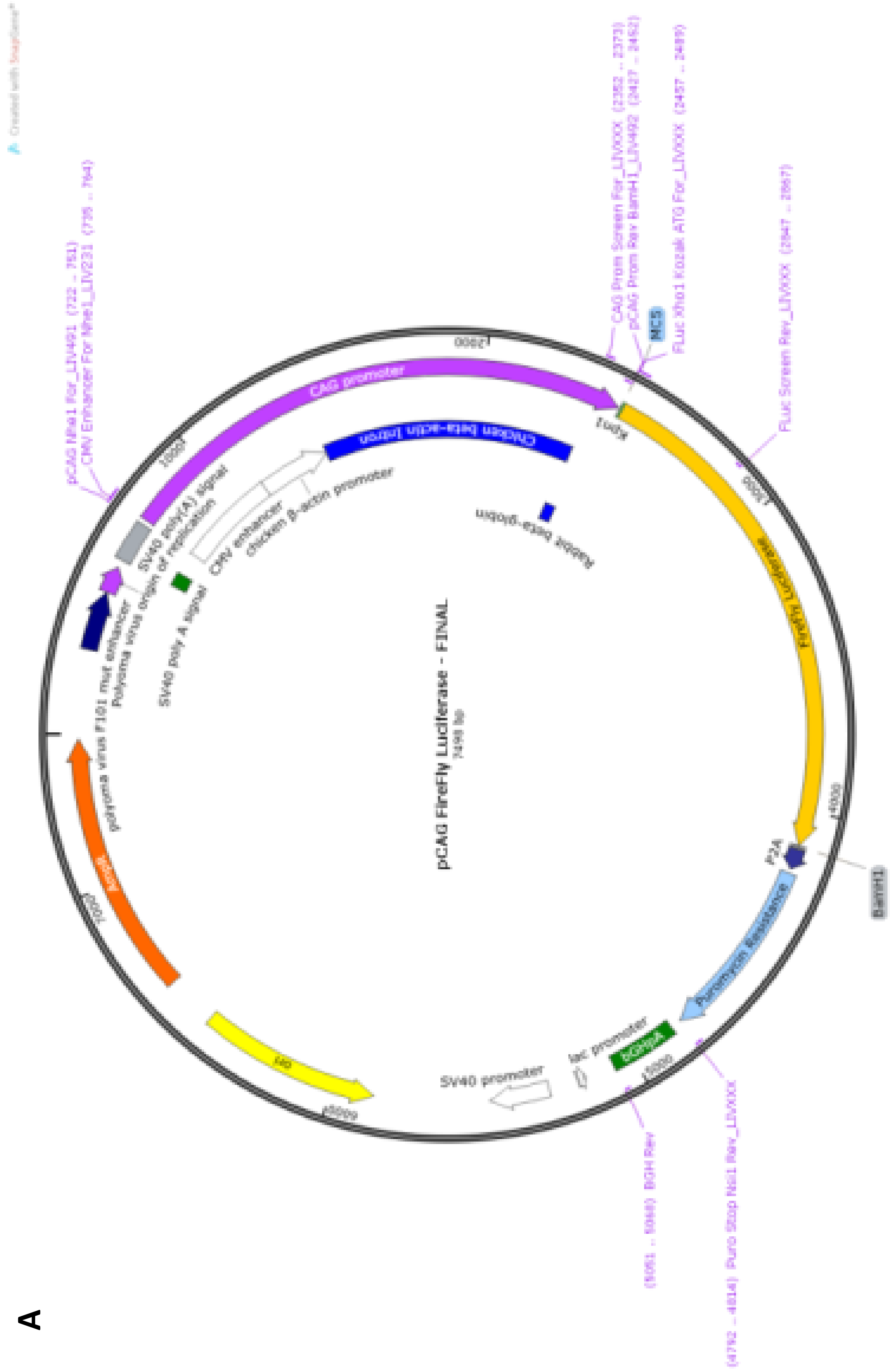
pCAG FireFly Luciferase - FINAL
7498 bp
CAG promoter
Chicken beta-actin intron
FireFly Luciferase
P2A
Puromycin Resistance
bGHpA
lac promoter
SV40 promoter
ori
AmpR
BamH1
MCS
Kpn1
rabbit beta-globin
SV40 poly A signal
SV40 poly(A) signal
CMV enhancer
chicken β-actin promoter

A

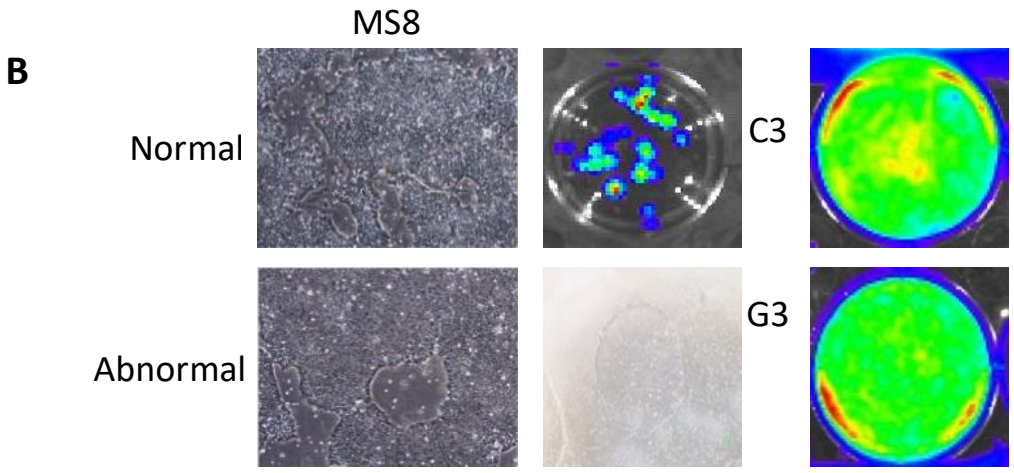
B
MS8
Normal
C3
Abnormal
G3

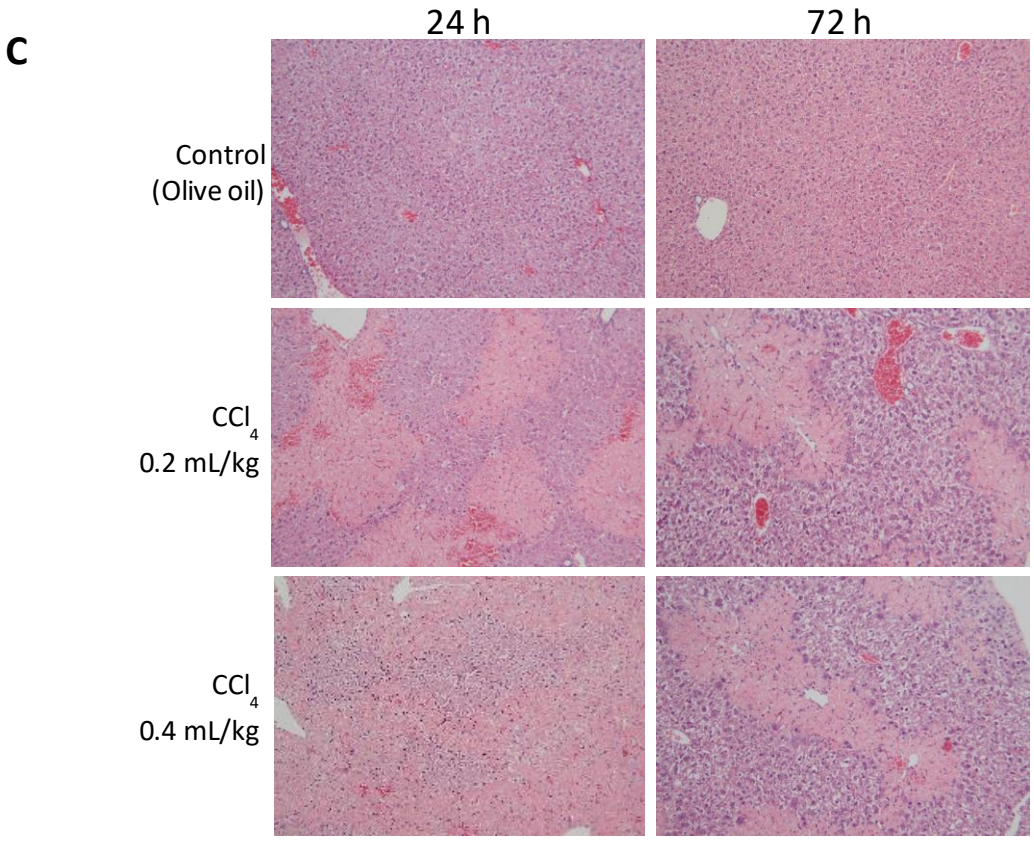
C
24 h
72 h
Control
(Olive oil)
CCl4
0.2 mL/kg
CCl4
0.4 mL/kg

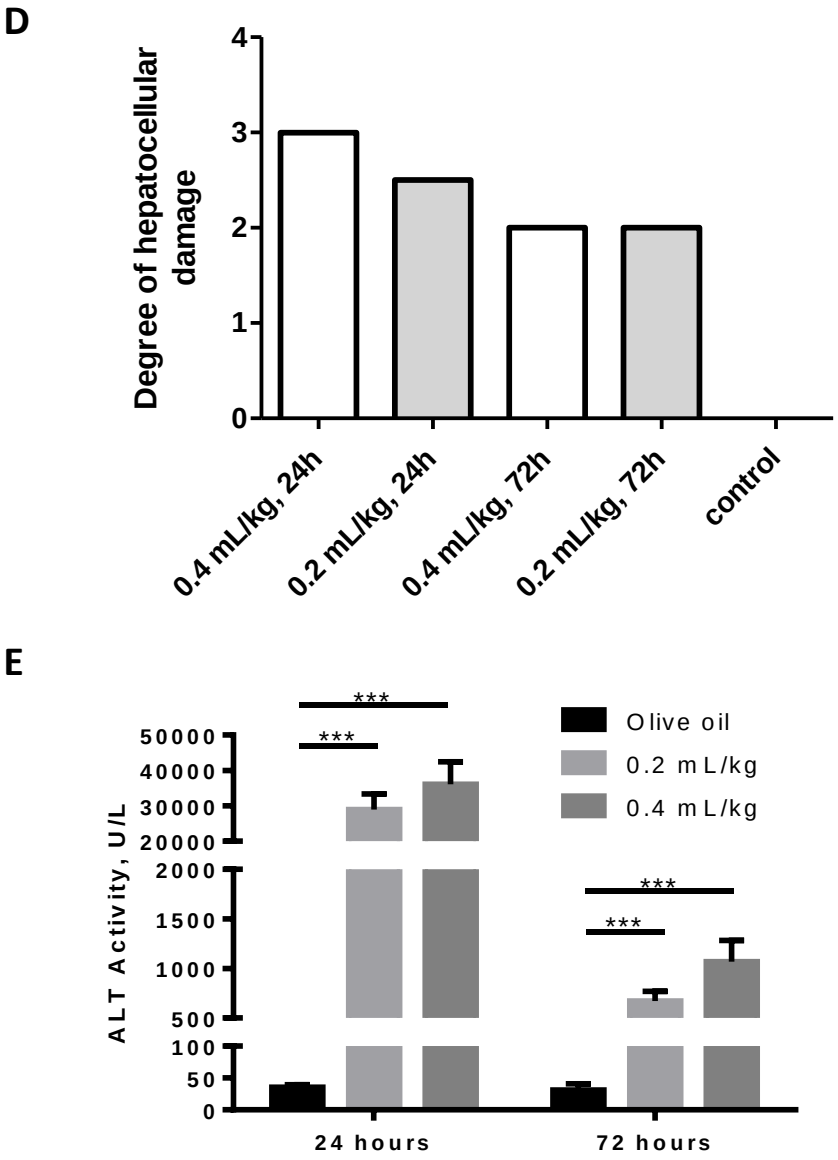

Figure 31

Transfection of undifferentiated hESCs with a luciferase construct and identification of appropriate dosage of CCl_4 for consistent induction of acute liver injury in Fox Chase SCID beige mice - **(A)** pCAG Firefly Luciferase-2A-Puro map **(B)** MasterShef 8 normal and abnormal cells transfected with pCAG Firefly Luciferase plasmid. Clones were selected with puromycin and the two most luminescent from each line were expanded. **(C)** H&E staining of liver tissue. Fox Chase SCID beige mice received a single dose of CCl_4 (0.2 or 0.4 mL/kg) or olive oil and were sacrificed at 24 or 72 h. After 24 h both 0.2 and 0.4 mL/kg induced severe coagulative necrosis of the centrilobular hepatocytes with or without the presence of acute haemorrhages. After 72 h, both groups showed a decreased degree of damage and a narrowing of the area of coagulative necrosis around the central vein with a continuous rim of hyper-basophilic regenerating hepatocytes and an increased number of mitotically active

hepatocytes within the intervening "healthy" parenchyma. Administration of olive oil as medium only in the control group did not elicit appreciable morphological degeneration of the hepatic parenchyma. **(D)** Mean hepatocellular damage. Scoring system for liver damage in this cohort scored according to Thoolen et al. (2010). (Table 9) **(E)** ALT activation in SCID-beige mice 24 and 72 hours after injection with CCl_4. Data are displayed as U/L and show the mean; error bars show standard deviation. Asterisks denote significance calculated using a two-tailed unpaired student's t-test. *** = P ≤0.0001

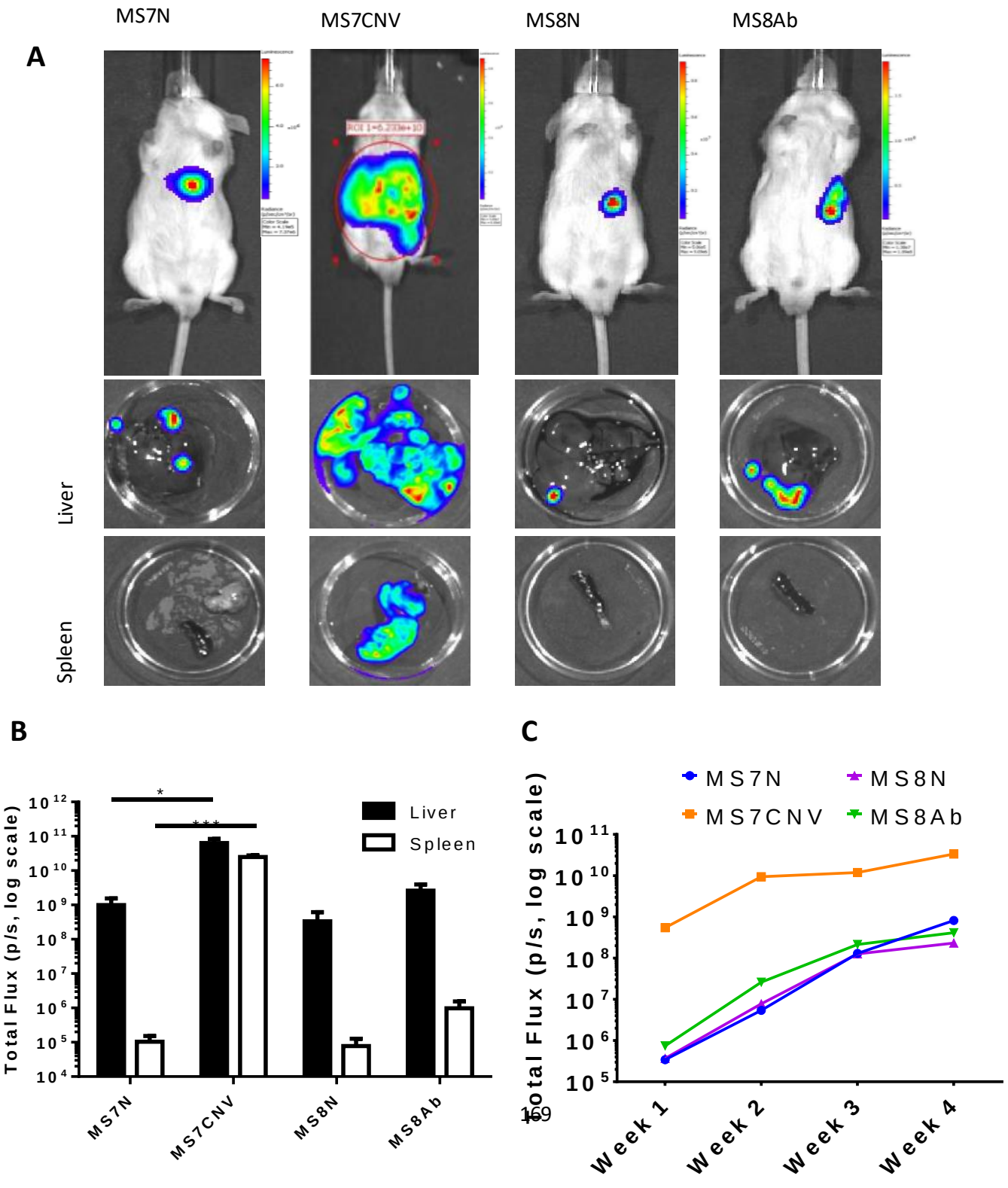

D

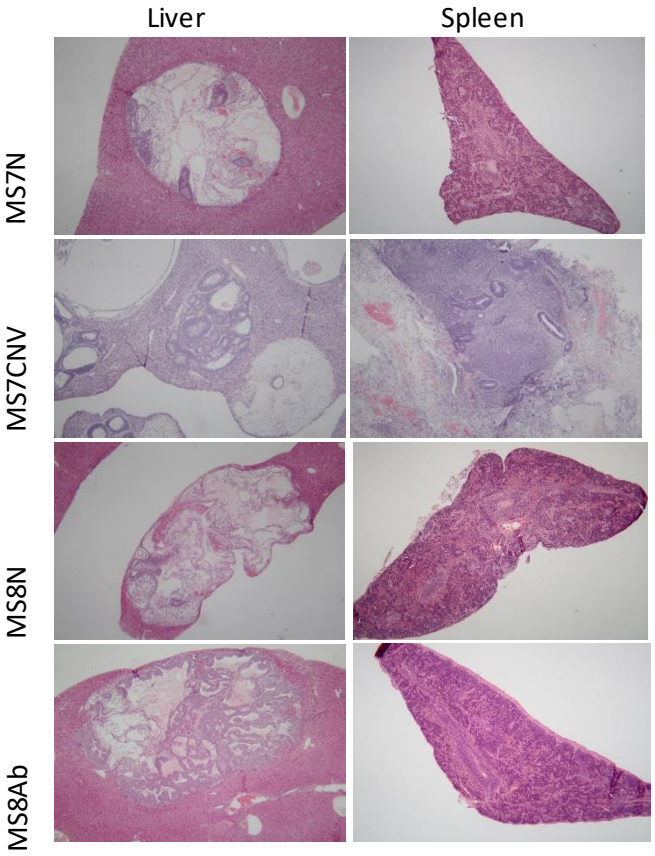

E

Cell line	Grade in Liver	Grade in spleen	Nature of masses
MS7N	0-1	0	Immature teratoma
MS7CNV	5	5	Immature teratoma
MS8N	0-3	0	Immature teratoma
MS8Ab	1-2	0	Immature teratoma with carcinomatous features

F

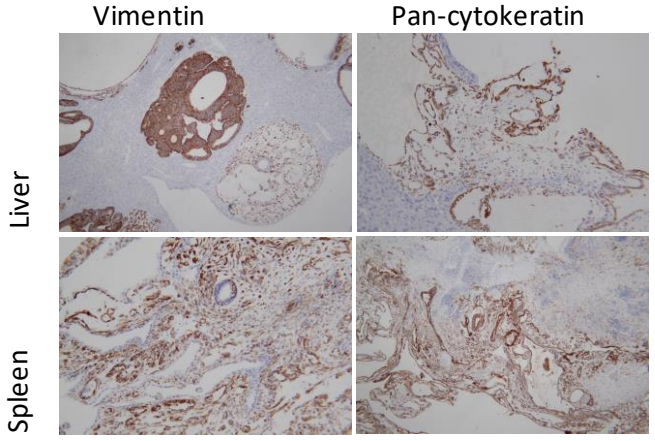

Figure 32

Undifferentiated hESCs with 20q11.21 amplicon induce extensive immature teratoma and teratocarcinoma in the murine liver. SCID beige mice were injected with 1×10^6 of undifferentiated MS7N, MS7CNV, MS8N and MS8Ab into the spleen **(A)** *In vivo* and *ex vivo* (liver and spleen) bioluminescence imaging of representative mice from each group after 28 days. See Supplementary Figure 1 for data from all mice. **(B)** Comparison of bioluminescence in livers and spleens imaged *ex vivo* in different cell lines. Values are plotted as total flux (photons/second) Total flux is determined by the total amount of luminescence detected from the animal in the IVIS Spectrum during the exposure period, error bars show SEM. MS7CNV and MS7N are significantly different for both liver and spleen (two-tailed, unpaired t-test, p= 0.0152 and 0.0002 respectively). **(C)** Bioluminescence over time *in vivo* grouped by cell line. Values are plotted as total flux (photons/second). **(D)** H&E staining of a representative liver and spleen tissue after injection with undifferentiated hESCs. **(E)** Grades of teratoma formation in the liver and spleen of mice injected with undifferentiated hESCs. Scoring was performed by a veterinary histopathologist and scored according to Thoolen et al. (2010) (Table 9). **(F)** Representative IHC staining of liver and spleen tissue for vimentin and Pan-cytokeratin to confirm the presence of teratoma.

In H&E staining, all four cell lines demonstrated immature teratoma and in MS8Ab carcinomatous features were also present (Figure 32D). The grade of cystic formation was higher in liver (5) and spleen (5) of mice injected with MS7CNV compared to liver (0-1) and spleen (0) with MS7N though this trend was not apparent in MS8N and MS8Ab (Figure 32B).

Vimentin and pan-cytokeratin proteins were expressed in liver and spleen (Figure 32F). Vimentin is the first intermediate filament expressed in the cytoplasm of embryonic cells, soon replaced by cytokeratins in epithelial tissues during cell differentiation. Therefore, coupled with the biphasic pattern of morphological differentiation of the neoplastic cells composing the nodular masses in both liver and spleen, the observation of specific cytokeratin labelling in structures resembling large acini is supporting of the hypothesis that initial epithelial commitment of a proportion of the neoplastic cells is well established. Therefore, both mesenchymal and epithelial differentiations are present within most of the neoplastic masses.

5.2.4 Pluripotency assessment of MasterShef hESCs

Since a random integration method was used to produce the luminescent reporter cells. It is possible that the pluripotency of these cells could have been affected. We used an embryoid body-forming assay where undifferentiated hESCs are allowed to differentiate spontaneously before staining for markers of the three germ layers. If markers of all three germ layers can be detected, the functional pluripotency of the cell is thereby demonstrated.

We generated embryoid bodies from each parental MasterShef line (Figure 33A) and two luminescent clones of each, and then stained for alpha-foetoprotein (AFP) as a marker of endoderm, neuron-specific beta -III tubulin (Tuj-1) as a marker of ectoderm, and alpha smooth muscle actin (α-SMA) as a marker of mesoderm and were able to detect all three markers in each line tested as indicated in green (Figure 33B), demonstrating that their pluripotency was unaffected.

The protocol described by Greenhough et al. for the prediction of differentiation propensity was adapted for use in this study. The original protocol measured the spontaneous expression of AFP, albumin and HNF4α in embryoid bodies in order to predict the ability of a stem cell line to form HLCs by directed differentiation (Greenhough et al., 2013). We adapted this protocol to examine the expression of AFP, albumin and HNF4α using qPCR to

determine if the propensity to differentiate towards HLCs had been altered by the random integration of the reporter plasmid.

Embryoid bodies were formed from each parental cell line and the two most luminescent clones were then assessed by qPCR. The results of this experiment (Figure 34) showed that in all cases the expression of these three genes was either similar or higher than the parental line indicating a similar or increased propensity to differentiate towards HLCs after integration of the reporter construct.

5.2.5 Differentiation protocol development

The protocol described by Medine et al. (2011) was initially chosen to produce HLCs in this study (Figure 35A). However, it was noted that luminescence was lost in HLCs after day 9 of differentiation (Figure 35C). Moreover, the proportion of cells expressing HNF4a was decreased at day 12 compared with day 8 (data not shown). Additionally, cells differentiated using this protocol failed to engraft, as determined by absence of luminescence. We reasoned that since luminescence was lost when moving into the final stage of differentiation, the cause of the loss of differentiation and luminescence was due to the composition of this medium. It was observed that the pH of the L-15 based medium was very low (<6) due to addition of 2% (w/v) ascorbic acid (Medine et al., 2011). The composition of this medium was adjusted based on a similarly composed medium described by Siller et al. (2015), replacing 2% (w/v) ascorbic acid with 50 ng/mL sodium-L-ascorbate. Cells differentiated using this adapted protocol (Figure 35E) retained luminescence until day 12 (Figure 35D) and were able to successfully engraft *in vivo* (Figure 35). Other aspects of this differentiation protocol remained unchanged.

5.2.6 Differentiation efficiency of MasterShef hESCs

Due to the potential for teratoma formation from undifferentiated cells is was necessary to assess the efficiency of the differentiation protocol prior to injection of the cells. The efficiency of the differentiation protocol in producing HLCs was assessed using flow cytometry where HNF4α expression at day 8 of the differentiation protocol was used as a marker of successful hepatic differentiation. A single luminescent clone of each MasterShef line (MS7N D6, MS7CNV D7, MS8N E3, MS8Ab D7) was differentiated until day 8 of the differentiation protocol described in chapter 2 and in Figure 35 before analysing their expression of HNF4α by flow cytometry. At day 8 of differentiation cells were stained for HNF4α as described in chapter 2 and their differentiation proportion was assessed. All lines showed a high proportion of HNF4a expression, i.e. 90.7%, 87.6%, 96.4% and 80.4% for

MS7N_D6, MS7CNV_D7, MS8N_E3 and MS8Ab_D7 respectively (Figure 33C). These differentiation proportions were deemed satisfactory and used to produce HLCs for injection.

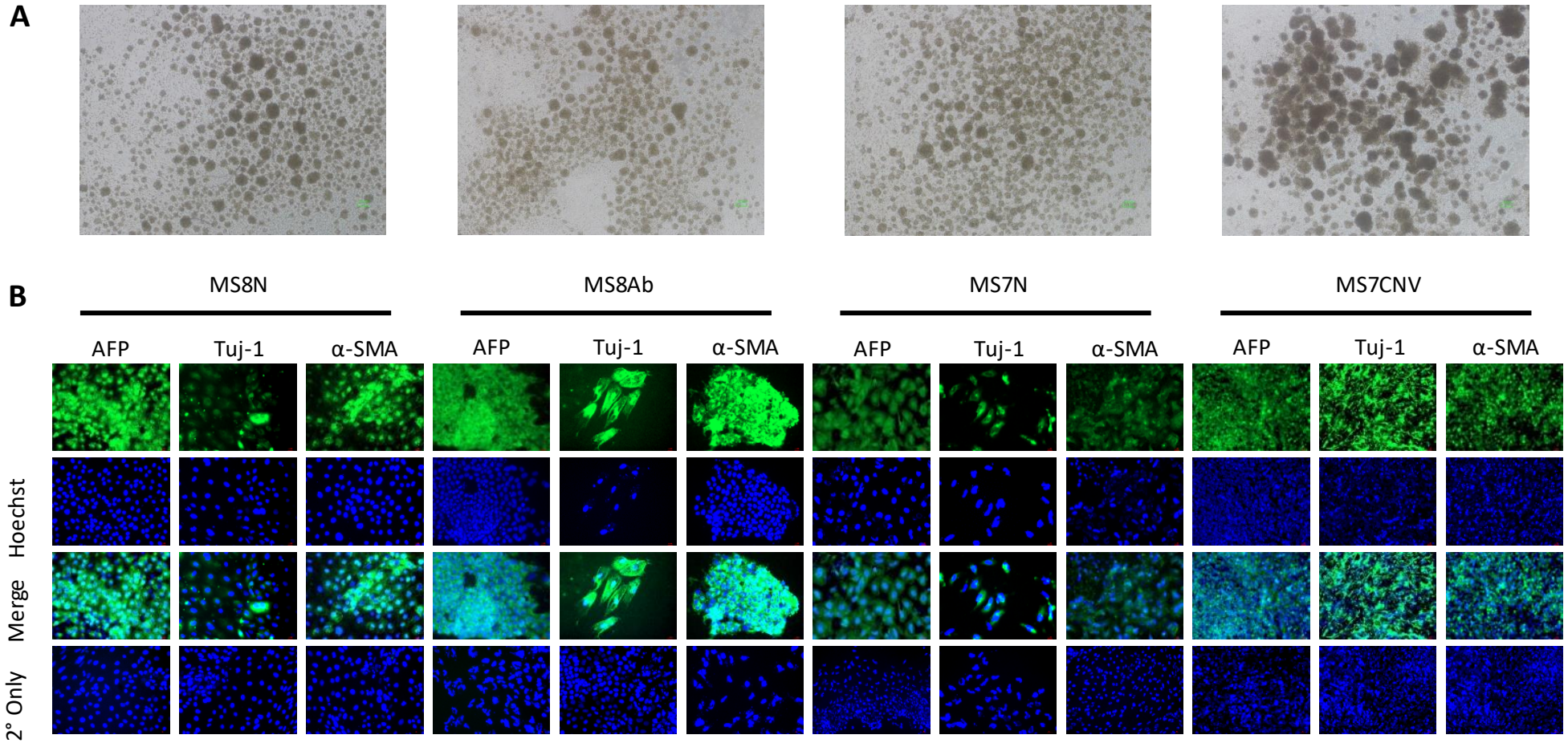
A
B
MS8N
MS8Ab
MS7N
MS7CNV
AFP
Tuj-1
α-SMA
Hoechst
Merge
2° Only

B (cont.)

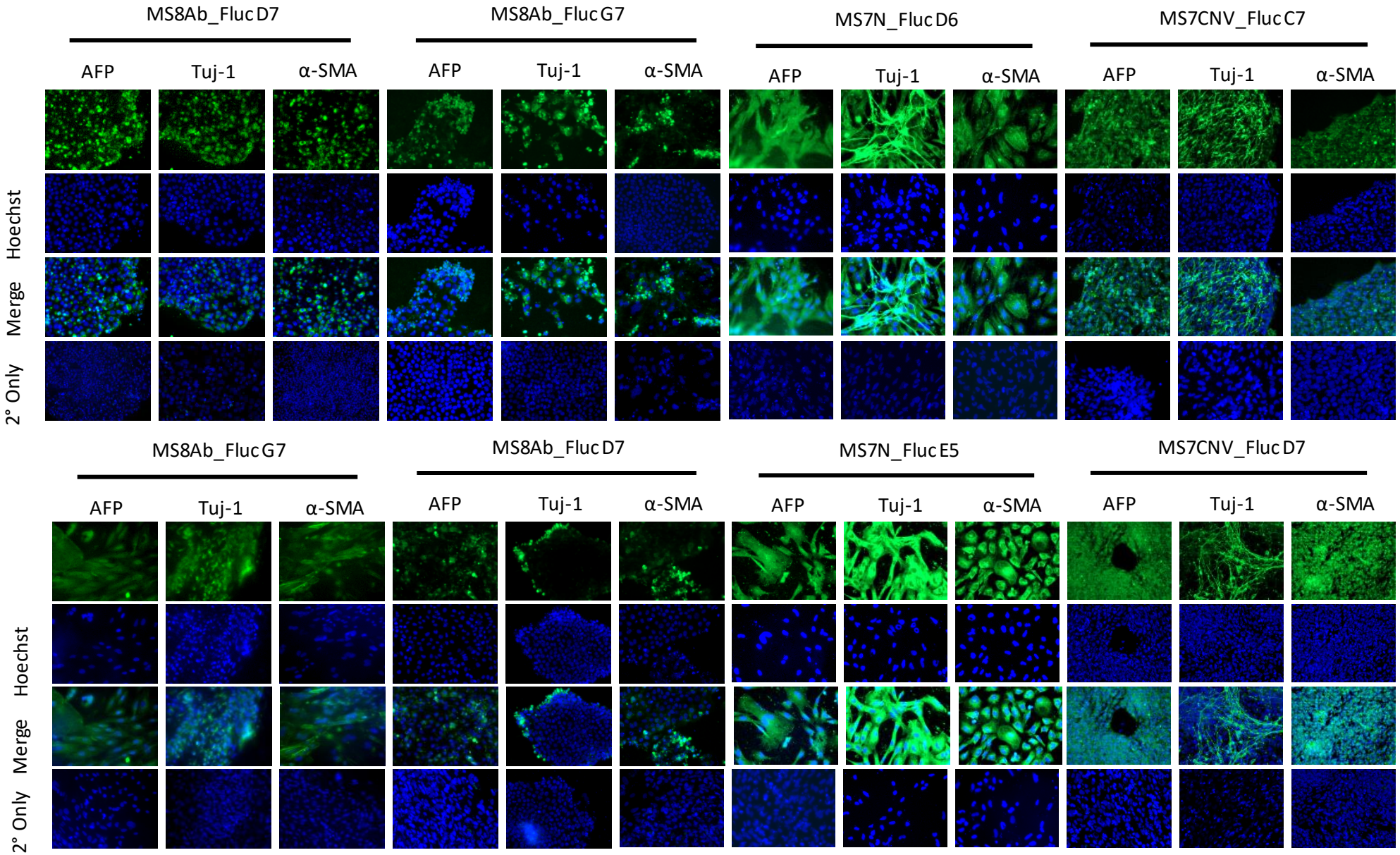
MS8Ab_Fluc D7
MS8Ab_Fluc G7
MS7N_Fluc D6
MS7CNV_Fluc C7
AFP
Tuj-1
α-SMA
Hoechst
Merge
2° Only
MS8Ab_Fluc G7
MS8Ab_Fluc D7
MS7N_Fluc E5
MS7CNV_Fluc D7

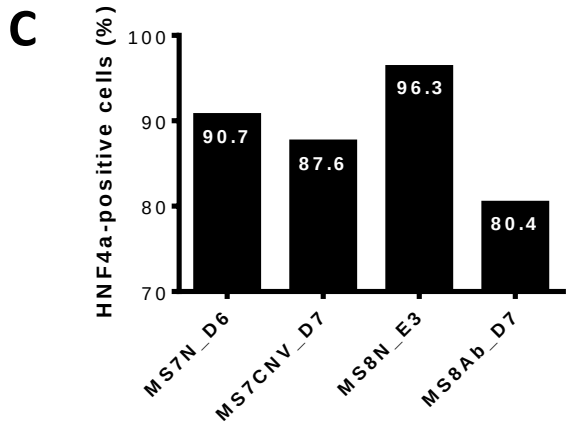

Figure 33

Demonstration of pluripotency in transformed MasterShef Fluc ESCs and characterisation of differentiation efficiency to HLCs. (A) Representative micrographs showing embryoid body formation in MS8N, MS8Ab, MS7N and MS7CNV ESCs 48 hours after seeding. Embryoid bodies were also formed for all the transformed lines in panel B but are not shown. **(B)** Representative fluorescence micrographs of spontaneously differentiating embryoid bodies adhered to a cell culture surface. Positive staining (in green) for AFP (endoderm), Tuj-1 (ectoderm) and a-SMA (mesoderm) demonstrates formation of the three major germ layers, and therefore, pluripotency. Hoechst was used as a nuclear stain and is shown in blue. Pluripotency was not affected in any of the tested transformed cell lines. **(C)** Differentiation efficiency towards HLCs shown by flow cytometry. Cells were stained for HNF4a as a marker of differentiation and assessed using flow cytometry, exact differentiation proportion is shown on each bar n=1

5.2.7 Tumorigenicity of MasterShef HLCs with amplicon in SCID beige mice

To test the hypothesis that the presence of amplicon 20q11.21 in human cells used therapeutically predisposes to a greater risk of tumorigenicity in a mouse model, 8 luminescent hESC lines, 4 without and 4 with amplicon 20q11.21, were differentiated into HLCs as described above. One million cells were injected into the spleens of 56 SCID Beige mice 72 h after induction of acute liver injury (n=7). After 7 days, the animals were imaged using an IVIS Spectrum either weekly or fortnightly for approximately 4 months (Figure 36A), after which some animals began to show signs of deteriorating health and the experiment was ended.

A positive control of a relative cancer cell type was used for the purposes of comparison in terms of engraftment and proliferation *in vivo*. HepG2 cells are an immortalised cell line which is routinely used as a liver cell model. Because of their liver phenotype and high rate of proliferation, they may reasonably be expected to engraft aggressively into the liver of an immunocompromised mouse. HepG2 cells expressing the same luciferase reporter were produced in the same manner and iPSCs and 1 x10^6 cells were injected intrasplenically into mice 72-hours after CCl_4-induced acute liver injury. These animals rapidly developed a strong luminescent signal which became saturated after 6 weeks, the health of these animals simultaneously began to decline at which point the experiment was ended (Figure 36A-D)

Thymus tumours were routinely checked for post-mortem and 6 were observed, animals with thymus tumours were excluded from all analyses. Luminescent signal was observed in livers from 3 animals and in the spleens of 3 animals (Figure 36B).

In vivo luminescence was tracked over the course of the experiment in each line (Figure 36C). These results demonstrate an increased luminescent signal on average in animals injected with cells containing the 20q11.21 amplicon. Figure 36D shows the mean luminescent signal from all lines grouped according to their 20q11.21 status and show increased signal in animals injected with cells containing the amplicon, though these values do not reach significance due to high inter-animal variation.

On average, there were more severe histology scores in the animals where cells containing the 20q11.21 amplicon were injected (Figure 36F, Table 8). The criteria for these histology scores are shown in Table 9. Moreover, the luminescent signal, where observed, was

greater in the cells containing the 20q11.21 amplicon. We also quantified the levels of human albumin present in the serum. If the cells had successfully engrafted, they would be expected to produce human albumin. However, there were undetectable levels of human albumin in all cases except for a single clone, MS8Ab D7, where the concentration was still extremely low compared to the levels of human albumin detected in the serum of animals injected with HepG2 cells (Figure 36E).

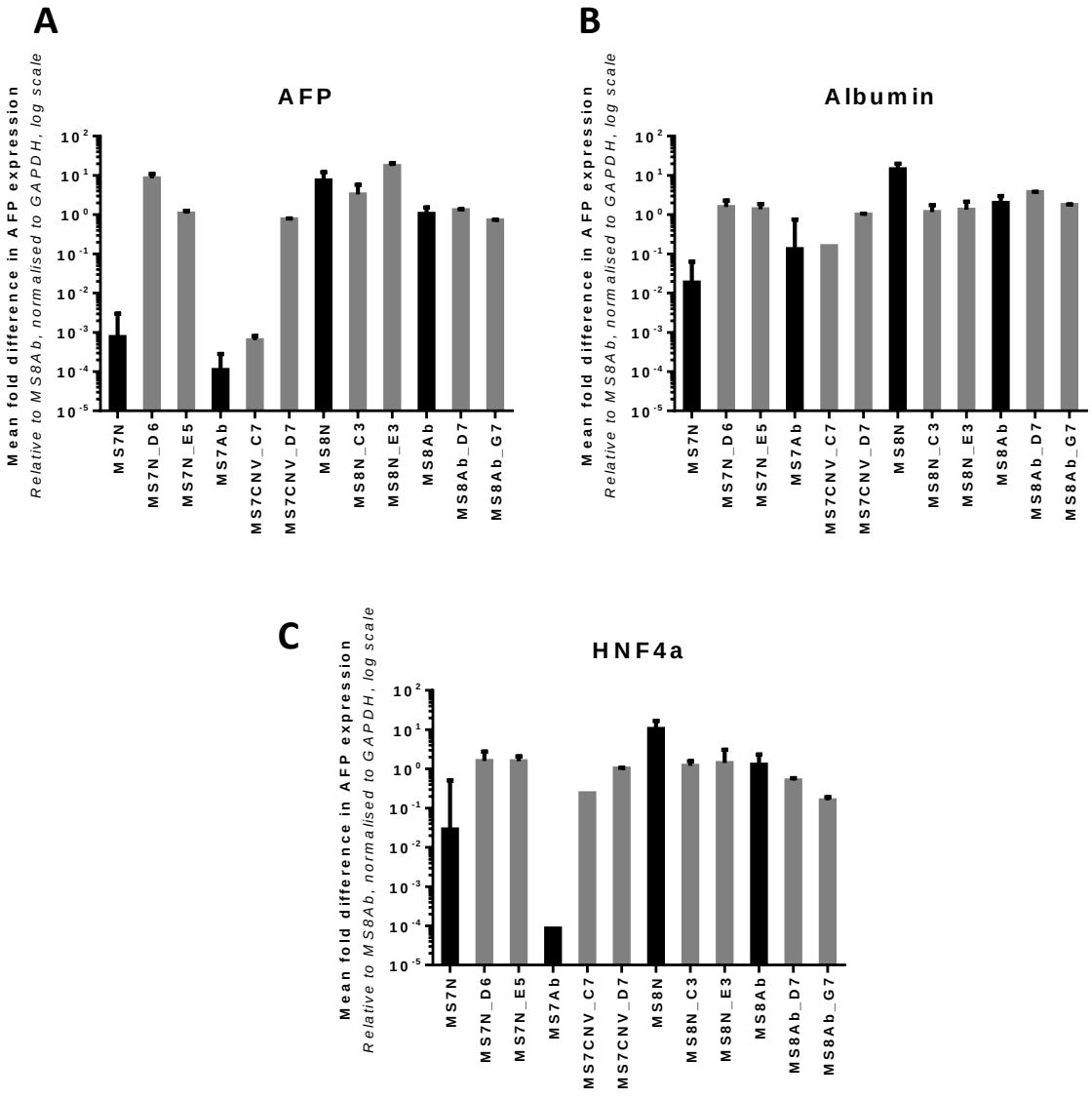

Figure 34

Gene expression in MasterShef Embryoid bodies to assess skewing of differentiation propensity – Embryoid bodies differentiate spontaneously, their tendency to differentiate into a particular germ layer has been suggested to indicate their ability to differentiate to that fate under directed differentiation (Greenhough et al., 2013). In this study it was determined whether that propensity to differentiate into the endoderm lineage had been affected by integration of luminescence plasmid. Expression of AFP **(A)**, albumin **(B)** and HNF4a **(C)** analysed using qPCR with SYBR green chemistry in embryoid bodies produced from MS7N, MS7CNV, MS8N and MS8Ab and their luminescent clones. Values are presented as mean fold change calculated using the $2^{-\Delta\Delta CT}$ method, error bars show error calculated using the same method (Livak and Schmittgen, 2001). All values are presented relative to expression in MS8Ab and are normalised to GAPDH. Gene expression in each cell

line is presented separately, bars in black show parental cell lines followed by the luminescent clones produced from that line in grey. n=3

A

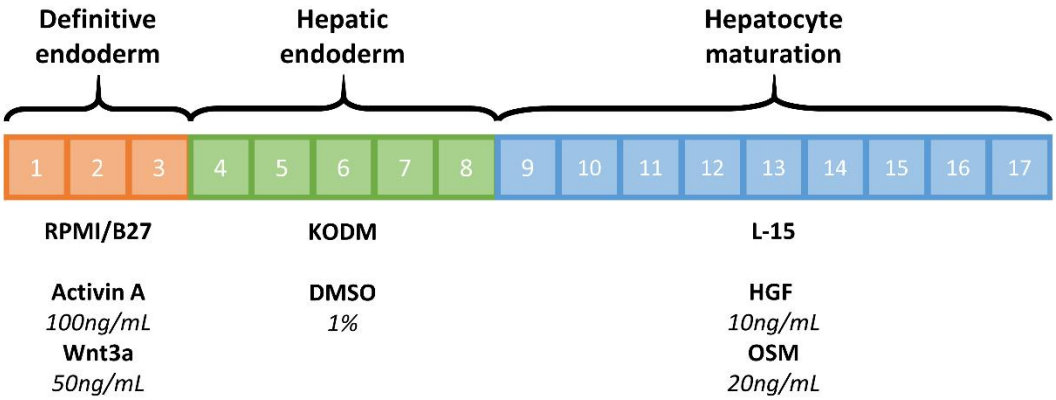

B **C** **D**

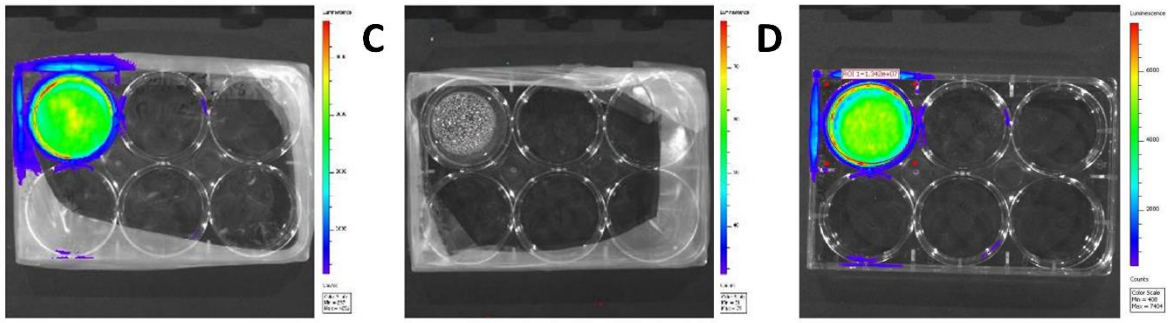

E

Version 1	Version 2
• Leibovitz's L-15 • 8.3% tryptose phosphate broth • 8.3% embryonic stem-cell FBS • 10 µM hydrocortisone 21-hemisuccinate • 1 µM Insulin (bovine pancreas) • 1% GlutaMAX • **0.2% ascorbic acid** • 100 nM dexamethasone • 20 ng/mL OSM • 10 ng/mL HGF	• Leibovitz's L-15 • 8.3% tryptose phosphate broth • 8.3% embryonic stem-cell FBS • 10 µM hydrocortisone 21-hemisuccinate • 1 µM insulin (bovine pancreas) • 1% GlutaMAX • **50ng/mL sodium-L-ascorbate** • 100 nM dexamethasone • 20 ng/mL OSM • 10 ng/mL HGF

Figure 35

Overview of the differentiation protocol used in this study - adapted from the protocol published by Medine et al. 2011. The top bar represents the day of the differentiation procedure and the medium and supplements used are shown underneath. Full details of the differentiation protocol are in chapter 2. **(A)** Overview of differentiation protocol used in this chapter, **(B)** Luminescence in ESC-HLCs at day 8 using version 1 of the protocol, **(C)** Luminescence at day 12 of the differentiation protocol using version 1 of the protocol, **(D)** Luminescence at day 12 using version 2 of the protocol, **(E)** Comparison of the composition of the hepatocyte maturation medium used in version 1 and version 2 of the differentiation protocol.

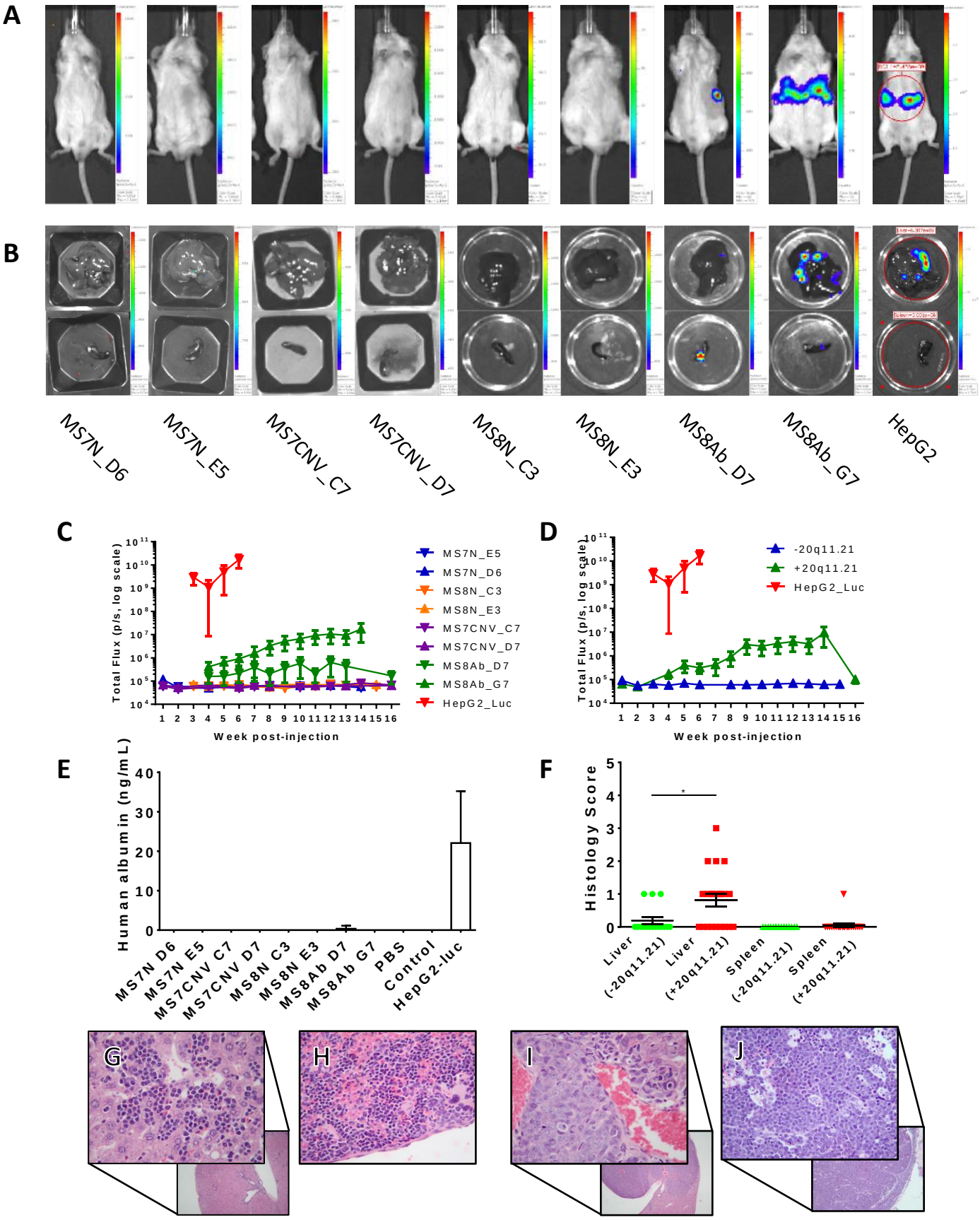
A
B
MS7N_D6
MS7N_E5
MS7CNV_C7
MS7CNV_D7
MS8N_C3
MS8N_E3
MS8Ab_D7
MS8Ab_G7
HepG2
C
Total Flux (p/s, log scale)
Week post-injection
MS7N_E5
MS7N_D6
MS8N_C3
MS8N_E3
MS7CNV_C7
MS7CNV_D7
MS8Ab_D7
MS8Ab_G7
HepG2_Luc
D
Total Flux (p/s, log scale)
Week post-injection
-20q11.21
+20q11.21
HepG2_Luc
E
Human albumin (ng/mL)
MS7N D6
MS7N E5
MS7CNV C7
MS7CNV D7
MS8N C3
MS8N E3
MS8Ab D7
MS8Ab G7
PBS
Control
HepG2-luc
F
Histology Score
Liver (-20q11.21)
Liver (+20q11.21)
Spleen (-20q11.21)
Spleen (+20q11.21)
G
H
I
J

Figure 36

MasterShef Fluc HLCs sporadically luminesce *in vivo* and increase liver tissue histology scores (A) Representative luminescence images of SCID beige mice 6 weeks post intrasplenic injection with MS Fluc HLCs or HepG2 Fluc cells. Luminescence is displayed in the coloured overlay with warmer colours indicating higher luminescence intensity. Not all animals displayed luminescence after injection with MS Fluc HLCs. **(B)** Representative ex vivo luminescence images of mouse organs. All images show liver (top) and spleen (bottom). Luminescence is indicated by the coloured overlays with warmer colours indicating greater luminescence intensity. **(C)** Luminescence over time for each injected cell line. Luminescence values were recorded for up to 4 months post-injection for each cell line using the IVIS. The values are plotted as total flux (photons/second) and error bars show SEM. The experiment with HepG2 Fluc cells was halted after 6 weeks since the luminescent signal was saturated in the IVIS scanner and the health of the animals began to deteriorate. **(D)** Luminescence over time grouped for cells with or without the 20q11.21 amplicon. Values are plotted as total flux (photons/second) and error bars show SEM. **(E)** Graph showing concentration of human albumin in the blood of SCID beige mice after injection with MS Fluc HLCs, HepG2 Fluc cells or controls. Blood was collected by cardiac puncture and assessed using human Albumin ELISA (Bethyl Laboratories). Values are presented as ng/mL. **(F)** Mean histology scores for liver and spleen tissues separated by tissue and amplicon status. Tissues were assessed by a histopathologist and were scored according to Thoolen et al. Horizontal black bars indicate the mean and SEM. Mean liver histology score was 0.81 with amplicon, 0.19 without, p=0.0281 using the Mann Whitney-U test with Bonferroni correction, mean spleen histology score was 0.05 with amplicon, 0.00 without, p=0.8264 using the Mann Whitney-U test with Bonferroni correction, details of the criteria for each score are shown in Table 9 **(G)** Haematoxylin and eosin staining of mouse liver after injection with MS Fluc HLCs showing hepatic lymphoma. **(H)** Haematoxylin and eosin staining of mouse spleen after injection with MS Fluc HLCs showing splenic lymphoma. **(I)** Haematoxylin and eosin staining of mouse liver after injection with MS Fluc HLCs showing carcinoma. **(J)** Haematoxylin and eosin staining of mouse thymus tumour after injection with MS Fluc HLCs showing thymic lymphoma.

Liver				Spleen			
-20q11.21	+20q11.21	HepG2	Control	-20q11.21	+20q11.21	HepG2	Control
0‡	0§	0	0	0‡	0§	0	0
0‡	3§	0	0	0‡	1§	0	0
0‡	0§	2	5	0‡	0§	0	4
0‡	0§		0	0‡	0§		0
0§	0§		0	0§	0§		0
0§	0§		0	0§	0§		0
0§	1‡			0§	0‡		
0§	0‡			0§	0‡		
0§	0‡			0§	0‡		
0*	0‡			0*	0‡		
1*	0‡			0*	0‡		
1*	2†			0*	0†		
1*	2†			0*	0†		
0*	2†			0*	0†		
0†	1†			0†	0†		
0†	1†			0†	0†		
	1*				0*		
	1*				0*		
	1*				0*		
	1*				0*		
	1*				0*		

Table 8

Histology scores for spleen and liver in animals injected with MS cells with or without 20q11.21 amplicon. Histology performed by a veterinary pathologist and scored according to Thoolen *et al.* For the columns marked '-20q11.21' an asterisk (*), dagger (†), double dagger (‡) or section mark (§) indicated that the animal was injected with MS7N E5, MS7N D6, MS8N C3 or MS8N E3 respectively. For the columns marked '+20q11.21' an asterisk (*), dagger (†), double dagger (‡) or section mark (§) indicated that the animal was injected with MS7CNV C7, MS7CNV D7, MS8Ab D7 or MS8Ab G7 respectively. Liver and spleen scores for +20q11.21 and -20q11.21 were compared using the Mann Whitney U test with Bonferroni correction using the wilcox.test() function in R. Mean liver histology score was 0.81 with amplicon, 0.19 without, p=0.0281. Mean spleen histology score was 0.05 with amplicon, 0.00 without, p=0.8264. Details for the criteria for each score are shown in Table 9.

Score	Details
0	No morphological abnormalities detected.
1	Discontinuous layers of centrilobular hepatocytes exhibiting coagulative necrosis, with kariolysis and kariorrhexis (only zone 3).
2	Thick continuous layer of centrilobular hepatocytes exhibiting coagulative necrosis, with kariolysis and kariorrhexis (only zone 3).
3	Thick and bridging areas of centrilobular coagulative necrosis (zone 3 and most of 2)
4	Extensive coagulative necrosis involving zones 3 and 2, sparing only a thin layer (~2 hepatocytes thick) of periportal hepatocytes
5	Extensive coagulative necrosis involving zones 3 and 2, and periportal hepatocytes including multiple diffuse foci

Table 9

Criteria for histology scoring of lesions in liver tissue – Histological scoring was performed by a veterinary pathologist according to Thoolen et al. (Thoolen et al., 2010). Though the scoring system described by Thoolen et al. was intended for use in Liver it was also arbitrarily applied to spleen. Scoring ranges from 0 to 5, where 0 indicates no detectable change in morphology from healthy tissue and 5 indicates the most severe form of lesion with even progression between each score.

H&E staining revealed hepatic lymphoma (Figure 36G), splenic lymphoma (Figure 36H), carcinoma (Figure 36I) and nodal lymphomas (Figure 36J). The tissues were also scored by a veterinary pathologist according to Thoolen et al. (Figure 36H); these scores were significantly higher in animals that received cells containing the 20q11.21 amplicon (Table 8).

5.3 Discussion

A major concern over the use of stem cell therapies is the perceived risk of tumorigenicity. This is highlighted by recent cases where tumours were found several years post stem cell transplantation. In one case, a tumour, derived from the transplanted material, was detected four years after foetal neural stem cell transplantation for ataxia telangiectasia (Amariglio et al., 2009). A similar case was also reported following the treatment of spinal injury with olfactory mucosal cell transplantation; 8 years after treatment, the patient was found to have developed a mucosal-like mass at the transplant location (Dlouhy et al., 2014). Pluripotent stem cells (PSCs) have been shown to cause benign teratomas in immune-deficient mice but may also create potentially malignant teratocarcinomas. In the short term, a pragmatic position on genetic changes will need to be adopted for the culture of human PSCs intended for clinical applications (Andrews et al., 2015), however, more data are required on which genetic variants are prone to tumorigenesis and which are safest.

It is of vital importance that cells used for therapy do not pose a substantial risk to their recipients be it from undifferentiated cell survival or by insidious changes to the genotype of cultured cells which makes them more prone to form tumours after transplantation (Nicolas et al., 2017). In this study we have examined the effects of a common amplicon- 20q11.21- which is known to confer a survival advantage *in vitro* (Nguyen et al., 2014). This amplicon contains several high risk genes including BCL2L2, ID1 and TPX2, and although the survival advantage has been demonstrated to operate via overexpression of BCL2L2 *in vitro* it is not clear whether the advantage will operate through the same mechanism, or at all *in vivo* (Avery et al., 2013). Therefore, we hypothesised that cells containing the 20q11.21 amplicon would show greater tumour forming potential *in vivo* than cells without the amplification

In this work we demonstrate for the first time, the engraftment of differentiated cells with known 20q11.21 status and show differences in their behaviour after engraftment depending on amplicon status. Cells with 20q11.21 engraft more readily in both a

differentiated and undifferentiated state. This is demonstrated by the extensive integration of undifferentiated MS7CNV cells (Figure 32A) and increased mean luminescent signal from lines containing the amplicon when differentiated (Figure 36A, B, I & J). Moreover, the extent of pathological change to tissues from cells with the 20q11.21 amplicon is greater as determined by mean histology score (Figure 36H, Table 8) (Thoolen et al., 2010).

These results are unsurprising given the mechanism of the survival advantage conferred by 20q11.21. Cells containing the amplicon are somewhat protected against cell death induced by single-cell passaging. In these experiments the cells were reduced to a single-cell suspension for injection, and it is clear that a survival advantage at this stage could lead to improved engraftment downstream (Nguyen et al., 2014). It should also be considered that the survival advantage conferred to hESCs *in vitro* may not provide a similar advantage *in vivo* and also that if an advantage is conferred it may not operate via the same mechanism. Specifically, although BCL-XL has been shown to be responsible for the survival advantage conferred *in vitro* and has been found to be upregulated in several cancers (Jin et al., 2017), ID1 and TPX2 were both considered as candidate drivers of the selective advantage of 20q11.21 *in vitro*. TPX2 is involved in the progression of the cell cycle and is often overexpressed in hepatocellular carcinoma (Shu et al., 2017), therefore the relevance of overexpression in transplanted cells is clear. The effects of ID1 are highly pleiotropic, however it is implicated in promoting cell-cycle progression, prevention of differentiation and tumour progression (Aloia et al., 2014; Roschger and Cabrele, 2017; Tournay and Benezra, 2015; Zhang et al., 2007). Additionally, ID1 is often found to be overexpressed in a number of cancer cell types including hepatocellular carcinoma (Roschger and Cabrele, 2017; Sharma et al., 2016). Therefore, it is also possible that an increase in tumorigenicity could be attributed to ID1 overexpression.

5.3.1 Pluripotency is maintained after transformation with luciferase reporter

Random integration of nucleic acids into the genome of a cell can produce unintended side effects should the integrated portion disrupt the expression of genes essential to cell function. Though unlikely given the size of the genome, it was important to determine that pluripotency and differentiation propensity had been maintained after transformation with the luciferase reporter. Using an embryoid body forming assay, the formation of all three germ layers was demonstrated at the protein level (Figure 33B). This is a positive result as pluripotency was required for this study. However, the genomic location of plasmid

integration was not determined and it was possible that even though pluripotency was maintained, the propensity to differentiate to each germ layer was changed. Not all stem cell lines share an equal propensity to differentiate towards hepatocyte like cells, and it is conceivable that disruption of an essential gene for the proper formation of the hepatic cell fate could be disrupted without damaging a cell's ability to form endoderm markers in the embryoid body forming assay. Moreover it has been suggested that the tendency to express hepatic markers spontaneously can dictate a stem cell line's ability to form HLCs (Greenhough et al., 2013). Therefore, we also quantitatively examined the expression of several hepatic markers in embryoid bodies produced from the transformed lines using qPCR (Figure 34).

The results in Figure 34 are unexpected, the expression of AFP in both MS7N and MS7CNV appears to be increased in the transformed lines relative to the parental line. Similarly, the expression of albumin appears to be improved in MS7N transformed lines versus parental and the expression of HNF4a is improved in transformed lines versus parental for MS7CNV. In other cases, expression is similar between parental and transformed lines as might be expected. These results seem initially paradoxical, the luciferase reporter construct may have integrated in such a way to produce deranged expression of these genes but this would not explain how multiple genes were affected (e.g. AFP and HNF4a in MS7CNV) nor the regularity with which they occurred. However, when the stochastic nature of embryoid body formation is considered these results may be understood. Since the differentiation of cells during embryoid body formation is non-directed the embryoid bodies in both MS7N and MS7CNV parental line have only poorly entered the endoderm germ layer. It is probable that were this experiment repeated these cells may form endoderm more readily and show similar expression to MS8N and MS8Ab. Ultimately, although there were discrepancies in the number of hepatic markers expressed, most of the transformed lines showed enough expression of the tested hepatic markers to proceed to directed differentiation and were later shown to differentiate without issue (Figure 35 & 36). Interestingly, these results did not predict the less complete differentiation of MS8Ab, which showed the lowest proportion of HNF4a-expressing cells at day 8 of differentiation (80%, Figure 33) compared with MS7CNV which formed HNF4a more efficiently (88%).

5.3.2 CCl_4-induced acute liver injury in SCID beige mice

To the best of our knowledge, this study is the first example of acute CCl_4-induced liver injury in SCID beige mice for engraftment of differentiated cells. SCID beige mice were

chosen for this study due to their SCID status, displaying severe B and T lymphocytopaenia and defective natural killer cells, making them suitable xenograft candidates. Additionally, albino fur is more suited to long-term luminescence imaging since it does not obscure the luminescent signal as much as dark fur and therefore does not require shaving. However, there are some shortcomings of this engraftment model which have limited the application of this study. The SCID beige mouse is not as widely used as other SCID strains, such as the NOD-SCID or NOG which have long been known to develop lifespan limiting thymus tumours at 6-8 months of age (Custer et al., 1985; Yasuda et al., 2017). Many of the SCID beige mice also shared this tendency to develop lifespan-limiting thymic lymphomas as 6 animals in this study were found to have developed tumours. This tendency was limiting to the overall goals of the study where the aim was to maintain the mice long-term (i.e. over 6 months) which was not possible. Though the development of lymphomas in SCID beige mice is not surprising, due to the shared mutation in *Prkdc*^{scid}, we are not aware of literature reports of this propensity.

5.3.3 Inconsistent detection of luminescent signal after injection of HLCs

In vivo imaging was used during this study to track the fate of luminescent cells in a repeatable and non-destructive manner. This allowed for the use of fewer animals than would have otherwise been possible, in line with the key tenets of the 3R's. Moreover, it was possible to observe the same animal and cells repeatedly to track how the engraftment progressed, we were able to determine from an early time point if the cells were successfully engrafted based on the presence of a luminescent signal. However, there were also limitations to this approach, imaging in this manner allows only a 2D view of the luminescent signal, although as shown in supplementary figures 2-10 imaging the animals in different directions can allow for better triangulation of the source of the signal. This proved problematic as it was not possible to reliably determine whether the observed signals originated from the liver, spleen or both. Moreover, the signal was partially attenuated by the animal's body meaning that only more intense signals could be detected. Future studies may consider the use of more sensitive techniques such as those utilising far-red luminescence recently employed by Yeh et al. (2017) or Iwano et al. (2018) which are reported to enable better tissue penetration and sensitivity.

Intrasplenic injection was chosen as the delivery route for both undifferentiated and differentiated cells, as it has previously been successfully used by Payne et al. (2011). Alternative methods including portal vein infusion were considered but ultimately not used

due to the higher technical complexity and potential for complications. In most animals, engraftment of undifferentiated cells could be detected by the presence of a luminescent signal (Figure 32). Supplementary figure 1 shows the time course of engraftment in detail, at least a small signal was observed in every animal except one injected with MS8Ab. The outcome of these signals was divided, in 6 animals the signal was lost over time and in those where the signal retained the intensity increased over time, with the exception of 2 animals injected with MS8N where the signal remained similar throughout the experiment. These results demonstrate the efficient engraftment and proliferation of undifferentiated cells *in vivo*.

After injection of differentiated cells, no luminescent signal was observed or became undetectable after several weeks in 42/45 animals which survived surgery, as shown in supplementary figures 2-10. The cause of the lack of signal is unclear, though we can predict several possibilities. The transplanted cells may have failed to integrate once differentiated, however, literature reports using similar protocols to this study observed long-term survival of engrafted cells *in vivo*, making this possibility unlikely (Payne et al., 2011; Takayama et al., 2017). There were minor differences in the differentiation protocol, strain of mice and cell lines used, therefore it is possible that these discrepancies may have prevented integration of HLCs in this study.

It is also possible that only the undifferentiated proportion of cells survived transplantation and formed the few luminescent signals observed in Figure 36 and supplementary figures 2-10 and that the differentiated cells have failed to engraft. This possibility is appealing because the engraftment potential of undifferentiated cells and their presence after this differentiation protocol has been demonstrated (Figure 32 & 33). Based on flow cytometry analysis (Figure 33C) it was demonstrated that a substantial proportion (19.4%) of the cells do not express HNF4α and likely did not form HLCs. Furthermore, the 3 animals which showed luminescent signals long-term were all injected with MS8Ab-derived HLCs, this line showed the lowest differentiation proportion of 80.6% (Figure 33C). The undifferentiated population of cells may give rise to the sporadic luminescent signals observed. However, were this the case it might be expected that the undifferentiated proportion of the cells would produce a luminescent signal more frequently. The presence of human albumin in Figure 36E suggests that at least some hESC-HLCs have engrafted but does not discount the possibility that the luminescent signal was derived from undifferentiated cells. This possibility would be relatively simple to evaluate through the use of cell sorting to purify only differentiated cells prior to injection or through the use of a more modern and highly

efficient differentiation protocol such as the recent study utilising laminins by Takayama *et al.* (2017).

Finally, the failure to produce a luminescent signal in many animals may be an indicator of inter-animal variation, though the animals are of the same strain, they cannot necessarily be expected to behave identically and minor discrepancies in the induction and extent of acute liver injury and injection of the HLCs may influence the propensity to integrate.

Taken together, these results show that consistent engraftment of cells in all mice with hESC-HLCs was not achieved, as indicated by the lack of luminescent signal in many animals (supplementary figures 2-10). Possibly, a different mouse model may have been more suitable for the purposes of this experiment. For example, NOD-SCID gamma mice are reported to have a lifespan in excess of 16 months whilst still retaining a severely immunocompromised status (Shultz et al., 2005). Alternatively, a more complete model of humanisation could have been used wherein the survival of the animal depends on the engraftment of the injected cells. For example, TK-NOG mice are a mouse humanisation model which express viral thymidine kinase specifically in the hepatocytes allowing for selective deletion of the host hepatocytes using ganciclovir allowing for efficient repopulation (Hasegawa et al., 2011). Other humanisation models exist, including fumarylacetoacetate hydrolase (fah) deficient mice which lack the fah gene. This phenotype is lethal without treatment with NTBC and is permissive of repopulation with non-fah deficient hepatocytes (Grompe, 2017). For the purpose of these experiments these animal models were prohibitively expensive, but future studies may consider their use. The use of a more complete humanisation model would provide greater confidence in the integration of the transplanted cells and the subsequent effects.

5.3.4 Poor expression of human albumin in HLC-injected mice

The expression of human albumin was examined in Figure 36E but was largely undetected except for a single clone. Interestingly, the animal from which the serum containing human albumin was taken did not show a luminescent signal, suggesting either attenuation of the signal or only a small number of cells. The lack of detectable albumin in almost all lines after 4 months (Figure 36C-E) suggests that the cells have engrafted poorly, failed to survive long-term or dedifferentiated after injection as reported by Payne et al. (2011), though we did not specifically test for this possibility. Human albumin was readily detectable in the serum of animals injected with HepG2 cells, however, these animals were only maintained for 6 weeks after injection as opposed to approximately four months for animals injected

with HLCs and it is possible that there would have been an increased quantity of human albumin in the HLC-injected animals at this time point. However, early experiments indicated that SCID beige mice failed to clot in response to collection of serum via tail bleeding, this was compounded by the small overall size of the animals and the relatively high serum requirement of albumin ELISA and therefore examination of albumin at additional time points was not possible.

The detection of human albumin, even at extremely low levels demonstrates that hESC-HLCs have engrafted and survived long-term in at least one animal, that there is no luminescent signal is concerning as it suggests possible attenuation of the signal either in the hESC-HLCs or by the body of the animal. This highlights a potential limitation of the imaging approach used as discussed previously.

5.3.5 SCID beige mice spontaneously form thymic lymphomas

The observation that SCID beige mice were similarly susceptible to spontaneous formation of thymic lymphoma as other SCID strains somewhat hampered these experiments. Initially it was planned to assess the long-term effects of engraftment over a period of 6 months after injection. However, given that mice were obtained at 8 weeks of age and began to develop lifespan-limiting thymic lymphomas around 6 months of age, this was not possible.

5.3.6 Conclusions

There are concerns that stem cell-derived cells pose an oncogenic risk when transplanted which must be allayed before they can progress to clinical use. However, testing for tumorigenicity is inherently challenging, *in vitro* models are unable to model engraftment and tumour growth to a satisfactory degree. Therefore, immunocompromised animal models must be used as an approximation of the response in humans. These results show for the first time the effects of transplant of an extremely common genetic aberration in human stem cells in a differentiated cell. It should also be considered that, like other therapies, stem cell therapies will always carry some degree of risk to the patient. By determining commonly occurring genetic risk factors such as 20q11.21 and other aberrations linked to increased tumorigenic potential, cells intended for transplant can be quickly triaged to minimise risk whilst allowing the use of potentially valuable therapies without an excessive burden of testing.

In summary, these results show engraftment of differentiated cells into an animal model and demonstration of a change in cell phenotype based on a commonly acquired culture

adaptation. Specifically, these results likely demonstrate an increased risk and severity of malignancies in animals injected with cells containing the 20q11.21 amplicon. The results are impactful to the wider field of translational medicine as future studies should take care to screen lines known to harbour common amplicons when they are being considered for use in transplant. Future studies in this area should also consider the use of a more complete humanisation model e.g. TK-NOG or fah (-/-) mice where survival of the animal depends on engraftment, or a longer-lived immunocompromised model such as a NOD-SCID gamma which would provide more certainty of the survival of the engrafting cells and their long-term effects respectively.

6 General Discussion

6.1 Introduction

This thesis represents our efforts to develop and characterise nascent stem cell-based *in vitro* hepatocyte models. This work is necessary to produce better models of hepatotoxicity than are currently possible and may eventually be used in cell therapies and for transplant once safety issues have been more thoroughly addressed. Current models of hepatotoxicity are insufficient to tackle drug-induced liver injury because they lack physiological relevance, in the case of commonly used cancer cell lines. Or fall short in stability, availability and reproducibility in the case of hPH.

PSC-derived HLCs are a promising alternative hepatocyte model. They can be produced non-invasively and can be readily expanded *in vitro*. Hepatic organoids are another nascent *in vitro* model of hepatocytes which exploit the regenerative mechanisms of the liver to produce HLCs. Organoids are most commonly isolated invasively and currently offer a closer approximation of *in vivo* liver than HLCs. Both models can reproducibly model multiple genotypes, but differ in terms of genetic stability.

Our work has used advanced techniques to better understand models of hepatotoxicity including iTRAQ and qPCR. The three main projects of this thesis were to examine the effects of a hypoxic environment on the differentiation of human induced pluripotent stem cells (iPSCs) to HLCs. Secondly, to establish human liver organoids in our laboratory and examine their phenotype on a proteomic level and thirdly, to examine the effects of the 20q11.21 amplicon on the tumorigenicity of human embryonic stem cell (hESC)-derived HLCs when transplanted into SCID beige mice with livers which were acutely damaged with CCl_4.

6.2 The effects of a hypoxic environment on the differentiation of iPSC-HLCs and comparison of two differentiation protocols

PSC-HLCs are a promising model to produce high-quality hepatocytes, however they are hindered by poor physiological relevance compared to hPH or organoids. The development of differentiation protocols for iPSC-HLCs has not changed dramatically in recent years in terms of additives to differentiation media. Instead there has been a focus on the adaptation of the culture conditions to improve physiological relevance, including 3D

culture and laminins to mimic the conditions of embryogenesis. Though oxygen levels have been modulated for the maintenance of PSCs, the use of lowered oxygen has not been widely examined for the differentiation of HLCs.

In chapter 3, the effects of low-oxygen on the differentiation of iPSC-HLCs were examined and two differentiation protocols were compared. The results of these experiments showed only minor separation between tested conditions. The use of low oxygen did not appear to improve the phenotype of the HLCs as predicted and the two protocols did not separate strongly based on principal component analysis or hierarchical clustering.

The lack of separation based on differentiation protocol suggests that protocol 2, which is cheaper, is the most suitable for large scale culture where the decreased costs and increased reproducibility offered by protocol 2 are key factors. However, the use of serum in this protocol should be considered, modern protocols are typically serum free, particularly those intended for medicinal use. Serum is a biological component whose composition is not defined. Future studies should consider the replacement of serum in this protocol with serum-free alternatives such as Knockout Serum Replacement as is used in earlier stages of the same protocol to produce a xeno- and serum-free differentiation protocol.

This work represents the first attempt that we are aware of to differentiate iPSCs to HLCs under hypoxic conditions, though similar methods using mesenchymal stem cells exist (Prasajak and Leeanansaksiri, 2013). We observed no evidence of adoption of a perivenous phenotype under hypoxic conditions and observed activation of hypoxia inducible factors under normoxic conditions.

This indicates a potential hypoxia response under normoxic conditions likely due to the increasing metabolic oxygen demand (MOD) of differentiating cells combined with the rate of diffusion of oxygen throughout the culture medium. As PSCs differentiate to HLCs, their MOD presumably increases to become like a hepatocyte (Figure 37). Increasing MOD likely produced a progressively increasing hypoxic cell environment even under normoxic conditions and cells cultured under hypoxic conditions likely experienced conditions of near-anoxia (Figure 37, Place et al. (2017)). These very low oxygen conditions likely explain the casually observed, poorer success rate of differentiations under hypoxic conditions and may have led to cells beginning to die off as cells became more metabolically active towards the end of the differentiation protocols.

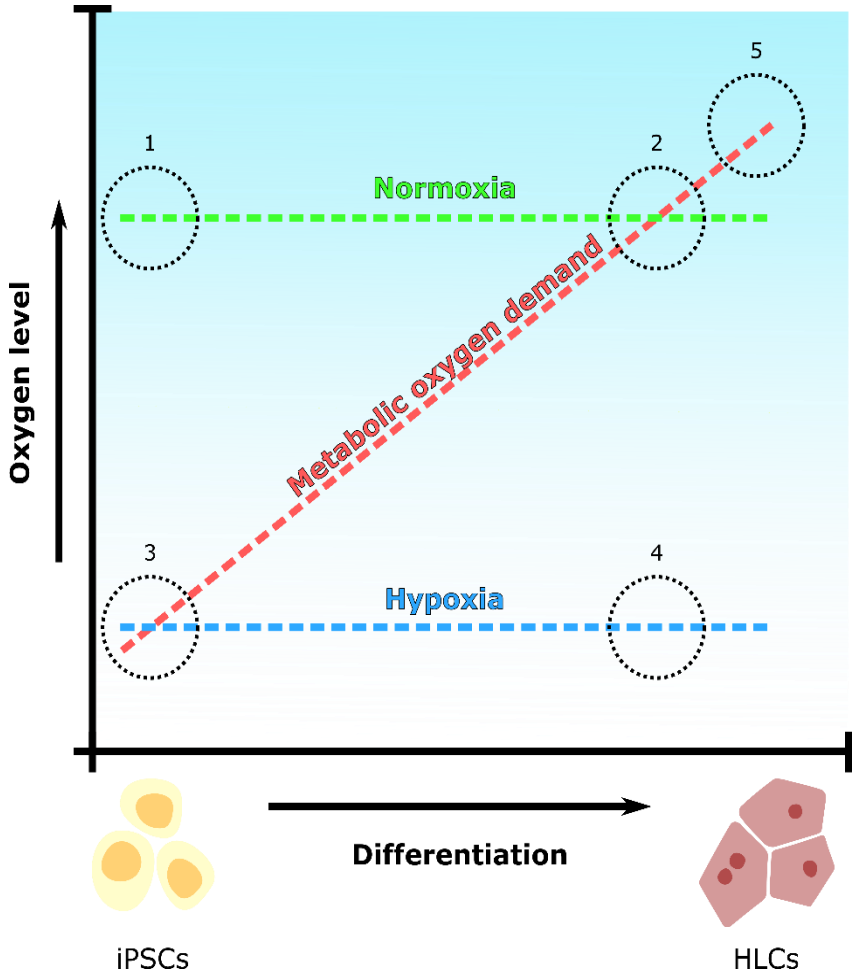

Figure 37

Schematic of increasing oxygen demand during differentiation and oxygen levels supplied by hypoxic and normoxic culture conditions – progress throughout differentiation from iPSCs to HLCs is shown on the x-axis. Arbitrary oxygen level is shown on the y axis. The red dotted line indicates increasing oxygen demand throughout the differentiation, the blue dotted line indicates the oxygen level of cells cultured under hypoxic conditions, the green dotted line shows the oxygen level of cells cultured under normoxic conditions. **(1)** levels of oxygen in normoxic culture are higher than physiological oxygen for iPSCs. **(2)** Normoxic culture provides near physiological oxygen levels during the later stages of differentiation but remains slightly hypoxic **(3)** Hypoxic conditions provide physiological conditions for oxygen demand for iPSCs. **(4)** hypoxic culture is insufficient to satisfy increased metabolic oxygen demand of HLCs. **(5)** Metabolic oxygen demand of HLCs increases beyond what can be provided by normoxic culture, hyperoxic culture may provide sufficient oxygen to meet this demand.

Furthermore, an improvement in the phenotype of hepatic cell lines when cultured under hyperoxic conditions was recently shown, improvements in CYP3A4 expression and ammonia elimination in HepaRG and C3A cells was observed (van Wenum et al., 2018). These results suggest that future studies should investigate the use of hyperoxia or increasing oxygen levels during differentiation to match increasing MOD and observe if HLCs under these conditions adopt a zonal phenotype.

6.3 The establishment of human liver organoids and characterisation by proteomic analysis

Liver organoids were recently established for the first time in a series of papers by the Clever's lab and show promise as a model of hepatotoxicity and liver regeneration. Two major types of liver organoids have been described to date which exploit the two main pathways of liver regeneration. In chapter 5 we established the culture of hepatic organoids derived from EpCAM-positive cells in our laboratory and examined their phenotype more closely than has previously been attempted using iTRAQ analysis.

Our results demonstrated that differentiated and undifferentiated organoids clustered separately by hierarchical clustering analysis, and though they separated from hPH, showed good recapitulation of key liver-specific proteins, with the expression of many CYPs, transporters and DMETs, not significantly different from hPH. Interestingly, although differentiated and undifferentiated organoids separated based on hierarchical clustering analysis, the expression of many liver-related proteins was not significantly changed by differentiation.

Overall these results show that hepatic organoids, derived from EpCAM-positive cells offer good recapitulation of the hepatic phenotype, particularly transporters. Future studies should aim to compare organoids with other emerging models such as iPSC-HLCs and organoids derived from hepatocytes to determine whether they represent a true improvement over these models.

There were some shortcomings of this study, cryopreservation severely retarded organoid growth after thawing and therefore, iTRAQ analysis was only completed in a single donor. Future work should repeat this analysis in additional donors to determine if the phenotype is reproducible and establish a cryopreservation protocol that does not cause growth retardation in cryopreserved organoids.

The expansion of EpCAM-positive cells *in vivo* is the minor pathway in the production of hepatocytes. Exploitation of the major method of cell repopulation i.e. from extant hepatocytes, may produce better quality cells as suggested by Hu et al. (2018). However, this study also uses RNA-based methods to determine phenotype so closer scrutiny with proteomic analysis may reveal a more accurate approximation of the true phenotype. Therefore, future studies should also attempt to produce organoids from hepatocytes and compare their proteome to those produced from EpCAM-positive cells. This experiment would reveal not only which type of organoid produces a better model for hepatotoxicity but may also provide insights into the differences, if any, between cells produced by the two major routes of hepatocyte repopulation in the liver.

Organoids show an improved hepatic phenotype compared with iPSC-HLCs as is apparent from the comparisons made to hPH in chapters 3 and 4. Their good recapitulation of mature liver characteristics makes them the best option for hepatotoxicity screening of the nascent models discussed in this thesis. However, the manner in which they are cultured i.e. in semi-solid domes, with imprecise control of cell numbers during passaging may hinder their use in high-throughput screening where he matrix may interfere with testing compounds and the precise cell number must be controlled. By comparison, iPSC-HLCs do not share these issues, using more traditional 2D cultures which are currently in use for toxicity testing though currently their phenotype is not necessarily a large enough improvement to warrant a switch away from simpler and cheaper immortalised cell lines.

In conclusion, organoids appear to be capable of good recapitulation of the hepatic phenotype, but this should be compared more thoroughly against other emerging models such as PSC-HLCs and other types of liver organoids. After which, their use in toxicity testing must be addressed. Currently, organoid toxicity testing is not yet fully realised and few toxicity screens have been reported to date (Van De Wetering et al., 2015). The manner in which organoids are cultured is labour-intensive and does not easily allow for close control of the number of cells per culture due to passaging using organoid fragments, future studies may investigate the development of single-cell passaging protocols to enable the necessary degrees of control over cell number. These issues must be overcome and automated, if the organoids are to be used in high-throughput screening.

6.4 The Effects of the 20q11.21 amplicon on the tumorigenicity of hESC-HLCs *in vivo*

With the advent of personalised medicine there is great potential for the use of isogenic cells for cell therapies and transplant. However, the safety of such techniques has not yet been fully established. Cells accrue mutations over time in culture which may make the more prone to tumour formation later. In chapter 5 we examined the effects of a common amplicon of the tumour forming potential of hESC- HLCs.

The results of this chapter showed significantly increased histology scores and increased luminescent signal in the livers of mice which were injected with cells containing the 20q11.21 amplicon. Therefore, we can conclude that cells should likely be screened for the presence of the 20q11.21 amplicon prior to use in transplantation. This is the first literature example of the transplant of cells with known 20q11.21 status which demonstrated a change in behaviour of the cells *in vivo* and is a key milestone in determining what characteristics of a pluripotent cells are potentially harmful if intended for transplant. Future studies may consider testing other commonly occurring amplicons in a similar manner to build a library of aberrations that are unacceptable for transplanted cells.

The work in this chapter used Fox Chase SCID beige mice, an uncommon SCID mouse strain which led to several drawbacks. We are not aware of previous reports of the tendency to form lifespan-limiting thymus tumours in this strain. Were this not the case, the study would have been continued for 6 months after transplantation of the cells. Future studies should consider the use of a longer-lived strain of SCID mouse such as the NOD SCID Gamma.

Additionally, results were hampered by loss of luminescence after injection of HLCs in many animals and the poor detection of albumin. This was interpreted largely as engraftment failure in the differentiated cells though the reasons for this failure are unclear. Future studies may consider the use of recent highly efficient differentiation protocols or the use of obligate humanisation models such as TK-NOG or fah deficient mice to increase the confidence that HLCs have survived *in vivo*.

6.5 Final Comments

To conclude, the hypotheses investigated in this thesis will be commented upon individually.

6.5.1 Hypothesis 1:

During embryonic development, hepatocytes are exposed to low oxygen conditions and the phenotype of mature hepatocytes varies across the lobule and is influenced by oxygen tension. By differentiating iPSC-HLCs under hypoxic conditions their phenotype will be improved and more closely mimic that of a perivenous hepatocyte.

Comment: Cells differentiated under hypoxic conditions showed little to no consistent improvement over those differentiated under normoxic conditions. Nor did cells differentiated in hypoxia show an increase in perivenous markers. Therefore, we find this hypothesis to be rejected. Future studies should investigate the use of hyperoxia to determine if a pericentral phenotype may be achieved.

6.5.2 Hypothesis 2:

Organoids have been demonstrated to show a mature hepatic phenotype by examining gene expression. Examining their proteomic phenotype will produce a truer representation of their hepatic phenotype.

Comment: Hepatic organoids were established in culture and differentiated. Assessment using iTRAQ analysis showed that although organoids cluster separately from hPH, their expression of a large number of liver-specific proteins is not significantly different from hPH and therefore the hepatic phenotype is well represented and the difference in clustering analysis is likely due to the proliferative nature of the cells or mixed cholangiocyte phenotype. Therefore the hypotheses cannot be rejected under the conditions of this study. Future studies should aim to increase the number of replicates in this experiment to confirm these findings and determine a cryopreservation technique that does not retard the growth of cryopreserved organoids and should also aim to confirm these findings using activity assays.

6.5.3 Hypothesis 3:

The presence of amplicon 20q11.21 confers a survival advantage to carrier cells *in vitro*. Similarly, differentiated cells which carry the amplification will be more prone to tumour formation when transplanted into the livers of an immunodeficient mouse model.

Comment: HLCs differentiated from ESCs containing the 20q11.21 amplicon produced greater luminescent signal *in vivo* and showed significantly increased histology scores in the liver. Therefore, we find this hypothesis to be supported. However, it should be noted that the injected HLCs were found to be non-functional *in vivo* as determined by albumin expression Future studies should make use of a humanisation model in which survival of the animal depends on engraftment of the transplanted cells to increase confidence in their long-term survival.

7 Appendices and supplementary figures

Protein	Abbreviation	Prot. 1 normoxia vs. prot. 1 hypoxia		Protocol 1 normoxia vs hPH		Protocol 1 normoxia vs UD		Protocol 1 hypoxia vs. hPH		Protocol 1 hypoxia vs. UD	
		Fold change	p-value	Fold change	p-value	Fold change	p-value	Fold change	p-value	Fold change	p-value
CYPs											
Cytochrome P450 1A2	CYP1A2	-1.537	3.36E-01	**-57.718**	**6.59E-07**	**3.425**	**1.41E-02**	**-37.549**	**2.15E-06**	**5.265**	**2.23E-03**
Cytochrome P450 2A6	CYP2D6	**2.201**	**3.60E-02**	**-21.283**	**9.26E-07**	**3.010**	**6.36E-03**	**-46.844**	**7.67E-08**	1.368	3.67E-01
Cytochrome P450 2C8	CYP3D6	-1.314	4.27E-01	**-46.699**	**7.19E-08**	**2.763**	**9.87E-03**	**-35.535**	**1.62E-07**	**3.631**	**2.17E-03**
Cytochrome P450 2C9	CYP2C9	-1.166	5.96E-01	**-88.185**	**2.04E-09**	**3.653**	**6.24E-04**	**-75.625**	**3.05E-09**	**4.259**	**2.48E-04**
Cytochrome P450 2D6	CYP2D6	**-2.831**	**2.34E-02**	**-57.893**	**3.12E-07**	1.537	3.04E-01	**-20.447**	**6.95E-06**	**4.352**	**3.21E-03**
Cytochrome P450 2E1	CYP2E1	-1.054	8.35E-01	**-38.610**	**4.30E-09**	**1.803**	**3.36E-02**	**-36.645**	**5.06E-09**	**1.900**	**2.28E-02**
Cytochrome P450 2S1	CYP2S1	-1.282	5.20E-01	1.437	3.53E-01	**-9.726**	**5.63E-05**	1.842	1.29E-01	**-7.584**	**1.60E-04**
Cytochrome P450 3A4	CYP3A4	1.041	9.46E-01	**-69.595**	**8.87E-06**	**5.738**	**1.05E-02**	**-72.434**	**8.07E-06**	**5.513**	**1.20E-02**
Cytochrome P450 4A11	CYP4A11	-1.131	8.23E-01	**-74.243**	**3.79E-06**	2.974	6.60E-02	**-65.647**	**5.09E-06**	**3.363**	**4.39E-02**
TRANSPORTERS											
ATP-binding cassette sub-family A member 6	ABCA6	-2.070	3.65E-01	**-6.690**	**3.01E-02**	1.206	8.13E-01	-3.232	1.55E-01	2.496	2.60E-01
ATP-binding cassette sub-family D member 1	ABCD1	1.537	2.74E-01	1.148	7.19E-01	**2.866**	**1.58E-02**	-1.339	4.52E-01	1.865	1.23E-01
ATP-binding cassette sub-family D member 3	ABCD3	**3.332**	**4.85E-02**	-3.153	5.81E-02	**7.967**	**2.59E-03**	**-10.503**	**1.05E-03**	2.391	1.38E-01
ATP-binding cassette sub-family E member 1	ABCE1	1.217	6.00E-01	1.057	8.82E-01	-1.722	1.62E-01	-1.152	7.05E-01	-2.096	6.53E-02
ATP-binding cassette sub-family F member 1	ABCF1	1.389	3.49E-01	**4.144**	**1.20E-03**	-2.057	5.39E-02	**2.983**	**7.11E-03**	**-2.858**	**9.00E-03**
ATP-binding cassette sub-family F member 3	ABCF3	-1.110	7.79E-01	-1.251	5.50E-01	-1.031	9.34E-01	-1.127	7.48E-01	1.076	8.43E-01
Calcium-binding mitochondrial carrier protein Aralar1	SLC25A12	1.748	9.66E-02	-1.041	9.00E-01	1.876	6.50E-02	-1.819	7.74E-02	1.073	8.24E-01
Protein	**Abbreviation**	**Prot. 1 normoxia vs.**		**Protocol 1 normoxia**		**Protocol 1 normoxia**		**Protocol 1 hypoxia**		**Protocol 1 hypoxia**	

		prot. 1 hypoxia		vs hPH		vs UD		vs. hPH		vs. UD	
		Fold change	p-value	Fold change	p-value	Fold change	p-value		Fold change	p-value	Fold change
Calcium-binding mitochondrial carrier protein Aralar2	SLC25A13	-1.022	9.55E-01	**-7.114**	**2.16E-04**	1.334	4.58E-01	**-6.962**	**2.38E-04**	1.363	4.26E-01
Calcium-binding mitochondrial carrier protein SCaMC-1	SLC25A24	1.198	5.96E-01	**7.703**	**5.04E-05**	**7.243**	**6.69E-05**	**6.428**	**1.17E-04**	**6.044**	**1.58E-04**
Equilibrative nucleoside transporter 1	ENT1	-2.039	1.13E-01	-1.335	5.02E-01	**-7.223**	**4.76E-04**	1.528	3.29E-01	**-3.542**	**1.04E-02**
Major vault protein	MVP	-1.015	9.79E-01	**4.758**	**1.55E-02**	**8.317**	**2.40E-03**	**4.830**	**1.47E-02**	**8.444**	**2.29E-03**
Multidrug resistance-associated protein 1	ABCC1, MRP1	1.876	9.61E-02	**2.646**	**1.63E-02**	-1.019	9.58E-01	1.411	3.43E-01	-1.911	8.77E-02
Solute carrier family 2, facilitated glucose transporter member 1	GLUT1	1.523	1.88E-01	**8.577**	**1.20E-05**	**2.208**	**2.21E-02**	**5.632**	**9.45E-05**	1.450	2.42E-01
Solute carrier family 2, facilitated glucose transporter member 2	GLUT2	1.463	5.62E-01	**-10.250**	**3.35E-03**	2.519	1.73E-01	**-14.994**	**1.14E-03**	1.722	4.11E-01
Solute carrier family 2, facilitated glucose transporter member 3	GLUT3	-2.384	1.62E-01	**13.304**	**8.02E-04**	1.947	2.75E-01	**31.715**	**6.88E-05**	**4.641**	**2.18E-02**
Voltage-dependent anion-selective channel protein 1	VDAC1	1.177	6.07E-01	-1.012	9.69E-01	**6.176**	**7.24E-05**	-1.191	5.81E-01	**5.248**	**1.67E-04**
Voltage-dependent anion-selective channel protein 2	VDAC2	**-2.181**	**7.62E-03**	**4.311**	**6.25E-05**	**2.558**	**2.29E-03**	**9.403**	**8.78E-07**	**5.580**	**1.33E-05**
Voltage-dependent anion-selective channel protein 3	VDAC3	**-1.711**	**1.26E-02**	1.163	4.27E-01	1.398	9.27E-02	**1.989**	**2.76E-03**	**2.392**	**4.66E-04**
PHASE II											
Catalase	CAT	-1.372	3.70E-01	**-36.761**	**1.89E-07**	1.738	1.30E-01	**-26.795**	**5.10E-07**	**2.384**	**2.51E-02**
Catechol O-methyltransferase	COMT	2.057	8.09E-02	**-4.325**	**2.23E-03**	**12.625**	**2.20E-05**	**-8.898**	**8.81E-05**	**6.137**	**4.38E-04**
Glutathione S-transferase A2	GSTA2	1.385	7.09E-01	**-12.744**	**1.13E-02**	**7.425**	**3.65E-02**	**-17.646**	**5.58E-03**	5.362	7.22E-02
Glutathione S-transferase kappa 1	GSTK1	**2.606**	**3.40E-02**	**-4.392**	**3.06E-03**	**9.695**	**1.03E-04**	**-11.446**	**5.43E-05**	**3.720**	**6.56E-03**
Glutathione S-transferase Mu 2	GSTM2	1.080	7.42E-01	1.210	4.21E-01	-1.006	9.80E-01	1.120	6.28E-01	-1.086	7.23E-01
Glutathione S-transferase Mu 3	GSTM3	1.419	4.74E-01	1.983	1.74E-01	2.512	7.56E-02	1.397	4.94E-01	1.770	2.51E-01

Protein	Abbreviation	Prot. 1 normoxia vs. prot. 1 hypoxia		Protocol 1 normoxia vs hPH		Protocol 1 normoxia vs UD		Protocol 1 hypoxia vs. hPH		Protocol 1 hypoxia vs. UD	
		Fold change	p-value	Fold change	p-value	Fold change			Fold change	p-value	Fold change
Glutathione S-transferase omega-1	GSTO1	-1.070	8.64E-01	**-13.634**	**2.04E-05**	**12.248**	**3.05E-05**	**-12.744**	**2.62E-05**	**13.103**	**2.36E-05**
Glutathione S-transferase P	GSTP1	1.267	5.01E-01	**28.141**	**4.45E-07**	-1.912	8.13E-02	**22.217**	**9.75E-07**	**-2.422**	**2.33E-02**
Glutathione S-transferase theta-1	GSTT1	-1.468	4.76E-01	**-16.044**	**1.84E-04**	1.060	9.13E-01	**-10.929**	**6.34E-04**	1.556	4.14E-01
Microsomal glutathione S-transferase 1	MGST1	1.454	5.49E-01	**-20.702**	**3.11E-04**	1.711	3.93E-01	**-30.101**	**1.14E-04**	1.177	7.93E-01
Microsomal glutathione S-transferase 3	MGST3	1.224	6.19E-01	-1.419	3.95E-01	**2.696**	**2.79E-02**	-1.737	1.89E-01	2.202	6.99E-02
NAD(P)H dehydrogenase [quinone] 1	NQO1	-1.232	6.04E-01	2.333	5.18E-02	1.495	3.26E-01	**2.875**	**1.96E-02**	1.842	1.45E-01
Sulfotransferase 1A1	SULT1A1	1.759	1.04E-01	**-28.577**	**2.26E-07**	**8.818**	**1.98E-05**	**-50.280**	**4.05E-08**	**5.012**	**3.01E-04**
UDP-glucuronosyltransferase 1-4	UGT1A4	**-3.721**	**4.33E-02**	**-42.856**	**3.11E-05**	-1.315	6.47E-01	**-11.516**	**1.23E-03**	2.831	9.88E-02
UDP-glucuronosyltransferase 1-6	UGT1A6	1.202	5.84E-01	**-6.331**	**1.07E-04**	1.831	8.88E-02	**-7.609**	**4.47E-05**	1.523	2.22E-01
UDP-glucuronosyltransferase 1-9	UGT1A9	1.459	5.27E-01	**-9.609**	**2.09E-03**	-1.566	4.54E-01	**-14.015**	**6.59E-04**	-2.284	1.80E-01
UDP-glucuronosyltransferase 2B10	UGT2B10	-1.124	8.21E-01	**-112.038**	**7.18E-07**	**3.478**	**2.92E-02**	**-99.711**	**9.36E-07**	**3.908**	**1.90E-02**
UDP-glucuronosyltransferase 2B15	UGT2B15	-2.797	1.43E-01	**-14.765**	**1.46E-03**	1.290	7.04E-01	**-5.280**	**2.61E-02**	3.609	7.41E-02
UDP-glucuronosyltransferase 2B4	UGT2B4	-1.437	5.36E-01	**-66.492**	**8.55E-06**	2.399	1.50E-01	**-46.275**	**2.08E-05**	3.447	5.04E-02
UDP-glucuronosyltransferase 2B7	UGT2B7	-1.842	1.46E-01	**-41.178**	**6.53E-07**	**5.122**	**1.34E-03**	**-22.355**	**4.26E-06**	**9.434**	**9.79E-05**
ZONAL MARKERS											
Arginase-1	ARG1	-1.459	2.25E-01	**-85.243**	**3.76E-09**	**3.908**	**5.98E-04**	**-58.425**	**1.03E-08**	**5.702**	**7.36E-05**
Phosphoenolpyruvate carboxykinase [GTP], mitochondrial	PCK2	**-1.446**	**4.91E-02**	**-10.702**	**7.98E-09**	**6.486**	**1.14E-07**	**-7.403**	**5.34E-08**	**9.375**	**1.53E-08**
Phosphoenolpyruvate carboxykinase, cytosolic [GTP]	PCK1	1.228	7.14E-01	**-38.139**	**2.35E-05**	**3.542**	**3.94E-02**	**-46.848**	**1.38E-05**	2.884	7.69E-02
Carbamoyl-phosphate synthase [ammonia], mitochondrial	CPS1	-1.022	7.06E-01	**-1.888**	**8.84E-08**	1.016	7.87E-01	**-1.848**	**1.29E-07**	1.038	5.20E-01

Protein	Abbreviation	Prot. 2 normoxia vs. prot. 2 hypoxia		Protocol 2 normoxia vs hPH		Protocol 2 normoxia vs UD		Protocol 2 hypoxia vs. hPH		Protocol 2 hypoxia vs. UD	
		Fold change	p-value	Fold change	p-value	Fold change	p-value	Fold change	p-value	Fold change	p-value
CYPs											
Cytochrome P450 1A2	CYP1A2	-1.360	4.88E-01	**-45.156**	**1.28E-06**	**4.378**	**4.89E-03**	**-33.212**	**3.07E-06**	**5.953**	**1.33E-03**
Cytochrome P450 2A6	CYP2D6	1.131	7.20E-01	**-24.582**	**5.67E-07**	**2.606**	**1.42E-02**	**-27.795**	**3.78E-07**	**2.305**	**2.80E-02**
Cytochrome P450 2C8	CYP3D6	1.225	5.53E-01	**-21.611**	**8.18E-07**	**5.971**	**1.65E-04**	**-26.469**	**4.13E-07**	**4.875**	**4.55E-04**
Cytochrome P450 2C9	CYP2C9	-1.221	4.93E-01	**-59.157**	**5.95E-09**	**5.445**	**6.20E-05**	**-48.449**	**1.05E-08**	**6.648**	**2.17E-05**
Cytochrome P450 2D6	CYP2D6	-1.067	8.75E-01	**-24.511**	**3.84E-06**	**3.631**	**7.39E-03**	**-22.977**	**4.73E-06**	**3.873**	**5.48E-03**
Cytochrome P450 2E1	CYP2E1	-1.590	8.36E-02	**-24.510**	**1.94E-08**	**2.840**	**1.13E-03**	**-15.417**	**1.11E-07**	**4.515**	**5.06E-05**
Cytochrome P450 2S1	CYP2S1	**-2.929**	**1.42E-02**	1.759	1.58E-01	**-7.943**	**1.31E-04**	**5.153**	**9.10E-04**	**-2.712**	**2.08E-02**
Cytochrome P450 3A4	CYP3A4	2.102	2.22E-01	**-60.808**	**1.22E-05**	**6.567**	**6.83E-03**	**-127.820**	**2.27E-06**	3.124	7.20E-02
Cytochrome P450 4A11	CYP4A11	-1.022	9.69E-01	**-42.855**	**1.49E-05**	**5.152**	**1.02E-02**	**-41.937**	**1.57E-05**	**5.265**	**9.49E-03**
TRANSPORTERS											
ATP-binding cassette sub-family A member 6	ABCA7	-3.415	1.38E-01	**-16.347**	**3.56E-03**	-2.027	3.79E-01	-4.787	6.57E-02	1.685	5.13E-01
ATP-binding cassette sub-family D member 1	ABCD1	1.162	6.95E-01	-1.644	2.10E-01	1.518	2.87E-01	-1.911	1.10E-01	1.306	4.90E-01
ATP-binding cassette sub-family D member 3	ABCD3	1.595	4.11E-01	-3.260	5.21E-02	**7.703**	**2.90E-03**	**-5.200**	**1.09E-02**	**4.829**	**1.40E-02**
ATP-binding cassette sub-family E member 1	ABCE1	1.380	3.94E-01	1.359	4.16E-01	-1.339	4.40E-01	-1.015	9.67E-01	-1.848	1.18E-01
ATP-binding cassette sub-family F member 1	ABCF1	-1.006	9.86E-01	**4.194**	**1.13E-03**	-2.032	5.74E-02	**4.220**	**1.09E-03**	-2.020	5.93E-02
ATP-binding cassette sub-family F member 3	ABCF3	1.759	1.47E-01	-1.415	3.60E-01	-1.166	6.81E-01	**-2.489**	**2.77E-02**	-2.051	7.21E-02
Calcium-binding mitochondrial carrier protein Aralar1	SLC25A12	**2.148**	**2.97E-02**	1.267	4.60E-01	**2.473**	**1.28E-02**	-1.696	1.14E-01	1.152	6.57E-01
Protein	**Abbreviation**	**Prot. 2 normoxia vs.**		**Protocol 2 normoxia**		**Protocol 2 normoxia**		**Protocol 2 hypoxia**		**Protocol 2 hypoxia**	

		prot. 2 hypoxia		vs hPH		vs UD		vs. hPH		vs. UD	
		Fold change	p-value	Fold change	p-value	Fold change	p-value	Fold change	p-value	Fold change	p-value
Calcium-binding mitochondrial carrier protein Aralar2	SLC25A13	1.776	1.53E-01	**-7.919**	**1.36E-04**	1.199	6.39E-01	**-14.063**	**1.38E-05**	-1.482	3.17E-01
Calcium-binding mitochondrial carrier protein SCaMC-1	SLC25A24	-1.437	2.97E-01	**5.345**	**2.90E-04**	**5.026**	**3.96E-04**	**7.680**	**5.11E-05**	**7.222**	**6.78E-05**
Equilibrative nucleoside transporter 1	ENT1	**-3.467**	**1.14E-02**	-1.958	1.33E-01	**-10.600**	**1.05E-04**	1.770	1.96E-01	**-3.057**	**2.00E-02**
Major vault protein	MVP	1.518	4.65E-01	2.083	2.10E-01	**3.641**	**3.77E-02**	1.372	5.78E-01	2.399	1.40E-01
Multidrug resistance-associated protein 1	ABCC1, MRP1	1.103	7.83E-01	**3.038**	**7.78E-03**	1.127	7.37E-01	**2.754**	**1.31E-02**	1.022	9.52E-01
Solute carrier family 2, facilitated glucose transporter member 1	GLUT1	**-2.583**	**8.44E-03**	**12.132**	**2.66E-06**	**3.123**	**2.64E-03**	**31.334**	**8.37E-08**	**8.066**	**1.60E-05**
Solute carrier family 2, facilitated glucose transporter member 2	GLUT2	-1.195	7.85E-01	**-9.787**	**3.82E-03**	2.638	1.54E-01	**-8.190**	**6.40E-03**	3.152	9.72E-02
Solute carrier family 2, facilitated glucose transporter member 3	GLUT3	**-9.206**	**2.48E-03**	**5.580**	**1.21E-02**	-1.225	7.34E-01	**51.367**	**2.01E-05**	**7.516**	**4.69E-03**
Voltage-dependent anion-selective channel protein 1	VDAC1	-1.240	5.00E-01	-1.556	1.77E-01	**4.018**	**7.17E-04**	-1.255	4.75E-01	**4.981**	**2.20E-04**
Voltage-dependent anion-selective channel protein 2	VDAC2	-1.131	6.23E-01	**4.181**	**7.59E-05**	**2.481**	**2.88E-03**	**4.728**	**3.53E-05**	**2.806**	**1.16E-03**
Voltage-dependent anion-selective channel protein 3	VDAC3	1.290	1.90E-01	1.206	3.27E-01	1.450	6.54E-02	-1.070	7.19E-01	1.124	5.36E-01
PHASE II											
Catalase	CAT	1.134	7.18E-01	-40.932	**1.37E-07**	1.561	2.15E-01	-46.417	**9.47E-08**	1.376	3.66E-01
Catechol O-methyltransferase	COMT	-1.195	6.47E-01	-6.386	**3.67E-04**	8.551	**1.04E-04**	-5.346	**8.22E-04**	**10.215**	**5.02E-05**
Glutathione S-transferase A2	GSTA2	-2.235	3.64E-01	-100.628	**1.57E-04**	-1.064	9.44E-01	-45.015	**7.68E-04**	2.102	4.00E-01
Glutathione S-transferase kappa 1	GSTK1	1.060	8.87E-01	-3.698	**6.74E-03**	11.514	**5.31E-05**	-3.920	**5.16E-03**	**10.864**	**6.63E-05**
Glutathione S-transferase Mu 2	GSTM2	2.256	**3.87E-03**	1.905	**1.53E-02**	1.566	7.29E-02	-1.184	4.73E-01	-1.441	1.35E-01
Protein	**Abbreviation**	**Prot. 2 normoxia vs. prot. 2 hypoxia**		**Protocol 2 normoxia vs hPH**		**Protocol 2 normoxia vs UD**		**Protocol 2 hypoxia vs. hPH**		**Protocol 2 hypoxia vs. UD**	

		Fold change	p-value	Fold change	p-value	Fold change			Fold change	p-value	Fold change
Glutathione S-transferase Mu 3	GSTM3	-1.086	8.64E-01	3.362	**2.50E-02**	4.259	**9.90E-03**	3.653	**1.81E-02**	**4.627**	**7.15E-03**
Glutathione S-transferase omega-1	GSTO1	-1.791	1.58E-01	-43.112	**4.82E-07**	3.873	**4.38E-03**	-24.066	**2.84E-06**	**6.939**	**3.06E-04**
Glutathione S-transferase P	GSTP1	1.566	2.13E-01	31.824	**3.01E-07**	-1.691	1.49E-01	20.326	**1.33E-06**	**-2.647**	**1.44E-02**
Glutathione S-transferase theta-1	GSTT1	-1.057	9.18E-01	**-16.695**	**1.63E-04**	1.019	9.72E-01	**-15.799**	**1.93E-04**	1.077	8.90E-01
Microsomal glutathione S-transferase 1	MGST1	-2.215	2.14E-01	**-54.109**	**2.61E-05**	-1.527	4.98E-01	**-24.431**	**1.98E-04**	1.450	5.51E-01
Microsomal glutathione S-transferase 3	MGST3	-1.206	6.45E-01	-1.675	2.18E-01	2.284	5.94E-02	-1.389	4.24E-01	**2.755**	**2.52E-02**
NAD(P)H dehydrogenase [quinone] 1	NQO1	1.251	5.78E-01	-1.314	4.99E-01	-2.051	9.19E-02	-1.645	2.29E-01	**-2.567**	**3.33E-02**
Sulfotransferase 1A1	SULT1A1	**2.038**	**4.68E-02**	**-45.995**	**5.24E-08**	**5.479**	**1.91E-04**	**-93.747**	**7.68E-09**	**2.688**	**9.59E-03**
UDP-glucuronosyltransferase 1-4	UGT1A4	1.318	6.43E-01	**-19.350**	**2.64E-04**	1.685	3.87E-01	**-25.509**	**1.22E-04**	1.278	6.81E-01
UDP-glucuronosyltransferase 1-6	UGT1A6	1.259	4.94E-01	**-6.349**	**1.05E-04**	1.825	9.01E-02	**-7.993**	**3.57E-05**	1.450	2.77E-01
UDP-glucuronosyltransferase 1-9	UGT1A9	-1.073	9.05E-01	**-11.732**	**1.13E-03**	-1.912	2.85E-01	**-10.929**	**1.40E-03**	-1.781	3.39E-01
UDP-glucuronosyltransferase 2B10	UGT2B10	-1.259	6.56E-01	**-74.015**	**1.89E-06**	**5.265**	**6.35E-03**	**-58.797**	**3.34E-06**	**6.627**	**2.74E-03**
UDP-glucuronosyltransferase 2B15	UGT2B15	-1.619	4.77E-01	**-22.556**	**4.73E-04**	-1.184	8.01E-01	**-13.930**	**1.72E-03**	1.368	6.42E-01
UDP-glucuronosyltransferase 2B4	UGT2B4	-1.294	6.59E-01	**-126.278**	**2.00E-06**	1.263	6.89E-01	**-97.595**	**3.53E-06**	1.634	4.05E-01
UDP-glucuronosyltransferase 2B7	UGT2B7	-2.122	7.99E-02	**-74.020**	**1.34E-07**	**2.849**	**2.07E-02**	**-34.887**	**1.06E-06**	**6.045**	**6.37E-04**
ZONAL MARKERS											
Arginase-1	ARG1	-1.331	3.53E-01	**-100.626**	**2.47E-09**	**3.311**	**1.61E-03**	**-75.630**	**5.13E-09**	**4.405**	**3.00E-04**
Phosphoenolpyruvate carboxykinase [GTP], mitochondrial	PCK2	1.151	4.19E-01	**-45.580**	**3.18E-11**	**1.523**	**2.80E-02**	**-52.483**	**2.07E-11**	1.322	1.23E-01
Phosphoenolpyruvate carboxykinase, cytosolic [GTP]	PCK1	-1.819	2.96E-01	**-47.714**	**1.32E-05**	2.831	8.15E-02	**-26.227**	**6.53E-05**	**5.151**	**1.12E-02**
Carbamoyl-phosphate synthase [ammonia], mitochondrial	CPS1	-1.006	9.15E-01	**-1.888**	**8.85E-08**	1.016	7.86E-01	**-1.877**	**9.84E-08**	1.022	7.06E-01

Appendix 1

Fold changes and associated significance in liver-related proteins from iTRAQ analysis of iPSC-HLCs differentiated under hypoxia or normoxia using two protocols - Names and abbreviations used for the proteins in Figure 9-14 divided into four categories: CYPs, transporters, phase II metabolism, and zonal markers. Five comparisons are made per differentiation protocol, where normoxia and hypoxia are compared against undifferentiated cells (UD), primary human hepatocytes (hPH) and one another. Fold changes are presented as a decimal where positive values indicate higher expression in the first comparator listed. Significance was calculated by ANOVA using Partek, p-values ≤ 0.05 were considered significant and are highlighted with the associated fold change in **bold**.

Cell line	Gene	Protocol	Oxygen condition	Mean fold change	Standard deviation	p-value vs. P1N	p-value vs. P1H	p-value vs. P2N
Liv6HB	FOXA2	1	Normoxia	563.9139	639.8217			
		1	Hypoxia	355.0282	76.8648	0.6920		
		2	Normoxia	2.0774	2.3652	0.1287	**0.0004**	
		2	Hypoxia	0.2185	0.3090	0.2017	**0.0031**	0.2424
	VEGFA	1	Normoxia	2.3019	0.9515			
		1	Hypoxia	1.6932	0.9714	0.5477		
		2	Normoxia	1.5295	1.2518	0.4211	0.8752	
		2	Hypoxia	1.1675	0.6459	0.1305	0.4285	0.6381
	HNF4α	1	Normoxia	356.9566	334.8480			
		1	Hypoxia	151.9462	38.2181	0.4729		
		2	Normoxia	9.6668	13.9270	0.0848	**0.0019**	
		2	Hypoxia	0.5043	0.7131	0.1394	**0.0049**	0.3438
	NRF2	1	Normoxia	3.8815	2.4596			
		1	Hypoxia	2.1201	2.3858	0.4748		
		2	Normoxia	2.7233	0.8545	0.3967	0.6323	
		2	Hypoxia	3.1936	2.5521	0.5626	0.7524	0.9701
	ALDOA	1	Normoxia	1.2729	0.3701			
		1	Hypoxia	1.1883	0.5841	0.8813		
		2	Normoxia	1.1243	0.3042	0.5385	0.7768	
		2	Hypoxia	1.3064	0.0737	0.8899	0.7663	0.3189
	HSF1	1	Normoxia	1.2168	0.1278			
		1	Hypoxia	0.6156	0.4284	0.0843		
		2	Normoxia	0.9405	0.2208	0.1540	0.2436	
		2	Hypoxia	1.0420	0.9203	0.5032	0.6338	0.8967
	HIF1A	1	Normoxia	2.7960	2.2310			
		1	Hypoxia	0.7890	0.4685	0.3250		
		2	Normoxia	2.1204	0.7995	0.5940	0.0958	
		2	Hypoxia	3.3960	2.6304	0.9863	0.3191	0.6024
	CTNNB1	1	Normoxia	0.9564	0.2432			
		1	Hypoxia	0.7188	0.1429	0.2782		
		2	Normoxia	0.6493	0.1942	0.0936	0.6530	
		2	Hypoxia	1.0209	0.9664	0.7427	0.8755	0.6751
	NANOG	1	Normoxia	1.0036	0.7977			
		1	Hypoxia	8.8407	8.7569	0.1907		
		2	Normoxia	0.0789	0.0180	0.0616	0.0820	
		2	Hypoxia	0.0411	0.0542	0.1035	0.1524	0.1010
Liv6HE	FOXA2	1	Normoxia	0.0655	0.0749			
		1	Hypoxia	0.0000	0.0000	0.1993		
		2	Normoxia	0.0009	0.0015	0.2044	0.3739	
		2	Hypoxia	0.0000	0.0001	0.1996	0.2174	0.3965
	VEGFA	1	Normoxia	0.5651	0.3365			
		1	Hypoxia	0.3877	0.6683	0.6597		
		2	Normoxia	0.1461	0.0473	0.0908	0.5661	
		2	Hypoxia	0.2788	0.0510	0.2129	0.7923	**0.0299**
	HNF4α	1	Normoxia	0.5455	0.8330			
		1	Hypoxia	0.0000	0.0000	0.3187		
		2	Normoxia	0.0086	0.0106	0.3256	0.2328	

		2	Hypoxia	0.0013	0.0014	0.3197	0.1747	0.3031
	NRF2	1	Normoxia	2.5857	0.9937			
		1	Hypoxia	0.0914	0.1582	**0.0084**		
		2	Normoxia	1.6901	0.3225	0.2009	**0.0015**	
		2	Hypoxia	0.8547	0.0248	**0.0321**	**0.0012**	**0.0110**
	ALDOA	1	Normoxia	0.9082	0.0931			
		1	Hypoxia	0.3399	0.5846	0.1052		
		2	Normoxia	0.5703	0.2169	**0.0356**	0.5570	
		2	Hypoxia	0.7428	0.2124	0.2149	0.3246	0.3805
	HSF1	1	Normoxia	1.4670	0.5243			
		1	Hypoxia	0.0563	0.0975	**0.0064**		
		2	Normoxia	0.5480	0.1156	**0.0332**	**0.0049**	
		2	Hypoxia	0.4277	0.0884	**0.0210**	**0.0081**	0.2254
	HIF1A	1	Normoxia	4.1888	2.2250			
		1	Hypoxia	0.1590	0.2753	**0.0286**		
		2	Normoxia	2.7443	2.4232	0.4495	0.1402	
		2	Hypoxia	1.4611	0.8603	0.1051	0.0670	0.4362
	CTNNB1	1	Normoxia	1.4882	0.4662			
		1	Hypoxia	0.0453	0.0785	**0.0035**		
		2	Normoxia	0.6209	0.2265	**0.0329**	**0.0142**	
		2	Hypoxia	0.3689	0.1163	**0.0106**	**0.0162**	0.1617
	NANOG	1	Normoxia	0.0487	0.0402			
		1	Hypoxia	0.7029	-	-		
		2	Normoxia	0.0355	0.0044	0.6051	-	
		2	Hypoxia	0.0136	0.0106	0.2084	-	**0.0292**
Liv7HE	FOXA2	1	Normoxia	10.1381	4.7647			
		1	Hypoxia	2.6917	4.4598	0.0868		
		2	Normoxia	0.6433	0.4184	**0.0093**	0.3957	
		2	Hypoxia	0.2430	0.3557	**0.0230**	0.3969	0.2415
	VEGFA	1	Normoxia	1.9626	0.5496			
		1	Hypoxia	1.7756	1.1698	0.8109		
		2	Normoxia	0.6820	0.2057	**0.0071**	0.1151	
		2	Hypoxia	0.5208	0.1361	**0.0116**	0.1309	0.2964
	HNF4α	1	Normoxia	412.5284	140.4492			
		1	Hypoxia	69.4695	131.7341	**0.0210**		
		2	Normoxia	8.7222	5.3866	**0.0019**	0.3923	
		2	Hypoxia	5.8517	9.6762	**0.0075**	0.4522	0.6334
	NRF2	1	Normoxia	8.9561	1.7914			
		1	Hypoxia	5.9987	3.2793	0.2226		
		2	Normoxia	4.7386	0.4645	**0.0056**	0.4755	
		2	Hypoxia	4.8882	1.6411	**0.0441**	0.6189	0.8654
	ALDOA	1	Normoxia	0.8866	0.0893			
		1	Hypoxia	0.8862	0.0720	0.9948		
		2	Normoxia	0.8299	0.2898	0.7615	0.7193	
		2	Hypoxia	0.8924	0.1715	0.9612	0.9495	0.7562
	HSF1	1	Normoxia	1.6592	0.1667			
		1	Hypoxia	1.2868	0.4873	0.2685		
		2	Normoxia	0.9986	0.1949	**0.0054**	0.3142	
		2	Hypoxia	0.6915	0.1918	**0.0027**	0.1065	0.0925
	HIF1A	1	Normoxia	1.5240	0.4233			

		1	Hypoxia	1.1168	0.3019	0.1940		
		2	Normoxia	1.7470	0.2974	0.4461	**0.0248**	
		2	Hypoxia	2.0093	0.4945	0.2662	**0.0304**	0.4171
	CTNNB1	1	Normoxia	1.0623	0.2613			
		1	Hypoxia	0.8598	0.2369	0.3322		
		2	Normoxia	1.2743	0.1652	0.2415	**0.0284**	
		2	Hypoxia	1.1079	0.2724	0.8443	0.2534	0.3567
	NANOG	1	Normoxia	0.2540	0.1923			
		1	Hypoxia	1.4604	2.7443	0.4915		
		2	Normoxia	0.1470	0.1579	0.4535	0.3761	
		2	Hypoxia	0.0173	0.0140	0.1007	0.4148	0.2247

Appendix 2

Fold changes, error and associated significance in expression of liver and hypoxia related genes - Fold changes and associated error and significance for the genes in Figure 15 separated based in iPSC line. Fold change was calculated using the $2^{-\Delta\Delta CT}$ method (Livak and Schmittgen, 2001) versus line-matched normoxic iPSCs and using GAPDH as a control gene. Fold changes are presented as a decimal where values greater than 1 indicate higher expression in iPSC-HLCs. p-values were calculated using an unpaired, two-tailed Student's t-test and values ≤ 0.05 were considered significant and are highlighted in **bold**.

MS7N		
	Side	**Front**
06/12/2017	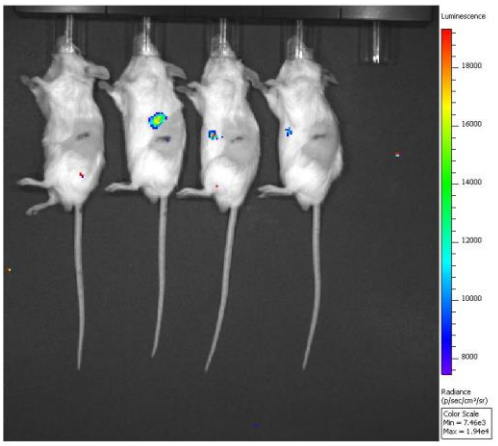	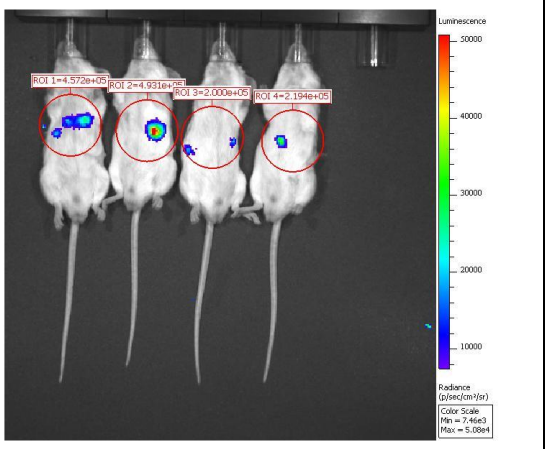
13/12/2017	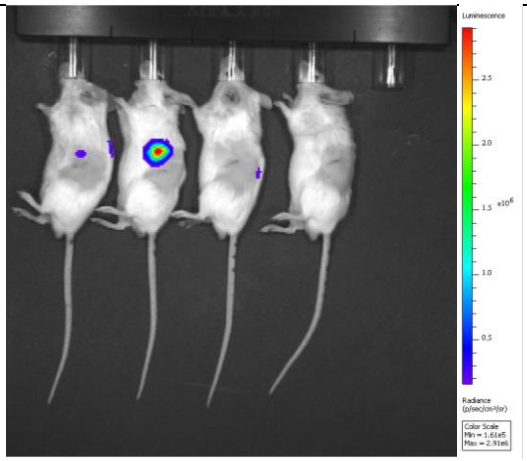	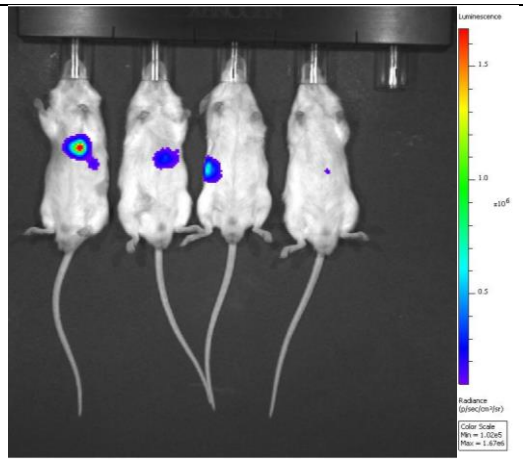
20/12/2017	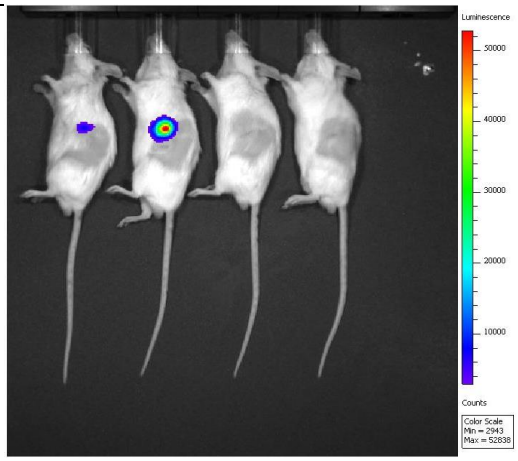	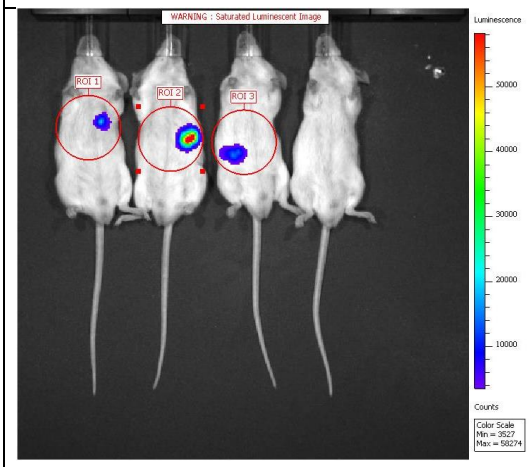

27/12/2017	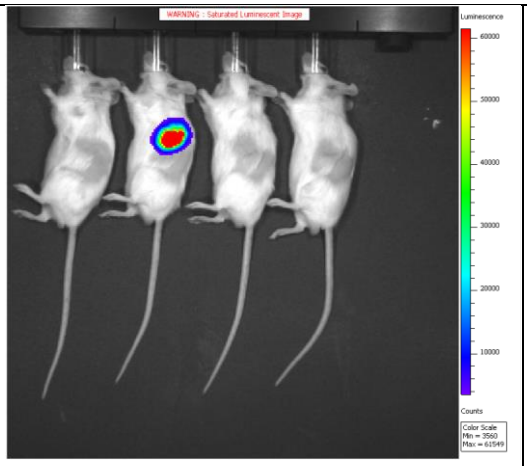	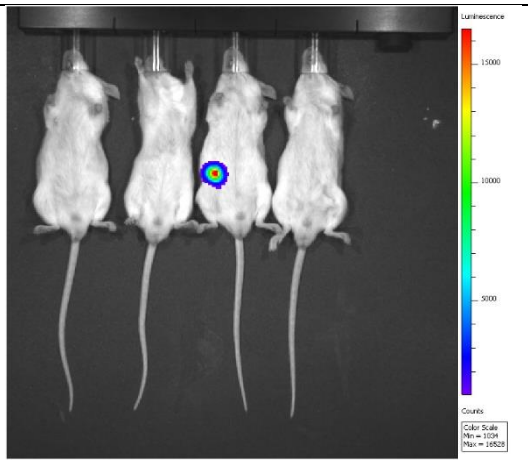

MS7CNV

	Side	Front
12/09/2017	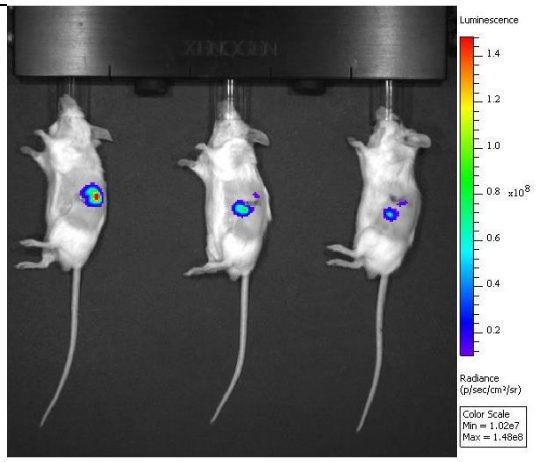	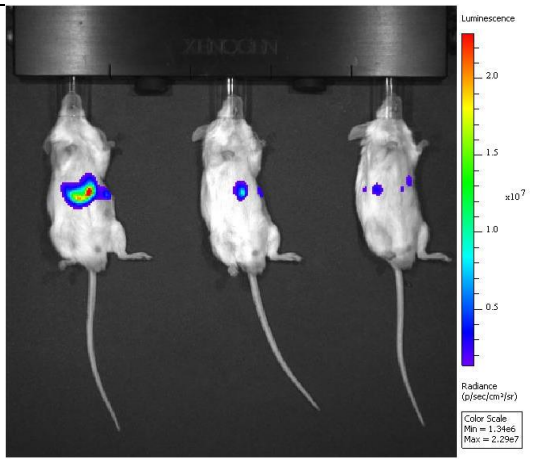
15/09/2017	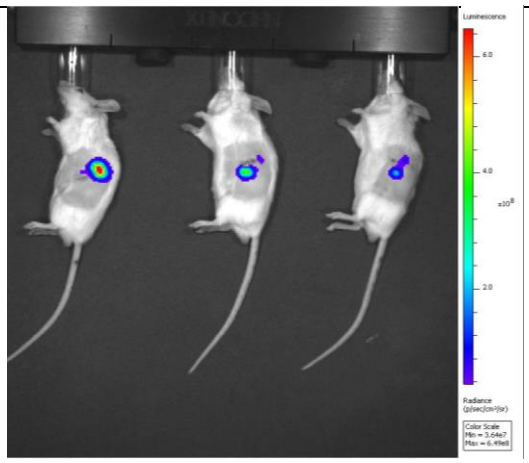	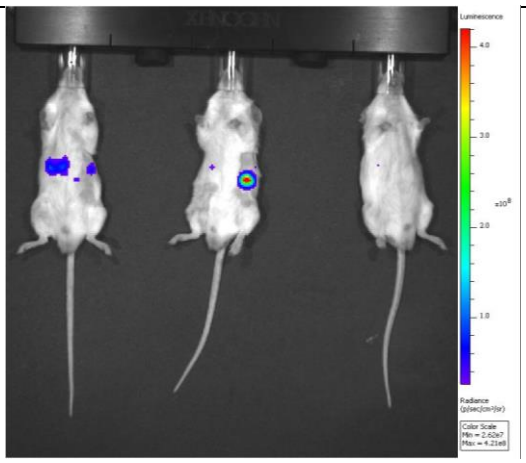

19/09/2017	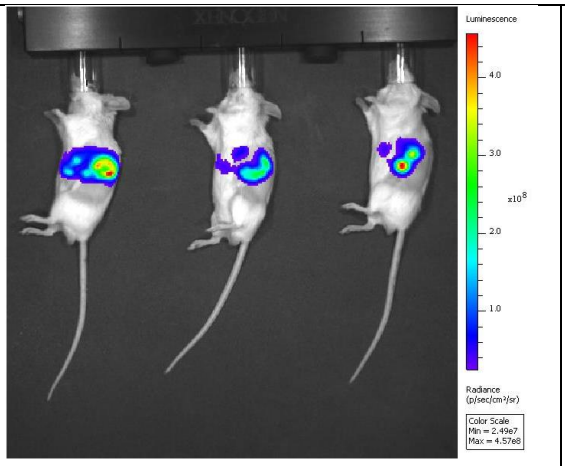	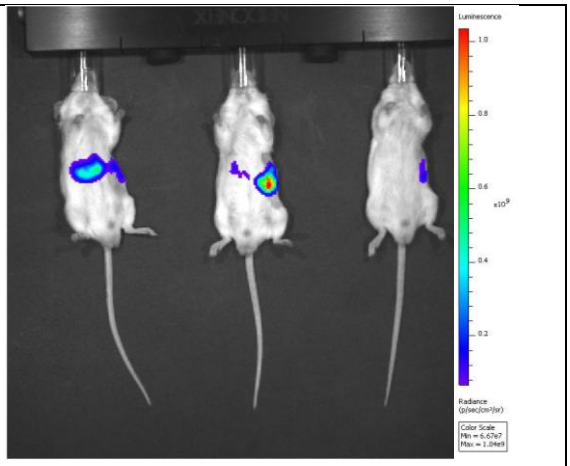
21/09/2017	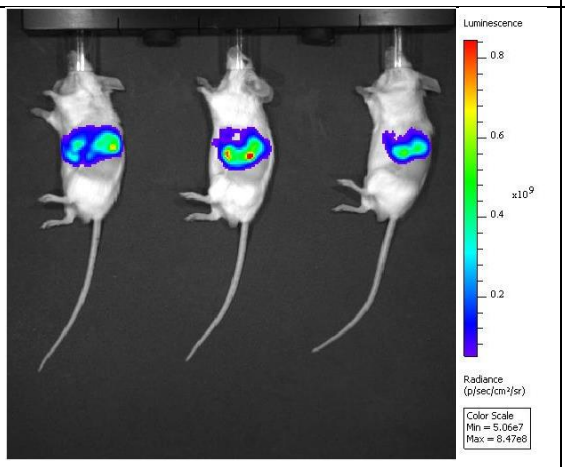	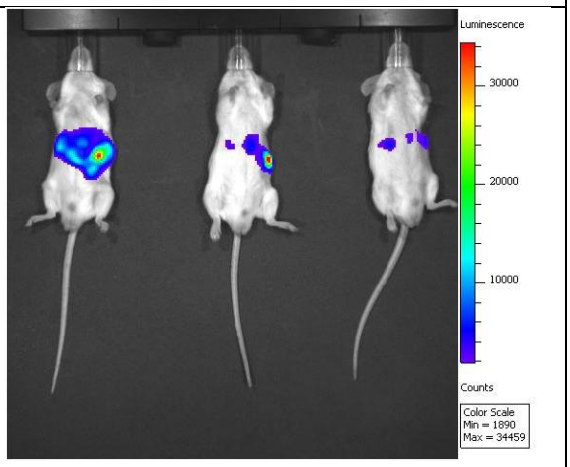
28/09/2017	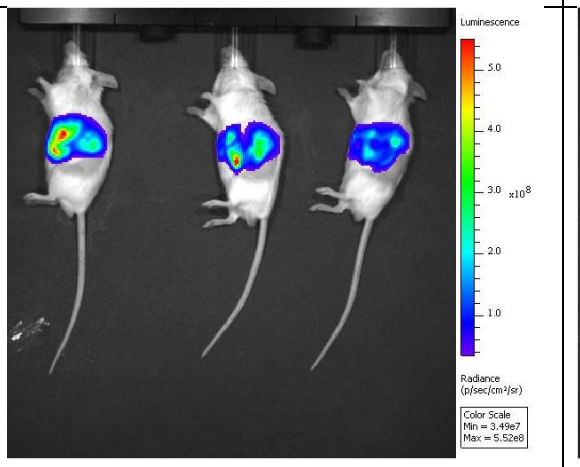	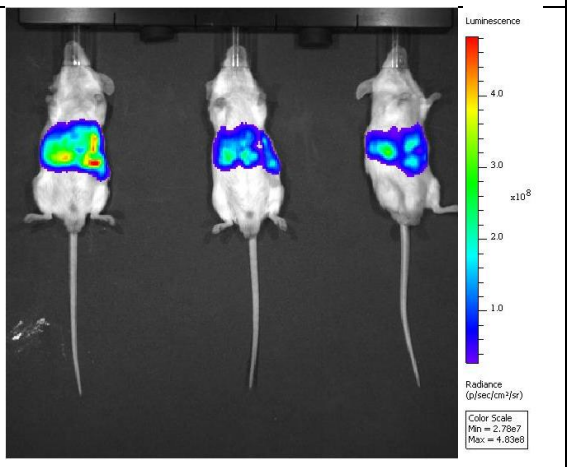

04/10/2017	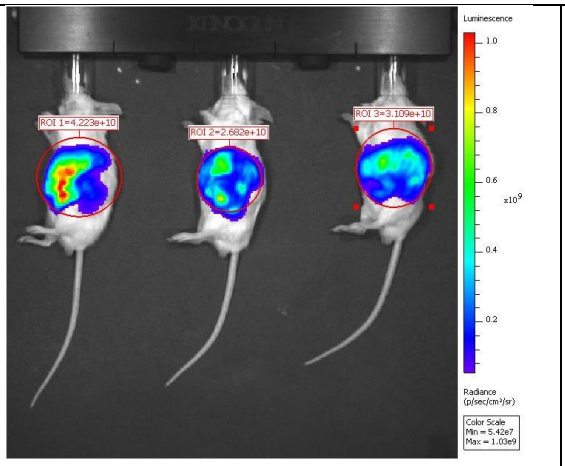	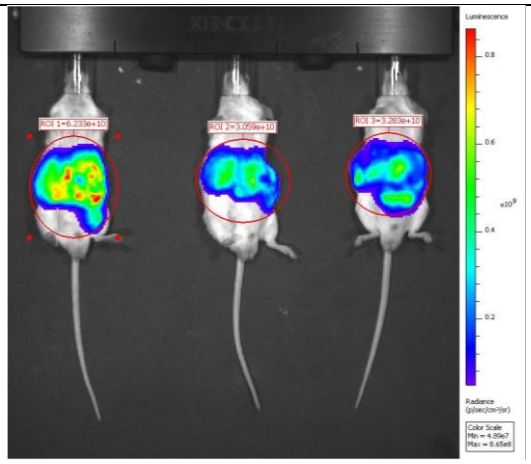

	MS8N	
	Side	Front
06/12/2017	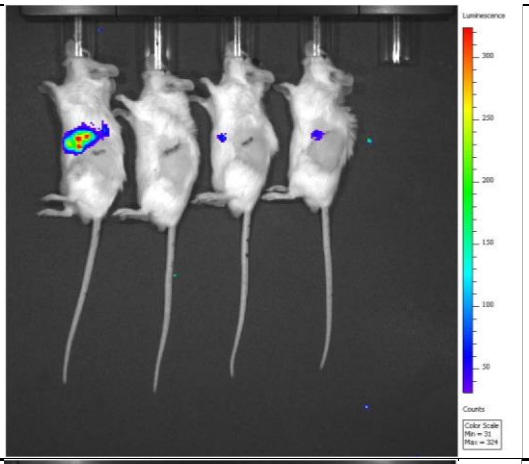	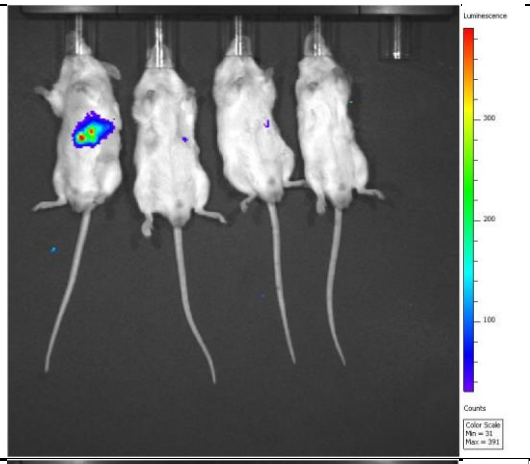
13/12/2017	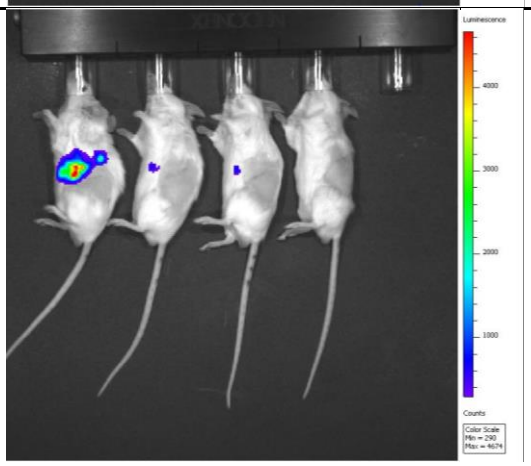	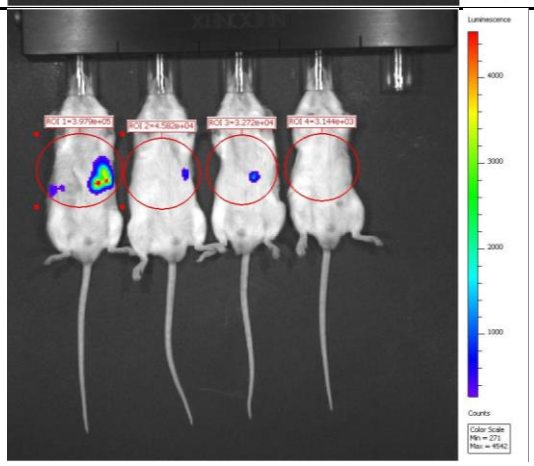

20/12/2017	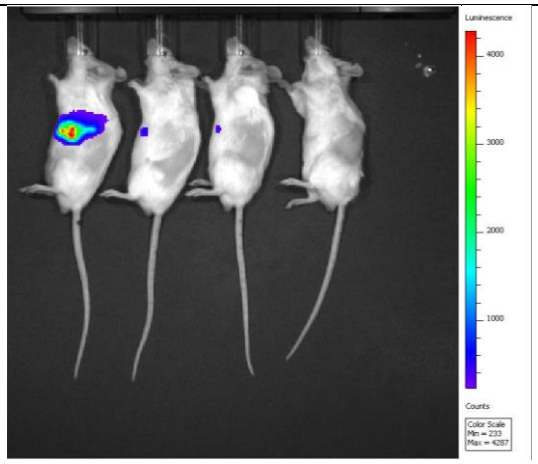	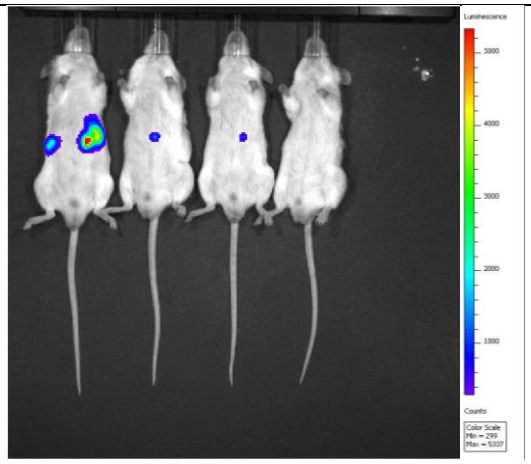
MS8Ab		
	Side	**Front**
06/12/2017	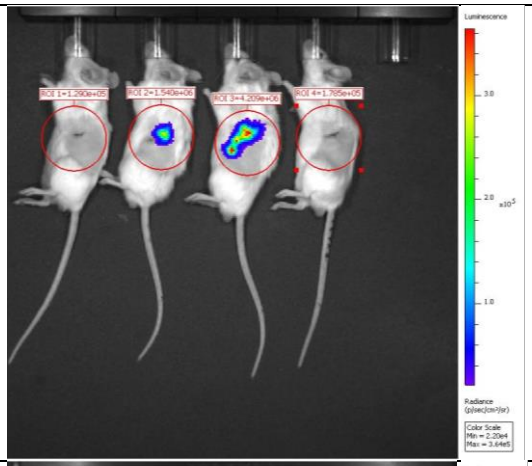	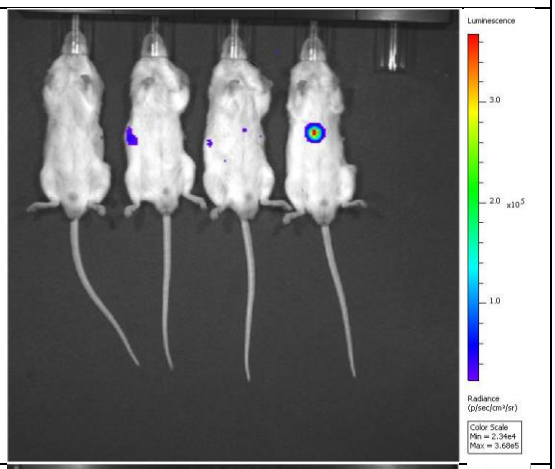
13/12/2017	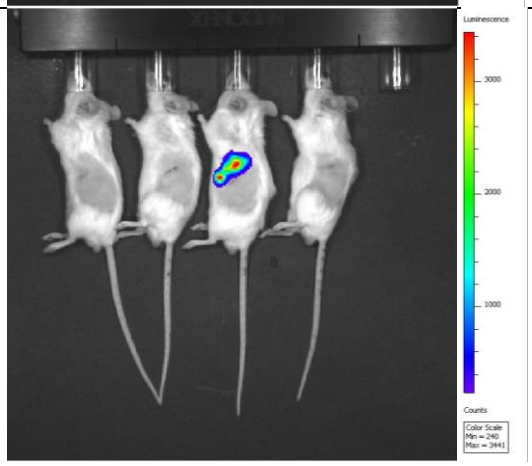	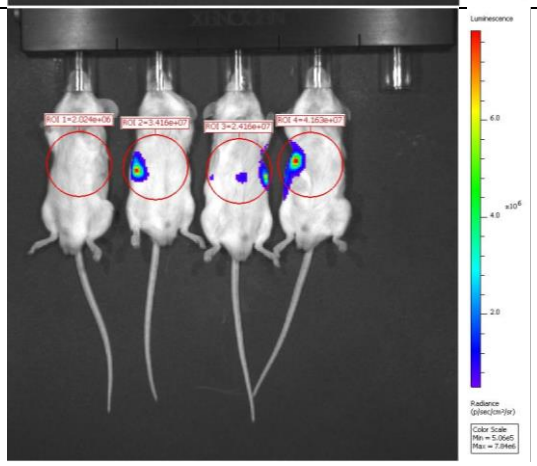

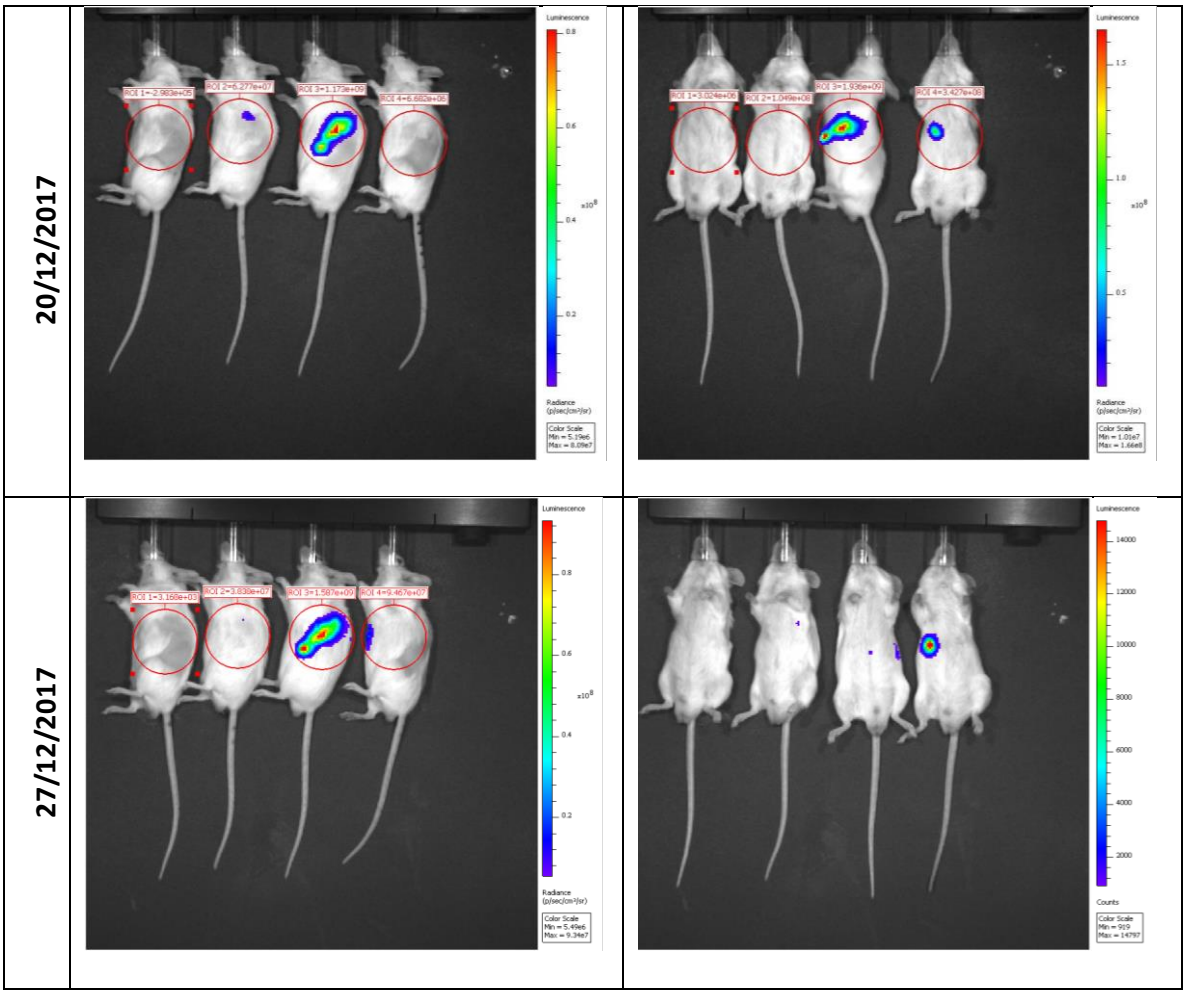

Supplementary Figure 1 - Representative bioluminescence images of SCID beige mice intrasplenically injected with undifferentiated luminescent hESCs – Animals were injected with 1 x10^6 undifferentiated luminescent hESCs 72-hours after induction of acute liver injury with 0.2mL/kg CCl_4. Each hESC line (i.e. MS7N, MS7CNV, MS8N and MS8AB) is shown individually. Images show luminescence over time from side and front elevations. Red circles show regions of interest used to determine luminescence intensity, in this case showing radiance (photons/second/cm^2/steradian), though total flux (photons/second) was also recorded and was used for later experiments. Luminescence intensity is represented by the coloured overlays with warmer colour indicating greater intensity. Each scale bar applies only to the image to its immediate left. The order of animals is consistent between images. Only values from the front elevation were used for subsequent analyses.

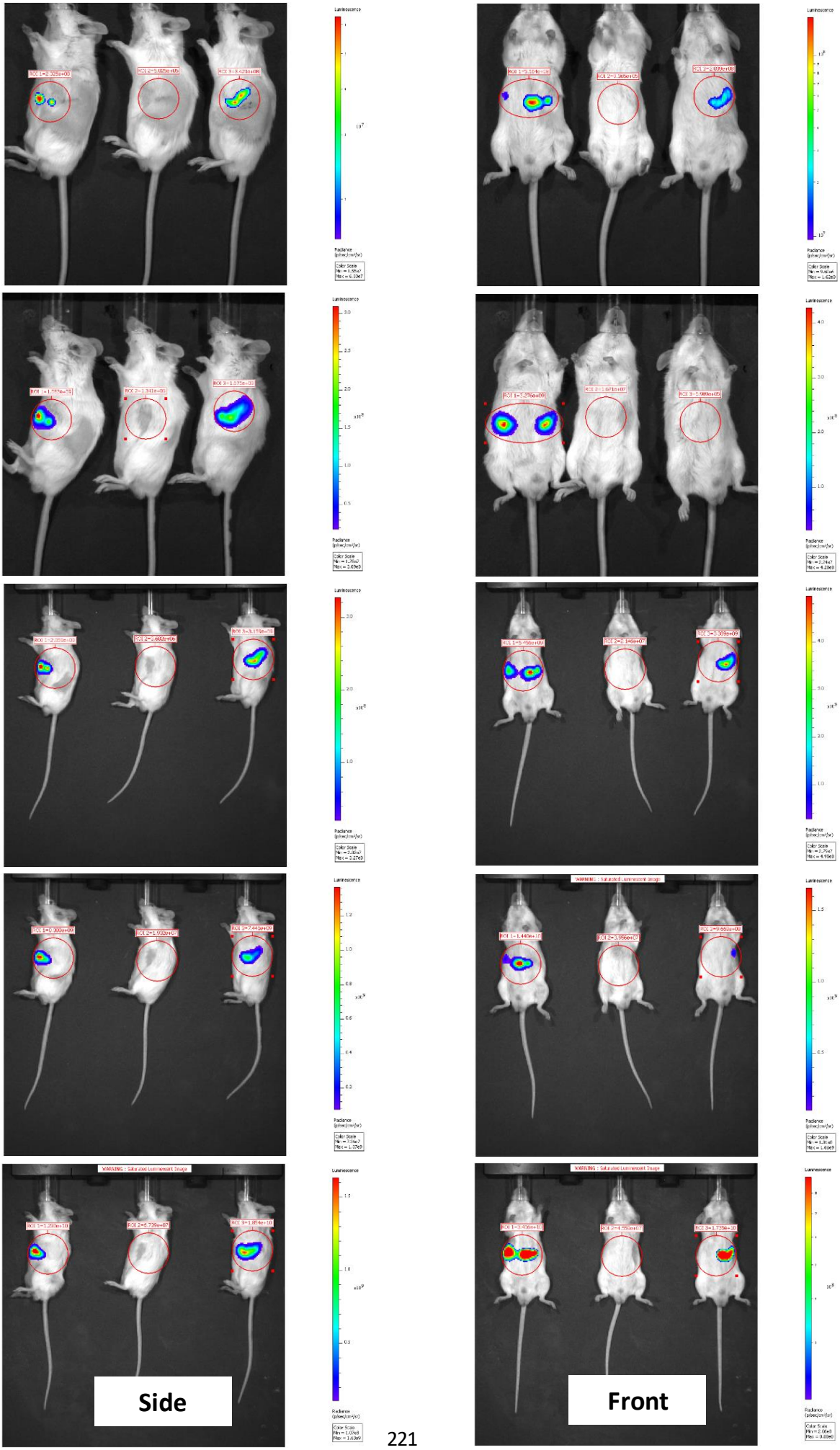
Side
Front

Supplementary Figure 2

Representative bioluminescence images of SCID beige mice intrasplenically injected with HepG2_Fluc – Animals were injected with 1 x10^6 luminescent HepG2 cells 72-hours after induction of acute liver injury with 0.2mL/kg CCl_4. Images show luminescence over time from side and front elevations. Red circles show regions of interest used to determine luminescence intensity, in this case showing radiance (photons/second/cm^2/steradian), though total flux (photons/second) was also recorded and was used for later experiments. Luminescence intensity is represented by the coloured overlays with warmer colour indicating greater intensity. Each scale bar applies only to the image to its immediate left. The order of animals is consistent between images. Only values from the front elevation were used for subsequent analyses.

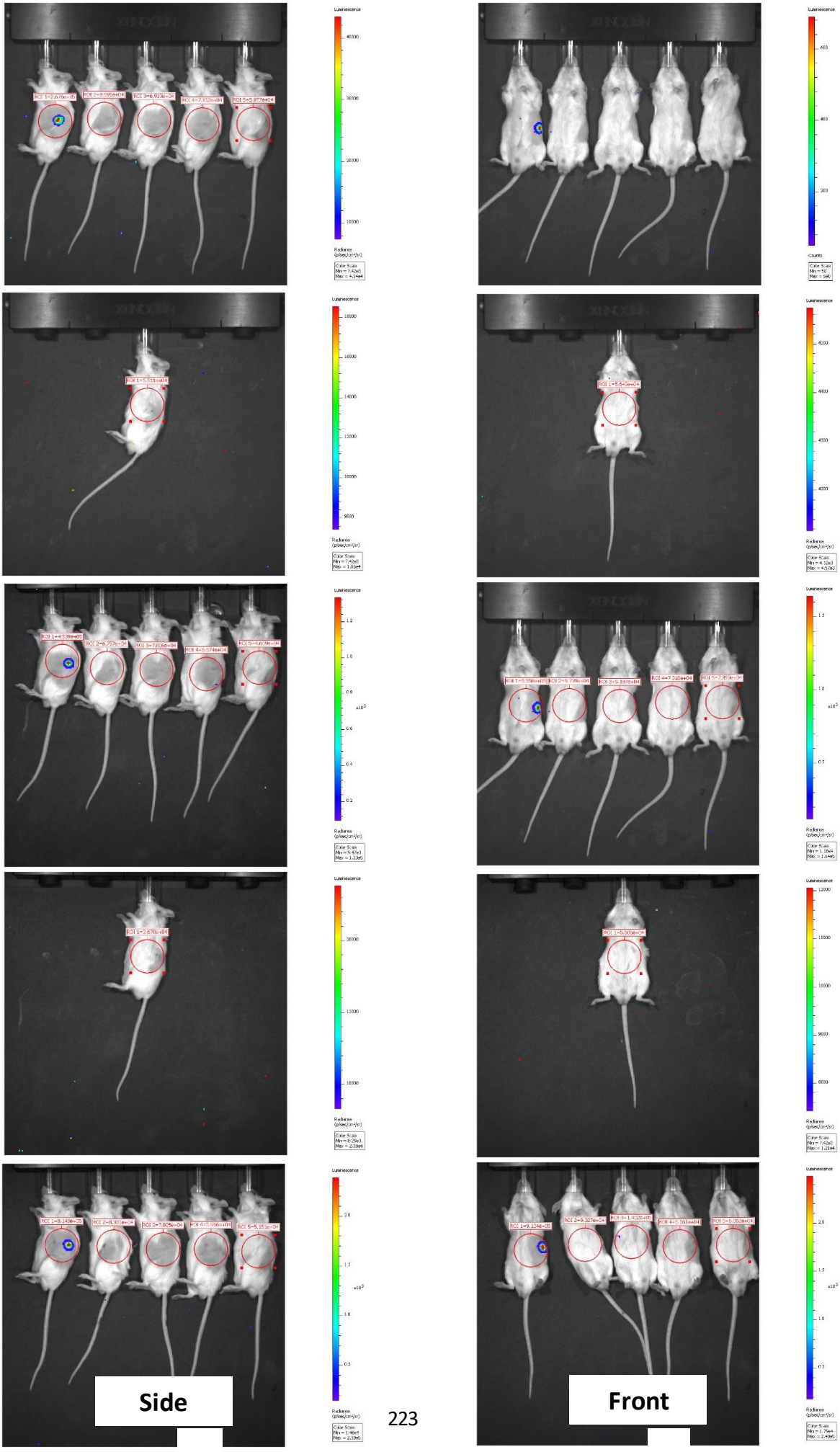
Side
Front

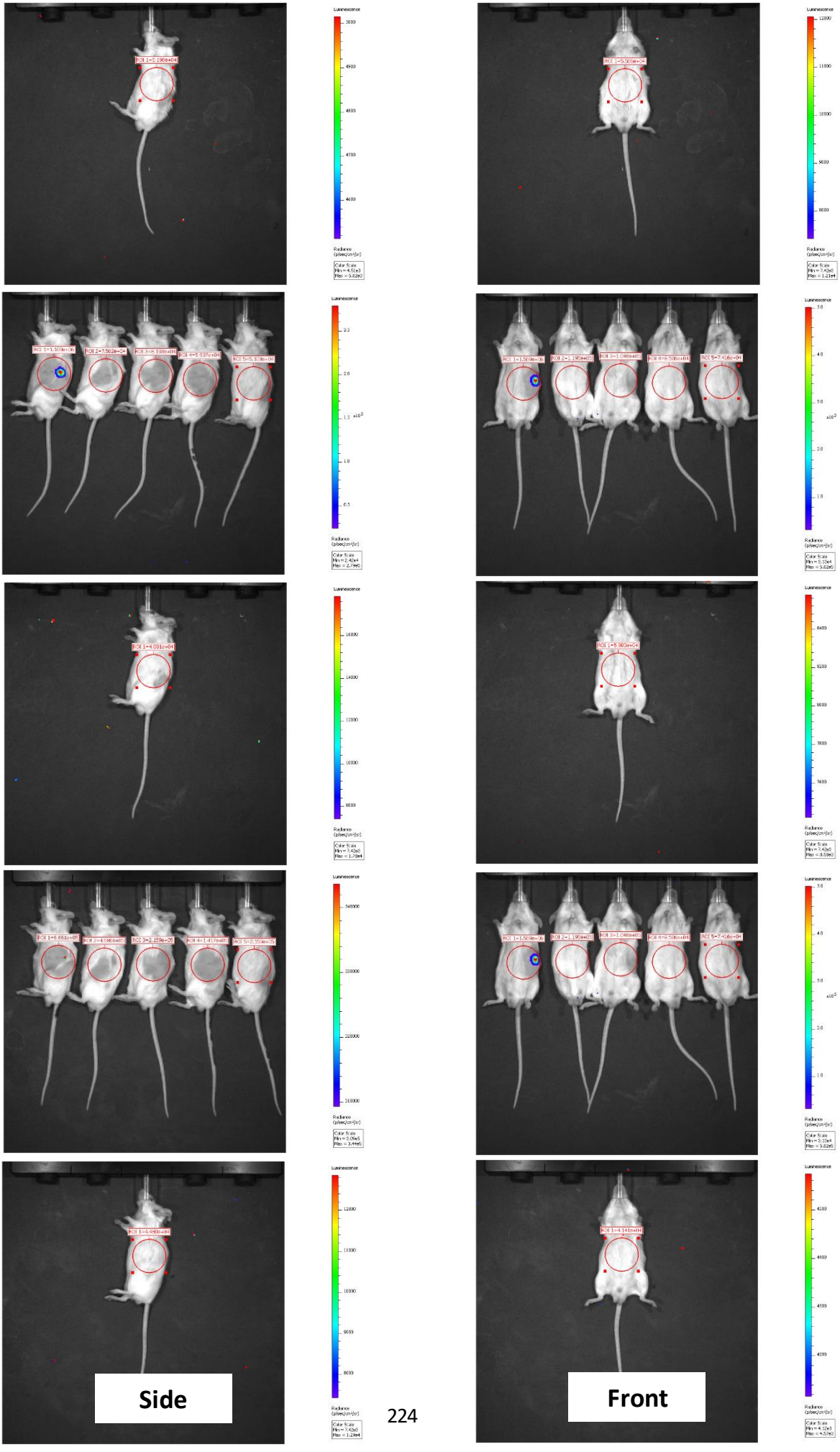
Side
Front

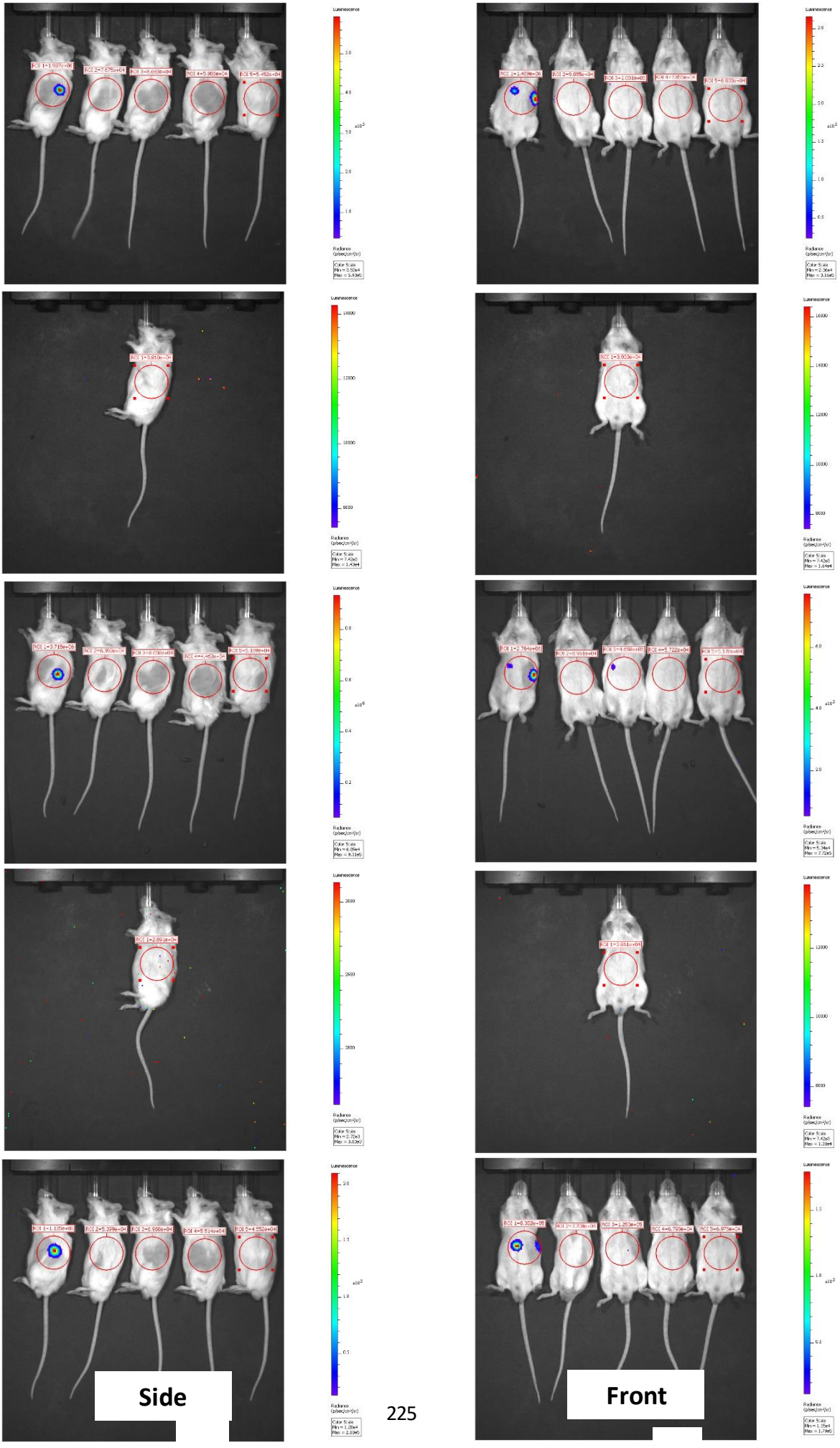
Side
Front

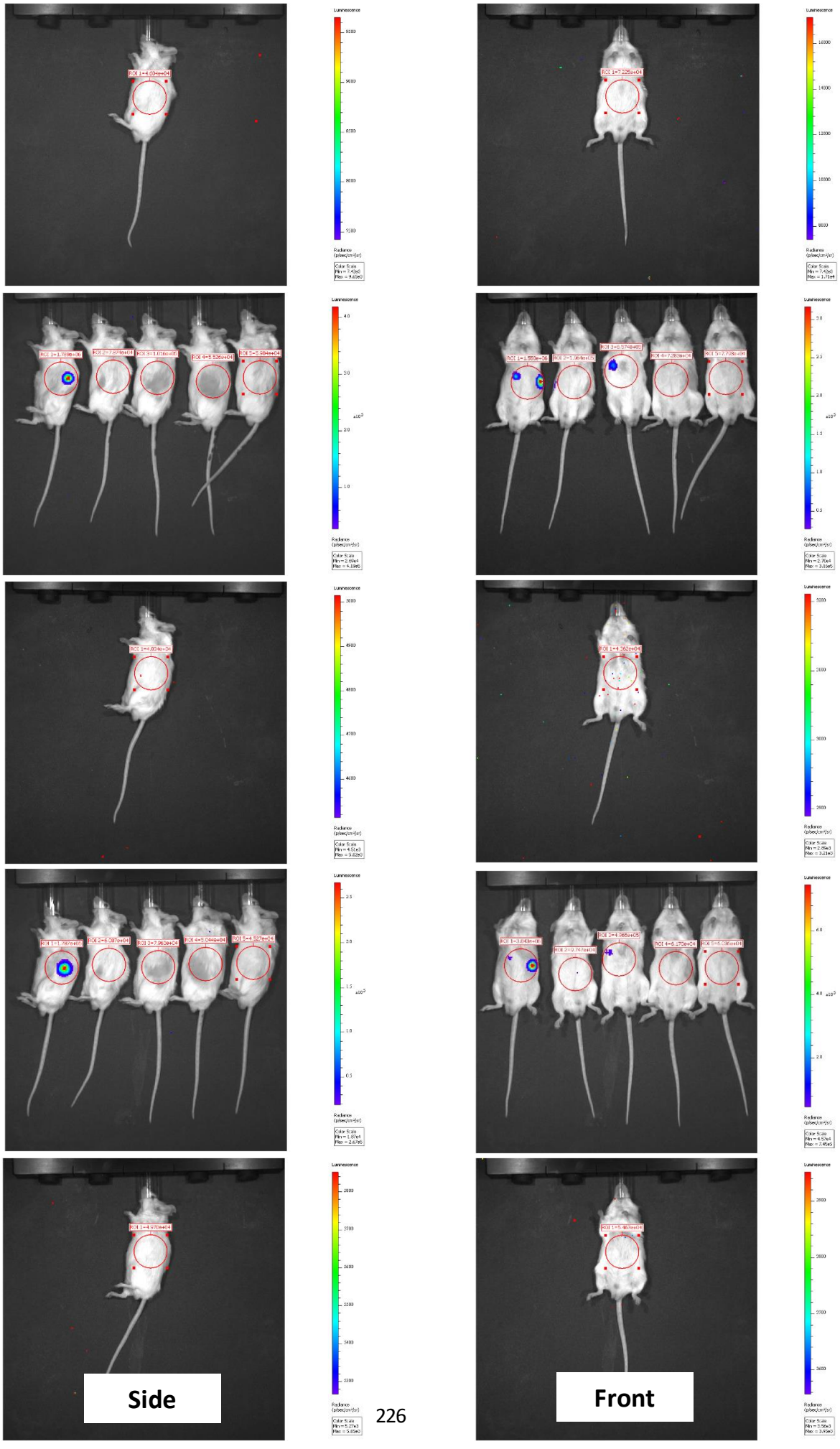
Side
Front

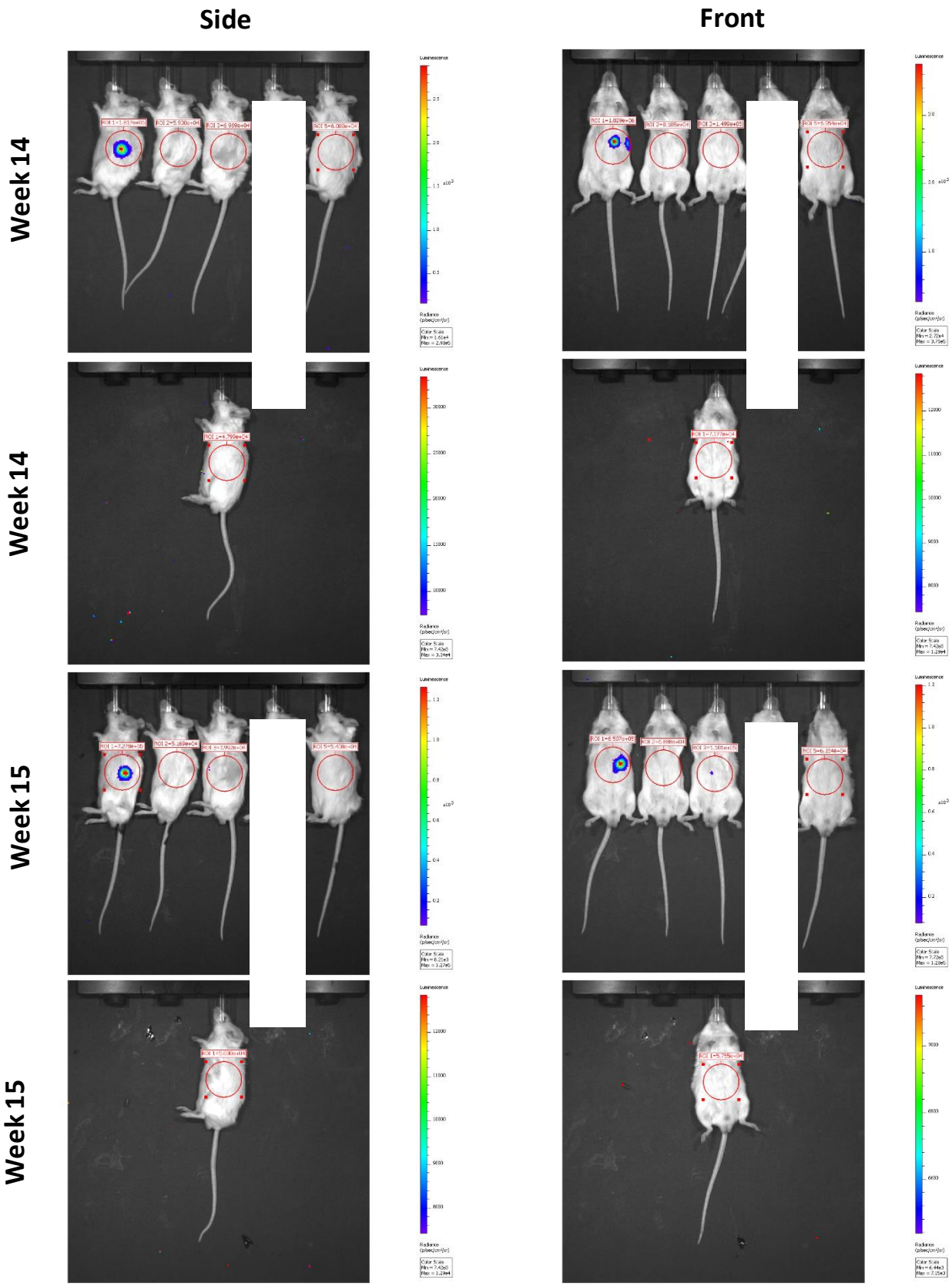

Supplementary Figure 3

Representative bioluminescence images of SCID beige mice intrasplenically injected with MS8Ab_D7 hESC-HLCs – Animals were injected with 1 x10^6 MS8Ab_D7 luminescent hESCs 72-hours after induction of acute liver injury with 0.2mL/kg CCl_4. Images show luminescence over time from side and front elevations. Red circles show regions of interest used to determine luminescence intensity, in this case showing radiance (photons/second/cm^2/steradian),

though total flux (photons/second) was also recorded and was used for later experiments. Luminescence intensity is represented by the coloured overlays with warmer colour indicating greater intensity. Each scale bar applies only to the image to its immediate left. The order of animals is consistent between images some animals were excluded due to thymic lymphoma discovered at the end of the experiment and are covered by white boxes. Only values from the front elevation were used for subsequent analyses.

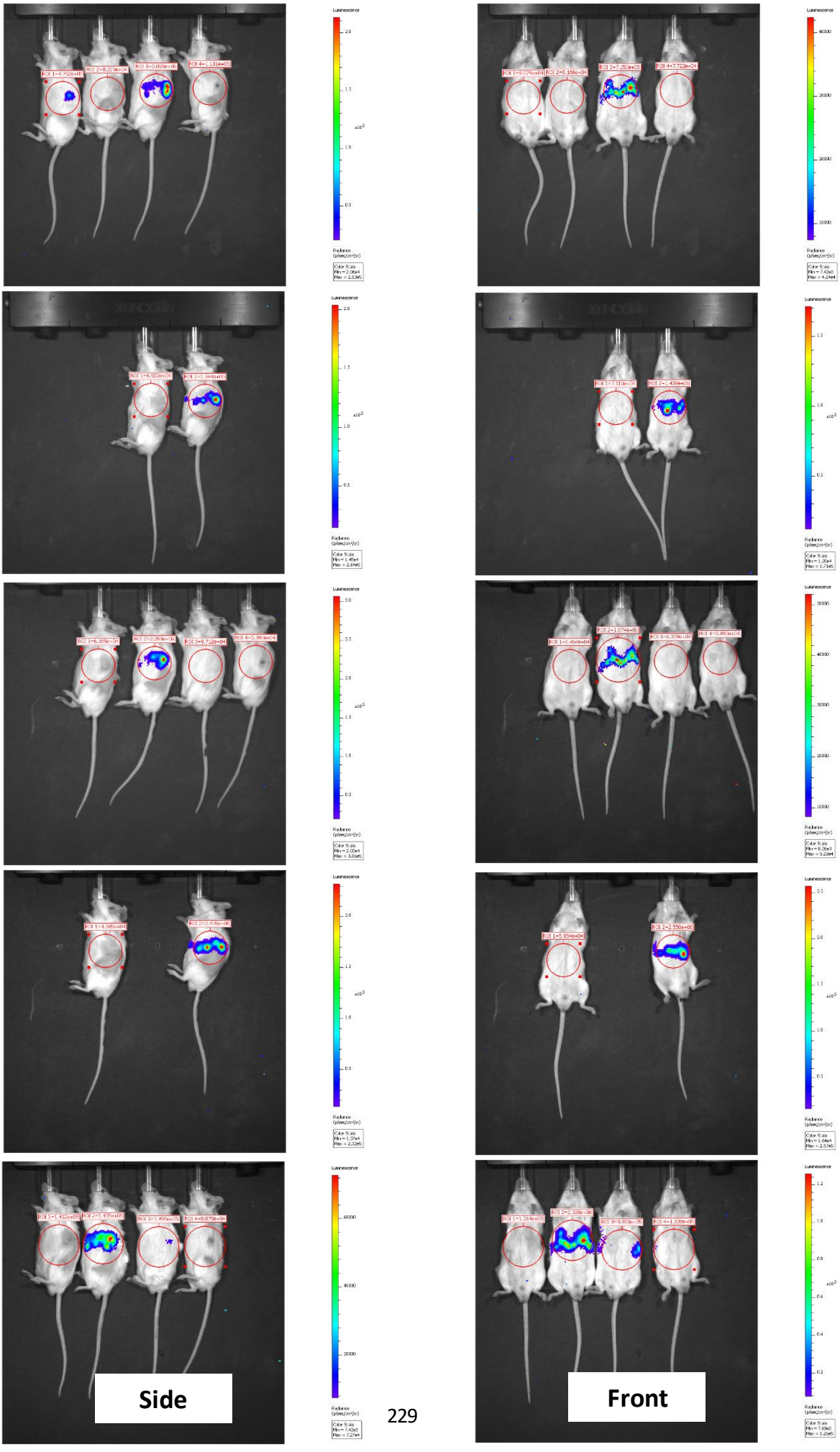
Side
Front

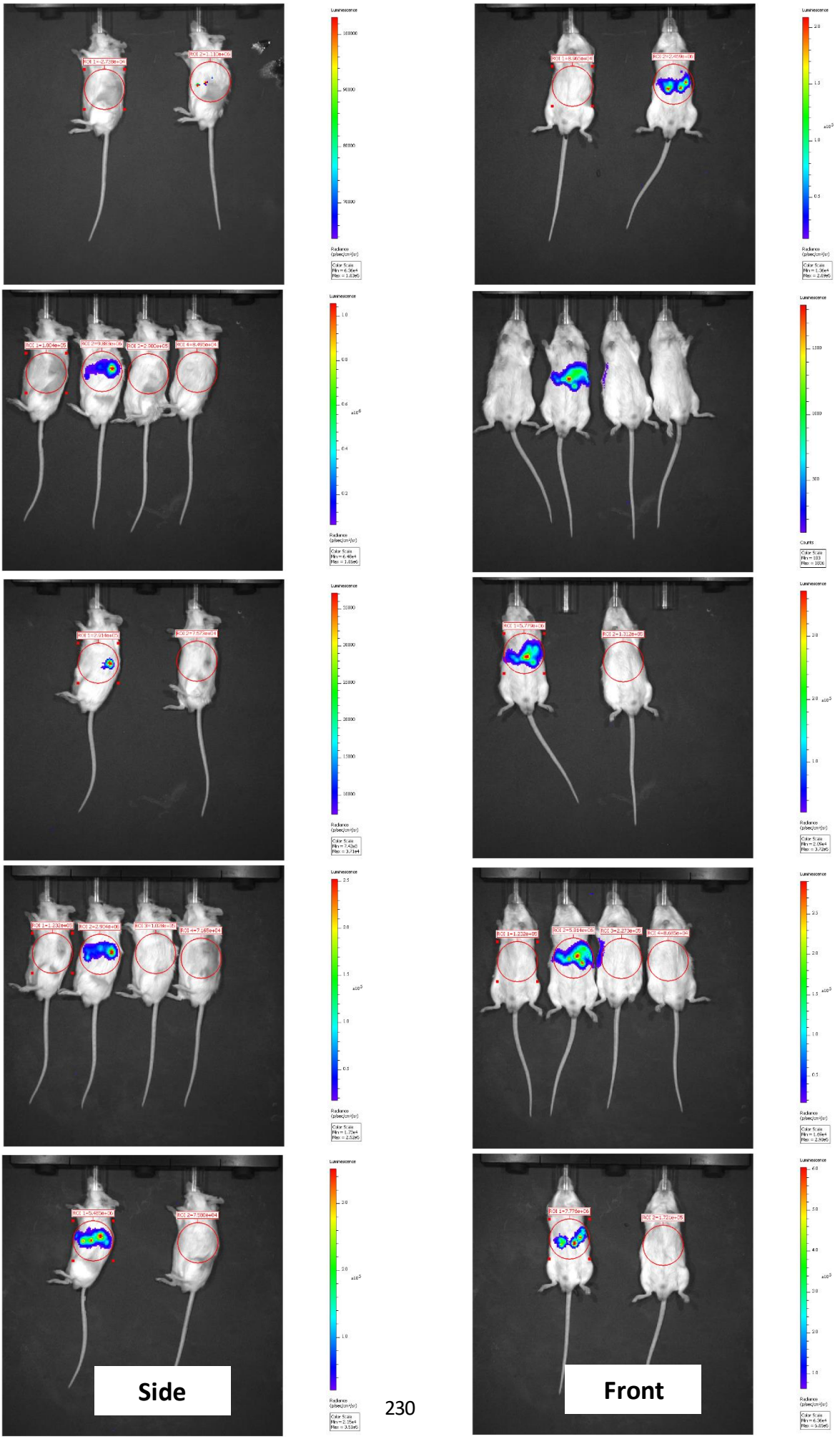
Side
Front

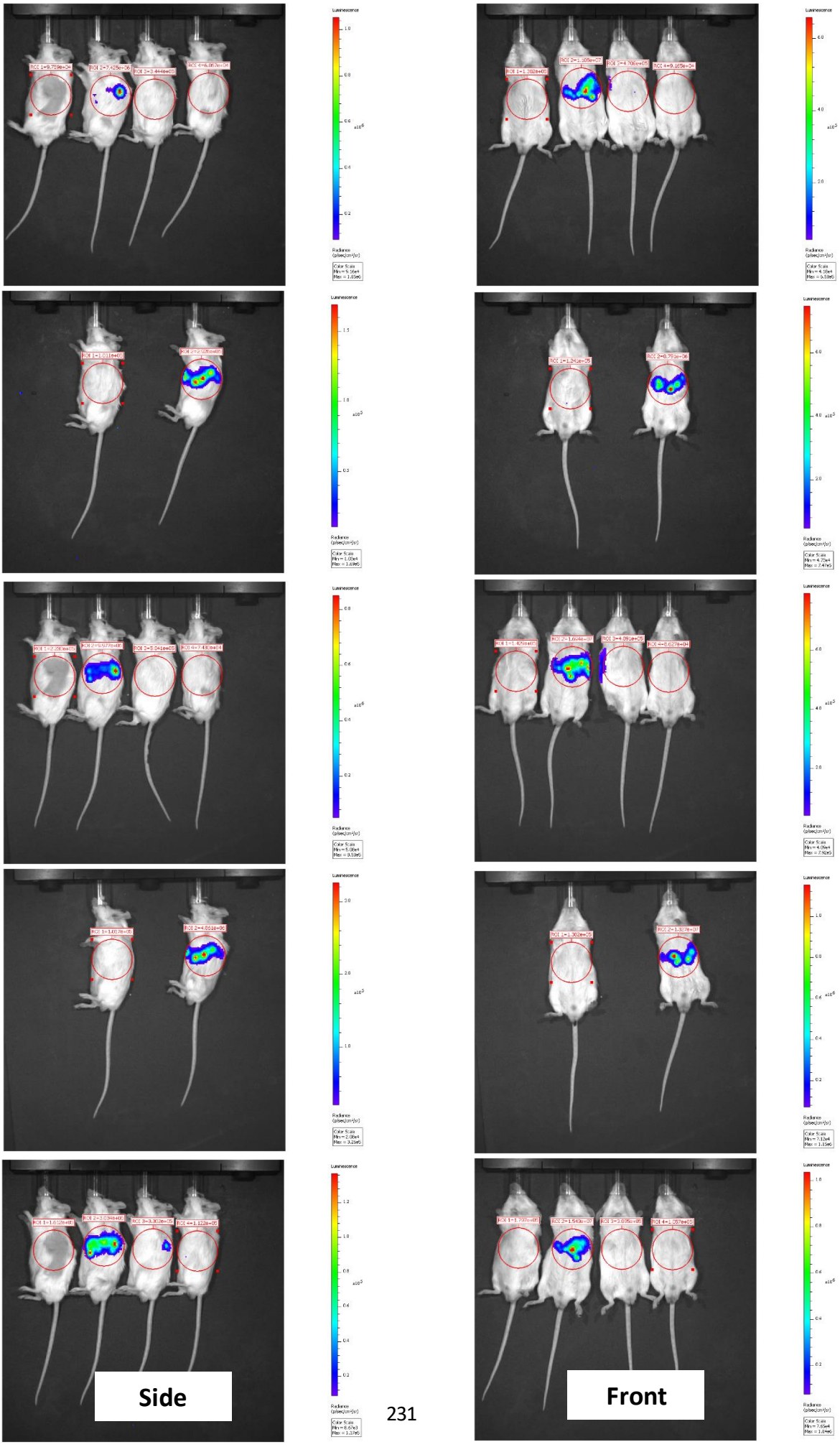
Side
Front

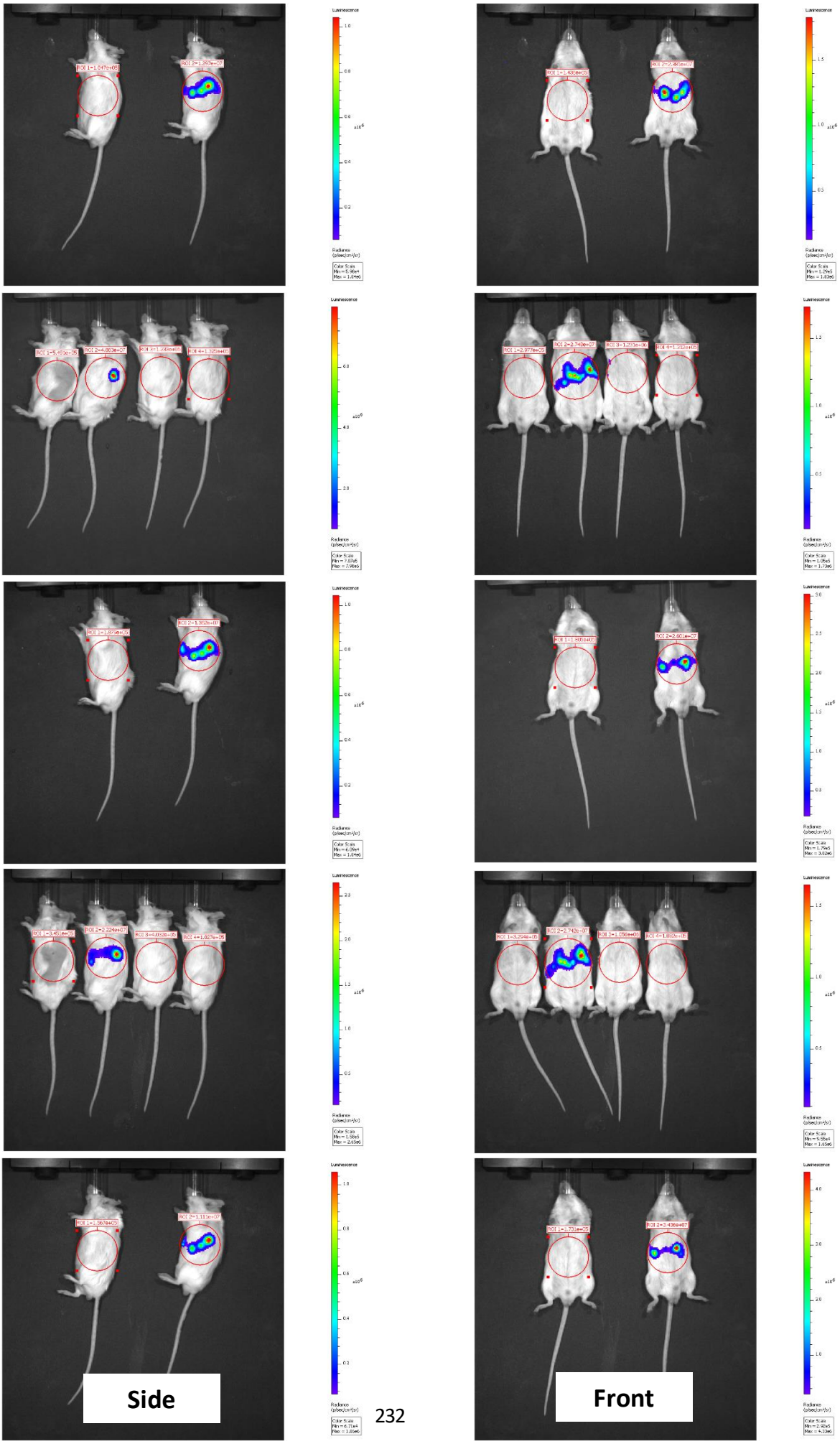
Side
Front

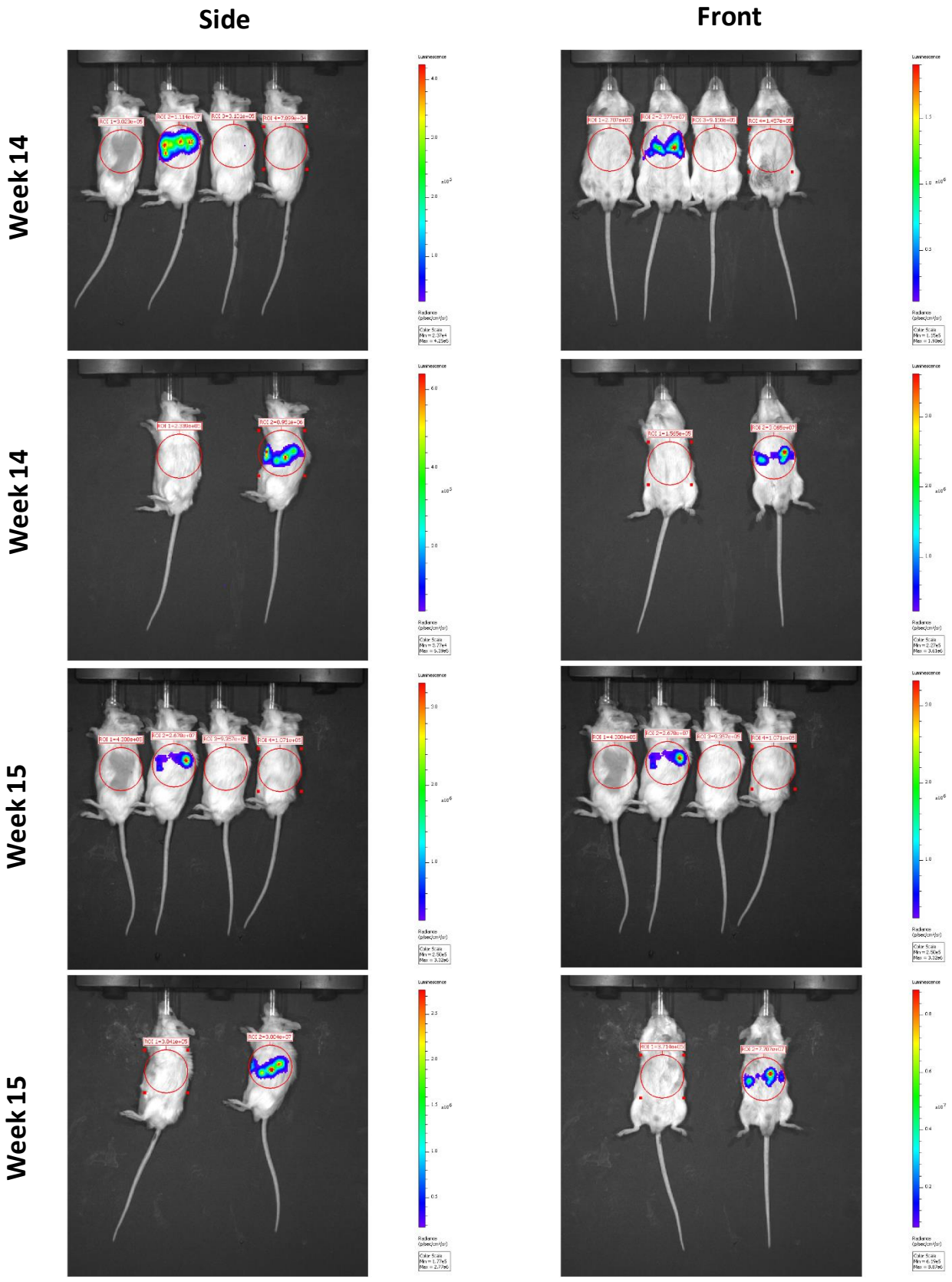

Supplementary Figure 4

Representative bioluminescence images of SCID beige mice intrasplenically injected with MS8Ab_G7 hESC-HLCs – Animals were injected with 1 x10^6 MS8Ab_G7 luminescent hESCs 72-hours after induction of acute liver injury with 0.2mL/kg CCl_4. Images show luminescence over time from side and front elevations. Red circles show regions of interest used to determine luminescence intensity, in this case showing radiance (photons/second/cm^2/steradian),

though total flux (photons/second) was also recorded and was used for later experiments. Luminescence intensity is represented by the coloured overlays with warmer colour indicating greater intensity. Each scale bar applies only to the image to its immediate left. The order of animals is consistent between images, after week 6, order of the animals in the second row (two animals) is reversed. Only values from the front elevation were used for subsequent analyses.

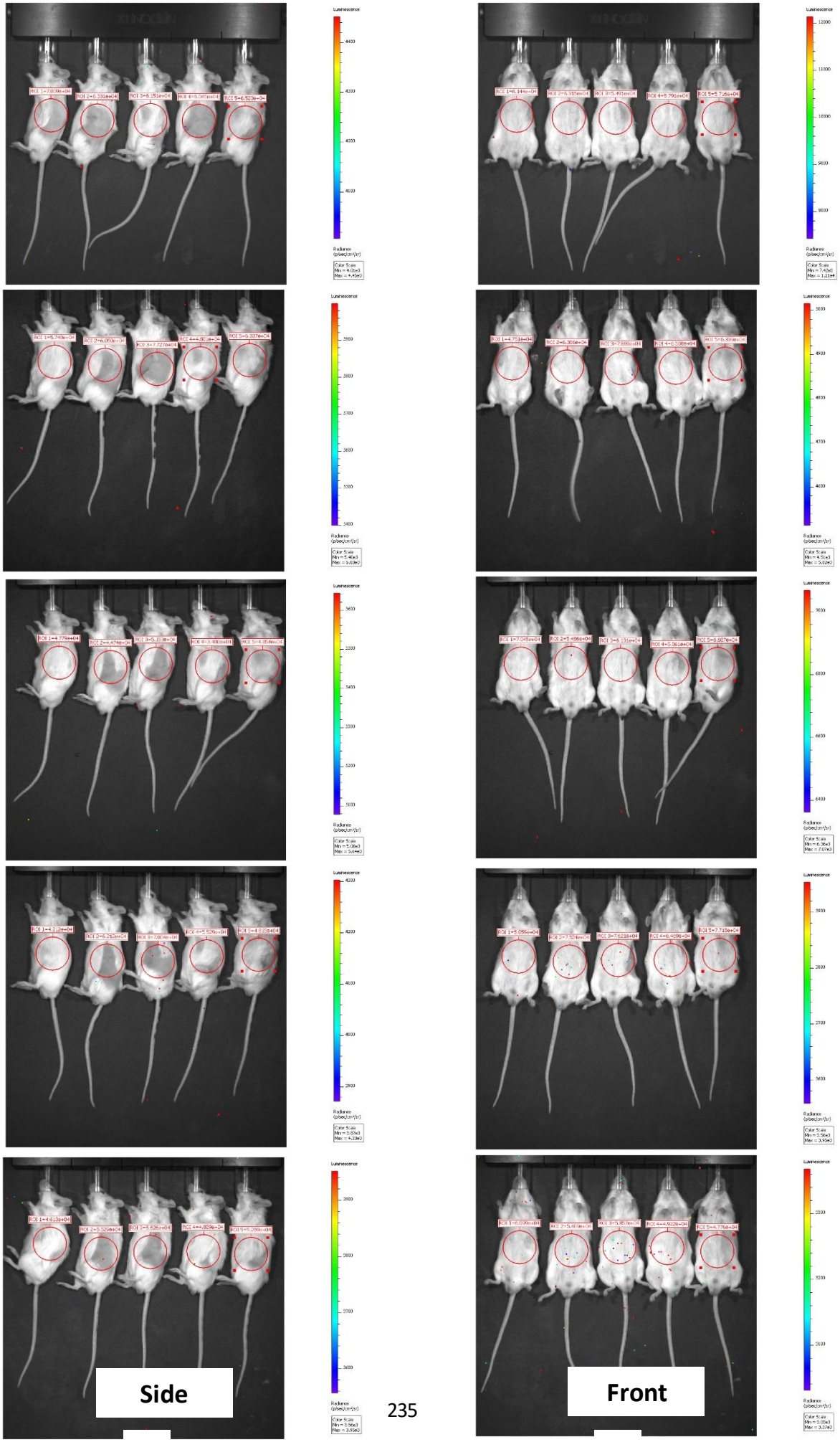
Side
Front

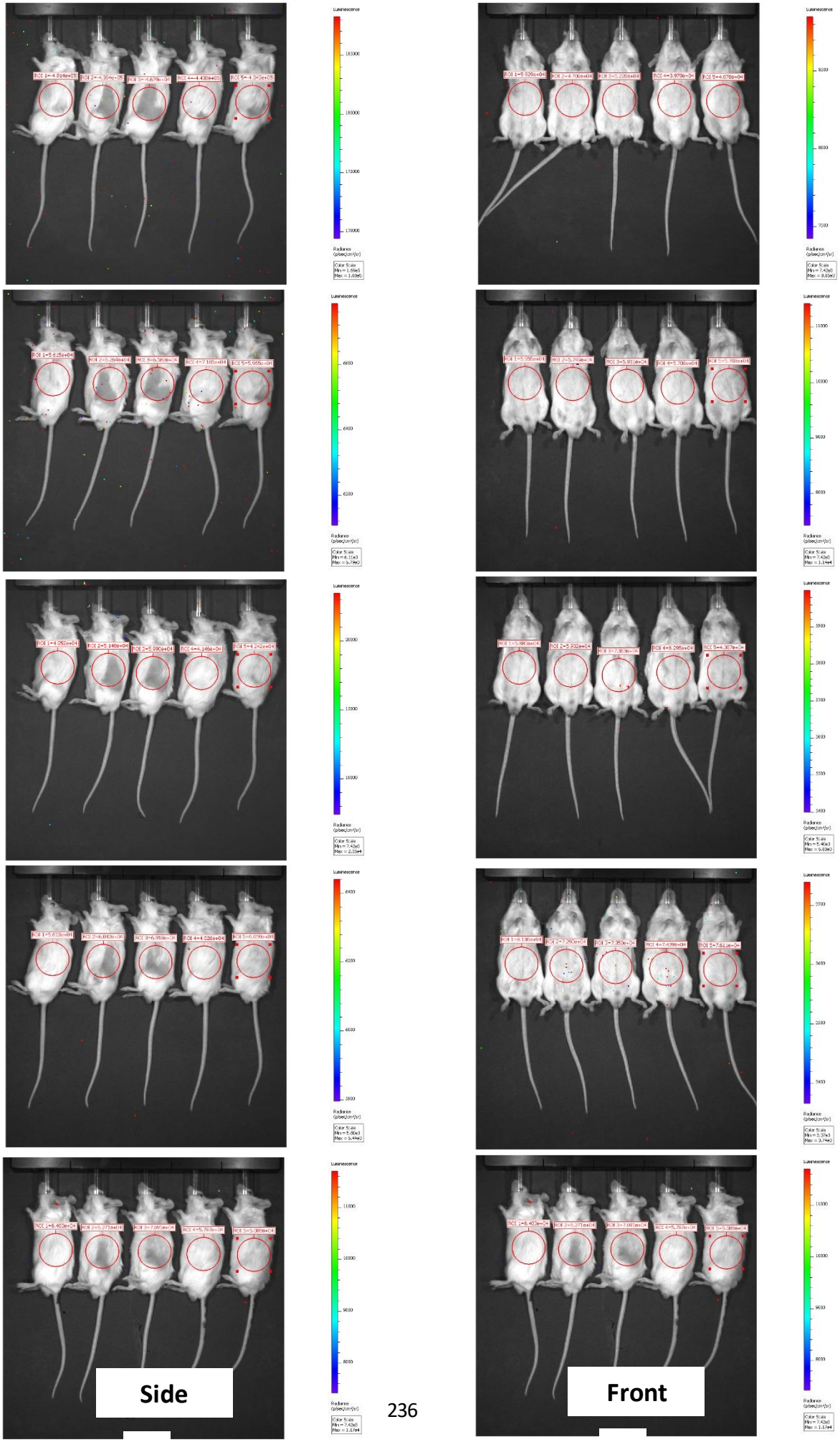
Side
Front

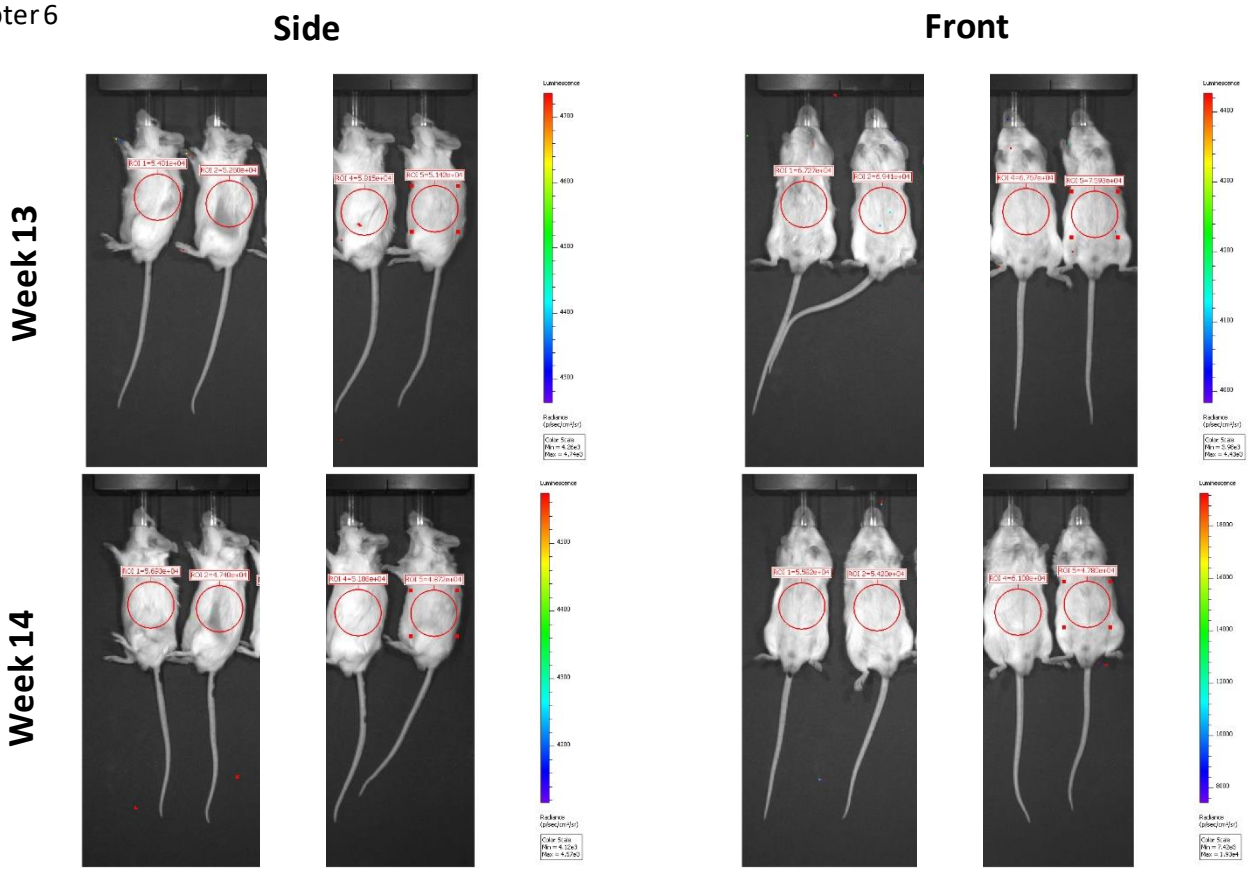

Supplementary Figure 5

Representative bioluminescence images of SCID beige mice intrasplenically injected with MS8N_C3 hESC-HLCs – Animals were injected with 1 x10^6 MS8N_C3 luminescent hESCs 72-hours after induction of acute liver injury with 0.2mL/kg CCl_4. Images show luminescence over time from side and front elevations. Red circles show regions of interest used to determine luminescence intensity in this case showing radiance (photons/second/cm^2/steradian), though total flux (photons/second) was also recorded and was used for later experiments. Luminescence intensity is represented by the coloured overlays with warmer colour indicating greater intensity. Each scale bar applies only to the image to its immediate left. The order of animals is consistent between images. Only values from the front elevation were used for subsequent analyses.

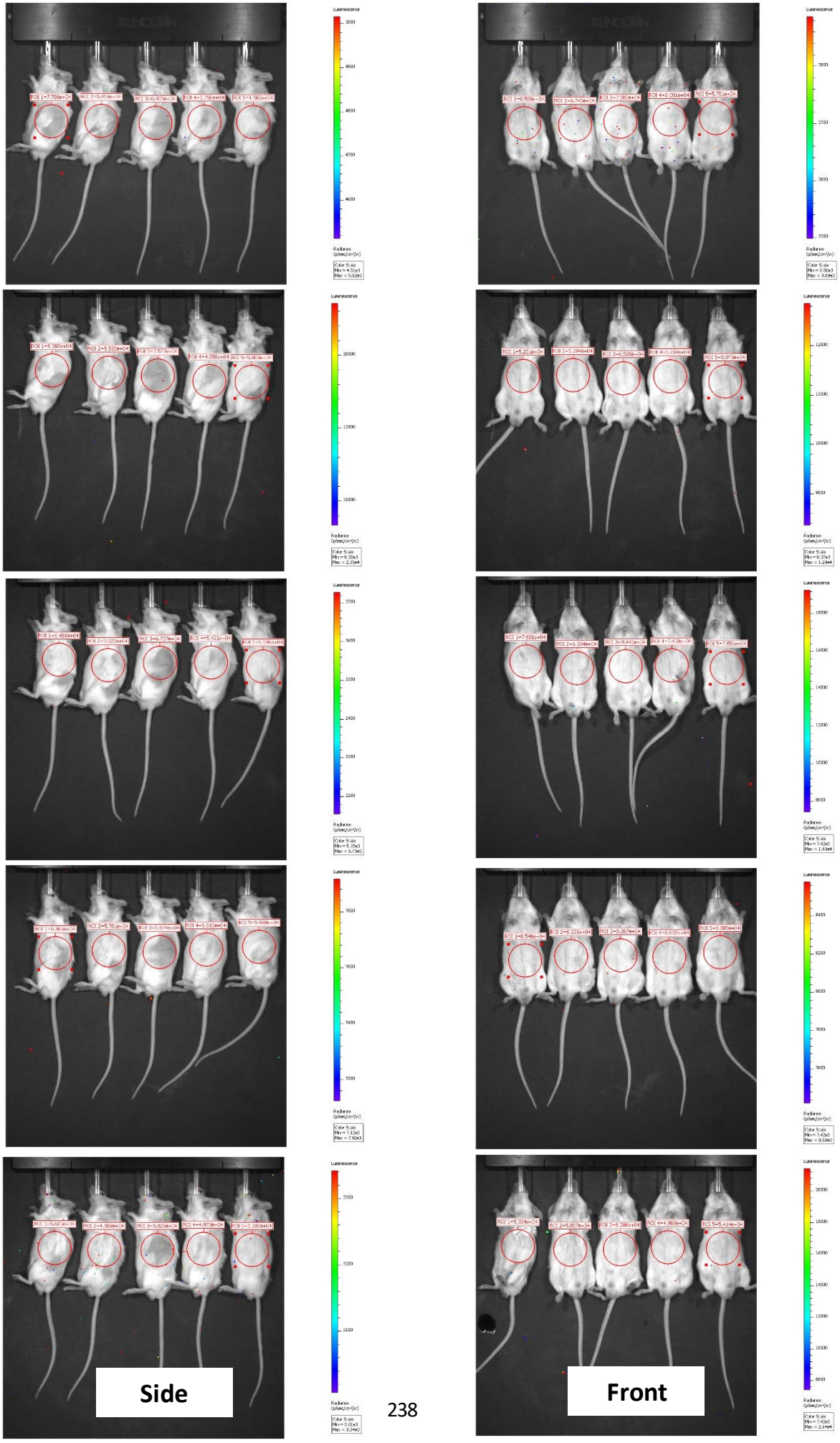
Side
Front

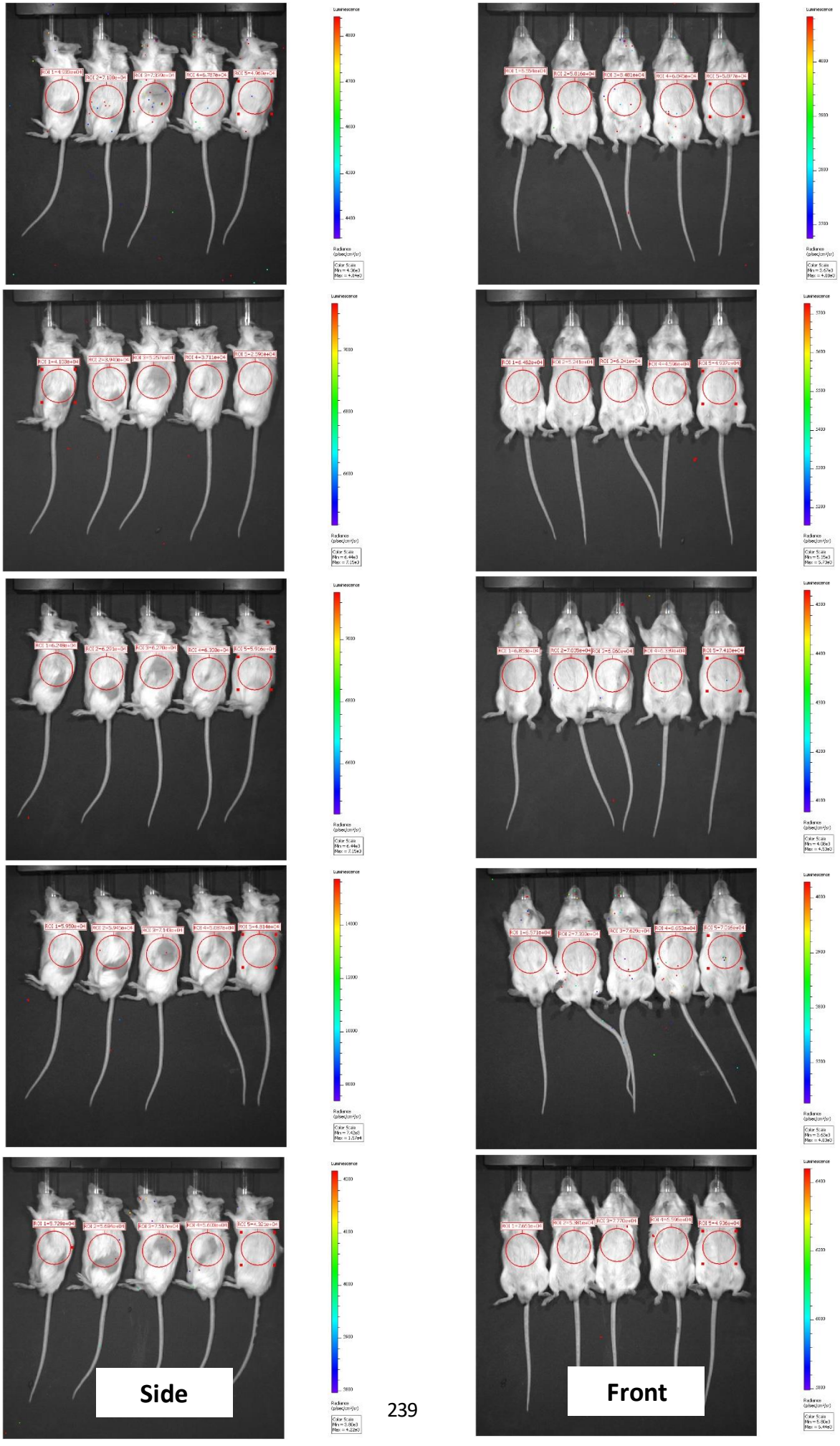
Side
Front

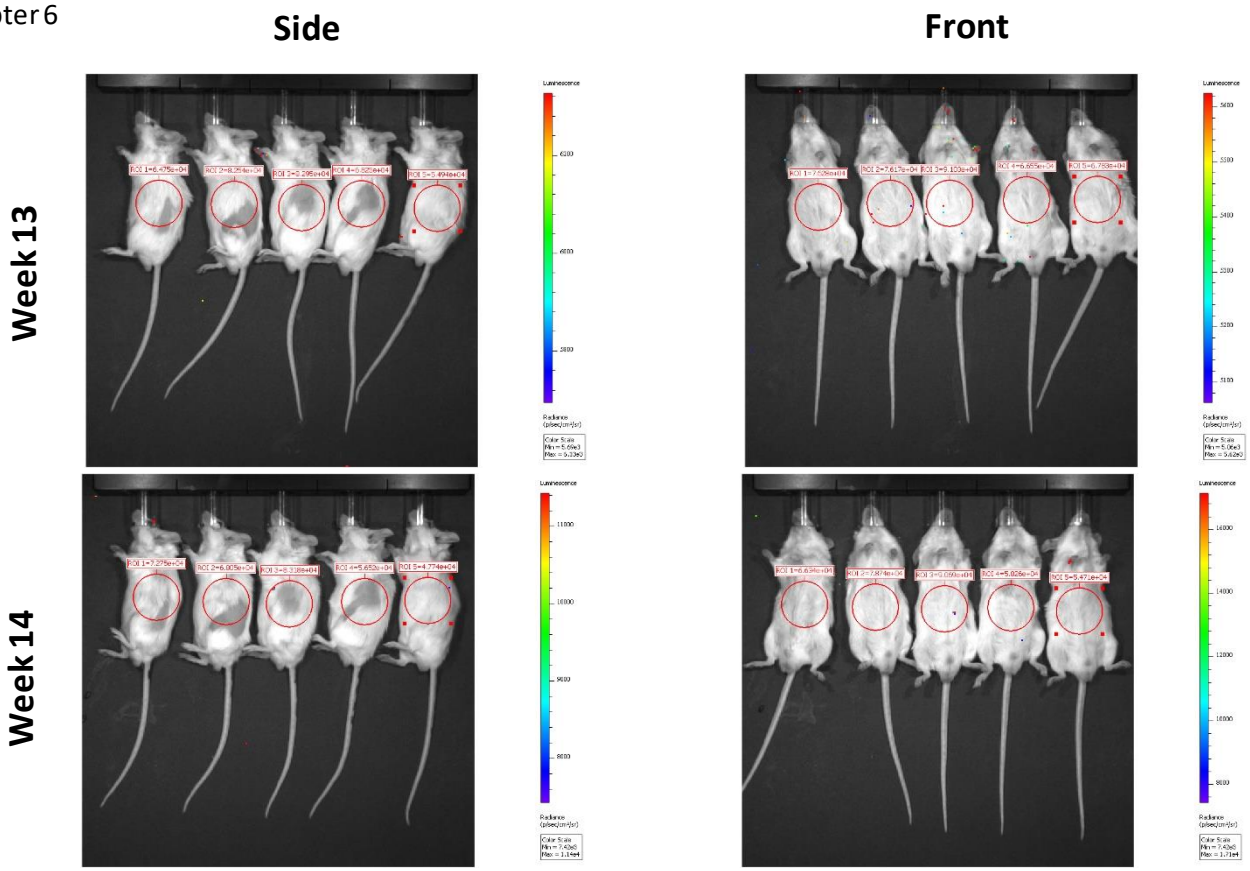

Supplementary Figure 6

Representative bioluminescence images of SCID beige mice intrasplenically injected with MS8N_E3 hESC-HLCs – Animals were injected with 1 x10^6 MS8N_E3 luminescent hESCs 72-hours after induction of acute liver injury with 0.2mL/kg CCl_4. Images show luminescence over time from side and front elevations. Red circles show regions of interest used to determine luminescence intensity, in this case showing radiance (photons/second/cm^2/steradian), though total flux (photons/second) was also recorded and was used for later experiments. Luminescence intensity is represented by the coloured overlays with warmer colour indicating greater intensity. Each scale bar applies only to the image to its immediate left. The order of animals is consistent between images. Only values from the front elevation were used for subsequent analyses.

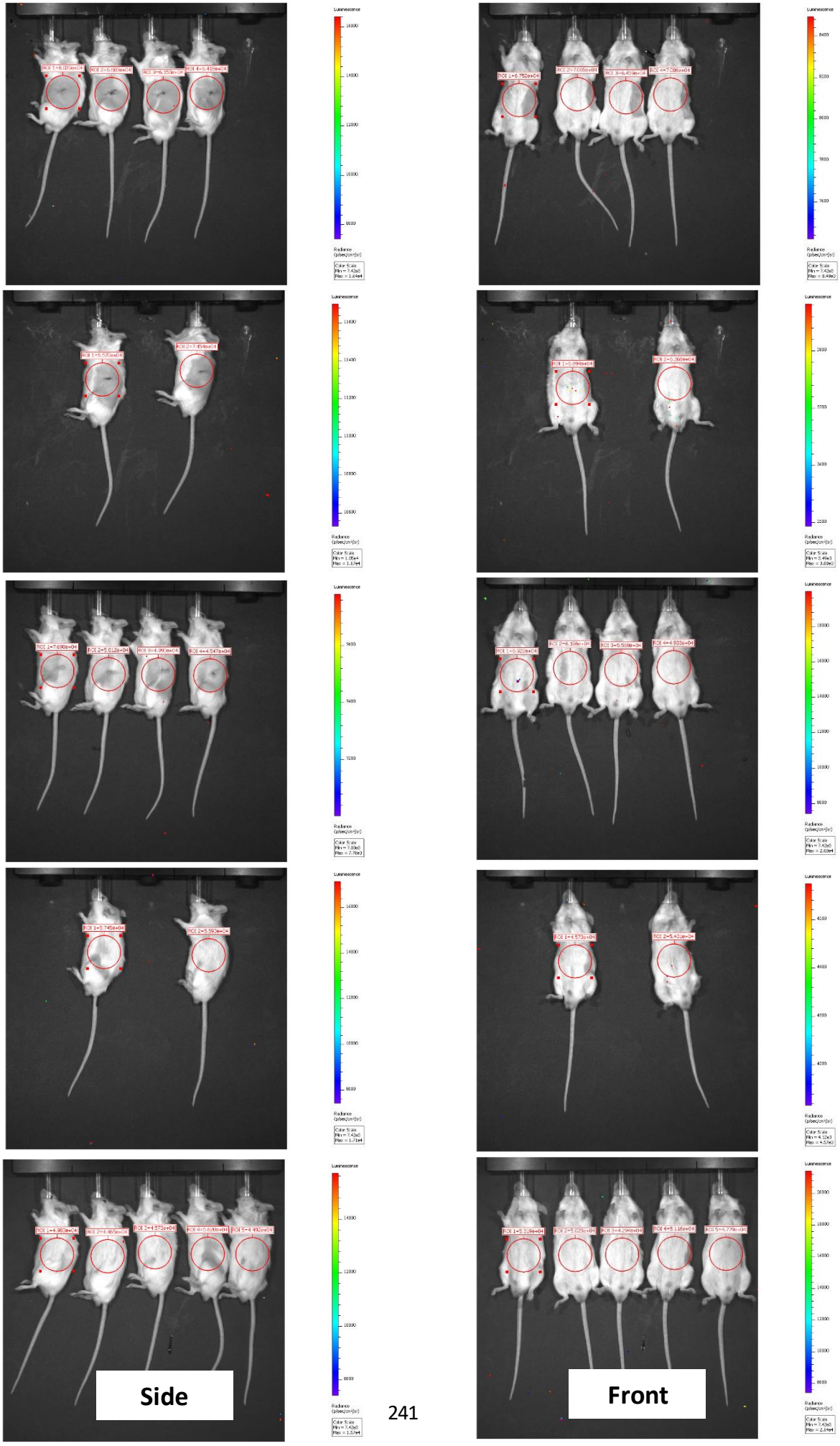
Side
Front

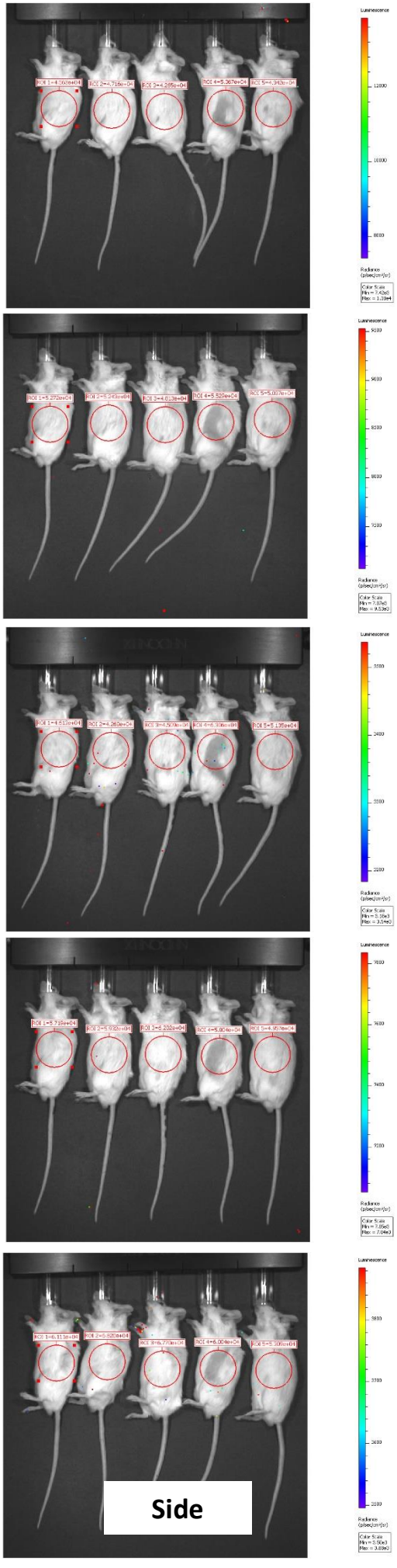
Side
Front

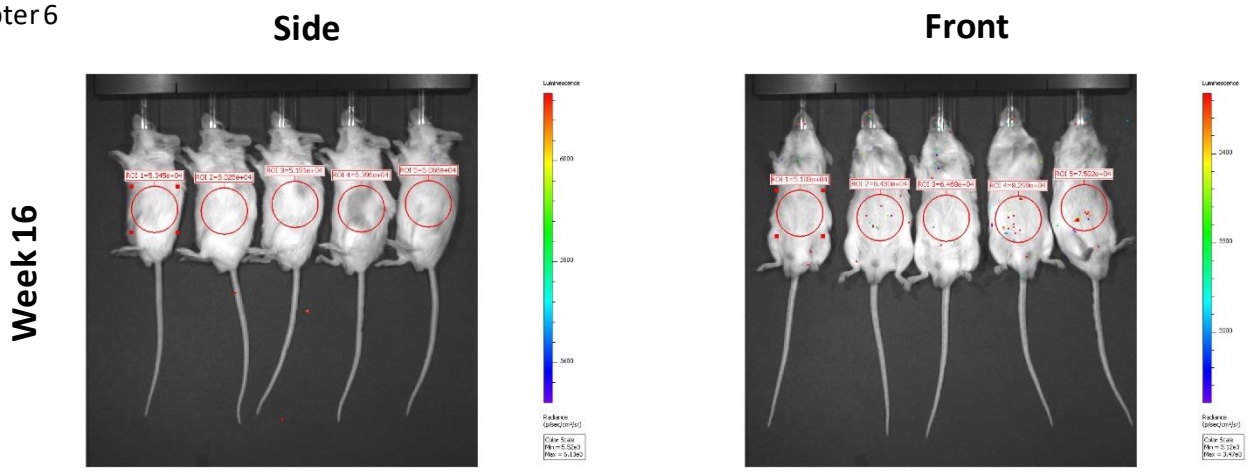

Supplementary Figure 7

Representative bioluminescence images of SCID beige mice intrasplenically injected with MS7CNV_C7 hESC-HLCs – Animals were injected with 1 x10^6 MS7CNV_C7 luminescent hESCs 72-hours after induction of acute liver injury with 0.2mL/kg CCl_4. Images show luminescence over time from side and front elevations. Red circles show regions of interest used to determine luminescence intensity, in this case showing radiance (photons/second/cm^2/steradian), though total flux (photons/second) was also recorded and was used for later experiments. Luminescence intensity is represented by the coloured overlays with warmer colour indicating greater intensity. Each scale bar applies only to the image to its immediate left. The order of animals is consistent between images, after week 4, one animal was sacrificed due to poor health and the remaining animal is that on the furthest right of the remaining images. Only values from the front elevation were used for subsequent analyses.

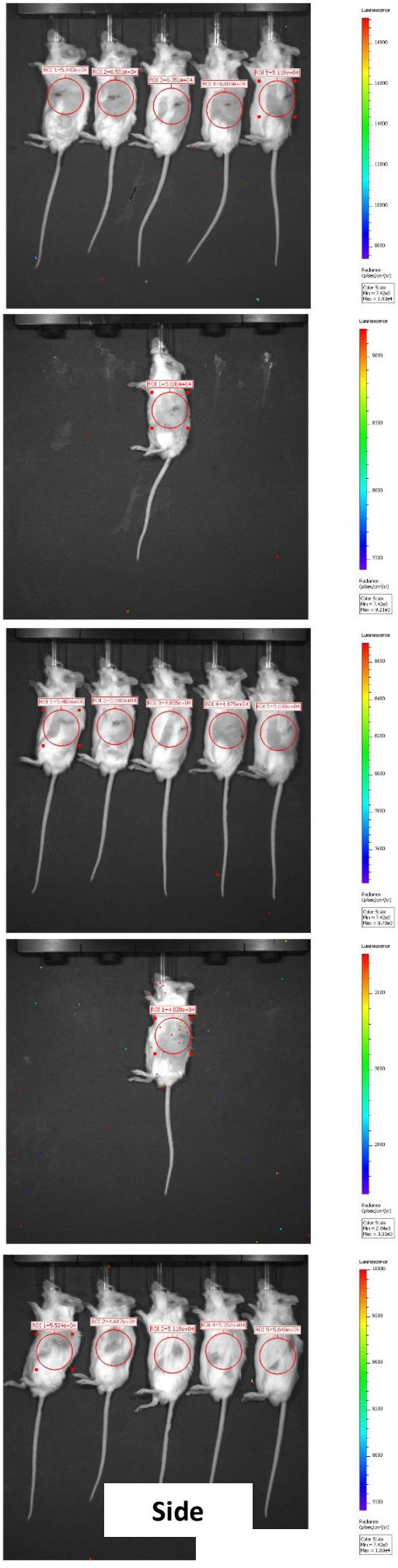
Side
Front

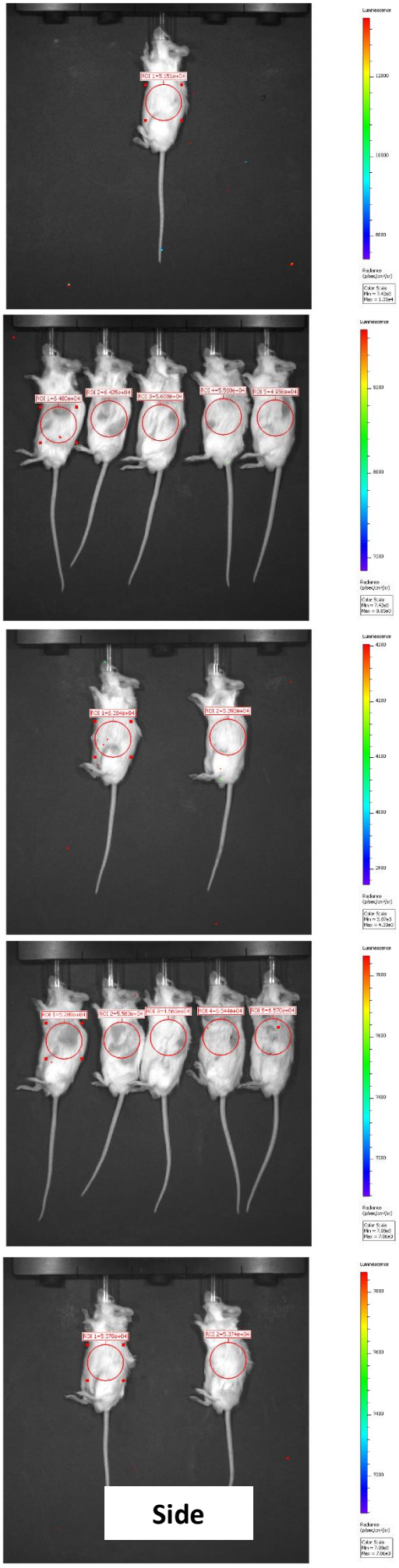
Side
Front

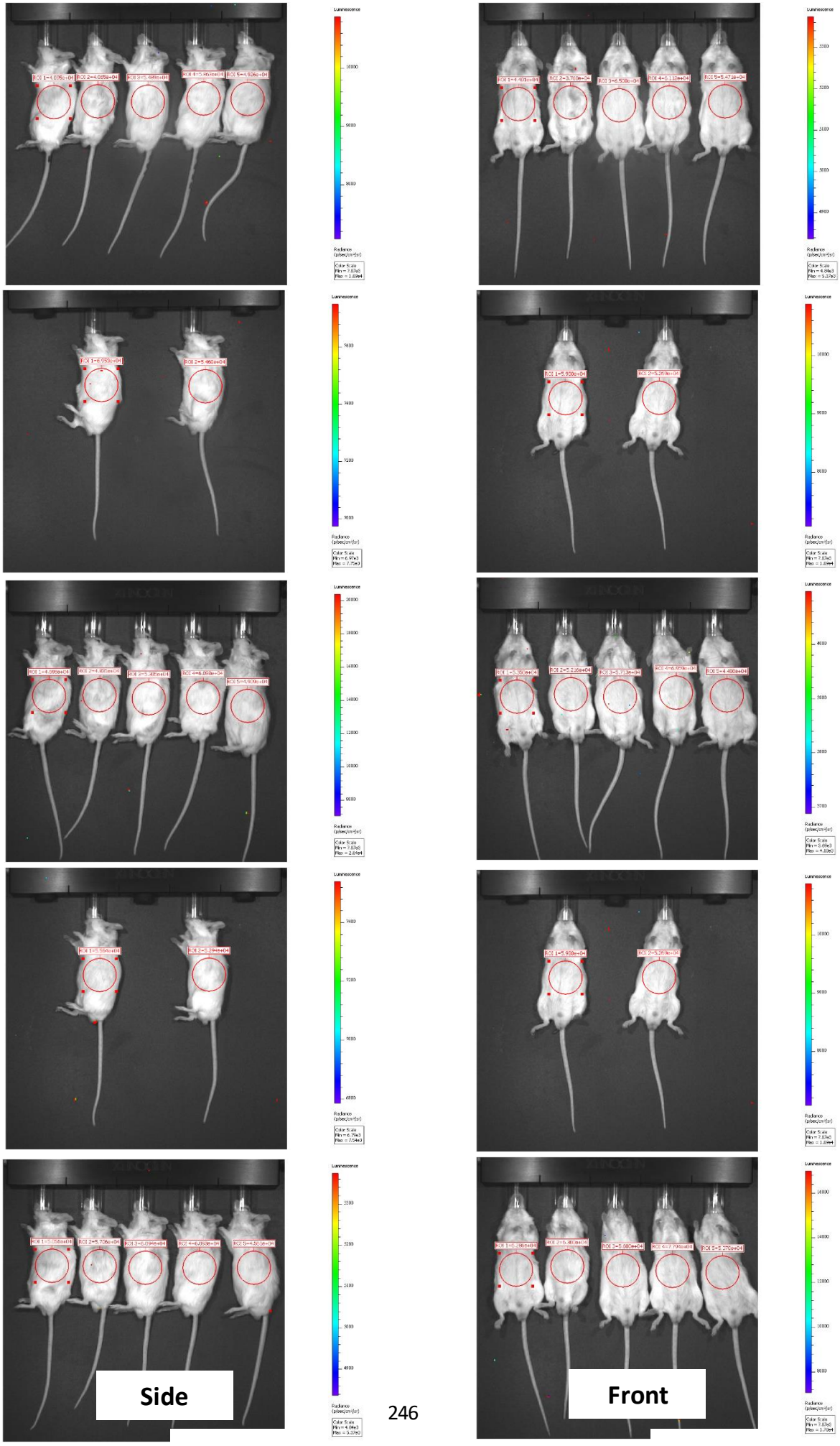
Side
Front

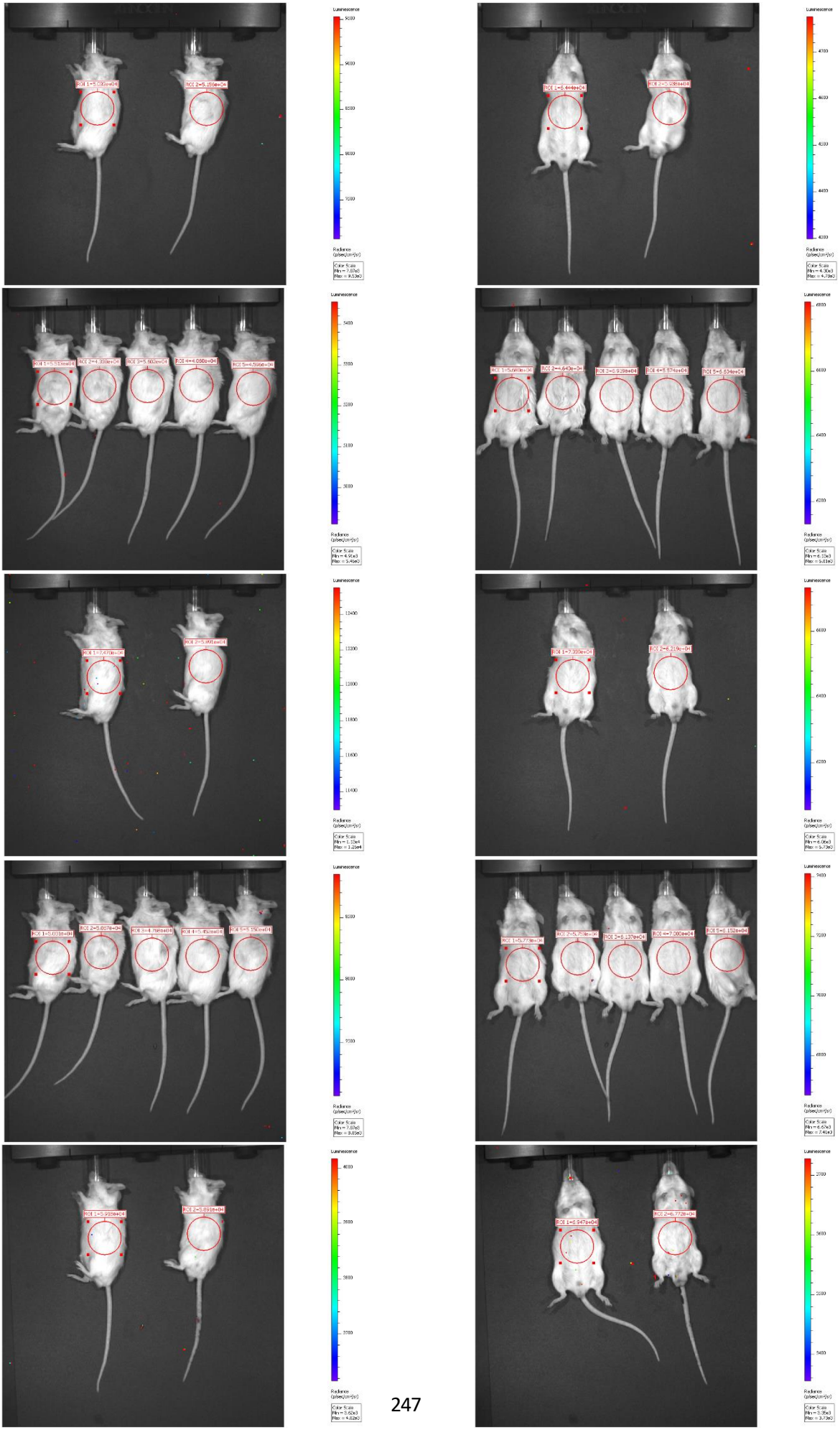

Supplementary Figure 8

Representative bioluminescence images of SCID beige mice intrasplenically injected with MS7CNV_D7 hESC-HLCs – Animals were injected with 1 x10^6 MS7CNV_D7 luminescent hESCs 72-hours after induction of acute liver injury with 0.2mL/kg CCl_4. Images show luminescence over time from side and front elevations. Red circles show regions of interest used to determine luminescence intensity, in this case showing radiance (photons/second/cm^2/steradian), though total flux (photons/second) was also recorded and was used for later experiments. Luminescence intensity is represented by the coloured overlays with warmer colour indicating greater intensity. Each scale bar applies only to the image to its immediate left. The order of animals is consistent between images, some animals were excluded due to thymic lymphoma discovered at the end of the experiment and are covered by white boxes. Only values from the front elevation were used in subsequent analyses.

Side **Front**

Week 1

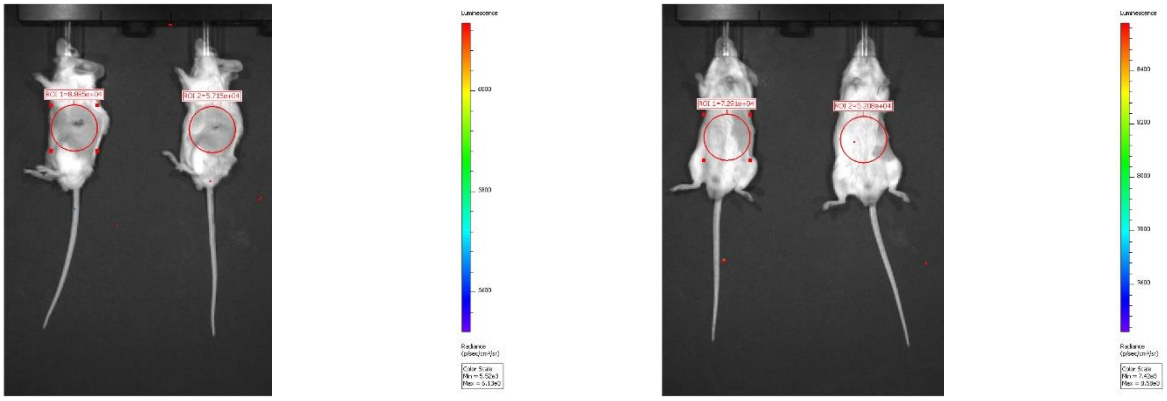

Week 4

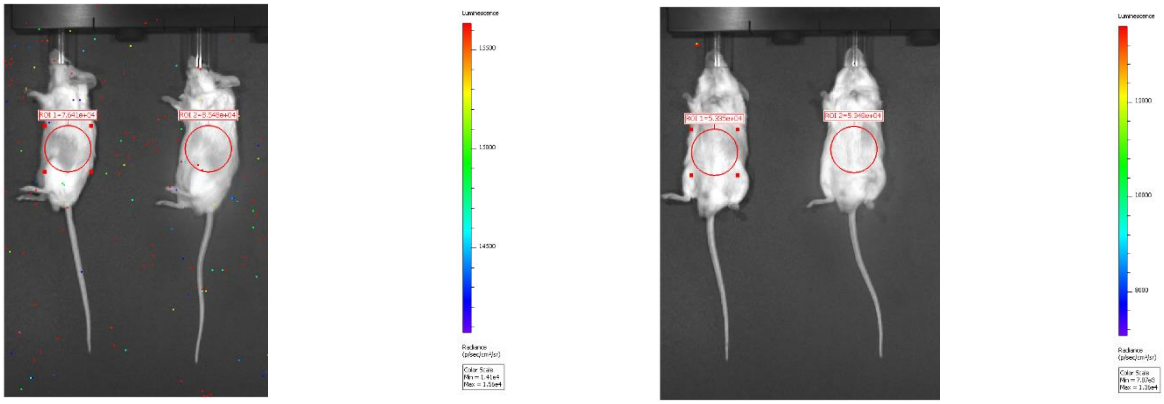

Week 6

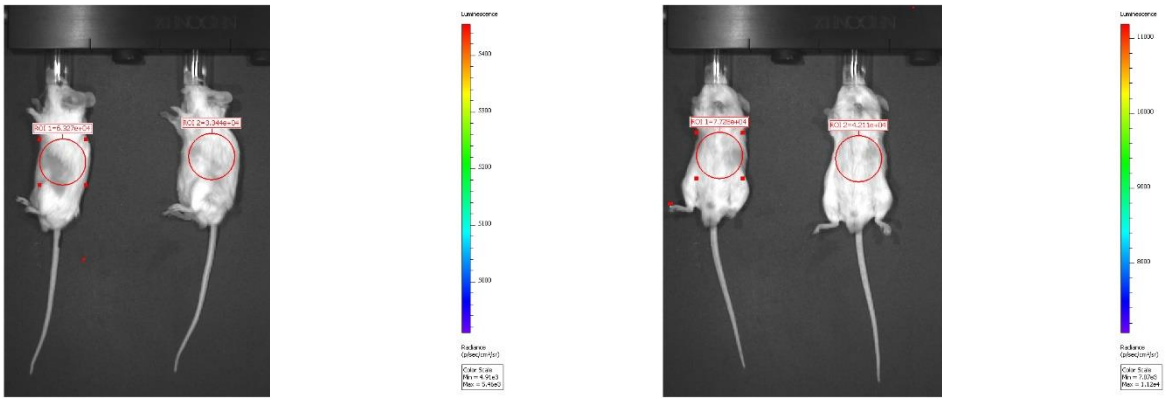

Week 8

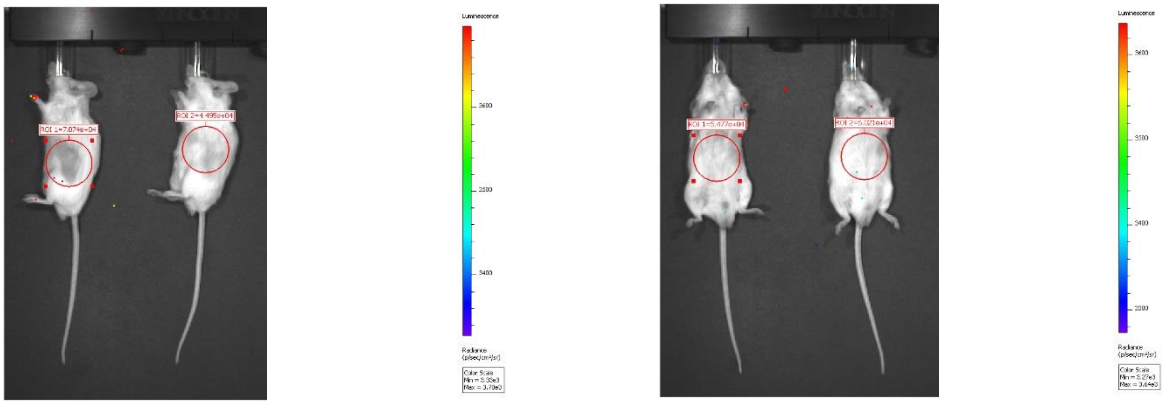

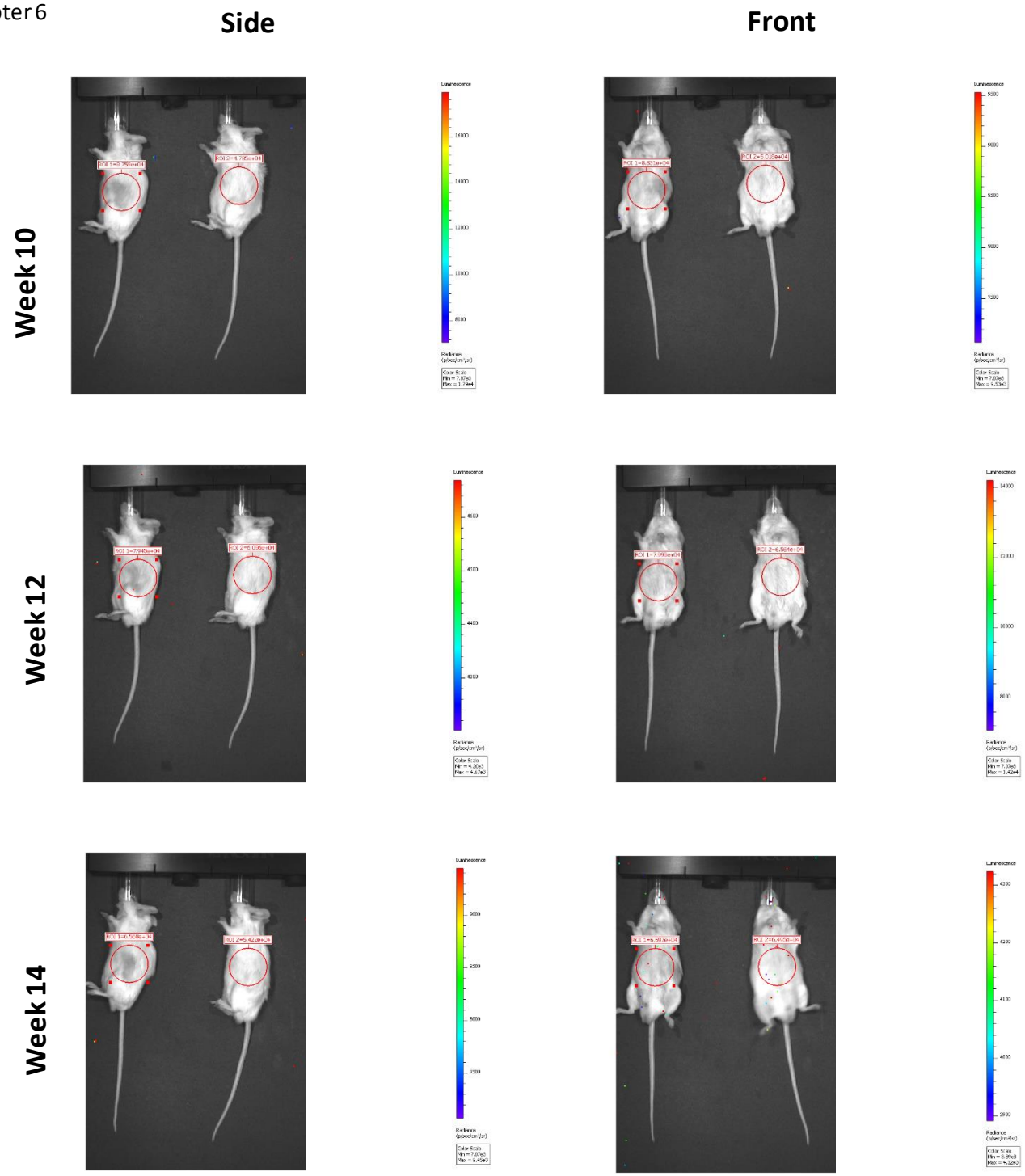

Supplementary Figure 9

Representative bioluminescence images of SCID beige mice intrasplenically injected with MS7N_D6 hESC-HLCs – Animals were injected with 1 x10^6 MS7N_D6 luminescent hESCs 72-hours after induction of acute liver injury with 0.2mL/kg CCl_4. Images show luminescence over time from side and front elevations. Red circles show regions of interest used to determine luminescence intensity, in this case showing radiance (photons/second/cm^2/steradian), though total flux (photons/second) was also recorded and was used for later experiments. Luminescence intensity is represented by the coloured overlays with warmer colour indicating greater intensity. Each scale bar applies only to

the image to its immediate left. The order of animals is consistent between images some animals were excluded after discovery of thymic lymphoma at the end of the experiment and are either not show or covered by white boxes. Only values from the front elevation were used for subsequent analyses.

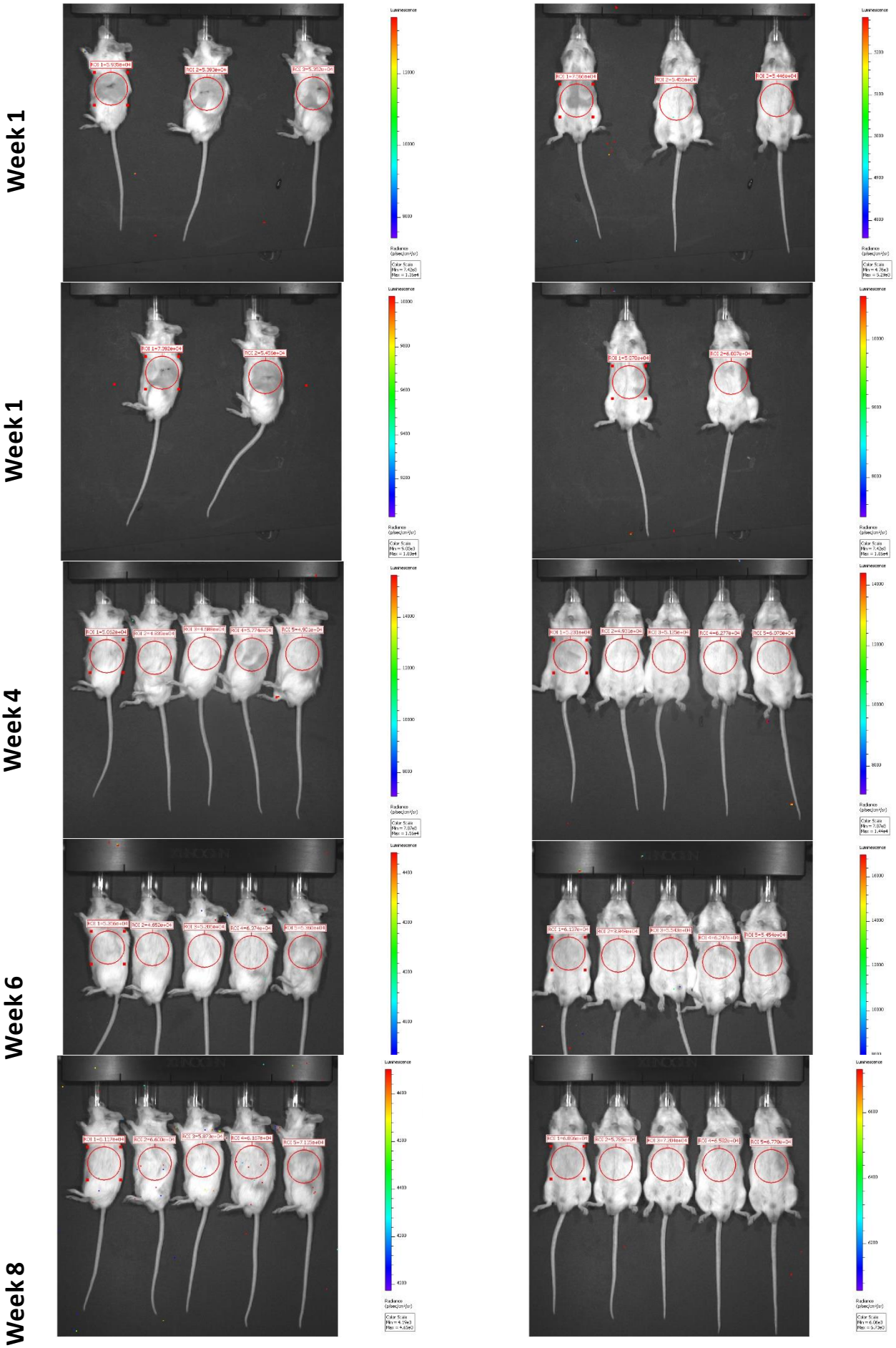
Side
Front
Week 1
Week 1
Week 4
Week 6
Week 8

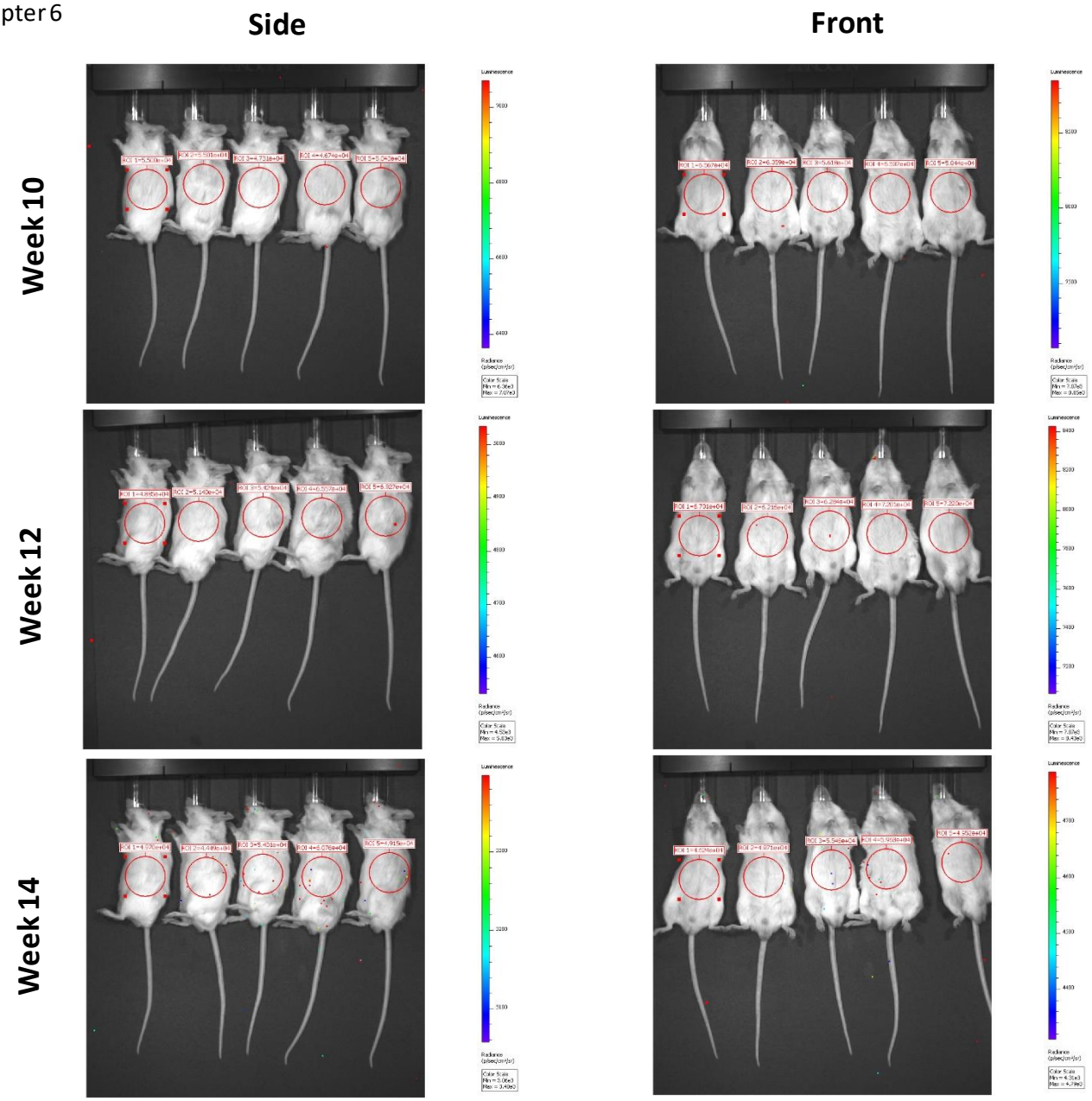

Supplementary Figure 10

Representative bioluminescence images of SCID beige mice intrasplenically injected with MS7N_E5 hESC-HLCs – Animals were injected with 1 x10^6 MS7N_E5 luminescent hESCs 72-hours after induction of acute liver injury with 0.2mL/kg CCl_4. Images show luminescence over time from side and front elevations. Red circles show regions of interest used to determine luminescence intensity, in this case showing radiance (photons/second/cm^2/steradian), though total flux (photons/second) was also recorded and was used for later experiments. Luminescence intensity is represented by the coloured overlays with warmer colour indicating greater intensity. Each scale bar applies only to the image to its immediate left. The order of animals is consistent between images, after week 1, the animals in the second row are the two animals to the furthest right in subsequent images. Only values from the front elevation were used for subsequent analyses.

8 Bibliography

Adam, R., Cailliez, V., Majno, P., Karam, V., McMaster, P., Calne, R.Y., O'Grady, J., Pichlmayr, R., Neuhaus, P., Otte, J.B., Hoeckerstedt, K., Bismuth, H., 2000. Normalised intrinsic mortality risk in liver transplantation: European Liver Transplant Registry study. Lancet 356, 621–627. https://doi.org/10.1016/S0140-6736(00)02603-9

Ahmed, N.E.-M.B., Murakami, M., Kaneko, S., Nakashima, M., 2016. The effects of hypoxia on the stemness properties of human dental pulp stem cells (DPSCs). Sci. Rep. 6, 35476. https://doi.org/10.1038/srep35476

Aloia, L., Gutierrez, A., Caballero, J.M., Di Croce, L., 2014. Direct interaction between Id1 and Zrf1 controls neural differentiation of embryonic stem cells. EMBO Rep. 16, 63–70. https://doi.org/10.15252/embr.201439560

Amariglio, N., Hirshberg, A., Scheithauer, B.W., Cohen, Y., Loewenthal, R., Trakhtenbrot, L., Paz, N., Koren-Michowitz, M., Waldman, D., Leider-Trejo, L., Toren, A., Constantini, S., Rechavi, G., 2009. Donor-Derived Brain Tumor Following Neural Stem Cell Transplantation in an Ataxia Telangiectasia Patient. PLoS Med. 6, e1000029. https://doi.org/10.1371/journal.pmed.1000029

Amps, K., Andrews, P.W., Anyfantis, G., Armstrong, L., Avery, S., Baharvand, H., Baker, J., Baker, D., Munoz, M.B., Beil, S., Benvenisty, N., Ben-Yosef, D., Biancotti, J.C., Bosman, A., Brena, R.M., Brison, D., Caisander, G., Camarasa, M. V., Chen, J., Chiao, E., Choi, Y.M., Choo, A.B.H., Collins, D., Colman, A., Crook, J.M., Daley, G.Q., Dalton, A., De Sousa, P.A., Denning, C., Downie, J., Dvorak, P., Montgomery, K.D., Feki, A., Ford, A., Fox, V., Fraga, A.M., Frumkin, T., Ge, L., Gokhale, P.J., Golan-Lev, T., Gourabi, H., Gropp, M., Guangxiu, L., Hampl, A., Harron, K., Healy, L., Herath, W., Holm, F., Hovatta, O., Hyllner, J., Inamdar, M.S., Irwanto, A.K., Ishii, T., Jaconi, M., Jin, Y., Kimber, S., Kiselev, S., Knowles, B.B., Kopper, O., Kukharenko, V., Kuliev, A., Lagarkova, M.A., Laird, P.W., Lako, M., Laslett, A.L., Lavon, N., Lee, D.R., Lee, J.E., Li, C., Lim, L.S., Ludwig, T.E., Ma, Y., Maltby, E., Mateizel, I., Mayshar, Y., Mileikovsky, M., Minger, S.L., Miyazaki, T., Moon, S.Y., Moore, H., Mummery, C., Nagy, A., Nakatsuji, N., Narwani, K., Oh, S.K.W., Oh, S.K., Olson, C., Otonkoski, T., Pan, F., Park, I.H., Pells, S., Pera, M.F., Pereira, L. V., Qi, O., Raj, G.S., Reubinoff, B., Robins, A., Robson, P., Rossant, J., Salekdeh, G.H., Schulz, T.C., Sermon, K., Mohamed, J.S., Shen, H., Sherrer, E., Sidhu, K., Sivarajah, S., Skottman, H., Spits, C., Stacey, G.N., Strehl, R., Strelchenko, N., Suemori, H., Sun, B., Suuronen, R., Takahashi, K., Tuuri, T., Venu, P., Verlinsky, Y., Oostwaard, D.W. Van, Weisenberger, D.J., Wu, Y., Yamanaka, S., Young, L., Zhou, Q., 2011. Screening ethnically diverse human embryonic stem cells identifies a chromosome 20 minimal amplicon conferring growth advantage. Nat. Biotechnol. 29, 1132–1144. https://doi.org/10.1038/nbt.2051

Andrews, P., Baker, D., Benvinisty, N., Miranda, B., Bruce, K., Brüstle, O., Choi, M., Choi, Y.-M., Crook, J., de Sousa, P., Dvorak, P., Freund, C., Firpo, M., Furue, M., Gokhale, P., Ha, H.-Y., Han, E., Haupt, S., Healy, L., Hei, D., Hovatta, O., Hunt, C., Hwang, S.-M., Inamdar, M., Isasi, R., Jaconi, M., Jekerle, V., Kamthorn, P., Kibbey, M., Knezevic, I., Knowles, B., Koo, S.-K., Laabi, Y., Leopoldo, L., Liu, P., Lomax, G., Loring, J., Ludwig, T., Montgomery, K., Mummery, C., Nagy, A., Nakamura, Y., Nakatsuji, N., Oh, S., Oh, S.-K., Otonkoski, T., Pera, M., Peschanski, M., Pranke, P., Rajala, K., Rao, M., Ruttachuk, R., Reubinoff, B., Ricco, L., Rooke, H., Sipp, D., Stacey, G., Suemori, H., Takahashi, T., Takada, K., Talib, S., Tannenbaum, S., Yuan, B.-Z., Zeng, F., Zhou, Q., 2015. Points to consider in the development of seed stocks of pluripotent stem cells for clinical applications: International Stem Cell Banking Initiative (ISCBI). Regen. Med. 10, 1–44. https://doi.org/10.2217/rme.14.93

Asgari, S., Moslem, M., Bagheri-Lankarani, K., Pournasr, B., Miryounesi, M., Baharvand, H.,

2013. Differentiation and Transplantation of Human Induced Pluripotent Stem Cell-derived Hepatocyte-like Cells. Stem Cell Rev. Reports 9, 493–504. https://doi.org/10.1007/s12015-011-9330-y

Astashkina, A., Grainger, D.W., 2014. Critical analysis of 3-D organoid in vitro cell culture models for high-throughput drug candidate toxicity assessments. Adv. Drug Deliv. Rev. 69–70, 1–18. https://doi.org/10.1016/j.addr.2014.02.008

Avery, S., Hirst, A.J., Baker, D., Lim, C.Y., Alagaratnam, S., Skotheim, R.I., Lothe, R.A., Pera, M.F., Colman, A., Robson, P., Andrews, P.W., Knowles, B.B., 2013. BCL-XL mediates the strong selective advantage of a 20q11.21 amplification commonly found in human embryonic stem cell cultures. Stem Cell Reports 1, 379–386. https://doi.org/10.1016/j.stemcr.2013.10.005

Avior, Y., Levy, G., Zimerman, M., Kitsberg, D., Schwartz, R., Sadeh, R., Moussaieff, A., Cohen, M., Itskovitz-Eldor, J., Nahmias, Y., 2015. Microbial-derived lithocholic acid and vitamin K2 drive the metabolic maturation of pluripotent stem cells-derived and fetal hepatocytes. Hepatology 62, 265–78. https://doi.org/10.1002/hep.27803

Badger, J.L., Byrne, M.L., Veraitch, F.S., Mason, C., Wall, I.B., Caldwell, M.A., 2012. Hypoxic culture of human pluripotent stem cell lines is permissible using mouse embryonic fibroblasts. Regen. Med. 7, 675–683. https://doi.org/10.2217/rme.12.55

Baharvand, H., Hashemi, S.M., Ashtiani, S.K., Farrokhi, A., 2006. Differentiation of human embryonic stem cells into hepatocytes in 2D and 3D culture systems in vitro. Int. J. Dev. Biol. 50, 645–652. https://doi.org/10.1387/ijdb.052072hb

Bai, F., Jones, D.C., Lau, S.S., Monks, T.J., 2001. Serotonergic neurotoxicity of 3,4-(+/-)-methylenedioxyamphetamine and 3,4-(+/-)-methylendioxymethamphetamine (ecstasy) is potentiated by inhibition of gamma-glutamyl transpeptidase. Chem. Res. Toxicol. 14, 863–70.

Bao, J., Wu, Q., Wang, Y., Li, Y., Li, L., Chen, F., Wu, X., Xie, M., Bu, H., 2016. Enhanced hepatic differentiation of rat bone marrow-derived mesenchymal stem cells in spheroidal aggregate culture on a decellularized liver scaffold. Int. J. Mol. Med. 38, 457–465. https://doi.org/10.3892/ijmm.2016.2638

Basma, H., Soto-Gutiérrez, A., Yannam, G.R., Liu, L., Ito, R., Yamamoto, T., Ellis, E., Carson, S.D., Sato, S., Chen, Y., Muirhead, D., Navarro-Alvarez, N., Wong, R.J., Roy-Chowdhury, J., Platt, J.L., Mercer, D.F., Miller, J.D., Strom, S.C., Kobayashi, N., Fox, I.J., Navarro-Álvarez, N., Wong, R.J., Roy-Chowdhury, J., Platt, J.L., Mercer, D.F., Miller, J.D., Strom, S.C., Kobayashi, N., Fox, I.J., 2009. Differentiation and transplantation of human embryonic stem cell-derived hepatocytes. Gastroenterology 136, 990–9. https://doi.org/10.1053/j.gastro.2008.10.047

Baxter, M., Withey, S., Harrison, S., Segeritz, C.P., Zhang, F., Atkinson-Dell, R., Rowe, C., Gerrard, D.T., Sison-Young, R., Jenkins, R., Henry, J., Berry, A.A., Mohamet, L., Best, M., Fenwick, S.W., Malik, H., Kitteringham, N.R., Goldring, C.E., Piper Hanley, K., Vallier, L., Hanley, N.A., 2015. Phenotypic and functional analyses show stem cell-derived hepatocyte-like cells better mimic fetal rather than adult hepatocytes. J. Hepatol. 62, 581–589. https://doi.org/10.1016/j.jhep.2014.10.016

Bedel, A., Taillepierre, M., Guyonnet-Duperat, V., Lippert, E., Dubus, P., Dabernat, S., Mautuit, T., Cardinaud, B., Pain, C., Rousseau, B., Lalanne, M., Ged, C., Duchartre, Y., Richard, E., De Verneuil, H., Moreau-Gaudry, F., 2012. Metabolic correction of congenital erythropoietic porphyria with iPSCs free of reprogramming factors. Am. J. Hum. Genet. 91, 109–121. https://doi.org/10.1016/j.ajhg.2012.05.026

Bell, C.C., Hendriks, D.F.G., Moro, S.M.L., Ellis, E., Walsh, J., Renblom, A., Fredriksson Puigvert, L., Dankers, A.C.A., Jacobs, F., Snoeys, J., Sison-Young, R.L., Jenkins, R.E., Nordling, Å., Mkrtchian, S., Park, B.K., Kitteringham, N.R., Goldring, C.E.P., Lauschke, V.M., Ingelman-Sundberg, M., 2016. Characterization of primary human hepatocyte

spheroids as a model system for drug-induced liver injury, liver function and disease. Sci. Rep. 6, 25187. https://doi.org/10.1038/srep25187

Ben-David, U., Arad, G., Weissbein, U., Mandefro, B., Maimon, A., Golan-Lev, T., Narwani, K., Clark, A.T., Andrews, P.W., Benvenisty, N., Carlos Biancotti, J., 2014. Aneuploidy induces profound changes in gene expression, proliferation and tumorigenicity of human pluripotent stem cells. Nat. Commun. 5. https://doi.org/10.1038/ncomms5825

Benoist, C.C., Kawas, L.H., Zhu, M., Tyson, K.A., Stillmaker, L., Appleyard, S.M., Wright, J.W., Wayman, G.A., Harding, J.W., 2014. The Procognitive and Synaptogenic Effects of Angiotensin IV-Derived Peptides Are Dependent on Activation of the Hepatocyte Growth Factor/c-Met System. J. Pharmacol. Exp. Ther. 351, 390–402. https://doi.org/10.1124/jpet.114.218735

Bergen, A.A.B., Plomp, A.S., Schuurman, E.J., Terry, S., Breuning, M., Dauwerse, H., Swart, J., Kool, M., Van Soest, S., Baas, F., Ten Brink, J.B., De Jong, P.T.V.M., 2000. Mutations in ABCC6 cause pseudoxanthoma elasticum. Nat. Genet. 25, 228–231. https://doi.org/10.1038/76109

Berger, W., Steiner, E., Grusch, M., Elbling, L., Micksche, M., 2009. Vaults and the major vault protein: Novel roles in signal pathway regulation and immunity. Cell. Mol. Life Sci. 66, 43–61. https://doi.org/10.1007/s00018-008-8364-z

Beyer, T.A., Xu, W., Teupser, D., auf dem Keller, U., Bugnon, P., Hildt, E., Thiery, J., Kan, Y.W., Werner, S., 2008. Impaired liver regeneration in Nrf2 knockout mice: role of ROS-mediated insulin/IGF-1 resistance. EMBO J. 27, 212–223. https://doi.org/10.1038/sj.emboj.7601950

Bigorgne, A.E., Farin, H.F., Lemoine, R., Mahlaoui, N., Lambert, N., Gil, M., Schulz, A., Philippet, P., Schlesser, P., Abrahamsen, T.G., Oymar, K., Graham Davies, E., Ellingsen, C.L., Leteurtre, E., Moreau-Massart, B., Berrebi, D., Bole-Feysot, C., Nischke, P., Brousse, N., Fischer, A., Clevers, H., De Saint Basile, G., 2014. TTC7A mutations disrupt intestinal epithelial apicobasal polarity. J. Clin. Invest. 124, 328–337. https://doi.org/10.1172/JCI71471

Bissell, M.J., Radisky, D.C., Rizki, A., Weaver, V.M., Petersen, O.W., 2002. The organizing principle: Microenvironmental influences in the normal and malignant breast. Differentiation 70, 537–546. https://doi.org/10.1046/j.1432-0436.2002.700907.x

Björnsson, E.S., Bergmann, O.M., Björnsson, H.K., Kvaran, R.B., Olafsson, S., 2013. Incidence, presentation, and outcomes in patients with drug-induced liver injury in the general population of iceland. Gastroenterology 144, 1419–1425.e3. https://doi.org/10.1053/j.gastro.2013.02.006

Böhme, M., Müller, M., Leier, I., Jedlitschky, G., Keppler, D., 1994. Cholestasis caused by inhibition of the adenosine triphosphate-dependent bile salt transport in rat liver. Gastroenterology 107, 255–265. https://doi.org/10.1016/0016-5085(94)90084-1

Boj, S.F., Hwang, C. Il, Baker, L.A., Chio, I.I.C., Engle, D.D., Corbo, V., Jager, M., Ponz-Sarvise, M., Tiriac, H., Spector, M.S., Gracanin, A., Oni, T., Yu, K.H., Van Boxtel, R., Huch, M., Rivera, K.D., Wilson, J.P., Feigin, M.E., Öhlund, D., Handly-Santana, A., Ardito-Abraham, C.M., Ludwig, M., Elyada, E., Alagesan, B., Biffi, G., Yordanov, G.N., Delcuze, B., Creighton, B., Wright, K., Park, Y., Morsink, F.H.M., Molenaar, I.Q., Borel Rinkes, I.H., Cuppen, E., Hao, Y., Jin, Y., Nijman, I.J., Iacobuzio-Donahue, C., Leach, S.D., Pappin, D.J., Hammell, M., Klimstra, D.S., Basturk, O., Hruban, R.H., Offerhaus, G.J., Vries, R.G.J., Clevers, H., Tuveson, D.A., 2015. Organoid models of human and mouse ductal pancreatic cancer. Cell 160, 324–338. https://doi.org/10.1016/j.cell.2014.12.021

Bokhari, M., Carnachan, R.J., Cameron, N.R., Przyborski, S.A., 2007. Culture of HepG2 liver cells on three dimensional polystyrene scaffolds enhances cell structure and function during toxicological challenge. J. Anat. 211, 567–576. https://doi.org/10.1111/j.1469-

7580.2007.00778.x

Braam, S.R., Zeinstra, L., Litjens, S., Ward-van Oostwaard, D., van den Brink, S., van Laake, L., Lebrin, F., Kats, P., Hochstenbach, R., Passier, R., Sonnenberg, A., Mummery, C.L., 2008. Recombinant Vitronectin Is a Functionally Defined Substrate That Supports Human Embryonic Stem Cell Self-Renewal via αVβ5 Integrin. Stem Cells 26, 2257–2265. https://doi.org/10.1634/stemcells.2008-0291

Broutier, L., Andersson-Rolf, A., Hindley, C.J., Boj, S.F., Clevers, H., Koo, B.K., Huch, M., 2016. Culture and establishment of self-renewing human and mouse adult liver and pancreas 3D organoids and their genetic manipulation. Nat. Protoc. 11, 1724–1743. https://doi.org/10.1038/nprot.2016.097

Byrne, J.A., Strautnieks, S.S., MieliVergani, G., Higgins, C.F., Linton, K.J., Thompson, R.J., 2002. The human bile salt export pump: Characterization of substrate specificity and identification of inhibitors. Gastroenterology 123, 1649–1658. https://doi.org/10.1053/gast.2002.36591

Cantòn, I., Cole, D.M., Kemp, E.H., Watson, P.F., Chunthapong, J., Ryan, A.J., MacNeil, S., Haycock, J.W., 2010. Development of a 3D human in vitro skin co-culture model for detecting irritants in real-time. Biotechnol. Bioeng. 106, 794–803. https://doi.org/10.1002/bit.22742

Caralt, M., Velasco, E., Lanas, A., Baptista, P.M., 2014. Liver bioengineering: From the stage of liver decellularized matrix to the multiple cellular actors and bioreactor special effects. Organogenesis 10, 250–259. https://doi.org/10.4161/org.29892

Castellanos-Gonzalez, A., Cabada, M.M., Nichols, J., Gomez, G., White, A.C., 2013. Human primary intestinal epithelial cells as an improved in vitro model for cryptosporidium parvum infection. Infect. Immun. 81, 1996–2001. https://doi.org/10.1128/IAI.01131-12

Chandra, V., Huang, P., Potluri, N., Wu, D., Kim, Y., Rastinejad, F., 2013. Multidomain integration in the structure of the HNF-4α nuclear receptor complex. Nature 495, 394–398. https://doi.org/10.1038/nature11966

Chatterjee, B., Echchgadda, I., Seog Song, C., 2005. Vitamin D receptor regulation of the steroid/bile acid sulfotransferase SULT2A1, in: Methods in Enzymology. pp. 165–191. https://doi.org/10.1016/S0076-6879(05)00010-8

Checa-Rojas, A., Delgadillo-Silva, L.F., Velasco-Herrera, M.D.C., Andrade-Domínguez, A., Gil, J., Santillán, O., Lozano, L., Toledo-Leyva, A., Ramírez-Torres, A., Talamas-Rohana, P., Encarnación-Guevara, S., 2018. GSTM3 and GSTP1: novel players driving tumor progression in cervical cancer. Oncotarget 9, 21696–21714. https://doi.org/10.18632/oncotarget.24796

Chen, G., Dellinger, R.W., Sun, D., Spratt, T.E., Lazarus, P., 2008. Glucuronidation of Tobacco-Specific Nitrosamines by UGT2B10. Drug Metab. Dispos. 36, 824–830. https://doi.org/10.1124/dmd.107.019406

Chen, X., Zhang, J., Yi, R., Mu, J., Zhao, X., Yang, Z., 2018. Hepatoprotective effects of lactobacillus on carbon tetrachloride-induced acute liver injury in mice. Int. J. Mol. Sci. 19. https://doi.org/10.3390/ijms19082212

Cheng, L., Hansen, N.F., Zhao, L., Du, Y., Zou, C., Donovan, F.X., Chou, B.K., Zhou, G., Li, S., Dowey, S.N., Ye, Z., Chandrasekharappa, S.C., Yang, H., Mullikin, J.C., Liu, P.P., 2012. Low incidence of DNA sequence variation in human induced pluripotent stem cells generated by nonintegrating plasmid expression. Cell Stem Cell 10, 337–344. https://doi.org/10.1016/j.stem.2012.01.005

Chien, Y., Chang, Y.L., Li, H.Y., Larsson, M., Wu, W.W., Chien, C.S., Wang, C.Y., Chu, P.Y., Chen, K.H., Lo, W.L., Chiou, S.H., Lan, Y.T., Huo, T.I., Lee, S.D., Huang, P.I., 2015. Synergistic effects of carboxymethyl-hexanoyl chitosan, cationic polyurethane-short branch PEI in miR122 gene delivery: Accelerated differentiation of iPSCs into mature

hepatocyte-like cells and improved stem cell therapy in a hepatic failure model. Acta Biomater. 13, 228–244. https://doi.org/10.1016/j.actbio.2014.11.018

Chitrangi, S., Nair, P., Khanna, A., 2017. Three-dimensional polymer scaffolds for enhanced differentiation of human mesenchymal stem cells to hepatocyte-like cells: a comparative study. J. Tissue Eng. Regen. Med. 11, 2359–2372. https://doi.org/10.1002/term.2136

Choi, D., Oh, H.J., Chang, U.J., Koo, S.K., Jiang, J.X., Hwang, S.Y., Lee, J.D., Yeoh, G.C., Shin, H.S., Lee, J.S., Oh, B., 2002. In vivo differentiation of mouse embryonic stem cells into hepatocytes. Cell Transpl. 11, 359–368.

Christensen, D.R., Calder, P.C., Houghton, F.D., 2015. GLUT3 and PKM2 regulate OCT4 expression and support the hypoxic culture of human embryonic stem cells. Sci. Rep. 5, 17500. https://doi.org/10.1038/srep17500

Cipriano, M., Freyer, N., Knöspel, F., Oliveira, N.G., Barcia, R., Cruz, P.E., Cruz, H., Castro, M., Santos, J.M., Zeilinger, K., Miranda, J.P., 2017. Self-assembled 3D spheroids and hollow-fibre bioreactors improve MSC-derived hepatocyte-like cell maturation in vitro. Arch. Toxicol. 91, 1815–1832. https://doi.org/10.1007/s00204-016-1838-0

Clark, A.M., Wheeler, S.E., Taylor, D.P., Pillai, V.C., Young, C.L., Prantil-Baun, R., Nguyen, T., Stolz, D.B., Borenstein, J.T., Lauffenburger, D.A., Venkataramanan, R., Griffith, L.G., Wells, A., 2014. A microphysiological system model of therapy for liver micrometastases. Exp. Biol. Med. 239, 1170–1179. https://doi.org/10.1177/1535370214532596

Colnot, S., Perret, C., 2011. Liver Zonation, in: Monga, S.P.S. (Ed.), Molecular Pathology of Liver Diseases. pp. 7–16. https://doi.org/10.1007/978-1-4419-7107-4_2

Committee for Medicinal Products for Human Use, 2007. Guideline on Strategies to Identify and Mitigate Risks for First-In-Human Clinical Trials with Investigational Medicinal Products [WWW Document]. Eur. Med. Agency. https://doi.org/EMEA/CHMP/SWP/28367/07

Concepcion, A.R., Lopez, M., Ardura-Fabregat, A., Medina, J.F., 2014. Role of AE2 for pHi regulation in biliary epithelial cells. Front. Physiol. 4. https://doi.org/10.3389/fphys.2013.00413

Coulouarn, C., Factor, V.M., Andersen, J.B., Durkin, M.E., Thorgeirsson, S.S., 2009. Loss of miR-122 expression in liver cancer correlates with suppression of the hepatic phenotype and gain of metastatic properties. Oncogene 28, 3526–3536. https://doi.org/10.1038/onc.2009.211

Croy, B.A., Chapeau, C., 1990. Evaluation of the pregnancy immunotrophism hypothesis by assessment of the reproductive performance of young adult mice of genotype scid/scid.bg/bg. J. Reprod. Fertil. 88, 231–9.

Custer, R.P., Bosma, G.C., Bosma, M.J., 1985. Severe combined immunodeficiency (SCID) in the mouse. Pathology, reconstitution, neoplasms. Am. J. Pathol. 120, 464–77.

Czysz, K., Minger, S., Thomas, N., 2015. Dmso efficiently down regulates pluripotency genes in human embryonic stem cells during definitive endoderm derivation and increases the proficiency of hepatic differentiation. PLoS One 10. https://doi.org/10.1371/journal.pone.0117689

Daly, A.K., Donaldson, P.T., Bhatnagar, P., Shen, Y., Pe'Er, I., Floratos, A., Daly, M.J., Goldstein, D.B., John, S., Nelson, M.R., Graham, J., Park, B.K., Dillon, J.F., Bernal, W., Cordell, H.J., Pirmohamed, M., Aithal, G.P., Day, C.P., 2009. HLA-B5701 genotype is a major determinant of drug-induced liver injury due to flucloxacillin. Nat. Genet. 41, 816–819. https://doi.org/10.1038/ng.379

Darnell, M., Schreiter, T., Zeilinger, K., Urbaniak, T., S??derdahl, T., Rossberg, I., Dilln??r, B., Berg, A.L., Gerlach, J.C., Andersson, T.B., 2011. Cytochrome P450-dependent metabolism in HepaRG cells cultured in a dynamic three-dimensional bioreactor. Drug

Metab. Dispos. 39, 1131–1138. https://doi.org/10.1124/dmd.110.037721
Davoodian, N., Lotfi, A.S., Soleimani, M., Mowla, S.J., 2014. MicroRNA-122 overexpression promotes hepatic differentiation of human adipose tissue-derived stem cells. J. Cell. Biochem. 115, 1582–1593. https://doi.org/10.1002/jcb.24822
Dayalan Naidu, S., Dinkova-Kostova, A.T., 2017. Regulation of the mammalian heat shock factor 1. FEBS J. 284, 1606–1627. https://doi.org/10.1111/febs.13999
Dekkers, J.F., Wiegerinck, C.L., De Jonge, H.R., Bronsveld, I., Janssens, H.M., De Winter-De Groot, K.M., Brandsma, A.M., De Jong, N.W.M., Bijvelds, M.J.C., Scholte, B.J., Nieuwenhuis, E.E.S., Van Den Brink, S., Clevers, H., Van Der Ent, C.K., Middendorp, S., Beekman, J.M., 2013. A functional CFTR assay using primary cystic fibrosis intestinal organoids. Nat. Med. 19, 939–945. https://doi.org/10.1038/nm.3201
Deng, X.G., Qiu, R.L., Wu, Y.H., Li, Z.X., Xie, P., Zhang, J., Zhou, J.J., Zeng, L.X., Tang, J., Maharjan, A., Deng, J.M., 2014. Overexpression of miR-122 promotes the hepatic differentiation and maturation of mouse ESCs through a miR-122/FoxA1/HNF4a-positive feedback loop. Liver Int. 34, 281–295. https://doi.org/10.1111/liv.12239
Dianat, N., Dubois-Pot-Schneider, H., Steichen, C., Desterke, C., Leclerc, P., Raveux, A., Combettes, L., Weber, A., Corlu, A., Dubart-Kupperschmitt, A., 2014. Generation of functional cholangiocyte-like cells from human pluripotent stem cells and HepaRG cells. Hepatology 60, 700–714. https://doi.org/10.1002/hep.27165
Dicker, E., Cederbaum, A.I., 1991. Increased Oxidation of Dimethylnitrosamine in Pericentral Microsomes after Pyrazole Induction of Cytochrome P-4502El. Alcohol. Clin. Exp. Res. 15, 1072–1076. https://doi.org/10.1111/j.1530-0277.1991.tb05214.x
DiMasi, J., Grabowski, H., Hansen, R., 2016. Innovation in the pharmaceutical industry: new estimates of R&D costs. Journal of Health Economics. J. Health Econ. 47, 20–33.
Dimos, J.T., Rodolfa, K.T., Niakan, K.K., Weisenthal, L.M., Mitsumoto, H., Chung, W., Croft, G.F., Saphier, G., Leibel, R., Goland, R., Wichterle, H., Henderson, C.E., Eggan, K., 2008. Induced pluripotent stem cells generated from patients with ALS can be differentiated into motor neurons. TL - 321. Science 321 VN-, 1218–1221. https://doi.org/10.1126/science.1158799
Ding, Q., Regan, S.N., Xia, Y., Oostrom, L.A., Cowan, C.A., Musunuru, K., 2013. Enhanced efficiency of human pluripotent stem cell genome editing through replacing TALENs with CRISPRs. Cell Stem Cell 12, 393–394. https://doi.org/10.1016/j.stem.2013.03.006
Dlouhy, B.J., Awe, O., Rao, R.C., Kirby, P.A., Hitchon, P.W., 2014. Autograft-derived spinal cord mass following olfactory mucosal cell transplantation in a spinal cord injury patient. J. Neurosurg. Spine 21, 618–622. https://doi.org/10.3171/2014.5.SPINE13992
Doddapaneni, R., Chawla, Y.K., Das, A., Kalra, J.K., Ghosh, S., Chakraborti, A., 2013. Overexpression of microRNA-122 enhances in vitro hepatic differentiation of fetal liver-derived stem/progenitor cells. J. Cell. Biochem. 114, 1575–1583. https://doi.org/10.1002/jcb.24499
Dunwoodie, S.L., 2009. The Role of Hypoxia in Development of the Mammalian Embryo. Dev. Cell 17, 755–773. https://doi.org/10.1016/j.devcel.2009.11.008
Eadie, L.N., Dang, P., Goyne, J.M., Hughes, T.P., White, D.L., 2018. ABCC6 plays a significant role in the transport of nilotinib and dasatinib, and contributes to TKI resistance in vitro, in both cell lines and primary patient mononuclear cells. PLoS One 13, e0192180. https://doi.org/10.1371/journal.pone.0192180
Ebert, A.D., Yu, J., Rose, F.F., Mattis, V.B., Lorson, C.L., Thomson, J.A., Svendsen, C.N., 2009. Induced pluripotent stem cells from a spinal muscular atrophy patient. Nature 457, 277–280. https://doi.org/10.1038/nature07677
Ejtehadifar, M., Shamsasenjan, K., Movassaghpour, A., Akbarzadehlaleh, P., Dehdilani, N., Abbasi, P., Molaeipour, Z., Saleh, M., 2015. The effect of hypoxia on mesenchymal stem cell biology. Adv. Pharm. Bull. 5, 141–149.

https://doi.org/10.15171/apb.2015.021
Elkayam, T., Amitay-Shaprut, S., Dvir-Ginzberg, M., Harel, T., Cohen, S., 2006. Enhancing the Drug Metabolism Activities of C3A— A Human Hepatocyte Cell Line—By Tissue Engineering Within Alginate Scaffolds. Tissue Eng. 12, 1357–1368. https://doi.org/10.1089/ten.2006.12.1357
Eltzschig, H.K., Abdulla, P., Hoffman, E., Hamilton, K.E., Daniels, D., Schönfeld, C., Löffler, M., Reyes, G., Duszenko, M., Karhausen, J., Robinson, A., Westerman, K.A., Coe, I.R., Colgan, S.P., 2005. HIF-1-dependent repression of equilibrative nucleoside transporter (ENT) in hypoxia. J. Exp. Med. 202, 1493–505. https://doi.org/10.1084/jem.20050177
Ezashi, T., Das, P., Roberts, R.M., 2005. Low O2 tensions and the prevention of differentiation of HES cells. Nat. Methods 2, 325. https://doi.org/10.1038/nmeth0505-325
Fey, S.J., Wrzesinski, K., 2012. Determination of drug toxicity using 3D spheroids constructed from an immortal human hepatocyte cell line. Toxicol. Sci. 127, 403–411. https://doi.org/10.1093/toxsci/kfs122
Finkbeiner, S.R., Zeng, X.L., Utama, B., Atmar, R.L., Shroyer, N.F., Estesa, M.K., 2012. Stem cell-derived human intestinal organoids as an infection model for rotaviruses. MBio 3, e00159. https://doi.org/10.1128/mBio.00159-12
Fontana, R.J., 2014. Pathogenesis of idiosyncratic drug-induced liver injury and clinical perspectives. Gastroenterology 146, 914–928.e1. https://doi.org/10.1053/j.gastro.2013.12.032
Forsyth, N.R., Musio, A., Vezzoni, P., Simpson, a H.R.W., Noble, B.S., McWhir, J., 2006. Physiologic oxygen enhances human embryonic stem cell clonal recovery and reduces chromosomal abnormalities. Cloning Stem Cells 8, 16–23. https://doi.org/10.1089/clo.2006.8.16
Friedman, J.R., Kaestner, K.H., 2006. The Foxa family of transcription factors in development and metabolism. Cell. Mol. Life Sci. 63, 2317–2328. https://doi.org/10.1007/s00018-006-6095-6
Fukuda, J., Sakai, Y., Nakazawa, K., 2006. Novel hepatocyte culture system developed using microfabrication and collagen/polyethylene glycol microcontact printing. Biomaterials 27, 1061–1070. https://doi.org/10.1016/j.biomaterials.2005.07.031
Gao, Y., Zhang, X., Zhang, L., Cen, J., Ni, X., Liao, X., Yang, C., Li, Y., Chen, X., Zhang, Z., Shu, Y., Cheng, X., Hay, D.C., Lai, D., Pan, G., Wei, G., Hui, L., 2017. Distinct Gene Expression and Epigenetic Signatures in Hepatocyte-like Cells Produced by Different Strategies from the Same Donor. Stem cell reports 9, 1813–1824. https://doi.org/10.1016/j.stemcr.2017.10.019
Gerets, H.H.J., Tilmant, K., Gerin, B., Chanteux, H., Depelchin, B.O., Dhalluin, S., Atienzar, F.A., 2012. Characterization of primary human hepatocytes, HepG2 cells, and HepaRG cells at the mRNA level and CYP activity in response to inducers and their predictivity for the detection of human hepatotoxins. Cell Biol. Toxicol. 28, 69–87. https://doi.org/10.1007/s10565-011-9208-4
Gieseck, R.L., Hannan, N.R.F., Bort, R., Hanley, N.A., Drake, R.A.L., Cameron, G.W.W., Wynn, T.A., Vallier, L., 2014. Maturation of induced pluripotent stem cell derived hepatocytes by 3D-culture. PLoS One 9, e86372. https://doi.org/10.1371/journal.pone.0086372
Glavinas, H., Krajcsi, P., Cserepes, J., Sarkadi, B., 2004. The role of ABC transporters in drug resistance, metabolism and toxicity. Curr. Drug Deliv. 1, 27–42.
Gonzalez, F., Boue, S., Izpisua Belmonte, J.C., 2011. Methods for making induced pluripotent stem cells: reprogramming a la carte. Nat Rev Genet 12, 231–242. https://doi.org/10.1038/nrg2937
Greenhough, S., Bradburn, H., Gardner, J., Hay, D.C., 2013. Development of an embryoid body-based screening strategy for assessing the hepatocyte differentiation potential

of human embryonic stem cells following single-cell dissociation. Cell. Reprogram. 15, 9–14. https://doi.org/10.1089/cell.2012.0049

Grompe, M., 2017. Fah knockout animals as models for therapeutic liver repopulation, in: Advances in Experimental Medicine and Biology. pp. 215–230. https://doi.org/10.1007/978-3-319-55780-9_20

Guo, C.W., Kawakatsu, M., Idemitsu, M., Urata, Y., Goto, S., Ono, Y., Hamano, K., Li, T.S., 2013. Culture under low physiological oxygen conditions improves the stemness and quality of induced pluripotent stem cells. J. Cell. Physiol. 228, 2159–2166. https://doi.org/10.1002/jcp.24389

Guo, L., Dial, S., Shi, L., Branham, W., Liu, J., Fang, J.L., Green, B., Deng, H., Kaput, J., Ning, B., 2011. Similarities and differences in the expression of drug-metabolizing enzymes between human hepatic cell lines and primary human hepatocytes. Drug Metab. Dispos. 39, 528–538. https://doi.org/10.1124/dmd.110.035873

Guo, R., Xu, X., Lu, Y., Xie, X., 2017. Physiological oxygen tension reduces hepatocyte dedifferentiation in in vitro culture. Sci. Rep. 7, 5923. https://doi.org/10.1038/s41598-017-06433-3

Gupta, S., Bhargava, K., Novikoff, P., 1999. Mechanisms of Cell Engraftment During Liver Repopulation with Hepatocyte Transplantation. Semin. Liver Dis. 19, 15–26. https://doi.org/10.1055/s-2007-1007094

Hackam, D.G., 2007. Translating animal research into clinical benefit. Br. Med. J. 334, 163–164. https://doi.org/10.1136/bmj.39104.362951.80

Hamazaki, T., Iiboshi, Y., Oka, M., Papst, P.J., Meacham, A.M., Zon, L.I., Terada, N., 2001. Hepatic maturation in differentiating embryonic stem cells in vitro. FEBS Lett. 497, 15–19. https://doi.org/10.1016/S0014-5793(01)02423-1

Hanahan, D., Weinberg, R.A., 2011. Hallmarks of cancer: The next generation. Cell. https://doi.org/10.1016/j.cell.2011.02.013

Hannan, N.R.F., Segeritz, C.-P., Touboul, T., Vallier, L., 2013. Production of hepatocyte-like cells from human pluripotent stem cells. Nat. Protoc. 8, 430–437. https://doi.org/10.1038/nprot.2012.153

Hasegawa, M., Kawai, K., Mitsui, T., Taniguchi, K., Monnai, M., Wakui, M., Ito, M., Suematsu, M., Peltz, G., Nakamura, M., Suemizu, H., 2011. The reconstituted "humanized liver" in TK-NOG mice is mature and functional. Biochem. Biophys. Res. Commun. 405, 405–410. https://doi.org/10.1016/j.bbrc.2011.01.042

Hendriks, D.F.G., Puigvert, L.F., Messner, S., Mortiz, W., Ingelman-Sundberg, M., 2016. Hepatic 3D spheroid models for the detection and study of compounds with cholestatic liability. Sci. Rep. 6, 35434. https://doi.org/10.1038/srep35434

Heslop, J.A., Kia, R., Pridgeon, C.S., Sison-Young, R.L., Liloglou, T., Elmasry, M., Fenwick, S.W., Mills, J.S., Kitteringham, N.R., Goldring, C.E., Park, B.K., 2017. Donor-dependent and other nondefined factors have greater influence on the hepatic phenotype than the starting cell type in induced pluripotent stem cell derived hepatocyte-like cells. Stem Cells Transl. Med. 6, 1321–1331. https://doi.org/10.1002/sctm.16-0029

Hodges, L.M., Markova, S.M., Chinn, L.W., Gow, J.M., Kroetz, D.L., Klein, T.E., Altman, R.B., 2011. Very important pharmacogene summary: ABCB1 (MDR1, P-glycoprotein). Pharmacogenet. Genomics 21, 152–161. https://doi.org/10.1097/FPC.0b013e3283385a1c

Holme, J.A., Jacobsen, D., 1986. MECHANISM OF PARACETAMOL TOXICITY. Lancet 327, 804–805. https://doi.org/10.1016/S0140-6736(86)91816-7

Hsu, D.C., Katelaris, C.H., 2009. Long-term management of patients taking immunosuppressive drugs. Aust. Prescr. https://doi.org/10.18773/austprescr.2009.035

Hu, H., Gehart, H., Artegiani, B., LÖpez-Iglesias, C., Dekkers, F., Basak, O., van Es, J., Chuva

de Sousa Lopes, S.M., Begthel, H., Korving, J., van den Born, M., Zou, C., Quirk, C., Chiriboga, L., Rice, C.M., Ma, S., Rios, A., Peters, P.J., de Jong, Y.P., Clevers, H., 2018. Long-Term Expansion of Functional Mouse and Human Hepatocytes as 3D Organoids. Cell 175, 1591–1606.e19. https://doi.org/10.1016/j.cell.2018.11.013

Huch, M., Dorrell, C., Boj, S.F., Van Es, J.H., Li, V.S.W., Van De Wetering, M., Sato, T., Hamer, K., Sasaki, N., Finegold, M.J., Haft, A., Vries, R.G., Grompe, M., Clevers, H., 2013. In vitro expansion of single Lgr5 + liver stem cells induced by Wnt-driven regeneration. Nature 494, 247–250. https://doi.org/10.1038/nature11826

Huch, M., Gehart, H., Van Boxtel, R., Hamer, K., Blokzijl, F., Verstegen, M.M.A., Ellis, E., Van Wenum, M., Fuchs, S.A., De Ligt, J., Van De Wetering, M., Sasaki, N., Boers, S.J., Kemperman, H., De Jonge, J., Ijzermans, J.N.M., Nieuwenhuis, E.E.S., Hoekstra, R., Strom, S., Vries, R.R.G., Van Der Laan, L.J.W., Cuppen, E., Clevers, H., 2015. Long-term culture of genome-stable bipotent stem cells from adult human liver. Cell 160, 299–312. https://doi.org/10.1016/j.cell.2014.11.050

Hussaini, S.H., Farrington, E.A., 2007. Idiosyncratic drug-induced liver injury: an overview. Expert Opin. Drug Saf. 6, 673–684. https://doi.org/10.1517/14740338.6.6.673

Hutchinson, L., Kirk, R., 2011. High drug attrition rates - Where are we going wrong? Nat. Rev. Clin. Oncol. 8, 189–190. https://doi.org/10.1038/nrclinonc.2011.34

Institute of Medicine and National Research Council, 2011. Chimpanzees in Biomedical and Behavioral Research, in: Altevogt, B.M., Pankevich, D.E., Shelton-Davenport, M.K., Kahn, J.P. (Eds.), Chimpanzees in Biomedical and Behavioral Research: Assessing the Necessity. National Academies Press (US), Washington (DC). https://doi.org/10.17226/13257

Itskovitz-Eldor, J., Schuldiner, M., Karsenti, D., Eden, a, Yanuka, O., Amit, M., Soreq, H., Benvenisty, N., 2000. Differentiation of human embryonic stem cells into embryoid bodies compromising the three embryonic germ layers. Mol. Med. 6, 88–95. https://doi.org/10859025

Iwano, S., Sugiyama, M., Hama, H., Watakabe, A., Hasegawa, N., Kuchimaru, T., Tanaka, K.Z., Takahashi, M., Ishida, Y., Hata, J., Shimozono, S., Namiki, K., Fukano, T., Kiyama, M., Okano, H., Kizaka-Kondoh, S., McHugh, T.J., Yamamori, T., Hioki, H., Maki, S., Miyawaki, A., 2018. Single-cell bioluminescence imaging of deep tissue in freely moving animals. Science (80-.). 359, 935–939. https://doi.org/10.1126/science.aaq1067

Jin, J., Xiong, Y., Cen, B., 2017. Bcl-2 and Bcl-xL mediate resistance to receptor tyrosine kinase-targeted therapy in lung and gastric cancer. Anticancer. Drugs 28, 1141–1149. https://doi.org/10.1097/CAD.0000000000000561

Jungermann, K., Kietzmann, T., 2000. Oxygen: Modulator of metabolic zonation and disease of the liver. Hepatology 31, 255–260. https://doi.org/10.1002/hep.510310201

Kamalian, L., Chadwick, A.E., Bayliss, M., French, N.S., Monshouwer, M., Snoeys, J., Park, B.K., 2015. The utility of HepG2 cells to identify direct mitochondrial dysfunction in the absence of cell death. Toxicol. Vitr. 29, 732–740. https://doi.org/10.1016/j.tiv.2015.02.011

Kamiike, W., Fujikawa, M., Koseki, M., Sumimura, J., Miyata, M., Kawashima, Y., Wada, H., Tagawa, K., 1989. Different patterns of leakage of cytosolic and mitochondrial enzymes. Clin. Chim. Acta 185, 265–270. https://doi.org/10.1016/0009-8981(89)90216-7

Karmen, A., Wroblewski, F., Ladue, J.S., 1955. Transaminase activity in human blood. J. Clin. Invest. 34, 126–131. https://doi.org/10.1172/JCI103055

Khetani, S.R., Bhatia, S.N., 2008. Microscale culture of human liver cells for drug development. Nat. Biotechnol. 26, 120–126. https://doi.org/10.1038/nbt1361

Kia, R., Kelly, L., Sison-Young, R.L.C., Zhang, F., Pridgeon, C.S., Heslop, J.A., Metcalfe, P.,

Kitteringham, N.R., Baxter, M., Harrison, S., Hanley, N.A., Burke, Z.D., Storm, M.P., Welham, M.J., Tosh, D., Küppers-Munther, B., Edsbagge, J., Starkey Lewis, P.J., Bonner, F., Harpur, E., Sidaway, J., Bowes, J., Fenwick, S.W., Malik, H., Goldring, C.E.P., Kevin Park, B., 2015. MicroRNA-122: A novel hepatocyte-enriched in vitro marker of drug-induced cellular toxicity. Toxicol. Sci. 144, 173–185. https://doi.org/10.1093/toxsci/kfu269

Kidambi, S., Yarmush, R.S., Novik, E., Chao, P., Yarmush, M.L., Nahmias, Y., 2009. Oxygen-mediated enhancement of primary hepatocyte metabolism, functional polarization, gene expression, and drug clearance. Proc. Natl. Acad. Sci. 106, 15714–15719. https://doi.org/10.1073/pnas.0906820106

Kietzmann, T., 2017. Metabolic zonation of the liver: The oxygen gradient revisited. Redox Biol. 11, 622–630. https://doi.org/10.1016/j.redox.2017.01.012

Kim, G.J., Rhee, H., Yoo, J.E., Ko, J.E., Lee, J.S., Kim, H., Choi, J.S., Park, Y.N., 2014. Increased expression of CCN2, epithelial membrane antigen, and fibroblast activation protein in hepatocellular carcinoma with fibrous stroma showing aggressive behavior. PLoS One 9, e105094. https://doi.org/10.1371/journal.pone.0105094

Kim, S.H., Naisbitt, D.J., 2016. Update on advances in research on idiosyncratic drug-induced liver injury. Allergy, Asthma Immunol. Res. 8, 3–11. https://doi.org/10.4168/aair.2016.8.1.3

Krahenbuhl, S., Talos, C., Fischer, S., Reichen, J., 1994. Toxicity of bile acids on the electron transport chain of isolated rat liver mitochondria. Hepatology 19, 471–479. https://doi.org/S027091399400039X [pii]

Kroemer, H.K., Eichelbaum, M., 1995. "It's the genes, stupid" Molecular bases and clinical consequences of genetic cytochrome P450 2D6 polymorphism. Life Sci. 56, 2285–2298. https://doi.org/10.1016/0024-3205(95)00223-S

Kumagai, A., Kondo, F., Sano, K., Inoue, M., Fujii, T., Hashimoto, M., Watanabe, M., Soejima, Y., Ishida, T., Tokairin, T., Saito, K., Sasajima, Y., Takahashi, Y., Uozaki, H., Fukusato, T., 2016. Immunohistochemical study of hepatocyte, cholangiocyte and stem cell markers of hepatocellular carcinoma: the second report: relationship with tumor size and cell differentiation. J. Hepatobiliary. Pancreat. Sci. 23, 414–21. https://doi.org/10.1002/jhbp.356

Labriet, A., Allain, E.P., Rouleau, M., Audet-Delage, Y., Villeneuve, L., Guillemette, C., 2018. Post-transcriptional Regulation of UGT2B10 Hepatic Expression and Activity by Alternative Splicing. Drug Metab. Dispos. 46, 514–524. https://doi.org/10.1124/dmd.117.079921

Lam, M.T., Longaker, M.T., 2012. Comparison of several attachment methods for human iPS, embryonic and adipose-derived stem cells for tissue engineering. J. Tissue Eng. Regen. Med. 6. https://doi.org/10.1002/term.1499

Lan, S.F., Starly, B., 2011. Alginate based 3D hydrogels as an in vitro co-culture model platform for the toxicity screening of new chemical entities. Toxicol. Appl. Pharmacol. 256, 62–72. https://doi.org/10.1016/j.taap.2011.07.013

Lancaster, M.A., Renner, M., Martin, C.-A., Wenzel, D., Bicknell, L.S., Hurles, M.E., Homfray, T., Penninger, J.M., Jackson, A.P., Knoblich, J.A., 2013. Cerebral organoids model human brain development and microcephaly. Nature 501, 373–379. https://doi.org/10.1038/nature12517

Langman, L., Van Gelder, T., Van Schaik, R.H.N., 2015. Pharmacogenomics Aspect of Immunosuppressant Therapy. Pers. Immunosuppr. Transplant. Role Biomark. Monit. Ther. Drug Monit. 109–124. https://doi.org/10.1016/B978-0-12-800885-0.00005-9

Larbcharoensub, N., Sornmayura, P., Sirachainan, E., Wilasrusmee, C., Wanmoung, H., Janvilisri, T., 2011. Prognostic value of ABCG2 in moderately and poorly differentiated intrahepatic cholangiocarcinoma. Histopathology 59, 235–246.

https://doi.org/10.1111/j.1365-2559.2011.03935.x

Larson, A.M., Polson, J., Fontana, R.J., Davern, T.J., Lalani, E., Hynan, L.S., Reisch, J.S., Schiødt, F. V., Ostapowicz, G., Shakil, A.O., Lee, W.M., 2005. Acetaminophen-induced acute liver failure: Results of a United States multicenter, prospective study. Hepatology 42, 1364–1372. https://doi.org/10.1002/hep.20948

Lauschke, V.M., Vorrink, S.U., Moro, S.M.L., Rezayee, F., Nordling, Å., Hendriks, D.F.G., Bell, C.C., Sison-Young, R., Park, B.K., Goldring, C.E., Ellis, E., Johansson, I., Mkrtchian, S., Andersson, T.B., Ingelman-Sundberg, M., 2016. Massive rearrangements of cellular MicroRNA signatures are key drivers of hepatocyte dedifferentiation. Hepatology 64, 1743–1756. https://doi.org/10.1002/hep.28780

Lazarou, J., Pomeranz, B.H., Corey, P.N., 1998. Incidence of Adverse Drug Reactions in Hospitalized Patients. Jama 279, 1200. https://doi.org/10.1001/jama.279.15.1200

Leclerc, E., Kimura, K., Shinohara, M., Danoy, M., Le Gall, M., Kido, T., Miyajima, A., Fujii, T., Sakai, Y., 2017. Comparison of the transcriptomic profile of hepatic human induced pluripotent stem like cells cultured in plates and in a 3D microscale dynamic environment. Genomics 109, 16–26. https://doi.org/10.1016/j.ygeno.2016.11.008

Lee, S.-A., No, D.Y., Kang, E., Ju, J., Kim, D.-S., Lee, S.-H., 2013. Spheroid-based three-dimensional liver-on-a-chip to investigate hepatocyte–hepatic stellate cell interactions and flow effects. Lab Chip 13, 3529. https://doi.org/10.1039/c3lc50197c

Leong, C.-F., Raudhawati, O., Cheong, S.-K., Sivagengei, K., Noor Hamidah, H., 2003. Epithelial membrane antigen (EMA) or MUC1 expression in monocytes and monoblasts. Pathology 35, 422–7.

Leuthold, S., Hagenbuch, B., Mohebbi, N., Wagner, C.A., Meier, P.J., Stieger, B., 2008. Mechanisms of pH-gradient driven transport mediated by organic anion polypeptide transporters. AJP Cell Physiol. 296, C570–C582. https://doi.org/10.1152/ajpcell.00436.2008

Li, S., Guo, J., Ying, Z., Chen, S., Yang, L., Chen, K., Long, Q., Qin, D., Pei, D., Liu, X., 2015. Valproic acid-induced hepatotoxicity in alpers syndrome is associated with mitochondrial permeability transition pore opening-dependent apoptotic sensitivity in an induced pluripotent stem cell model. Hepatology 61, 1730–1739. https://doi.org/10.1002/hep.27712

Li, Y., Lindsay, J., Wang, L.-L., Zhou, S.-F., 2008. Structure, Function and Polymorphism of Human Cytosolic Sulfotransferases. Curr. Drug Metab. 9, 99–105. https://doi.org/10.2174/138920008783571819

Liu, H., Radisky, D.C., Wang, F., Bissell, M.J., 2004. Polarity and proliferation are controlled by distinct signaling pathways downstream of PI3-kinase in breast epithelial tumor cells. J. Cell Biol. 164, 603–612. https://doi.org/10.1083/jcb.200306090

Livak, K.J., Schmittgen, T.D., 2001. Analysis of relative gene expression data using real-time quantitative PCR and the 2-ΔΔCT method. Methods 25, 402–408. https://doi.org/10.1006/meth.2001.1262

Lo, B., Parham, L., 2009. Ethical issues in stem cell research. Endocr. Rev. 30, 204–213. https://doi.org/10.1210/er.2008-0031

Louie, S.M., Grossman, E.A., Crawford, L.A., Ding, L., Camarda, R., Huffman, T.R., Miyamoto, D.K., Goga, A., Weerapana, E., Nomura, D.K., 2016. GSTP1 Is a Driver of Triple-Negative Breast Cancer Cell Metabolism and Pathogenicity. Cell Chem. Biol. 23, 567–578. https://doi.org/10.1016/j.chembiol.2016.03.017

Madden, D., 2006. Body Mass Index and the Measurement of Obesity. HEDG Work. Pap.

Majmundar, A.J., Wong, W.J., Simon, M.C., 2010. Hypoxia-Inducible Factors and the Response to Hypoxic Stress. Mol. Cell 40, 294–309. https://doi.org/10.1016/j.molcel.2010.09.022

March, S., Ramanan, V., Trehan, K., Ng, S., Galstian, A., Gural, N., Scull, M.A., Shlomai, A.,

Mota, M.M., Fleming, H.E., Khetani, S.R., Rice, C.M., Bhatia, S.N., 2015. Micropatterned coculture of primary human hepatocytes and supportive cells for the study of hepatotropic pathogens. Nat. Protoc. 10, 2027–2053. https://doi.org/10.1038/nprot.2015.128

Marek, C.J., Tucker, S.J., Koruth, M., Wallace, K., Wright, M.C., 2007. Expression of CYP2S1 in human hepatic stellate cells. FEBS Lett. 581, 781–786. https://doi.org/10.1016/j.febslet.2007.01.056

Martignano, F., Gurioli, G., Salvi, S., Calistri, D., Costantini, M., Gunelli, R., De Giorgi, U., Foca, F., Casadio, V., 2016. GSTP1 Methylation and Protein Expression in Prostate Cancer: Diagnostic Implications. Dis. Markers 2016, 1–6. https://doi.org/10.1155/2016/4358292

Martin, A.M., Nolan, D., Gaudieri, S., Almeida, C.A., Nolan, R., James, I., Carvalho, F., Phillips, E., Christiansen, F.T., Purcell, A.W., McCluskey, J., Mallal, S., 2004. Predisposition to abacavir hypersensitivity conferred by HLA-B*5701 and a haplotypic Hsp70-Hom variant. Proc. Natl. Acad. Sci. U. S. A. 101, 4180–4185. https://doi.org/10.1073/pnas.0307067101

Martin, L.J., Lau, E., Singh, H., Vergnes, L., Tarling, E.J., Mehrabian, M., Mungrue, I., Xiao, S., Shih, D., Castellani, L., Ping, P., Reue, K., Stefani, E., Drake, T.A., Bostrom, K., Lusis, A.J., 2012. ABCC6 localizes to the mitochondria-associated membrane. Circ. Res. 111, 516–520. https://doi.org/10.1161/CIRCRESAHA.112.276667

Mathur, A., Loskill, P., Shao, K., Huebsch, N., Hong, S.G., Marcus, S.G., Marks, N., Mandegar, M., Conklin, B.R., Lee, L.P., Healy, K.E., 2015. Human iPSC-based cardiac microphysiological system for drug screening applications. Sci. Rep. 5, 8883. https://doi.org/10.1038/srep08883

Matsukuma, S., Takeo, H., Kono, T., Nagata, Y., Sato, K., 2012. Aberrant cytokeratin 7 expression of centrilobular hepatocytes: A clinicopathological study. Histopathology 61, 857–862. https://doi.org/10.1111/j.1365-2559.2012.04278.x

McGill, M.R., 2016. The past and present of serum aminotransferases and the future of liver injury biomarkers. EXCLI J. 15, 817–828. https://doi.org/10.17179/excli2016-800

McKenzie, R., Fried, M.W., Sallie, R., Conjeevaram, H., Di Bisceglie, A.M., Park, Y., Savarese, B., Kleiner, D., Tsokos, M., Luciano, C., 1995. Hepatic failure and lactic acidosis due to fialuridine (FIAU), an investigational nucleoside analogue for chronic hepatitis B. N. Engl. J. Med. 333, 1099–1105. https://doi.org/10.1056/NEJM199510263331702

McPhalen, C.A., Vincent, M.G., Picot, D., Jansonius, J.N., Lesk, A.M., Chothia, C., 1992. Domain closure in mitochondrial aspartate aminotransferase. J. Mol. Biol. 227, 197–213. https://doi.org/10.1016/0022-2836(92)90691-C

Medine, C.N., Lucendo-Villarin, B., Zhou, W., West, C.C., Hay, D.C., 2011. Robust Generation of Hepatocyte-like Cells from Human Embryonic Stem Cell Populations. J. Vis. Exp. e2969–e2969. https://doi.org/10.3791/2969

Meier, Y., Cavallaro, M., Roos, M., Pauli-Magnus, C., Folkers, G., Meier, P.J., Fattinger, K., 2005. Incidence of drug-i'nduced liver injury in medical inpatients. Eur. J. Clin. Pharmacol. 61, 135–143. https://doi.org/10.1007/s00228-004-0888-z

Miyazaki, T., Futaki, S., Hasegawa, K., Kawasaki, M., Sanzen, N., Hayashi, M., Kawase, E., Sekiguchi, K., Nakatsuji, N., Suemori, H., 2008. Recombinant human laminin isoforms can support the undifferentiated growth of human embryonic stem cells. Biochem. Biophys. Res. Commun. 375, 27–32. https://doi.org/10.1016/j.bbrc.2008.07.111

Mobasheri, A., Richardson, S., Mobasheri, R., Shakibaei, M., Hoyland, J.A., 2005. Hypoxia inducible factor-1 and facilitative glucose transporters GLUT1 and GLUT3: putative molecular components of the oxygen and glucose sensing apparatus in articular chondrocytes. Histol. Histopathol. 20, 1327–38. https://doi.org/10.14670/HH-20.1327

Moore, N., 2016. Lessons from the fatal french study BIA-10-2474. BMJ 353, i2727.

https://doi.org/10.1136/bmj.i2727
Musunuru, K., 2013. Genome editing of human pluripotent stem cells to generate human cellular disease models. Dis. Model. Mech. 6, 896–904. https://doi.org/10.1242/dmm.012054
Mutter, F.E., Park, B.K., Copple, I.M., 2015. Value of monitoring Nrf2 activity for the detection of chemical and oxidative stress. Biochem. Soc. Trans. 43, 657–662. https://doi.org/10.1042/bst20150044
Nagamoto, Y., Tashiro, K., Takayama, K., Ohashi, K., Kawabata, K., Sakurai, F., Tachibana, M., Hayakawa, T., Furue, M.K., Mizuguchi, H., 2012. The promotion of hepatic maturation of human pluripotent stem cells in 3D co-culture using type I collagen and Swiss 3T3 cell sheets. Biomaterials 33, 4526–4534. https://doi.org/10.1016/j.biomaterials.2012.03.011
Nakajima, T., Takayama, T., Miyanishi, K., Nobuoka, A., Hayashi, T., Abe, T., Kato, J., Sakon, K., Naniwa, Y., Tanabe, H., Niitsu, Y., 2003. Reversal of multiple drug resistance in cholangiocarcinoma by the glutathione S-transferase-pi-specific inhibitor O1-hexadecyl-gamma-glutamyl-S-benzylcysteinyl-D-phenylglycine ethylester. J. Pharmacol. Exp. Ther. 306, 861–9. https://doi.org/10.1124/jpet.103.052696
Nguyen, H.N., Byers, B., Cord, B., Shcheglovitov, A., Byrne, J., Gujar, P., Kee, K., Schüle, B., Dolmetsch, R.E., Langston, W., Palmer, T.D., Pera, R.R., 2011. LRRK2 mutant iPSC-derived da neurons demonstrate increased susceptibility to oxidative stress. Cell Stem Cell 8, 267–280. https://doi.org/10.1016/j.stem.2011.01.013
Nguyen, H.T., Geens, M., Mertzanidou, A., Jacobs, K., Heirman, C., Breckpot, K., Spits, C., 2014. Gain of 20q11.21 in human embryonic stem cells improves cell survival by increased expression of Bcl-xL. Mol. Hum. Reprod. 20, 168–177. https://doi.org/10.1093/molehr/gat077
Nguyen, H.T., Geens, M., Spits, C., 2013. Genetic and epigenetic instability in human pluripotent stem cells. Hum. Reprod. Update. https://doi.org/10.1093/humupd/dms048
Nicolas, C.T., Hickey, R.D., Chen, H.S., Mao, S.A., Lopera Higuita, M., Wang, Y., Nyberg, S.L., 2017. Concise Review: Liver Regenerative Medicine: From Hepatocyte Transplantation to Bioartificial Livers and Bioengineered Grafts. Stem Cells 35, 42–50. https://doi.org/10.1002/stem.2500
Nicolas, C.T., Wang, Y., Nyberg, S.L., 2016. Cell therapy in chronic liver disease. Curr. Opin. Gastroenterol. https://doi.org/10.1097/MOG.0000000000000262
Nicoletti, P., Werk, A.N., Sawle, A., Shen, Y., Urban, T.J., Coulthard, S.A., Bjornsson, E.S., Cascorbi, I., Floratos, A., Stammschulte, T., Gundert-Remy, U., Nelson, M.R., Aithal, G.P., Daly, A.K., 2016. Hla-Drb1*16. Pharmacogenet. Genomics 26, 218–224. https://doi.org/10.1097/FPC.0000000000000209
Nyblom, H., Berggren, U., Balldin, J., Olsson, R., 2004. High AST/ALT ratio may indicate advanced alcoholic liver disease rather than heavy drinking. Alcohol Alcohol. 39, 336–339. https://doi.org/10.1093/alcalc/agh074
O'Grady, J.G., 2005. Acute liver failure. Postgrad. Med. J. 81, 148–154. https://doi.org/10.1136/pgmj.2004.026005
Obokata, H., Sasai, Y., Niwa, H., Kadota, M., Andrabi, M., Takata, N., Tokoro, M., Terashita, Y., Yonemura, S., Vacanti, C.A., Wakayama, T., 2014a. Bidirectional developmental potential in reprogrammed cells with acquired pluripotency. Nature 505, 676–680. https://doi.org/10.1038/nature12969
Obokata, H., Wakayama, T., Sasai, Y., Kojima, K., Vacanti, M.P., Niwa, H., Yamato, M., Vacanti, C.A., 2014b. Stimulus-triggered fate conversion of somatic cells into pluripotency. Nature 505, 641–647. https://doi.org/10.1038/nature12968
Oh, E.T., Park, H.J., 2015. Implications of NQO1 in cancer therapy. BMB Rep. 48, 609–617.

https://doi.org/10.5483/BMBRep.2015.48.11.190
Ohkura, T., Ohta, K., Nagao, T., Kusumoto, K., Koeda, A., Ueda, T., Jomura, T., Ikeya, T., Ozeki, E., Wada, K., Naitoh, K., Inoue, Y., Takahashi, N., Iwai, H., Arakawa, H., Ogihara, T., 2014. Evaluation of Human Hepatocytes Cultured by Three-dimensional Spheroid Systems for Drug Metabolism. Drug Metab. Pharmacokinet. 29, 373–378. https://doi.org/10.2133/dmpk.DMPK-13-RG-105
Onakpoya, I.J., Heneghan, C.J., Aronson, J.K., 2016. Post-marketing withdrawal of 462 medicinal products because of adverse drug reactions: A systematic review of the world literature. BMC Med. 14, 10. https://doi.org/10.1186/s12916-016-0553-2
Ostapowicz, G., 2002. Results of a Prospective Study of Acute Liver Failure at 17 Tertiary Care Centers in the United States. Ann. Intern. Med. 137, 947. https://doi.org/10.7326/0003-4819-137-12-200212170-00007
Otsuka, H., Hirano, A., Nagasaki, Y., Okano, T., Horiike, Y., Kataoka, K., 2004. Two-dimensional multiarray formation of hepatocyte spheroids on a microfabricated PEG-brush surface. ChemBioChem 5, 850–855. https://doi.org/10.1002/cbic.200300822
Pal, R., Mamidi, M.K., Das, A.K., Bhonde, R., 2012. Diverse effects of dimethyl sulfoxide (DMSO) on the differentiation potential of human embryonic stem cells. Arch. Toxicol. 86, 651–661. https://doi.org/10.1007/s00204-011-0782-2
Payne, C.M., Samuel, K., Pryde, A., King, J., Brownstein, D., Schrader, J., Medine, C.N., Forbes, S.J., Iredale, J.P., Newsome, P.N., Hay, D.C., 2011. Persistence of functional hepatocyte-like cells in immune-compromised mice. Liver Int. 31, 254–262. https://doi.org/10.1111/j.1478-3231.2010.02414.x
Peracchi, A., Veiga-da-Cunha, M., Kuhara, T., Ellens, K.W., Paczia, N., Stroobant, V., Seliga, A.K., Marlaire, S., Jaisson, S., Bommer, G.T., Sun, J., Huebner, K., Linster, C.L., Cooper, A.J.L., Van Schaftingen, E., 2017. Nit1 is a metabolite repair enzyme that hydrolyzes deaminated glutathione. Proc. Natl. Acad. Sci. 114, E3233–E3242. https://doi.org/10.1073/pnas.1613736114
Perland, E., Fredriksson, R., 2017. Classification Systems of Secondary Active Transporters. Trends Pharmacol. Sci. 38, 305–315. https://doi.org/10.1016/j.tips.2016.11.008
Pettinato, G., Ramanathan, R., Fisher, R.A., Mangino, M.J., Zhang, N., Wen, X., 2016. Scalable Differentiation of Human iPSCs in a Multicellular Spheroid-based 3D Culture into Hepatocyte-like Cells through Direct Wnt/β-catenin Pathway Inhibition. Sci. Rep. 6, 32888. https://doi.org/10.1038/srep32888
Pirmohamed, M., 2004. Adverse drug reactions as cause of admission to hospital: prospective analysis of 18 820 patients. Bmj 329, 15–19. https://doi.org/10.1136/bmj.329.7456.15
Place, T.L., Domann, F.E., Case, A.J., 2017. Limitations of oxygen delivery to cells in culture: An underappreciated problem in basic and translational research. Free Radic. Biol. Med. 113, 311–322. https://doi.org/10.1016/j.freeradbiomed.2017.10.003
Prasad, S.M., Czepiel, M., Cetinkaya, C., Smigielska, K., Weli, S.C., Lysdahl, H., Gabrielsen, A., Petersen, K., Ehlers, N., Fink, T., Minger, S.L., Zachar, V., 2009. Continuous hypoxic culturing maintains activation of Notch and allows long-term propagation of human embryonic stem cells without spontaneous differentiation. Cell Prolif. 42, 63–74. https://doi.org/10.1111/j.1365-2184.2008.00571.x
Prasajak, P., Leeanansaksiri, W., 2013. Developing a New Two-Step Protocol to Generate Functional Hepatocytes from Wharton's Jelly-Derived Mesenchymal Stem Cells under Hypoxic Condition. Stem Cells Int. 2013, 1–10. https://doi.org/10.1155/2013/762196
Raghunath, A., Sundarraj, K., Arfuso, F., Sethi, G., Perumal, E., 2018. Dysregulation of Nrf2 in Hepatocellular Carcinoma: Role in Cancer Progression and Chemoresistance. Cancers (Basel). 10, 481. https://doi.org/10.3390/cancers10120481
Ramachandran, A., Jaeschke, H., 2018. Acetaminophen toxicity: Novel insights into

mechanisms and future perspectives. Gene Expr. 18, 19–30. https://doi.org/10.3727/105221617X15084371374138

Ramaiahgari, S.C., Den Braver, M.W., Herpers, B., Terpstra, V., Commandeur, J.N.M., Van De Water, B., Price, L.S., 2014. A 3D in vitro model of differentiated HepG2 cell spheroids with improved liver-like properties for repeated dose high-throughput toxicity studies. Arch. Toxicol. 88, 1083–1095. https://doi.org/10.1007/s00204-014-1215-9

Ramasamy, T.S., Yu, J.S.L., Selden, C., Hodgson, H., Cui, W., 2013. Application of Three-Dimensional Culture Conditions to Human Embryonic Stem Cell-Derived Definitive Endoderm Cells Enhances Hepatocyte Differentiation and Functionality. Tissue Eng. Part A 19, 360–367. https://doi.org/10.1089/ten.tea.2012.0190

Rambhatla, L., Chiu, C.P., Kundu, P., Peng, Y., Carpenter, M.K., 2003. Generation of hepatocyte-like cells from human embryonic stem cells. Cell Transpl. 12, 1–11. https://doi.org/10.3727/000000003783985179

Raya, Á., Rodríguez-Piz, I., Guenechea, G., Vassena, R., Navarro, S., Barrero, M.J., Consiglio, A., Castell, M., Río, P., Sleep, E., González, F., Tiscornia, G., Garreta, E., Aasen, T., Veiga, A., Verma, I.M., Surrallés, J., Bueren, J., Belmonte, J.C.I., 2009. Disease-corrected haematopoietic progenitors from Fanconi anaemia induced pluripotent stem cells. Nature 460, 53–59. https://doi.org/10.1038/nature08129

Recknagel, R.O., 1967. Carbon Tetrachloride Hepatotoxicity. Pharmacol. Rev. 19, 145–208.

Reinhardt, P., Schmid, B., Burbulla, L.F., Schöndorf, D.C., Wagner, L., Glatza, M., Höing, S., Hargus, G., Heck, S.A., Dhingra, A., Wu, G., Müller, S., Brockmann, K., Kluba, T., Maisel, M., Krüger, R., Berg, D., Tsytsyura, Y., Thiel, C.S., Psathaki, O.E., Klingauf, J., Kuhlmann, T., Klewin, M., Müller, H., Gasser, T., Schöler, H.R., Sterneckert, J., 2013. Genetic correction of a lrrk2 mutation in human iPSCs links parkinsonian neurodegeneration to ERK-dependent changes in gene expression. Cell Stem Cell 12, 354–367. https://doi.org/10.1016/j.stem.2013.01.008

Reuben, A., Koch, D.G., Lee, W.M., 2010. Drug-induced acute liver failure: Results of a U.S. multicenter, prospective study. Hepatology 52, 2065–2076. https://doi.org/10.1002/hep.23937

Rivera, S.P., Wang, F., Saarikoski, S.T., Taylor, R.T., Chapman, B., Zhang, R., Hankinson, O., 2007. A novel promoter element containing multiple overlapping xenobiotic and hypoxia response elements mediates induction of cytochrome P4502S1 by both dioxin and hypoxia. J. Biol. Chem. 282, 10881–10893. https://doi.org/10.1074/jbc.M609617200

Rodin, S., Antonsson, L., Niaudet, C., Simonson, O.E., Salmela, E., Hansson, E.M., Domogatskaya, A., Xiao, Z., Damdimopoulou, P., Sheikhi, M., Inzunza, J., Nilsson, A.S., Baker, D., Kuiper, R., Sun, Y., Blennow, E., Nordenskj??ld, M., Grinnemo, K.H., Kere, J., Betsholtz, C., Hovatta, O., Tryggvason, K., 2014. Clonal culturing of human embryonic stem cells on laminin-521/E-cadherin matrix in defined and xeno-free environment. Nat. Commun. 5, 3195. https://doi.org/10.1038/ncomms4195

Rodin, S., Domogatskaya, A., Ström, S., Hansson, E.M., Chien, K.R., Inzunza, J., Hovatta, O., Tryggvason, K., 2010. Long-term self-renewal of human pluripotent stem cells on human recombinant laminin-511. Nat. Biotechnol. 28, 611–615. https://doi.org/10.1038/nbt.1620

Roschger, C., Cabrele, C., 2017. The Id-protein family in developmental and cancer-associated pathways Fritz Aberger. Cell Commun. Signal. 15. https://doi.org/10.1186/s12964-016-0161-y

Rose, J.B., Naydenova, Z., Bang, A., Eguchi, M., Sweeney, G., Choi, D.-S., Hammond, J.R., Coe, I.R., 2010. Equilibrative nucleoside transporter 1 plays an essential role in cardioprotection. Am. J. Physiol. Circ. Physiol. 298, H771–H777.

https://doi.org/10.1152/ajpheart.00711.2009
Rose, K.A., Holman, N.S., Green, A.M., Andersen, M.E., LeCluyse, E.L., 2016. Co-culture of Hepatocytes and Kupffer Cells as an In Vitro Model of Inflammation and Drug-Induced Hepatotoxicity. J. Pharm. Sci. 105, 950–964. https://doi.org/10.1016/S0022-3549(15)00192-6
Roth, A., Singer, T., 2014. The application of 3D cell models to support drug safety assessment: Opportunities & challenges. Adv. Drug Deliv. Rev. 69–70, 179–189. https://doi.org/10.1016/j.addr.2013.12.005
Rowe, C., Gerrard, D.T., Jenkins, R., Berry, A., Durkin, K., Sundstrom, L., Goldring, C.E., Park, B.K., Kitteringham, N.R., Hanley, K.P., Hanley, N.A., 2013. Proteome-wide analyses of human hepatocytes during differentiation and dedifferentiation. Hepatology 58, 799–809. https://doi.org/10.1002/hep.26414
Rowe, C., Taylor, I., Large, E., Cornforth, T., Robinson, A., Sceats, E., Hughes, D., 2014a. LiverChip ™ supports enhanced maturation of hepatocyte-like cells from human induced pluripotent stem cells . CN Bio Innov. Ltd. 1–8.
Rowe, C., Taylor, I., Large, E., Cornforth, T., Sceats, E., Hughes, D., Bio, C.N., 2014b. LiverChip TM identifies compounds with different mechanisms of toxicity and has utility as a predictive tool for drug development . 8.
Rowland, A., Miners, J.O., Mackenzie, P.I., 2013. The UDP-glucuronosyltransferases: Their role in drug metabolism and detoxification. Int. J. Biochem. Cell Biol. 45, 1121–1132. https://doi.org/10.1016/j.biocel.2013.02.019
Rowland, T.J., Miller, L.M., Blaschke, A.J., Doss, E.L., Bonham, A.J., Hikita, S.T., Johnson, L. V., Clegg, D.O., 2010. Roles of Integrins in Human Induced Pluripotent Stem Cell Growth on Matrigel and Vitronectin. Stem Cells Dev. 19, 1231–1240. https://doi.org/10.1089/scd.2009.0328
Russell, W., Burch, K., 1992. The principles of humane experimental technique., UFAW, London. Methuen London, London: Methuen & Co. Ltd.
Saarikoski, S.T., Rivera, S.P., Hankinson, O., Husgafvel-Pursiainen, K., 2005. CYP2S1: A short review. Toxicol. Appl. Pharmacol. 207, 62–69. https://doi.org/10.1016/j.taap.2004.12.027
Saffron, M.K., 1975. Antivivisection and Medical Science in Victorian Society, History: Reviews of New Books. https://doi.org/10.1080/03612759.1975.9945058
Sato, T., Vries, R.G., Snippert, H.J., Van De Wetering, M., Barker, N., Stange, D.E., Van Es, J.H., Abo, A., Kujala, P., Peters, P.J., Clevers, H., 2009. Single Lgr5 stem cells build crypt-villus structures in vitro without a mesenchymal niche. Nature 459, 262–265. https://doi.org/10.1038/nature07935
Satoh, K., Itoh, K., Yamamoto, M., Tanaka, M., Hayakari, M., Ookawa, K., Yamazaki, T., Sato , T., Tsuchida, S., Hatayama, I., 2002. Nrf2 transactivator-independent GSTP1-1 expression in "GSTP1-1 positive" single cells inducible in female mouse liver by DEN: A preneoplastic character of possible initiated cells. Carcinogenesis 23, 457–462. https://doi.org/10.1093/carcin/23.3.457
Sawers, L., Ferguson, M.J., Ihrig, B.R., Young, H.C., Chakravarty, P., Wolf, C.R., Smith, G., 2014. Glutathione S-transferase P1 (GSTP1) directly influences platinum drug chemosensitivity in ovarian tumour cell lines. Br. J. Cancer 111, 1150–1158. https://doi.org/10.1038/bjc.2014.386
Scheffer, G.L., Wijngaard, P.L., Flens, M.J., Izquierdo, M.A., Slovak, M.L., Pinedo, H.M., Meijer, C.J., Clevers, H.C., Scheper, R.J., 1995. The drug resistance-related protein LRP is the human major vault protein. Nat. Med. 1, 578–82.
Schepers, A., Li, C., Chhabra, A., Seney, B.T., Bhatia, S., 2016. Engineering a perfusable 3D human liver platform from iPS cells. Lab Chip 16, 2644–2653. https://doi.org/10.1039/C6LC00598E

Schneider, C.A., Rasband, W.S., Eliceiri, K.W., 2012. NIH Image to ImageJ: 25 years of image analysis. Nat. Methods 9, 671–675. https://doi.org/10.1038/nmeth.2089

Schönenberger, M.J., 2015. Hypoxia signaling pathways: modulators of oxygen-related organelles. Front. Cell Dev. Biol. 3. https://doi.org/10.3389/fcell.2015.00042

Schwanhüusser, B., Busse, D., Li, N., Dittmar, G., Schuchhardt, J., Wolf, J., Chen, W., Selbach, M., 2011. Global quantification of mammalian gene expression control. Nature 473, 337–342. https://doi.org/10.1038/nature10098

Schwartz, R.E., Linehan, J.L., Painschab, M.S., Hu, W.S., Verfaillie, C.M., Kaufman, D.S., 2005. Defined conditions for development of functional hepatic cells from human embryonic stem cells. Stem Cells Dev 14, 643–655. https://doi.org/10.1089/scd.2005.14.643

Sekine, S., Ogawa, R., Mcmanus, M.T., Kanai, Y., Hebrok, M., 2009. Dicer is required for proper liver zonation. J. Pathol. 219, 365–372. https://doi.org/10.1002/path.2606

Sgro, C., Clinard, F., Ouazir, K., Chanay, H., Allard, C., Guilleminet, C., Lenoir, C., Lemoine, A., Hillon, P., 2002. Incidence of drug-induced hepatic injuries: A French population-based study. Hepatology 36, 451–455. https://doi.org/10.1053/jhep.2002.34857

Shafa, M., Sjonnesen, K., Yamashita, A., Liu, S., Michalak, M., Kallos, M.S., Rancourt, D.E., 2012. Expansion and long-term maintenance of induced pluripotent stem cells in stirred suspension bioreactors. J. Tissue Eng. Regen. Med. 6, 462–472. https://doi.org/10.1002/term.450

Shan, J., Schwartz, R.E., Ross, N.T., Logan, D.J., Thomas, D., Duncan, S.A., North, T.E., Goessling, W., Carpenter, A.E., Bhatia, S.N., 2013. Identification of small molecules for human hepatocyte expansion and iPS differentiation. Nat. Chem. Biol. 9, 514–520. https://doi.org/10.1038/nchembio.1270

Sharma, B.K., Kolhe, R., Black, S.M., Keller, J.R., Mivechi, N.F., Satyanarayana, A., 2016. Inhibitor of differentiation 1 transcription factor promotes metabolic reprogramming in hepatocellular carcinoma cells. FASEB J. 30, 262–275. https://doi.org/10.1096/fj.15-277749

Shen, M.M., 2007. Nodal signaling: developmental roles and regulation. Development 134, 1023–1034. https://doi.org/10.1242/dev.000166

Shibuya, M., Kondo, F., Sano, K., Takada, T., Asano, T., 2011. Immunohistochemical study of hepatocyte, cholangiocyte and stem cell markers of hepatocellular carcinoma. J. Hepatobiliary. Pancreat. Sci. 18, 537–543. https://doi.org/10.1007/s00534-010-0365-2

Shin, S.M., Yang, J.H., Ki, S.H., 2013. Role of the Nrf2-ARE Pathway in Liver Diseases. Oxid. Med. Cell. Longev. 2013, 1–9. https://doi.org/10.1155/2013/763257

Shirahashi, H., Wu, J., Yamamoto, N., Catana, A., Wege, H., Wager, B., Okita, K., Zern, M.A., 2004. Differentiation of human and mouse embryonic stem cells along a hepatocyte lineage. Cell Transpl. 13, 197–211. https://doi.org/10.3727/000000004783984016

Shu, C.-W., Su, H.-H., Wu, T.T.-L., Hsu, C.-W., Chen, Y.-C., Pan, H.-W., Huang, G.-J., 2017. Targeting TPX2 Suppresses the Tumorigenesis of Hepatocellular Carcinoma Cells Resulting in Arrested Mitotic Phase Progression and Increased Genomic Instability. J. Cancer 8, 1378–1394. https://doi.org/10.7150/jca.17478

Shultz, L.D., Lyons, B.L., Burzenski, L.M., Gott, B., Chen, X., Chaleff, S., Kotb, M., Gillies, S.D., King, M., Mangada, J., Greiner, D.L., Handgretinger, R., 2005. Human Lymphoid and Myeloid Cell Development in NOD/LtSz-scid IL2R γ null Mice Engrafted with Mobilized Human Hemopoietic Stem Cells. J. Immunol. 174, 6477–6489. https://doi.org/10.4049/jimmunol.174.10.6477

Si-Tayeb, K., Noto, F.K., Nagaoka, M., Li, J., Battle, M.A., Duris, C., North, P.E., Dalton, S., Duncan, S.A., 2010. Highly efficient generation of human hepatocyte-like cells from induced pluripotent stem cells. Hepatology 51, 297–305. https://doi.org/10.1002/hep.23354

Siegel, D., Yan, C., Ross, D., 2012. NAD(P)H:quinone oxidoreductase 1 (NQO1) in the

sensitivity and resistance to antitumor quinones. Biochem. Pharmacol. 83, 1033–1040. https://doi.org/10.1016/j.bcp.2011.12.017

Siller, R., Greenhough, S., Naumovska, E., Sullivan, G.J., 2015. Small-molecule-driven hepatocyte differentiation of human pluripotent stem cells. Stem Cell Reports 4, 939–952. https://doi.org/10.1016/j.stemcr.2015.04.001

Smith, G.S., Walter, G.L., Walker, R.M., 2013. Clinical Pathology in Non-Clinical Toxicology Testing, in: Haschek and Rousseaux's Handbook of Toxicologic Pathology. pp. 565–594. https://doi.org/10.1016/B978-0-12-415759-0.00018-2

Söderdahl, T., Küppers-Munther, B., Heins, N., Edsbagge, J., Björquist, P., Cotgreave, I., Jernström, B., 2007. Glutathione transferases in hepatocyte-like cells derived from human embryonic stem cells. Toxicol. Vitr. 21, 929–937. https://doi.org/10.1016/j.tiv.2007.01.021

Sokol, S.Y., 2011. Maintaining embryonic stem cell pluripotency with Wnt signaling. Development 138, 4341–4350. https://doi.org/10.1242/dev.066209

Soldner, F., Hockemeyer, D., Beard, C., Gao, Q., Bell, G.W., Cook, E.G., Hargus, G., Blak, A., Cooper, O., Mitalipova, M., Isacson, O., Jaenisch, R., 2009. Parkinson's Disease Patient-Derived Induced Pluripotent Stem Cells Free of Viral Reprogramming Factors. Cell 136, 964–977. https://doi.org/10.1016/j.cell.2009.02.013

Somerville, G.A., Proctor, R.A., 2013. Cultivation conditions and the diffusion of oxygen into culture media: The rationale for the flask-to-medium ratio in microbiology. BMC Microbiol. 13, 9. https://doi.org/10.1186/1471-2180-13-9

Steijns, L.S.W., Van Der Weide, J., 1998. Ultrarapid drug metabolism: PCR-based detection of CYP2D6 gene duplication. Clin. Chem. 44, 914–917.

Stüven, T., Griese, E.U., Kroemer, H.K., Eichelbaum, M., Zanger, U.M., 1996. Rapid detection of CYP2D6 null alleles by long distance- and multiplex-polymerase chain reaction. Pharmacogenetics 6, 417–421. https://doi.org/10.1097/00008571-199610000-00005

Subramanian, K., Owens, D.J., Raju, R., Firpo, M., O'Brien, T.D., Verfaillie, C.M., Hu, W.-S., 2014. Spheroid Culture for Enhanced Differentiation of Human Embryonic Stem Cells to Hepatocyte-Like Cells. Stem Cells Dev. 23, 124–131. https://doi.org/10.1089/scd.2013.0097

Sui, L., Bouwens, L., Mfopou, J.K., 2013. Signaling pathways during maintenance and definitive endoderm differentiation of embryonic stem cells. Int. J. Dev. Biol. 57, 1–12. https://doi.org/10.1387/ijdb.120115ls

Suntharalingam, G., Perry, M.R., Ward, S., Brett, S.J., Castello-Cortes, A., Brunner, M.D., Panoskaltsis, N., 2006. Cytokine Storm in a Phase 1 Trial of the Anti-CD28 Monoclonal Antibody TGN1412. N. Engl. J. Med. 355, 1018–1028. https://doi.org/10.1056/NEJMoa063842

Takahashi, K., Tanabe, K., Ohnuki, M., Narita, M., Ichisaka, T., Tomoda, K., Yamanaka, S., 2007. Induction of Pluripotent Stem Cells from Adult Human Fibroblasts by Defined Factors. Cell 131, 861–872. https://doi.org/10.1016/j.cell.2007.11.019

Takahashi, K., Yamanaka, S., 2006. Induction of Pluripotent Stem Cells from Mouse Embryonic and Adult Fibroblast Cultures by Defined Factors. Cell 126, 663–676. https://doi.org/10.1016/j.cell.2006.07.024

Takahashi, R., Sonoda, H., Tabata, Y., Hisada, A., 2010. Formation of hepatocyte spheroids with structural polarity and functional bile canaliculi using nanopillar sheets. Tissue Eng. Part A 16, 1983–1995. https://doi.org/10.1089/ten.TEA.2009.0662

Takayama, K., Akita, N., Mimura, N., Akahira, R., Taniguchi, Y., Ikeda, M., Sakurai, F., Ohara, O., Morio, T., Sekiguchi, K., Mizuguchi, H., 2017. Generation of safe and therapeutically effective human induced pluripotent stem cell-derived hepatocyte-like cells for regenerative medicine. Hepatol. Commun. 1, 1058–1069. https://doi.org/10.1002/hep4.1111

Takayama, K., Kawabata, K., Nagamoto, Y., Kishimoto, K., Tashiro, K., Sakurai, F., Tachibana, M., Kanda, K., Hayakawa, T., Furue, M.K., Mizuguchi, H., 2013. 3D spheroid culture of hESC/hiPSC-derived hepatocyte-like cells for drug toxicity testing. Biomaterials 34, 1781–1789. https://doi.org/10.1016/j.biomaterials.2012.11.029

Takayama, K., Morisaki, Y., Kuno, S., Nagamoto, Y., Harada, K., Furukawa, N., Ohtaka, M., Nishimura, K., Imagawa, K., Sakurai, F., Tachibana, M., Sumazaki, R., Noguchi, E., Nakanishi, M., Hirata, K., Kawabata, K., Mizuguchi, H., 2014. Prediction of interindividual differences in hepatic functions and drug sensitivity by using human iPS-derived hepatocytes. Proc. Natl. Acad. Sci. 111, 16772–16777. https://doi.org/10.1073/pnas.1413481111

Takebe, T., Zhang, R.R., Koike, H., Kimura, M., Yoshizawa, E., Enomura, M., Koike, N., Sekine, K., Taniguchi, H., 2014. Generation of a vascularized and functional human liver from an iPSC-derived organ bud transplant. Nat. Protoc. 9, 396–409. https://doi.org/10.1038/nprot.2014.020

Teh, L.K., Bertilsson, L., 2012. Pharmacogenomics of CYP2D6: Molecular Genetics, Interethnic Differences and Clinical Importance. Drug Metab. Pharmacokinet. 27, 55–67. https://doi.org/10.2133/dmpk.DMPK-11-RV-121

Teratani, T., Yamamoto, H., Aoyagi, K., Sasaki, H., Asari, A., Quinn, G., Sasaki, H., Terada, M., Ochiya, T., 2005. Direct hepatic fate specification from mouse embryonic stem cells. Hepatology 41, 836–846. https://doi.org/10.1002/hep.20629

Terry, C., Dhawan, A., Mitry, R.R., Hughes, R.D., 2006. Cryopreservation of isolated human hepatocytes for transplantation: State of the art. Cryobiology 53, 149–159. https://doi.org/10.1016/j.cryobiol.2006.05.004

Terry, C., Dhawan, A., Mitry, R.R., Lehec, S.C., Hughes, R.D., 2010. Optimization of the cryopreservation and thawing protocol for human hepatocytes for use in cell transplantation. Liver Transplant. 16, 229–237. https://doi.org/10.1002/lt.21983

Thoolen, B., Maronpot, R.R., Harada, T., Nyska, A., Rousseaux, C., Nolte, T., Malarkey, D.E., Kaufmann, W., Küttler, K., Deschl, U., Nakae, D., Gregson, R., Vinlove, M.P., Brix, A.E., Singh, B., Belpoggi, F., Ward, J.M., 2010. Proliferative and nonproliferative lesions of the rat and mouse hepatobiliary system. Toxicol. Pathol. https://doi.org/10.1177/0192623310386499

Thorens, B., 2015. GLUT2, glucose sensing and glucose homeostasis. Diabetologia 58, 221–232. https://doi.org/10.1007/s00125-014-3451-1

Tomizawa, M., Shinozaki, F., Sugiyama, T., Yamamoto, S., Sueishi, M., Yoshida, T., 2013. Survival of Primary Human Hepatocytes and Death of Induced Pluripotent Stem Cells in Media Lacking Glucose and Arginine. PLoS One 8, e71897. https://doi.org/10.1371/journal.pone.0071897

Tong, W.H., Fang, Y., Yan, J., Hong, X., Hari Singh, N., Wang, S.R., Nugraha, B., Xia, L., Fong, E.L.S., Iliescu, C., Yu, H., 2016. Constrained spheroids for prolonged hepatocyte culture. Biomaterials 80, 106–120. https://doi.org/10.1016/j.biomaterials.2015.11.036

Tournay, O., Benezra, R., 2015. Transcription of the dominant-negative helix-loop-helix protein Id1 is regulated by a protein complex containing the immediate-early response gene Egr-1. Mol. Cell. Biol. 16, 2418–2430. https://doi.org/10.1128/mcb.16.5.2418

Uhlen, M., Zhang, C., Lee, S., Sjöstedt, E., Fagerberg, L., Bidkhori, G., Benfeitas, R., Arif, M., Liu, Z., Edfors, F., Sanli, K., von Feilitzen, K., Oksvold, P., Lundberg, E., Hober, S., Nilsson, P., Mattsson, J., Schwenk, J.M., Brunnström, H., Glimelius, B., Sjöblom, T., Edqvist, P.-H., Djureinovic, D., Micke, P., Lindskog, C., Mardinoglu, A., Ponten, F., 2017. A pathology atlas of the human cancer transcriptome. Science (80-.). 357, eaan2507. https://doi.org/10.1126/science.aan2507

Ulvestad, M., Nordell, P., Asplund, A., Rehnstrom, M., Jacobsson, S., Holmgren, G.,

Davidson, L., Brolen, G., Edsbagge, J., Björquist, P., Küppers-Munther, B., Andersson, T.B., 2013. Drug metabolizing enzyme and transporter protein profiles of hepatocytes derived from human embryonic and induced pluripotent stem cells. Biochem. Pharmacol. 86, 691–702. https://doi.org/10.1016/j.bcp.2013.06.029

Uotila, L., Koivusalo, M., 1974. Purification and properties of S formylglutathione hydrolase from human liver. J. Biol. Chem. 249, 7664–7672.

Van De Wetering, M., Francies, H.E., Francis, J.M., Bounova, G., Iorio, F., Pronk, A., Van Houdt, W., Van Gorp, J., Taylor-Weiner, A., Kester, L., McLaren-Douglas, A., Blokker, J., Jaksani, S., Bartfeld, S., Volckman, R., Van Sluis, P., Li, V.S.W., Seepo, S., Sekhar Pedamallu, C., Cibulskis, K., Carter, S.L., McKenna, A., Lawrence, M.S., Lichtenstein, L., Stewart, C., Koster, J., Versteeg, R., Van Oudenaarden, A., Saez-Rodriguez, J., Vries, R.G.J., Getz, G., Wessels, L., Stratton, M.R., McDermott, U., Meyerson, M., Garnett, M.J., Clevers, H., 2015. Prospective derivation of a living organoid biobank of colorectal cancer patients. Cell 161, 933–945. https://doi.org/10.1016/j.cell.2015.03.053

van Wenum, M., Adam, A.A.A., van der Mark, V.A., Chang, J.-C., Wildenberg, M.E., Hendriks, E.J., Jongejan, A., Moerland, P.D., van Gulik, T.M., Oude Elferink, R.P., Chamuleau, R.A.F.M., Hoekstra, R., 2018. Oxygen drives hepatocyte differentiation and phenotype stability in liver cell lines. J. Cell Commun. Signal. 12, 575–588. https://doi.org/10.1007/s12079-018-0456-4

Vasiliou, V., Vasiliou, K., Nebert, D.W., 2009. Human ATP-binding cassette (ABC) transporter family. Hum. Genomics 3, 281–90. https://doi.org/10.1186/1479-7364-3-3-281

Vihervaara, A., Sistonen, L., 2014. HSF1 at a glance. J. Cell Sci. 127, 261–266. https://doi.org/10.1242/jcs.132605

Vivares, A., Salle-Lefort, S., Arabeyre-Fabre, C., Ngo, R., Penarier, G., Bremond, M., Moliner, P., Gallas, J.F., Fabre, G., Klieber, S., 2015. Morphological behaviour and metabolic capacity of cryopreserved human primary hepatocytes cultivated in a perfused multiwell device. Xenobiotica 45, 29–44. https://doi.org/10.3109/00498254.2014.944612

Vogel, C., Marcotte, E.M., 2012. Insights into the regulation of protein abundance from proteomic and transcriptomic analyses. Nat. Rev. Genet. 13, 227–232. https://doi.org/10.1038/nrg3185

Wang, B., Yang, L.., Al, E., 2009. New insights into the structural characteristic and functional relevance of the human cytochrome PY4502D6 enzyme. Drug Metab. Rev. 41, 573–643.

Wang, D.H., Wang, Y.N., Ge, J.Y., Liu, H.Y., Zhang, H.J., Qi, Y., Liu, Z.H., Cui, X.L., 2013. Role of activin A in carbon tetrachloride-induced acute liver injury. World J. Gastroenterol. 19, 3802–3809. https://doi.org/10.3748/wjg.v19.i24.3802

Wang, Z., Luo, X., Anene-Nzelu, C., Yu, Y., Hong, X., Singh, N.H., Xia, L., Liu, S., Yu, H., 2015. HepaRG culture in tethered spheroids as an in vitro three-dimensional model for drug safety screening. J. Appl. Toxicol. 35, 909–917. https://doi.org/10.1002/jat.3090

Ware, B.R., Berger, D.R., Khetani, S.R., 2015. Prediction of drug-induced liver injury in micropatterned co-cultures containing iPSC-derived human hepatocytes. Toxicol. Sci. 145, 252–262. https://doi.org/10.1093/toxsci/kfv048

Weber, L.W.D., Boll, M., Stampfl, A., 2003. Hepatotoxicity and mechanism of action of haloalkanes: Carbon tetrachloride as a toxicological model. Crit. Rev. Toxicol. 33, 105–136. https://doi.org/10.1080/713611034

Wesselschmidt, R.L., 2011. The teratoma assay: An in vivo assessment of pluripotency. Methods Mol. Biol. 767, 231–241. https://doi.org/10.1007/978-1-61779-201-4_17

Wickham, S., West, M.B., Cook, P.F., Hanigan, M.H., 2011. Gamma-glutamyl compounds: Substrate specificity of gamma-glutamyl transpeptidase enzymes. Anal. Biochem. 414,

208–214. https://doi.org/10.1016/j.ab.2011.03.026

World Health Organisation, 2004. Environmental Health Criteria 208 : CARBON TETRACHLORIDE. World Heal. Organ.

Xu, D., Nishimura, T., Nishimura, S., Zhang, H., Zheng, M., Guo, Y.Y., Masek, M., Michie, S.A., Glenn, J., Peltz, G., 2014. Fialuridine Induces Acute Liver Failure in Chimeric TK-NOG Mice: A Model for Detecting Hepatic Drug Toxicity Prior to Human Testing. PLoS Med. 11, e1001628. https://doi.org/10.1371/journal.pmed.1001628

Xu, R.-R., Zhang, C.-W., Cao, Y., Wang, Q., 2013. [Mir122 Deficiency Inhibits Differentiation of Zebrafish Hepatoblast Into Hepatocyte]. Yi Chuan 35, 488–494.

Yanger, K., Knigin, D., Zong, Y., Maggs, L., Gu, G., Akiyama, H., Pikarsky, E., Stanger, B.Z., 2014. Adult hepatocytes are generated by self-duplication rather than stem cell differentiation. Cell Stem Cell 15, 340–349. https://doi.org/10.1016/j.stem.2014.06.003

Yasuda, M., Ogura, T., Goto, T., Yagoto, M., Kamai, Y., Shimomura, C., Hayashimoto, N., Kiyokawa, Y., Shinohara, H., Takahashi, R., Kawai, K., 2017. Incidence of spontaneous lymphomas in non-experimental NOD/Shi-scid, IL-2Rγnull (NOG) mice. Exp. Anim. 66, 425–435. https://doi.org/10.1538/expanim.17-0034

Ye, L., Chang, J.C., Lin, C., Sun, X., Yu, J., Kan, Y.W., 2009. Induced pluripotent stem cells offer new approach to therapy in thalassemia and sickle cell anemia and option in prenatal diagnosis in genetic diseases. Proc. Natl. Acad. Sci. 106, 9826–9830. https://doi.org/10.1073/pnas.0904689106

Yeh, H.W., Karmach, O., Ji, A., Carter, D., Martins-Green, M.M., Ai, H.W., 2017. Red-shifted luciferase-luciferin pairs for enhanced bioluminescence imaging. Nat. Methods 14, 971–974. https://doi.org/10.1038/nmeth.4400

Yoshimitsu, R., Hattori, K., Sugiura, S., Kondo, Y., Yamada, R., Tachikawa, S., Satoh, T., Kurisaki, A., Ohnuma, K., Asashima, M., Kanamori, T., 2014. Microfluidic perfusion culture of human induced pluripotent stem cells under fully defined culture conditions. Biotechnol. Bioeng. 111, 937–947. https://doi.org/10.1002/bit.25150

Yusa, K., Rashid, S.T., Strick-Marchand, H., Varela, I., Liu, P.Q., Paschon, D.E., Miranda, E., Ordóñez, A., Hannan, N.R.F., Rouhani, F.J., Darche, S., Alexander, G., Marciniak, S.J., Fusaki, N., Hasegawa, M., Holmes, M.C., Di Santo, J.P., Lomas, D.A., Bradley, A., Vallier, L., 2011. Targeted gene correction of α1-antitrypsin deficiency in induced pluripotent stem cells. Nature 478, 391–394. https://doi.org/10.1038/nature10424

Zanger, U.M., Schwab, M., 2008. Cytochrome P450 enzymes in drug metabolism: regulation of gene expression, enzyme activities, and impact of genetic variation. Pharmacol. Ther. 138, 103–141.

Zeng, Y., Lee, T.-S., Yu, P., Low, H.-T., 2007. Numerical simulation on mass transport in a microchannel bioreactor for co-culture applications. J. Biomech. Eng. 129, 365–73. https://doi.org/10.1115/1.2720913

Zhang, J., Wang, J.H.C., 2013. Human Tendon Stem Cells Better Maintain Their Stemness in Hypoxic Culture Conditions. PLoS One 8, e61424. https://doi.org/10.1371/journal.pone.0061424

Zhang, R.-R., Takebe, T., Miyazaki, L., Takayama, M., Koike, H., Kimura, M., Enomura, M., Zheng, Y.-W., Sekine, K., Taniguchi, H., 2014. Efficient Hepatic Differentiation of Human Induced Pluripotent Stem Cells in a Three-Dimensional Microscale Culture. Methods Mol. Biol. 1210, 131–141. https://doi.org/10.1007/978-1-4939-1435-7_10

Zhang, X., Ling, M.T., Wang, Q., Lau, C.K., Leung, S.C.L., Lee, T.K., Cheung, A.L.M., Wong, Y.C., Wang, X., 2007. Identification of a novel Inhibitor of Differentiation-1 (ID-1) binding partner, caveolin-1, and its role in epithelial-mesenchymal transition and resistance to apoptosis in prostate cancer cells. J. Biol. Chem. 282, 33284–33294. https://doi.org/10.1074/jbc.M705089200

Zhou, H., Liu, H., Ezzelarab, M., Schmelzer, E., Wang, Y., Gerlach, J., Gridelli, B., Cooper, D.K.C., 2015. Experimental hepatocyte xenotransplantation - A comprehensive review of the literature. Xenotransplantation 22, 239–248. https://doi.org/10.1111/xen.12170

Zorn, A.M., 2008. Liver development, Stembook, http://www.stembook.org. Sci. Collab. Framew. 2010. https://doi.org/10.3824/stembook.1.25.1

Zou, Y., Lee, J., Nambiar, S.M., Hu, M., Rui, W., Bao, Q., Chan, J.Y., Dai, G., 2014. Nrf2 is involved in maintaining hepatocyte identity during liver regeneration. PLoS One 9. https://doi.org/10.1371/journal.pone.0107423